A Theory/Experience Description of Support Effects in Carbon-Supported Catalysts

I.C. Gerber, Philippe Serp

A theory/experience description of support effects in carbon-supported catalysts

Iann C. Gerber,[1]* Philippe Serp[2]*

[1]*LPCNO, Université de Toulouse, CNRS, INSA, UPS, 135 avenue de Rangueil, F-31077 Toulouse, France*

[2]*LCC-CNRS, Université de Toulouse, UPR 8241 CNRS, INPT, Toulouse, France*

Abstract. The support plays an important role for supported metal catalysts by positioning itself as a macromolecular ligand, which conditions the nature of the active site and contributes indirectly, but also sometimes directly to the reactivity. Metal species such as nanoparticles, clusters or single atoms can be deposited on carbon materials for various catalytic reactions. All the carbon materials used as catalyst support constitute a large family of compounds that can vary both at textural and structural levels. Today, the recent developments of well-controlled synthesis methodologies, advanced characterization techniques and modeling tools allow one to correlate the relationships between metal/support/reactant at the molecular level. Based on these considerations, in this Review article, we wish to provide some answers to the question "*How and why anchoring metal nanoparticles, clusters or single atoms on carbon materials for catalysis?*". To do this, we will rely on both experimental and theoretical studies. We will first analyze what sites are available on the surface of a carbon support for the anchoring of the active phase. Then, we will describe some important effects in catalysis inherent to the presence of a carbon-type support (metal-support interaction, confinement, spillover and surface functional group effects). These effects will be commented on by putting

into perspective catalytic results obtained in numerous reactions of thermal catalysis, electrocatalysis or photocatalysis.

1. Introduction

2. How interact metal nanoparticles, clusters or single metal atoms with carbon (nano)materials?

2.1 Anchoring sites on carbon surfaces

2.1.1 0D materials

2.1.2 Nanotubes

2.1.3 Graphene and few layer graphene

2.1.4 Graphite (intercalation) + mesoporous (edges, activated carbon, carbon nanofibers) and hybrid structures

2.2 Atom, cluster, and nanoparticle anchoring

2.2.1 Atom anchoring

2.2.2 Cluster (< 13 atoms, 0.5 nm) anchoring

2.2.3 Nanoparticle anchoring

3. Why anchoring metal nanoparticles, clusters or metal single atoms on carbon materials for catalysis?

3.1 Metal-support interaction

3.1.1 Geometric effects

3.1.2 Charge transfer

1. Introduction

It has long been recognized that some activated carbons, developed for gas mask during the First World War may be used not only for their own catalytic activity but also as support for a metallic phase.[1] In fact, the development of metal impregnated carbon was firstly accomplished in order to increase the catalytic activity of the carbon itself,[2] and there is now more than a century that carbon materials are used industrially as catalyst or catalyst support.[3,4] Carbon supported metallic catalysts are exploited for a wide range of reactions involving noble metals (Pd ≈ Pt > Rh > Ru ≈ Ir),[5] such as (selective) hydrogenations, hydrogenolysis, dehydrogenation, dehalogenation or coupling reactions.[4,5] Reactions involving non-noble metals also exist as for vinyl acetate production (Zn) or hydrocarbon sweetening by oxidative dehydrogenation on Cu-Mn-Fe-Co catalysts. One of the oldest industrial application of activated carbon as catalyst support is for $HgCl_2$ supported catalyst. This catalyst was used for many years for the vapor phase production of vinyl chloride monomer from acetylene and HCl. Interestingly, commercialization of a new carbon supported gold catalysts for acetylene hydrochlorination has been recently reported.[6] X-ray spectroscopic studies of the working catalysts and computational modeling have shown that the active species are single-site Au cations.[7] This example among many others illustrates the continuous interest in using carbon materials in catalysis, and how the tremendous progresses in surface science and modeling allow the development and understanding of carbon-supported metallic catalysts.

The most used carbon support material is activated carbon, followed by carbon black and graphite or graphitized materials. In addition to a tailorable porous structure and surface chemistry, carbon materials present several advantages to be used as catalyst support, such as: (i) an easy reduction of the metallic phase; (ii) a good resistance to acids and bases; (iii) a stable

structure to high temperatures (even above 1023 K under inert atmosphere); (iv) porous carbon catalysts can be prepared in different physical forms as granules, clothes, fibers, pellets, etc.; (v) the active phase can be easily recovered; and (vi) the cost of conventional carbon supports is usually lower than that of other conventional supports, such as alumina and silica.[8] Although it was soon recognized that the nature of the carbon material, and particularly its electronic properties, structure, and surface chemistry, has an influence on its own catalytic performances,[9,10] studies aiming at investigating its influence on (electro)catalytic performances of supported catalysts only appears several years later.[11-13] Thus, the importance of electronic interactions between Pt particles and a carbon support on the electrocatalytic performances of Pt/C catalysts was reported in 1965 by Hillenbrand and Lacksonen.[11] For an appreciation of the possible variations in the electronic properties of carbons, Mrozowski *et al*. proposed in 1954 a model from aromatic hydrocarbons through defective graphites to near ideal graphite, that involves progressive reduction of a finite energy gap between the full π-electron band and the conduction band (Figure 1a).[14] Thus, as stated by Coughlin,[10] in any given microcrystalline carbon we might expect to find islands of order, differing in degree of perfection and, therefore, corresponding to several of the stages shown in Figure 1a. Consequently, we might find, within a typical sample, well-ordered carbon whose electronic behavior approaches that of a metal, as well as some highly disordered carbon with electronic behavior similar to that of an insulator. This reflects the difficulty to draw structure-property relationship with this kind of material. The porous structure impact's of the carbon support on hydrogen transport limitations from the bulk liquid phase to catalyst particles was highlighted in 1972 by Acres and Cooper.[13] The first attempt to understand the structure of carbons was made by Franklin in the 1950s.[15] She put forward a simple model based on small graphitic crystallites joined together by cross-links, without explaining the nature of these links (Figure 1b). Still today, the precise atomic structure of activated carbon remains unknown.[16] The first

works on the understanding of the surface chemistry of carbonaceous materials and its involvement in catalyst preparation and even catalysis appeared in the 1980s. Some landmark papers were published during this period, related to the influence of surface functionality on the preparation and the activity of carbon(-supported) catalysts.[17-19] The unambiguous identification of surface hetero-element species is a delicate art, and requires much experience. The presence of surface oxygen-containing groups (Fig 1c) formed upon oxidation of carbon proposed in 1913,[20] and highlighted by H.P. Boehm and others in the 60's,[21,22] is an important parameter that influences catalyst performances. It is also worth to keep in mind that it has been verified both experimentally and theoretically that pure (*i.e.* without any impurities) carbon materials can exhibit magnetism.[23] The presence of vacancies or radical species (Figure 1d) could be at the origin of magnetism.[24] If generated, the high chemical reactivity of the carbon atoms involved should be considered during the preparation of catalysts or during catalysis.[25] Furthermore, graphitic crystals, exhibiting highly anisotropic properties due to difference in bonding between basal planes and within basal planes, show large differences in surface energies in their different crystallographic directions: about 0.11 $J.m^{-2}$ in the basal plane and 5 $J.m^{-2}$ in the prismatic planes.[26] The edge surface would be expected to react much more rapidly than does the basal plane surface.

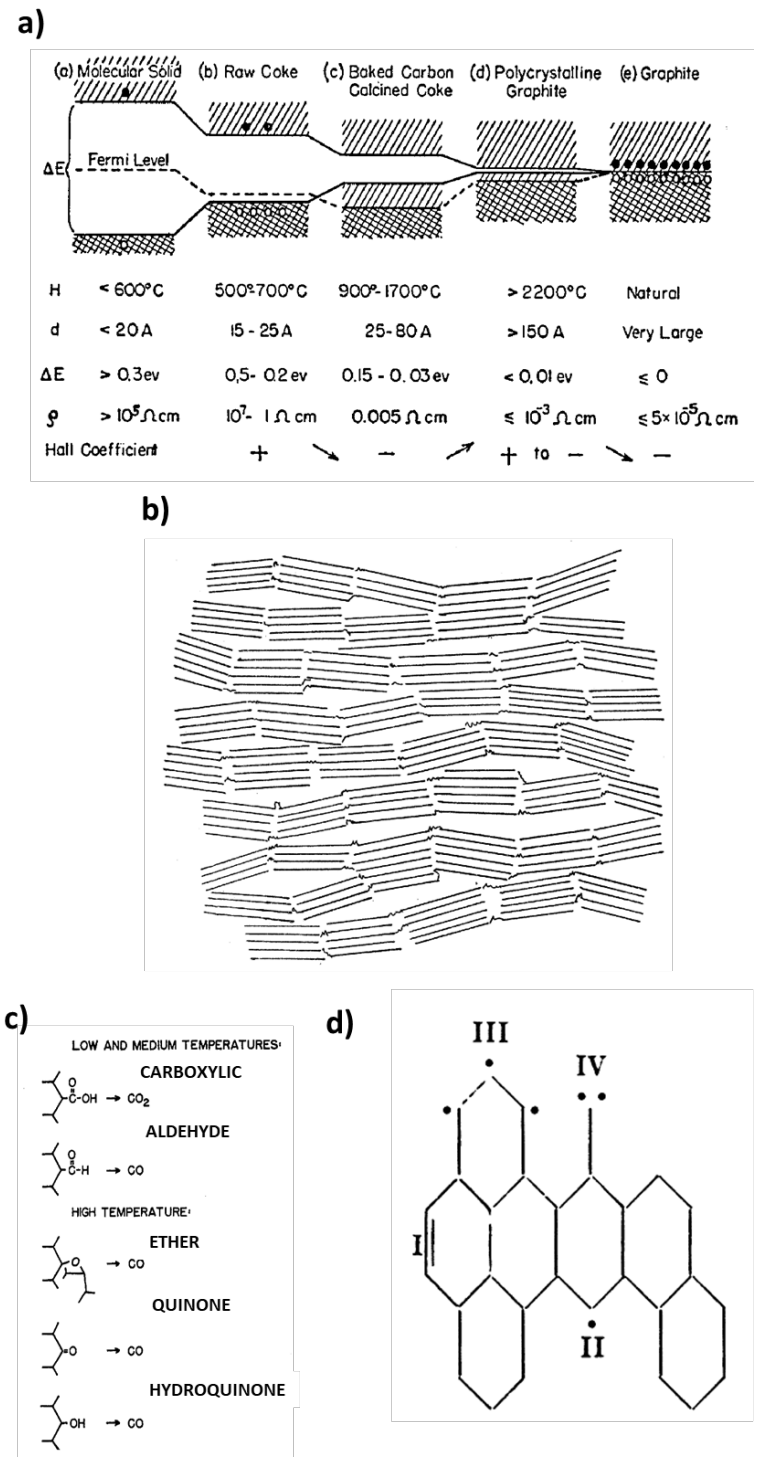

Figure 1. a) Schematic diagram of the energy bands and the position of the Fermi level for the aromatic solids starting from molecular van der Waals solids (a) and ending on a perfect graphite crystal (e). Reprinted from ref [14]; b) Schematic representation of the structure of a graphitizing (but non graphitic) carbon. Reprinted with permission from ref [15] Copyright 1951 from the Royal Society; c) Decomposition of isolated surface oxygenated groups. Reprinted

with permission from Coltharp, M. T.; *et al*. *J. Phys. Chem*. **1968**, *72*, 1171-1177.[22] Copyright 1968 from the American Chemical Society; and d) Types of reactive sites on carbon materials: I. banana bonds, free valence = 0.75, reactive, II. π-orbital electron unpaired, free valence = 1.70, radical, very reactive, III. resonance, stabilized, less reactive than II, IV. Extremely reactive. Reprinted with permission from Binford, J. S. In Literature of the Combustion of Petroleum; American Chemical Society, **1958**, *20*, 39-48.[24] Copyright 1958 from the American Chemical Society.

The 1990s saw significant advances in the surface characterization of carbon materials, and in particular surface groups containing heteroatoms such as oxygen, nitrogen or sulfur. Consequently, advances in the understanding of the influence of carbon surface chemistry on catalyst preparation and use have been made.[27] For example, the role of surface carboxyl groups in the catalyst loading stage and of surface carbonyl groups in anchoring the active phase has been discussed, and at the same time the importance of carbon surface inertness in the activity and selectivity of many carbon-supported catalysts has also been shown.[28] Since the beginning of the century, the field of carbon (nano)materials for catalysis is rapidly expanding, and many reviews[29-38] and entire books have already been devoted to the subject.[39-42] This is mainly due to: i) the (re)discovery of new types of carbon materials or allotropes, such as fullerene, carbon nanotubes (CNT) and graphene (G), which present outstanding properties, including for catalysis; ii) the emergence of new demanding applications, particularly in the field of energy, environment and biomass conversion;[43-45] and iii) the development of metal-free-,[46] photo-[47] and electro-catalysis.[48] Among the enormous recent advances due to the use of carbon (nano)materials as support for catalysis, we can point several highly important articles dealing with the use of (i) carbon black in Proton Exchange Membrane Fuel Cell (PEMFC)[49] or in Oxygen Evolution Reaction (OER),[50] ii) (nano-)fibers for CO oxidation[51] or Oxygen Reduction

Reaction (ORR),[52] (ii) carbon nanotubes in Direct Methanol Fuel Cells (DMFC)[53] or for ORR purpose,[54] (iii) graphene for ORR[55] or CO/methanol oxidation,[56] or iv) the discovery, development, and commercialization of a new Au/C catalyst for vinyl chloride production by acetylene hydrochlorination.[6,7]

In parallel, recent developments of characterization techniques, modeling tools, and progresses in surface coordination chemistry have allowed significant advances. Representative examples are shown on Figure 2, which can be considered in perspective from those presented in Figure 1. Figure 2a shows density of state (DoS) analysis carried out to examine the electronic structure of several defective sites in graphene.[57] Sharp spikes exist within 0.5 eV from the Fermi level on the DoS curves of all these defects, denoting the localized character of those reactive states. Charge densities of these states were extracted, which further prove that these features in the DoS are associated to defect states localized on carbon atoms involved in defect sites. Such defects alter the electronic properties of graphene and modify the chemical reactivity toward adsorbates. Recent investigation by aberration-corrected Transmission Electron Microscopy (TEM) suggests that activated carbon has a structure related to that of fullerenes, consisting of curved fragments containing pentagons and other non-hexagonal rings in addition to hexagons.[16,58] Figure 2b shows a molecular model based on a random packing of fullerene-like fragments, functionalized with carboxylic groups.[59] Experimental data combined with Density Functional Theory (DFT) calculations have shown that both metal precursor and metallic nanoparticles (NPs) can be anchored on the surface of the carbon support *via* these carboxylic surface groups, presumably *via* surface acetato ligands. Figure 2c shows a Ru_{13} cluster adsorbed on a site of graphene combining a double vacancy and two -COOH groups before (on left panel) and after a proton jump from the –COOH group to the metal.[60] Finally, while perfect graphite is nonmagnetic, experimental observations of magnetic ordering in carbon materials are often explained by the presence of defects, such as vacancies or hydrogen chemisorption defects.[61]

Figure 2d shows the spin-density projection in μ_B/a.u.^{2} on the graphene plane around these types of defects. Calculated magnetic moments are 1 μ_B per hydrogen chemisorption defect, and 1.1-1.5 μ_B per vacancy defect, depending on the defect concentration.

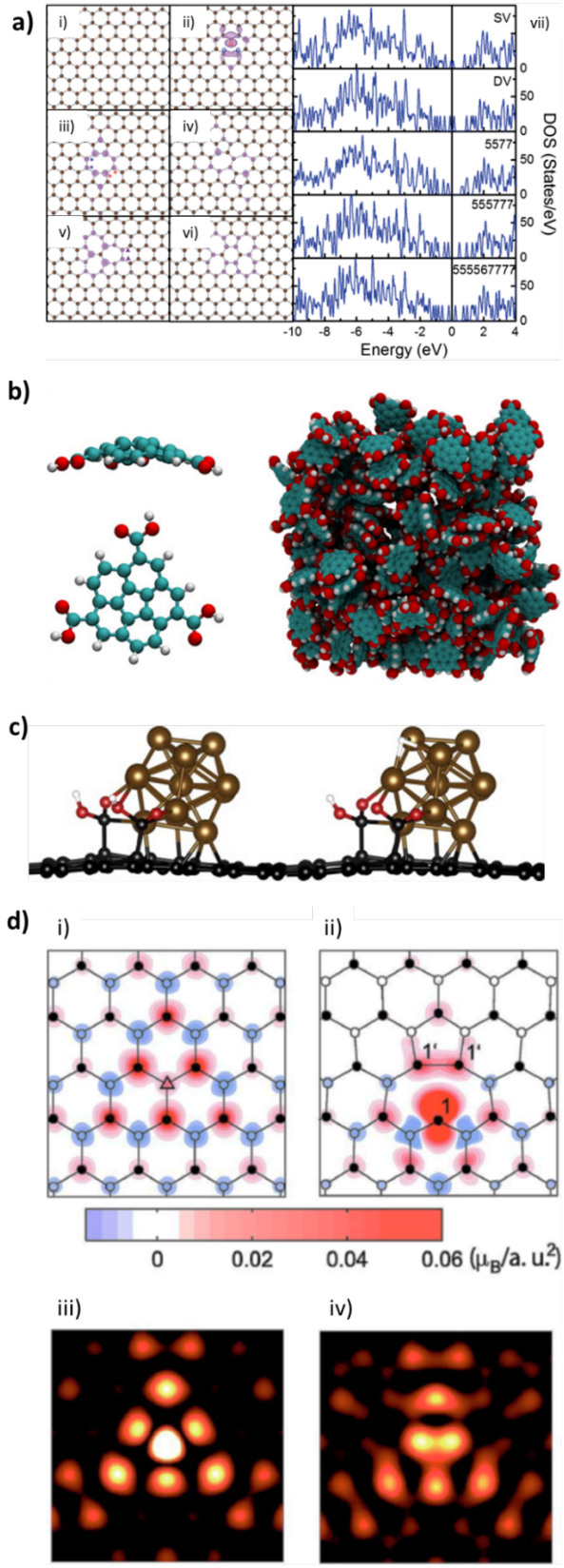

Figure 2. a) Structures of i) pristine graphene (G), ii) single vacancy (SV-G), iii) double vacancy (DV-G) and several haeckelite-like structures, namely iv) 5775, v) 555-777 vi), 5555

-6-7777 and their corresponding DoS curves vii). The charge densities of defective states at the Fermi level in vii) are shown in purple in ii)-vi) with an iso-value of ±0.003 a.u. Reprinted with permission from ref [57]. Copyright 2014 from the Royal Society of Chemistry; b) Molecular model of a corannulene-like element functionalized with three carboxylic groups from two different perspectives in the cpk representation (on the left). The final structure (190 elements in a cubic cell of 60 Å in size) obtained from random packing of the individual elements (on the right). Cyan: carbon, red: oxygen, white: hydrogen. Reprinted with permission from ref [59] Copyright 2017 from Elsevier; c) Side-views of Ru_{13} adsorbed on Gr-DV-2COOH site before (on left panel) and after a proton jump (right panel). C atoms are in black, O in red, H in with white and Ru in mocha. Reprinted with permission from ref [60] Copyright 2014 from Elsevier; and d) Spin-density projection in $\mu B/a.u.^2$ on the graphene plane around i) the hydrogen chemisorption defect (Δ) and ii) the vacancy defect in the α sublattice. Carbon atoms corresponding to the α sublattice (o) and to the β sublattice (●) are distinguished. Simulated STM images of the defects are shown in iii) and iv), respectively. Reprinted with permission from ref [61]. Copyright 2007 American Physical Society.

Despite the fact that syntheses and applications in various fields of catalysis of carbon-supported metal catalysts have been largely covered in many recent review articles or book chapters, we do believe that a comprehensive review ***covering from both theoretical and experimental point of views*** the critical issues dealing with this central question "How and why anchoring metal nanoparticles, clusters or single atoms on carbon (nano)materials for catalysis?" is definitively missing. Indeed, modern approaches for an in-depth understanding of the complex and rich surface chemistry as well as structural characteristics of carbon materials, and their influence on metal nanoparticle/cluster/atom anchoring and activity/selectivity, pass by a strong interaction between experiment and theory. We also believe that this review article

that cover the period 2000-2018 will open new perspectives for researchers exploring the reactivity of carbon and metallic surfaces in many other fields than catalysis.

2. How interact metal nanoparticles, clusters or single metal atoms with carbon (nano)materials?

As mentioned in the introduction, already in the late 1960s, R. W. Coughlin suggested in a landmark paper that the catalytic activity and selectivity of carbon catalysts was related to their surface chemistry and electronic properties.[10] We only recall that pure nanostructured carbon materials can be (i) 0D (carbon black or fullerene) (ii) 1D (nanotubes), (iii) 2D (graphene, graphene oxide) or even (iv) 3D (mesoporous carbon, graphite) for instance. A very large amount of experimental and theoretical works in the field are devoted to describe and/or tune the anchoring modes of supported metallic catalysts (be it a single atom, a small aggregate or even a NP) on all possible nanostructured carbon-based materials. A well-accepted concept is that specific sites on the carbon support, irrespective of their type, are required to trap the chemically active species. The next section is firstly devoted to present the major results concerning the description of those anchoring sites, and in a second time, to describe how atoms, clusters and NPs interact with them.

Adsorption on carbon materials is related to their surface physico-chemical properties. The sp^2 type carbon material surface chemistry is mainly dictated: (i) by basal and edge carbon atoms,[62,63] and (ii) point-defects such as structural carbon vacancies or non-aromatic rings.[64] The presence of such defects along the edges of graphene layers, and also incorporated in the graphene layer, is at the origin of their high reactivity since many unpaired electrons are indeed localized at these specific sites. Two types of carbon appear then, some carbene type on zigzag sites, or carbyne-like for armchair configurations.[62] Heteroatoms, mainly oxygen, hydrogen,

nitrogen, and sulfur can be also adsorbed or even substitute carbon atoms, resulting in very stable surface compounds, which induce a complex surface chemistry, especially in conjunction with structural point-defects.

Among the heteroatoms, nitrogen is particularly appealing, due to its chemical versatility and to the induced doping produced by a single substitution N/C.[65-67] If most of the adsorption sites for chemisorption on sp^2 and $sp^{2+\delta}$ carbon materials are on the basal planes and inner or outer surface in the case of CNT, the presence of heterogeneous groups,[68] mainly oxygenated ones, can also reinforce the overall adsorption capacity. This is due to a higher activity compared to pure sp^2 carbon of basal planes, or even carbon atoms involved in CNT sidewall, which are usually more pyramidalized. It is of great interest to get a better understanding at the atomic-scale, which necessitates the use of precise computational approaches combined with various experimental techniques, of how all these defects, substitutions and or functionalized groups grafted on carbon support interact with the active metal. Of course, computational chemistry is precious to elucidate the molecular scale interfacial structure, see ref. 69 for bright prospects and emerging challenges in the field of graphene-based energy applications for instance.

2.1 Anchoring sites on carbon surfaces

Direct atomic-scale pictures of nano-hybrid systems are difficult to obtain experimentally. However, in conjunction with the most advanced characterization technics such as FT-IR, Raman, XANES, EXAFS, HR-TEM, XPS, STEM-EELS, HAADF-STEM, theoretical works mainly using DFT, based on more and more realistic models, can provide useful insights of the metal-carbon interactions. The precise understanding of single atom catalysts (SAC), clusters or NP anchoring modes on advanced carbon materials, and potentially its engineering are key issues to obtain new catalytic properties. Nowadays, those fundamental studies mainly relies

on the fine-tuning of metal-carbon interaction through either the presence of structural surface defects, and/or by substitutional-doping and/or by chemical functionalization of the carbon surfaces. For instance, such studies should allow the development of highly efficient electrocatalysts for ORR,[70] since nitrogen-modified carbon are used as supports,[71] by mainly increasing the stability of metallic NP on the support. Supports with a high level of graphitization, such as CNT and graphene have been extensively considered. Indeed it has been thought that a higher level of graphitization yields to a higher stability due to a lower density of edge and defect sites. Other supports for which both the level of graphitization and support microstructure can be tailored have been considered too, such as nanofibers, hierarchical carbon, aerogels, and ordered mesoporous carbon. Surface functionalized and chemically modified carbon nanomaterials have been getting increased attention over the past few years. In these materials, surface functional groups can help to stabilize the carbon structure, and at the same time can also provide a bonding site for metal, by increasing its dispersion and stability at the same time.[72] If the introduction of hetero-atoms (N, B, P, S) in the carbon graphitic network usually alters locally the electronic properties, it usually increases the carbon sites' reactivity upon functionalization, making them efficient localized grounds for further SAC, clusters or metal NP anchoring. Although the interaction between functional groups and metal has been studied by various characterization techniques, the success of TEM is considerable in this field, see ref. 73 for a recent review. Finding correlation between catalytic performances and atomic scale pictures of the systems obtained from theoretical models, is an object of intense research work, especially for the elucidation of the nature and the role of heteroatoms.[74]

In last years, the newly emerging N-doped carbon-supported metal catalysts have arguably experienced great progresses and brought the most attention since nitrogen doping can tailor the properties of carbon for various applications of interest. Compared with pristine carbon-supported metal catalysts, these catalysts normally show superior catalytic performances in

many reactions because of specific metal-support interactions resulting from N-doping.[75] We will focus our attention, in the next subsections, on the interaction of (non-)noble metals with various carbon nanostructures employed for catalytic purposes, namely 0D (fullerene-like), 1D (nanotubes) and 2D (graphene-like). In a last part, the occurrence of surface modification to induce metal anchorage on more complex systems like graphitic of carbon nanofibers (CNF), will be discussed.

2.1.1 0D materials

The early significant atomic scale investigations of the interaction between transition metals (TM) with fullerenes dated from the 2000s, in the context of hydrogen storage,[76] with the aim of building polymerized structures, see ref. 77 for an overview. Metal fullerides have been the subject of intensive investigations over the past 20 years, and mostly compounds of C_{60} with alkali and alkaline metals (A-C_{60}) have been synthesized.[78] In contrast, only a few reports claiming the existence of fullerides or metal-fullerene complexes with transition metals are known.[79-84] The characterization of those complexes based on Pd or Ru metals is not easy, since various dispersion morphologies of palladium and ruthenium particles on the C_{60} matrix are obtained, depending on the synthesis conditions.[85]

Theoretically, most of the reports found in the literature deal with the interaction of a single TM atom adsorbed on a single C_{60} molecule, which is a versatile ligand, with various hapticity.[68,86] Usually are reported the binding energy, the most stable adsorption sites either hollow (η^6), pentagonal (η^5), bridge on a single bond ($\eta^{2(5-6)}$) or on a double bond ($\eta^{2(6)}$), or top position, see Figure 3a, as well as the geometric parameters such as bond-lengths, and angles. For light TM, Sc and Ti prefer hollow sites with a binding energy of 48.4 kcal.mol^{-1}, while V and Cr prefer $\eta^{2(6)}$ sites with binding energies of 29.9 and 18.5 kcal.mol^{-1}, respectively. In the same work, it

is reported that heavier metals such as Mn, Fe, and Co do not bond on C_{60}.[76] However, experimental evidences were reported for the formation of: i) Co-C_{60} polymeric structure with a complex covalent ionic bond character between the two moieties,[87] and ii) $Co_n(C_{60})_m^+$ mixed clusters with various compositions. Pd and Pt single atoms bind strongly with a $\eta^{2(6)}$ coordination mode and a corresponding adsorption energy of 34.1 and 63.9 kcal.mol^{-1} respectively.[88,89] Nickel atoms also possess a strong affinity with C_{60}.[89] We recall that this kind of study is only ideal in the sense that further molecular adsorption on the metallic center will occur, due to the presence of H_2, CO, or some ligands associated to the metallic precursors decomposition[90] or even other C_{60}.[91]

In the case of Ru fullerides, EXAFS techniques, which are site-specific tools,[92] corroborated by DFT calculations have shown that single Ru atoms can adopt a $\eta^{2(6)}$-η^6 coordination mode between two fullerenes. Charge transfer from the metal to the C_{60}, known as good electron acceptor, has been evidenced, by Raman spectroscopy and DFT calculations too.[91] For a single Pd atom embedded in a C_{60}-polymeric 1/1 ratio, the preferential coordination is $\eta^{2(6)}$-$\eta^{2(6)}$, and remains the same even in a 3D organization.[93] The adsorption of small clusters of Ni_n, Pd_n and Pt_n, with $n \leq 4$ on fullerenes, have been also studied theoretically.[89] In the Pd and Pt cluster cases, when increasing the number of involved atoms, the formation energy also increases, meaning that larger clusters are more favorable energetically. The same conclusion has been drawn for larger C_{60}-supported Pt_n clusters, with adsorption energy of the different clusters ranging from 34.6 to 71.5 kcal.mol^{-1}.[88] Fullerenes can be either functionalized[68,94,95] or can be also used to anchor organometallic complexes, to provide new homogenous type of catalysts; see ref. [68,96] for a review, which is out the scope of the present review.

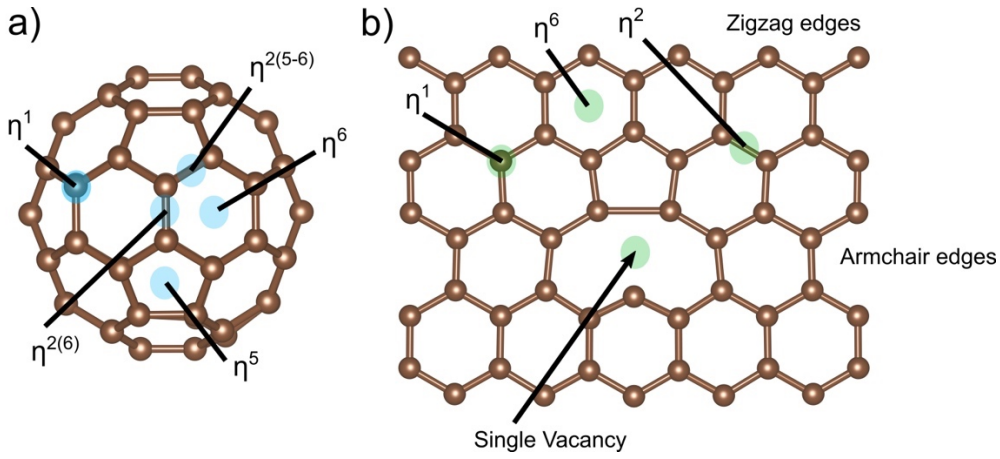

Figure 3. Typical adsorption modes on: a) C_{60}, and b) graphene layer presenting also armchair and zigzag edges as well as single vacancy.

Even if theoretically, activated carbon or carbon black (CB) have been less studied, due to the large size of these systems, we can mention the work of Dutta *et al*. They have systematically investigated by DFT calculations performed on a curved polyaromatic hydrogenated (PAH) molecule, used as a model of activated carbon surface, the mechanism of dihydrogen molecule dissociation to form metal hydride on supported small rhodium clusters, catalyzed by bare and activated carbon.[97] Five- as well as six-member rings of the activated carbon act as the support for hydrogen-adsorbed rhodium clusters. When a rhodium cluster is linked with a five-member ring of activated carbon, it has the enhanced ability to activate H_2 molecule.

Activated carbon can be also functionalized by acid groups for instance, to anchor small Rh NP with good dispersion.[98] In ref. [99], the authors report on the use of phosphorus-doped activated carbon made of 50 nm nanospheres, as support to grow *via* chemical reduction ultra-small (1-3 nm) and ligand-free precious metal NPs. The valence states of surface phosphorus species are critical in tuning the affinity between the carbon support and metal precursors, which rationally controls the loading, size and uniformity of resultant materials. Five metals (Ru, Ag, Au, Rh, and Pd) were grown *in situ* to demonstrate the key role of surface phosphorus sites.

2.1.2 Nanotubes

Theoretically, the interaction of single TM atom or small clusters with CNT has been studied since 15 years. Because the electronisc structure of CNT is crucially dependent of their diameter and helicity, it is expected that adsorption of metal is affected by these two properties.[100,101] Many publications dealing with the anchorage of TM single atom on pristine or functionalized nanotube sidewalls in the single context of hydrogen storage have been published, supported by strong orbital analyses.[102-105] It has been shown that the curvature of the surface has an impact on the surface diffusion of metallic adatoms[106-108] as well as on the type of binding sites for the metal.[109,110] Most of the results clearly indicated that defects, such as Stone-Wales (SW) defects or vacancies, which may be present either inherently or induced during purification process, play a crucial role in the adsorption or surface diffusion of TM atoms on CNT. Vacancies (Figure 3b) usually reinforce the bonding between TM atoms and the neighboring C atoms, since a factor of 2 in the adsorption energy values is found.[111] Clearly, the presence of σ-bonding of metal to carbon atoms around the defect edge provide stabilization. It has also been shown that the *3d* TM atoms acting as substitutional defects can substantially modify the electronic structure of CNT. Due to bonding character differences with C atoms, adsorption energies can vary considerably from one *3d* TM atom to the other.[111] Endohedral coordination, which is much less favorable thermodynamically is generally not favored.[112] This is the case for Fe in interaction with a (6,6) single-walled CNT.[113] However in some specific cases, the interactions and reactions of some specific TM clusters (Os, Re, W) with the interior of single-walled CNT have been modeled.[114]

A major challenge for NP catalysis is the synthesis and stabilization of small (< 2 nm) NP. Owing to their high reactivity and mobility, sub-2 nm metal NP easily merge to form larger ones, and thus many of the valuable physical properties are lost, especially their catalytic

activity can be suppressed. In this respect, single-walled CNTs appear to be an interesting support since curvature effects may reduce NP sintering even without any chemical treatment of the CNT sidewalls, see Figure 4a.

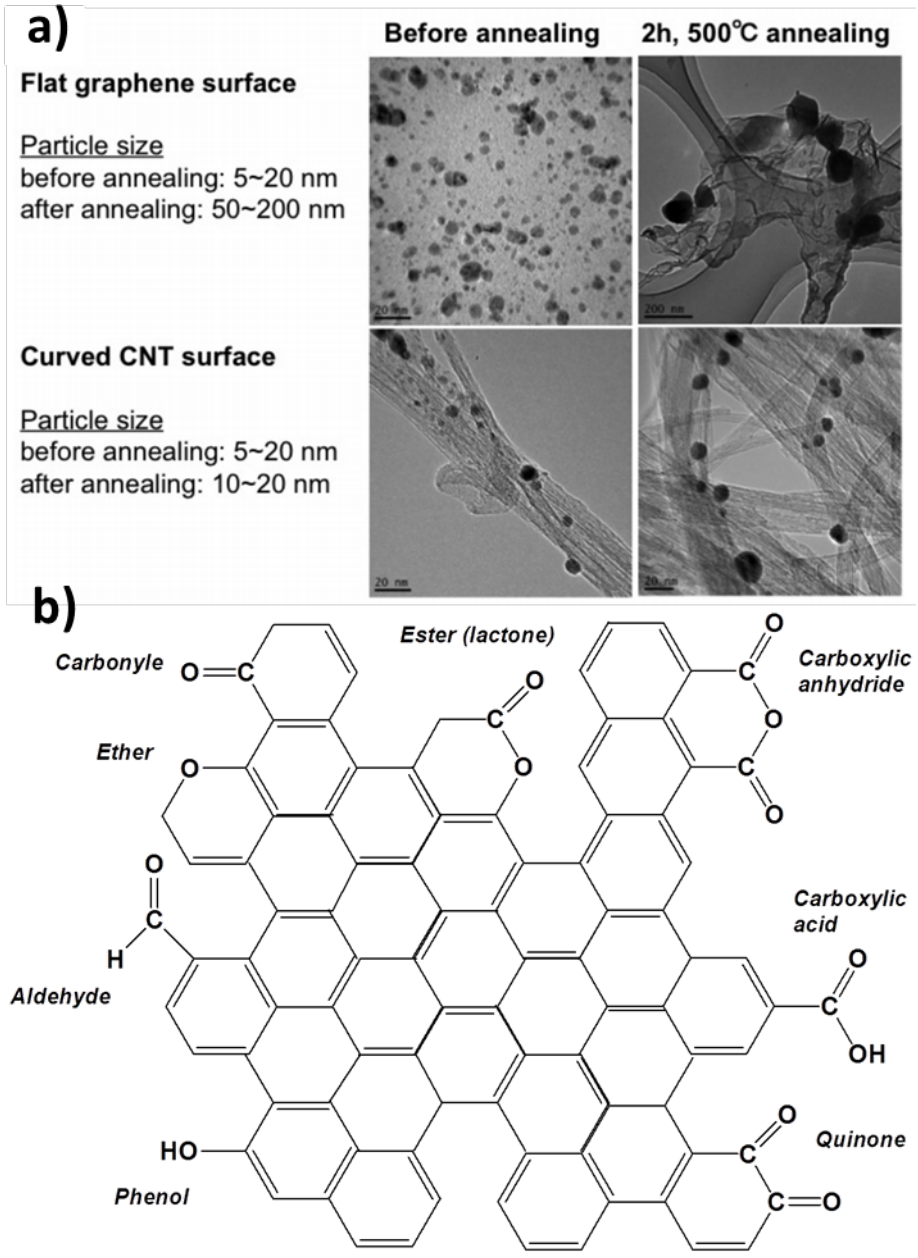

Figure 4. a) TEM images of Pd nanoparticles on graphene surface and on 1-2 nm diameter CNT surfaces. Images were taken after the loading and after sequential annealing for 2 h at 773 K. Reprinted with permission from Staykov, A.; *et al. J. Phys. Chem. C* **2014**, *118*, 8907-

8916.[115] Copyright 2014 from the American Chemical Society; and b) schematic representation of major possible oxygen functional groups present on carbon-based nanomaterials for further NP anchoring.

In the case of Pd or Au clusters, DFT calculations combined with experiments have proven the superiority of CNT over graphene supports to reduce significantly the sintering of small NP, after annealing, especially with small diameter CNT (Figure 4a).[115] Interestingly, important effects of metallic NP morphology on their dispersity and thus on their catalytic stability have been addressed in the case of small icosahedra Pt NP deposited on commercial single-walled CNT. When comparing small Pt nanocubes with icosahedra, the latter are highly mono-dispersed on CNT support due to their unique geometry, showing in return better electrocatalytic activity and stability.[116] One can suspect that this strong anchorage of Pt icosahedra is the result of combined effects due to the curvature and the presence of inherent defects on the carbon support with highly reactive facets of icosahedra Pt. Obtaining atomic dispersion, with very low metal loading, as in ref. [117], increases the portion of the surface active-atom sites and therefore, notably lowers the Pt loading needed for attaining a high Hydrogen Evolution Reaction (HER) catalytic activity.

Chemical treatments such as surface functionalization are also efficient to reinforce the interaction between the CNT and the metallic NP.[118,119] Those treatments often involved surface oxidation, with the formation of various functional groups (Figure 4b) such as ketones, phenols, lactones, carboxyls, ethers and acid anhydrides[120,121] from gas-phase reactions or nitric acid treatment.[122] In 2011, Chiang *et al* have stressed the importance of the oxidation treatment of CNT, which introduced primarily -OH and -COOH groups on CNT sidewalls, as revealed by XPS. This treatment enhanced the reduction of Pt ionic species, resulting in smaller Pt particles

with improved dispersion. Pt NP supported on oxidized CNT usually display superior durability than those on pristine CNT or commercially available Pt/C.[123]

Halogenation either during the CNT synthesis step[124] or *via* direct contact with chlorine, bromine or iodine vapor[125] can be used to better trap NP. Besides, sulfonation reaction is an alternative route to anchor metallic NP, either through the formation of -SO_3H group on the CNT surface,[126] or *via* non-covalent functionalization with the aim of forming oxidized groups[127] to anchor Pd[128] or Pt NP.[129] Hetero-atoms doping is also possible, for instance as in sulfur-doped CNT, which are highly-efficient Pt catalyst support toward methanol oxidation reaction,[130] or nitrogen-doped carbon supports[131] that enhance the dispersion and the stability of Pt NP,[132] since strong metal-nitrogen bonds enhanced the metal-support interactions thus limiting the coalescence of neighboring NP.[133]

2.1.3 Graphene and few layer graphene

Due to its high electronic conductivity and excellent mechanical properties, graphene meets the requirements of an ideal electrocatalyst support. For a review with a particular focus on the microscopic thermodynamic and kinetic mechanisms, concerning the fabrication of graphene-metal NP composites using vapor-phase depositions of metals on/in graphene-based materials, see ref. [134]. Numerous DFT studies of *3d*, *4d*, and *5d* TM atom adsorption on a pristine graphene surface, have been reported, few of them have even compiled complete series of adsorption energies.[135-138] Figure 3b recalls the most favorable adsorption sites on graphene. Generally, TM atoms stand in hollow (η^6) sites when they are chemisorbed (with typical $E_{ads} \geq 23$ kcal.mol^{-1}) with a strong hybridization between the TM *d* orbitals and the π orbital of the graphene layer, inducing spin state change.[139,140] Bridge (η^2) or top (η^1) sites are more eager to be occupied since the interaction involved only weak van der Waals forces. This physisorption process

occurs mainly for half-filled and completely filled *d* orbital atoms, and energy differences between different hapticity configurations are rather small. Among Few Layer Graphene (FLG), the adsorption on pristine Bilayer Graphene (BLG) has been theoretically studied,[141] and on model of graphite as well.[142] An increase of the binding energy is generally obtained, when more graphene layers are stacked.[143] Edges sites reactivity of graphene and FLG towards Au, Cr, and Al atom adsorption has been investigated,[143,144] and all edge sites were found to be good traps for all TM atoms with large binding energies, due to the presence of dangling bonds. More than 60 kcal.mol^{-1} for adsorption site on armchair edges and even 120 kcal.mol^{-1} for zigzag ones have been reported.[145] A study combining HRTEM and XPS experiments have allowed to elucidate the bonding of single Pt atoms at graphene step-edges, after plasma sputtering, revealing a large binding energy shift of the Pt *4f* state. Thanks to DFT, it was shown that the Pt $5d_{xy}$-orbital in the step edge plays a crucial role in the formation of chemical bonds to C atoms and in the considerable charge transfer from Pt to C atoms, resulting in the large binding energy shift of the Pt *4f* state.[146] However, due to experimental setup (chemical vapor deposition), the probability is high that most of those edge sites are passivated by hydrogen. In the case of a Fe atom adsorbed on a H-terminated site, the binding energy drops off, but remains still larger by 10 kcal.mol^{-1} than the adsorption on pristine graphene.[147]

Intrinsic, essentially vacancies, line of defects or grain boundaries as well as extrinsic, such as impurities defects are also good candidates for a strong anchoring of TM atoms, due to their high reactivity.[148,149] The presence of such defects thanks to the versatile nature of carbon atoms embedded in the graphene layer allows easy reconstruction by forming non-hexagonal rings. The numerous energetic aspects of changes in graphene atomic structures have been detailed recently,[150] we only present here important results considering further TM adsorption.

The simplest defect in any graphene-based materials, observed by TEM[151,152] or STM,[153] despite its high formation energy around 170 kcal.mol^{-1},[154,155] and thus the most studied one so

far,[23,61,154,156,157] is obviously the single vacancy (SV). See Figure 3b for the corresponding atomic structure induced by the formation of a five aromatic ring,[158] leaving one highly reactive dangling bond on the opposite C atom. Moreover, molecular orbital analysis have shown a small energy separation between the singlet and triplet state, pointing the carbene character of those mobile point defects.[121] Thus, such sites are usually involved in the anchoring of small metallic and well-dispersed NP in oxygen-free FLG samples.[159]

The migration barrier of such defect has been estimated to be around 30 kcal.mol^{-1} for graphene and small diameter single-walled CNTs,[154,155] meaning that slightly above room temperature these defects start to move. With the coalescence of two SVs, and possible rotation of C-C bonds,[64] a divacancy (DV) presenting a 5-8-5 structure (Figure 5a) is created with an energy gain per missing C atoms of 80 kcal.mol^{-1}, . Upon a rotation of one of the C-C bonds in the octagon, the so called 555-777 DV (Figure 5a) is obtained, yielding a more stable structure by around 20 kcal.mol^{-1},[160] but with a large activation energy barrier ~115 kcal.mol^{-1}.[161] DV defects appear to be immobile due to their high energy migration barriers,[154] justifying the use of 5-8-5 DV as model in several studies.

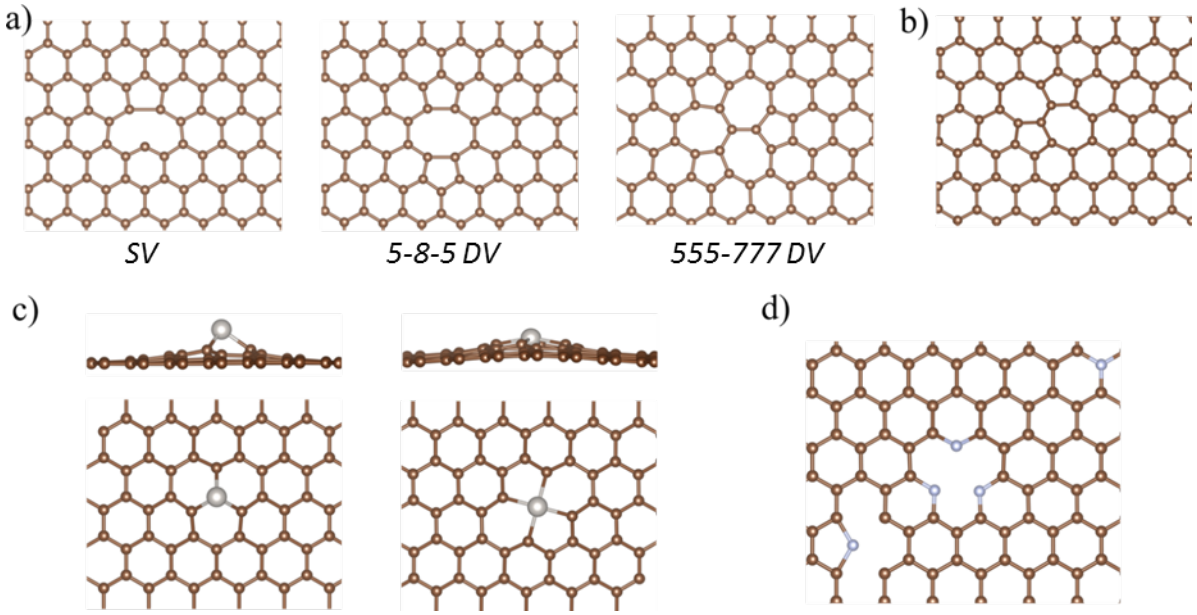

Figure 5. a) Examples of single vacancy, 5-8-5 *vs.* 555-777 divacancy atomic structures, b) Stone Wales (5775) defect, c) adsorption of Pt atom in SV and 5-8-5 DV, and d) various nitrogen doping configurations: graphitic, pyridinic and pyrrolic.

DFT studies of TM adatoms adsorbed on graphene sheet with carbon vacancies have all stressed that the strain fields around these rather localized defects spread far away from the adsorption site.[162,163] Moreover, it has been reported that metal atoms usually bind more strongly to vacancies than to pristine carbon-support, forming covalent bonds.[164-167] Those extensive studies have shown that the binding energies for a TM atom in SV defect are in typical range of 45-190 kcal.mol^{-1}. Similar values were obtained for DVs.[164] Thus, the presence of vacancies should prevent metal clustering on the carbon-support surface.[167] Interestingly, such defect passivation by Fe atoms have been observed experimentally by aberration-corrected TEM by Robertson *et al.*[168] The typical atomic configurations of TM SV/DV complexes are shown in Figure 5c.[164]. Those localized defects induce strain extending for at least 2 nm away from the defect, as it can be seen in Figure 6. TM atoms are thus attracted by the reconstructed defects. The increased reactivity of the strained graphene makes it possible to attach metal atoms much more firmly than to pristine graphene and supplies a tool for tailoring the electronic structure of graphene.

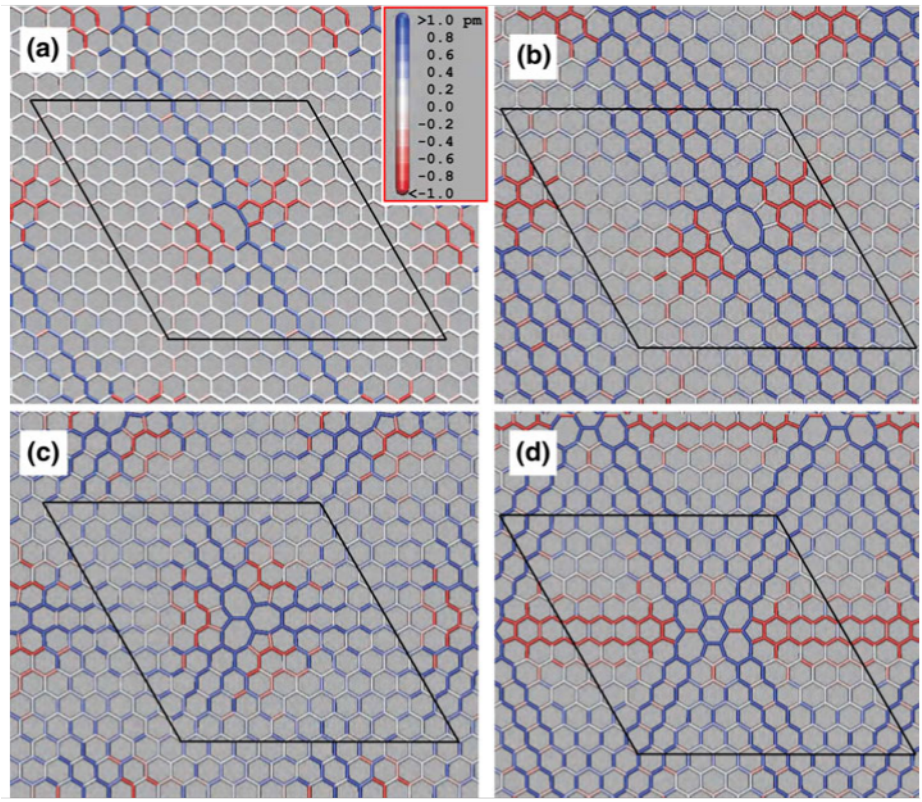

Figure 6. Strain fields in: a) SV, b) DV (5-8-5 defect), c) reconstructed DV (555-777 defect), and d) 5555-6-7777 defect. The bonds are colored according to an increase (blue) or decrease (red) in the bond length (given in picometers). The bonds close to pentagons are contracted, but most C–C bonds are stretched. Reprinted with permission from ref [169]. Copyright 2011 from Springer Nature.

Since TM atomic radii are larger than the carbon one, the TM atom tends to be displaced outward from the graphene plane, more strongly for SV than for DV, inducing a long range buckling of the graphene support.[164] For small clusters such as Pd_4, it has been shown that the larger is the vacancy, the stronger is the adsorption, due to more Pd-C bond formations.[170] The interaction of single Pt atom and very small clusters (up to Pt_4) with two stacked graphene ML decorated by various vacancies, to model irradiated Highly Oriented Pyrolytic Graphite (HOPG) was investigated thanks to DFT calculations.[171] For Pt clusters supported on HOPG

with vacancy aggregations, this study shows that a strong driving force for nucleation and a much enhanced tendency for particle ripening is present.

SW defects[172] have been also proposed as efficient point defects for further atomic adsorption since they do not involve any removed or added atoms. It implies a single 90°-rotation of a single C-C bond, which transforms 4 hexagons into 2 pentagons and 2 heptagons (5775-defect), as depicted in Figure 5b.[173] Despite their rather large formation energy, *i.e.* 70-115 kcal.mol^{-1} depending on model's curvature,[173-176] they have been observed experimentally.[177-179] Due to the presence of more reactive bonds, TM atoms bind more strongly to SW defects than pristine graphene layer, *i.e*. by almost 10 kcal.mol^{-1} for a single Co atom.[180] Due to curvature effect in nanotubes, SW defects are even better sites for metal anchoring.[181,182] In the case of Ti, Pd, Pt or Au small metallic clusters, SW defects tend to bind more strongly than pristine support.[183]

Another type of point defects usually used as anchoring site are substitutional foreign atoms,[184] mainly nitrogen, see ref. 67 for a review of synthesis and characterization of N-doped graphene (N-G), boron (B-G)[185] and in a lesser extend others elements like S or P.[186] Embedding a single hetero-atom, as B, in the graphene layer usually induced important out-of-plane distortions, as well as introducing a hole, acting thus as a p-dopant.[187] As a consequence, the incorporation of boron into graphene substantially enhances the adsorption strength for small metallic clusters. For Pt_4 the gain is already larger than 25 kcal.mol^{-1}.[188]

Nitrogen doping can be achieved by several methods,[189] and has been particularly studied in several contexts such as for supercapacitor applications,[190] and electrocatalysts for ORR,[191] in PEMFC.[192] As schematically illustrated in Figure 5d, three common bonding configurations of N atoms in graphene have been evidenced,[193] including pyrrolic, pyridinic, and substitutional (also denoted quaternary or graphitic) N. Experimentally, the atomic structure, electronic structure, and dynamic behavior of those defects have been systematically studied at the atomic

level by using a scanning transmission electron microscope.[194] Comparisons between XPS measurements and DFT calculations have proven its utility for site characterization.[195] Such N atoms can change the local density state around the Fermi level of N-doped graphitic carbons, which may play a vital role in tailoring the electronic and adsorption properties. Experimentally, the pyridinic-N exhibit higher chemical reactivity and thus appear to be better traps for single atoms; Mg, Al, Ca, Ti, Cr, Mn and Fe were successfully tested.[194] DFT results have clearly shown that the nitrogen incorporation into CNT or FLG could not only facilitate the immobilization, but also modifies the electronic structures of the TM atoms, which provides a promising approach for optimizing SAC.[196,197] The electron distribution in carbon atoms next to a nitrogen dopant is significantly disturbed, causing differences in the electron scattering and consequently contrast-differences in high resolution TEM images.[198,199] In the case of extensive N-doping, N_4-TM configurations can be produced, which have been proven to be highly active, like N_4-Co to build efficient counter electrode for dye-sensitized solar cells,[200] or N_4-Mn for ORR.[201] The structural stability of N-G with graphitic-N, pyridinic-N and pyrrolic-N, and TM atoms (from Sc to Ni) embedded into N-G have been investigated by DFT.[197] The TM atoms embedded in a N_4-DV, by substituting four C atoms in a DV site with N atoms, form a N_4-centered structure, which provides strong anchoring mode with binding energy larger than 160 kcal.mol^{-1}. By increasing the nitrogen concentration, graphitic carbon nitride (g-C_3N_4,) although not so in-depth characterized, can be formed,[202] as well as carbon nitride nanotubes.[203,204] C_3N_4 conjugated polymer can also be synthesized under specific conditions. We refer to ref. 47 for further information since metal/g-C_3N_4 nanohybrids have been reported. It has been recently proposed that the stabilization of single metal atoms on g-C_3N_4 is due to the presence of defects.[205] In the same work, DFT calculations of the adsorption, stabilization and diffusion of metals, established the stable location close to the six-fold interstices between tri-s-triazine units composing the g-C_3N_4. Even CNF can be N-doped, and it was shown that

for ORR efficiency trade-offs between nitrogen content, electrical conductivity and surface density of active sites must be reached.[206]

It was proposed that these g-C_3N_4 porous materials show, as graphene, a honeycomb-like structure but with six-membered carbon-nitrogen rings, that opens a gap in the electronic band structure, and presenting various type of cavities. The adsorption of *3d* TMs on those sites have been reported using DFT calculations.[207-210] The binding energies are usually strong, however in some cases, they remain smaller than the corresponding metal cohesive energies, still below the most favorable N_4 sites. For Pt clusters supported on HOPG with nitrogen defects, calculations have shown a greater driving force for nucleation and greater particle tethering, due to the disruption of the regular graphene bonding near the defect. For instance positively charged neighboring C atoms attract Pt more strongly.[171] Finally, edge doping of graphene nano-ribbons (GNRs) has also been reported by annealing graphene ribbons in ammonia,[211] presenting pyridinic-type N atoms. It appears that metal NP chemical reactivity are enhanced upon deposition, due to the creation of a Mott-Schottky heterojunction at the planar metal-semiconductor interface, inducing charge transfer.[212]

One dimensional defects have been observed in several experimental studies on graphene.[151,213-215] Generally, these line defects are tilt boundaries, with a tilt axis normal to the plane, which separate two graphene domains with different lattice orientations. These defect lines can be viewed as a line of reconstructed point defects presenting or not some dangling bonds.[64] In the case of FLG, the layers can interconnect either by direct atomic bonding, forming grain boundaries, or by overlapping, holding by van der Waals interactions.[216] Because of its low dimensionality and the rigid bonding structure of graphene, the structural variety along these lines is typically governed by the presence of 7-5 rings and 8-5 ring defects.[217] Grain boundaries in graphene have been studied extensively and are predicted to have specific electronic,[218-220] magnetic[221] and thus chemical properties.[222] Their activity allows for very

localized metal deposition.[223] The presence of such line defects induces a very localized strain, which provides better reactivity than pristine graphene.[224] This enhanced chemical reactivity at the grain boundary, makes graphene ML with engineered line defects a highly promising candidate for gas sensor applications,[225] or even for ORR.[226] It can also act like very localized anchoring sites, with stronger adsorption energies on the line defects for metal[163,227] or Li atoms,[228] and at the same lower diffusion barrier energy along the grain boundary. Besides, by increasing the concentration of the TM adatoms, nano-lines can be formed due to the strengthening of the energetic stability of the TM/grain boundary systems.[229]

Graphene oxide (GO) is a complex nonstoichiometric material possessing a layered structure, with physico-chemical properties, which are highly dependent on synthesis procedures and post-synthesis treatments.[230-232] The various strategies and application of metal NP deposition on GO have been reported elsewhere.[233,234] The efficiency of GO support for HER has been proven, since this support can be used simultaneously as an electron acceptor that allows electron transport, as co-catalyst, photocatalyst or photo-sensitizer.[235] Due to the use of strong oxidants under acidic conditions during GO synthesis, the graphene surface and edges are fully functionalized by a wide range of groups such as alcohols, epoxide and carboxylic, making: i) the O/C ratio the critical parameter that defines the atomic structure, usually extracted from XPS experiments,[236,237] and ii) GO modeling a challenging task.[238] In the literature, several different structural models exist for GO. All of them present epoxy[239] (mainly oxygen in bridge) or hydroxyl (-OH) groups adsorbed on graphene basal plane,[238,240,241] less with -COOH groups, despite their fundamental roles in reactivity.[242,243] Then, the component, the structure, and O/C ratio depend much on the different chemical oxidation processes.[244,245] Most of the possible applications of GO as support imply its reduction, to restore partially graphene's structure and physico-chemical properties. Depending on the reduction process, various properties of the reduced GO (rGO) can be obtained and thus different performances

achieved.[246] It has been suggested that by removing -OH and -COOH groups, the sp^2 character of the carbon atoms is restored.[247] Only few theoretical studies have addressed the adsorption of metals (or other elements) on GO or rGO.[244,248-250] As expected, those theoretical works have pointed stronger binding energies when GO is used as support when compared to pristine graphene. In the case of a single iron atom, the most favorable anchoring mode gives an adsorption energy of -160 kcal.mol^{-1}, quite similar to defective graphene values, when on a pristine graphene it is only ~ 20 kcal.mol^{-1}. Combined with a high migration barrier of 75 kcal.mol^{-1}, GO should ensure strong metal stability and avoid metal clustering. The presence of oxygen atoms allows for the anchoring of a single Pt as well as small Pt_{13} clusters, with a strong enhancement (~7 times) of the adsorption energies compared to the undoped situation,[251] when it is even unfavorable thermodynamically on pristine graphene.[252] The introduction of epoxy and hydroxyl groups on a graphene layer modifies its chemical properties, due to the deformation of the basal plane, which depends on the type and the concentration of these functional groups. It can even results in the formation of surface dangling bonds, which can greatly stabilize Pt single atom adsorption.[253] Experimentally, Raman and XANES analyses have allowed to identify TM-C and TM-O-C bond formation in the case of Pd/graphene catalysts.[254]

Considering the interaction of graphene ML, FLG and GO with metallic atoms, clusters and NP, very similar strategies, as exposed in the previous section devoted to CNT, have been developed: the use of surface functionalization and/or heteroatom doping in the presence of intrinsic defects. Several reviews on that topic are available in the literature.[205,255-259] Energy-related applications have benefited from these major progresses. In the context of fuel cells, doped graphene-supported nano-electrocatalysts have been widely considered. See ref. [260] for a comprehensive review on synthesis, physico-chemical characterization and applications in this particular topic, especially for Pt and Pd catalysts. For instance, stabilized Pt atoms and

clusters were obtained when numerous N-dopant types were incorporated in the graphene support, followed by an atomic layer deposition procedure.[261] Applications of mixing those chemical approaches in ORR and HER contexts have been reviewed too.[262-264] A further functionalization of rGO to covalently graft *p*-phenyl SO_3H- or *p*-phenyl NH_2- groups facilitates the homogeneous surface distribution of Pt NP and reduces the NP size since the strong interaction between the Pt atoms and the functionalized groups avoids the migration/coalescence of the NP, during durability tests.[265] In the context of ORR, it has been demonstrated that even without metals, a specific structure made of nitrogen pair doped SW defect provides a very active site.[266] The effect of curvature was also addressed, and its beneficial outcome clearly proven.[267,268] In the same spirit, the combined presence of defects, oxygenated groups (-OH mainly) and nitrogen groups (-N and -NH_2) on rGO insures the formation of ultrafine and well-dispersed NiPd NP with high activity for dehydrogenation reaction.[269] XPS results have shown that using N-doped rGO support for Pt NP deposition leads to formation of Pt-N chemical bonds, with an electronic transfer from Pt to the carbon support. It has also been demonstrated that *ca.* 25% of the total amount of N atoms were bound to Pt ones.[270] Sulfur-doped graphene, for which S is located either on edges or in the vicinity of a SW defect are very favorable configurations,[271] and are also ideal candidate for metal deposition. Finally, line defects can be further stabilized by N-doping, due to the occupation of frontier orbitals, thus enhancing the ultimate tensile strength,[272] but the effect on TM deposition is still lacking.

2.1.4 Graphite (intercalation) + mesoporous (edges, activated carbon, carbon nano fibers) and hybrid structures

A novel sandwich-structured graphene-Pt-graphene catalyst has been synthesized and well characterized by X-ray diffraction (XRD), XPS, scanning electron microscopy, HRTEM, and

electrochemical measurements.[273] All these experiments have shown that Pt NP are anchored between two adjacent graphene sheets, see Figure7a for schematic representation, substantially enhancing the metal-support interaction. Such configuration (G-Pt-G) allows preventing Pt to leach into the electrolyte in fuel cells, increasing catalyst overall stability. Moreover, electrochemical measurements have shown that this nano-hybrid has higher activity for methanol electro-oxidation than Pt/graphene catalyst.

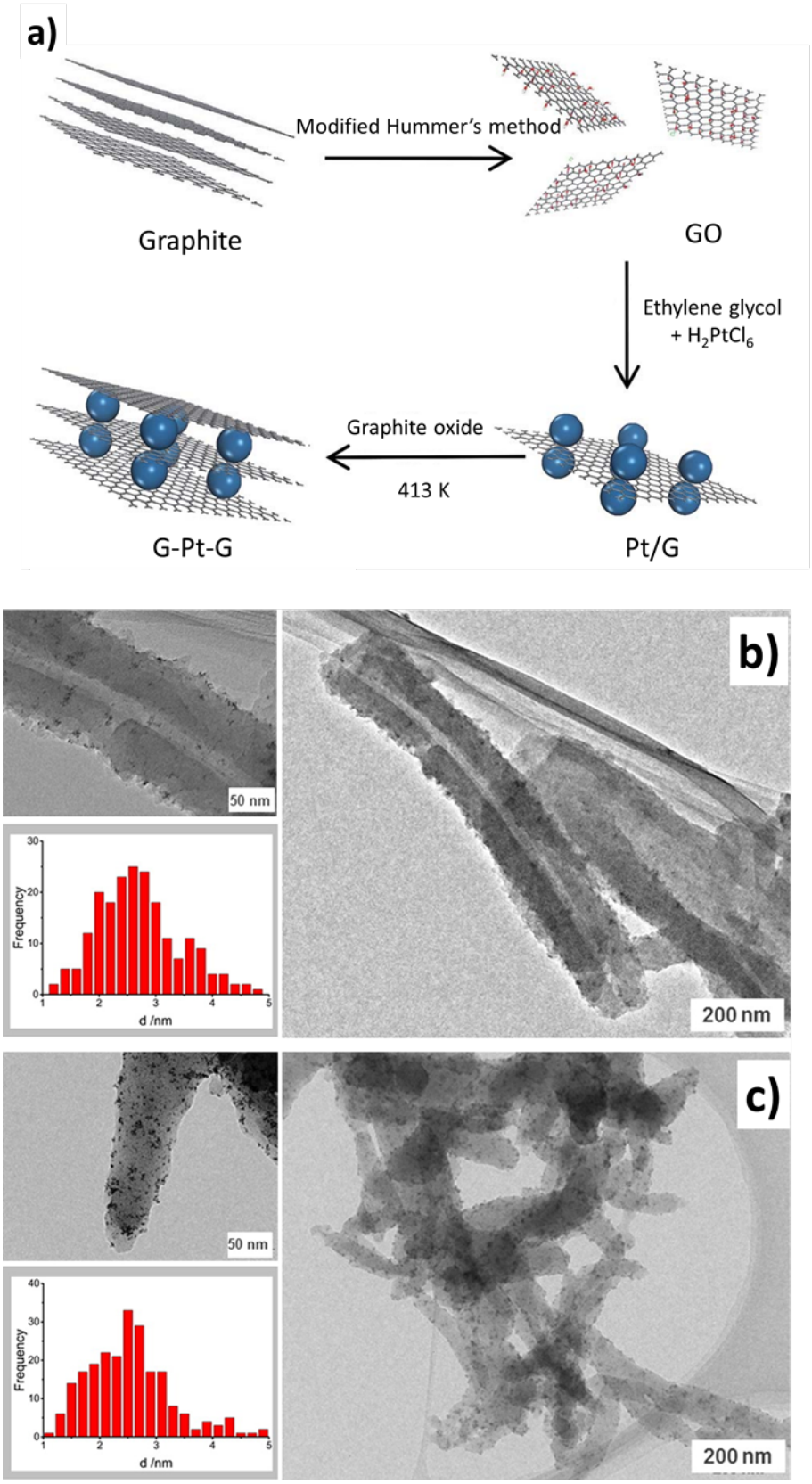

Figure 7. a) Schematic illustration of the preparation of the sandwich-structured graphene-Pt-graphene hybrid catalyst. Adapted with permission from ref [273] Copyright 2015 from the Royal

Society of Chemistry.; b) and c) TEM images and histograms of the Pt NP size distribution of Pt/polyalanine nanofiber precursors carbonized at 1023 K b) and Pt/polyalanine nanofiber precursors carbonized at 1273 K c). Reprinted with permission from Melke, J.; *et al*. *ACS Appl. Mater. Interfaces* **2016**, *8*, 82-90.[274] Copyright 2016 from the American Chemical Society.

Carbon nanofibers

Concerning CNF, aberration-corrected TEM observations showed that the degree of the surface graphitization strongly influences the structures of supported gold NP. With CNF presenting more ordered graphitic layers, Au NP prefer to bind to the CNF by their (111) plane, exhibiting more facet area. For disordered CNF surfaces, random orientation of supported NP is obtained. The different shape of similarly sized Au NP allowed determining the effect of support surface structures on the selectivity of the catalyst in the liquid-phase oxidation of glycerol.[275]

The preparation of Pt NP supported on N-doped CNF from a polyaniline nanofiber precursor (Figure 7b) has been investigated for ORR. Initially, Pt NP are deposited on polyaniline nanofiber precursor. By NEXAFS, it has been shown that electrons from the Pt are being transferred toward the π-conjugated systems of polyaniline nanofiber precursors. Due to this strong interaction, a high dispersion of Pt NP on the nanofiber is obtained. After carbonization of polyalanine nanofiber precursors at different temperatures, structurally different N-CNF are obtained. There are strong evidence of interaction between N-groups and Pt NP in all investigated N-CNF, despite the differences in composition of N-species and Pt NP dispersion. Interestingly, the presence of pyridinic sites favors a small mean Pt NP size with a narrow size distribution, when graphitic and pyrrolic N-groups induce an increase in the average Pt NP size with a broad size distribution.[274] In a similar manner N-functionalized carbon by pyridine N,

amine and amide groups modulate the size of Ir NP compared to pure carbon support. In XPS, a shift in Ir^0 $4f_{7/2}$ is experienced, confirming electronic interaction between Ir NP and N-doped carbon substrates.[276]

Complex hybrid materials

Hollow graphitized nanofibers are unique carbon nanomaterial possessing a topologically complex nanoscale structure comprising a series of stacked cups encased within concentric tubes.[277] The conjunction of typical internal diameters between 50 and 70 nm, and nanofiber tips opening allows efficient transport of molecules through the internal structure. Moreover, anchoring sites for TM NP are also present due to the distinctive internal herringbone structure resulting in a succession of 3-4 nm high steps formed by rolled-up sheets of graphene.[278] Depending on the Pd NP synthesis conditions, small Pd NP (1.1 nm) can be obtained and mainly located at the internal graphitic step-edges.[279]

Deposition of *fcc*-Pd NP on multi-scale hierarchical carbon supports that have exceptionally high surface area per volume, has been investigated. The proposed supports consist of porous carbon foam whose surface has been either chemically functionalized, or morphologically altered by grafting of carbon-nanotubes.[280] Even without further surface CNT etching, Pd NP were anchored on CNT sidewalls, presumably due to the very high density of the CNT forest grown by CVD, which insures sufficient surface active defects and confines sufficiently Pd precursor during NP formation.

A hierarchical N-doped carbon nanotube-graphene hybrid nanostructure, in which the graphene layers are distributed inside the CNT inner cavities, was designed to efficiently support well dispersed noble metal PtRu NP with 2-4 nm diameters, even inside the N-doped

CNT.[281] Again the presence of nitrogen allows to firmly anchor the PtRu NP, resulting in a better stability and enhanced activity for methanol oxidation.

A comparison between electro-deposited of Pd NP on carbon black (Vulcan Carbon XC-72) and functionalized GNRs has shown that in the context of ORR toward hydrogen peroxide formation,[282] the changes in selectivity and activity between GNR and Vulcan are explained by: i) the higher dispersion of Pd on GNR due to the presence of oxygen- and nitrogen-containing anchoring sites, and ii) the different porosity (determinant for the diffusivity and residence time of peroxide on the catalysts) and mass transport within layers, also related to different layer thicknesses or loadings. In the same spirit, by using inelastic neutron scattering (INS) that is able to probe surface hydrogen nature on the NP as well as on the support,[283,284] it was shown that depending of the support nature more isolated/clustering C-H groups could be observed on Ru catalysts, influencing the further activity of deposited Ru NP.[285]

Several TM-N-C catalysts were synthesized by pyrolysis of organometallic complexes and nicarbazin.[286] Their characterization has shown atomic dispersion of the TMs, with explicit TM-N bonds; where pyridinic and graphitic sites were used as anchoring sites for single Cu or Co cations for instance. These observations were obtained by using electron energy loss spectroscopy (EELS) in combination with AC-TEM, as extracted from data given in Figure 8.[287] In the case of Fe NP incorporated into a N-doped carbon matrix, XPS analyses have clearly demonstrated the formation of Fe-N_x bonds too.[288]

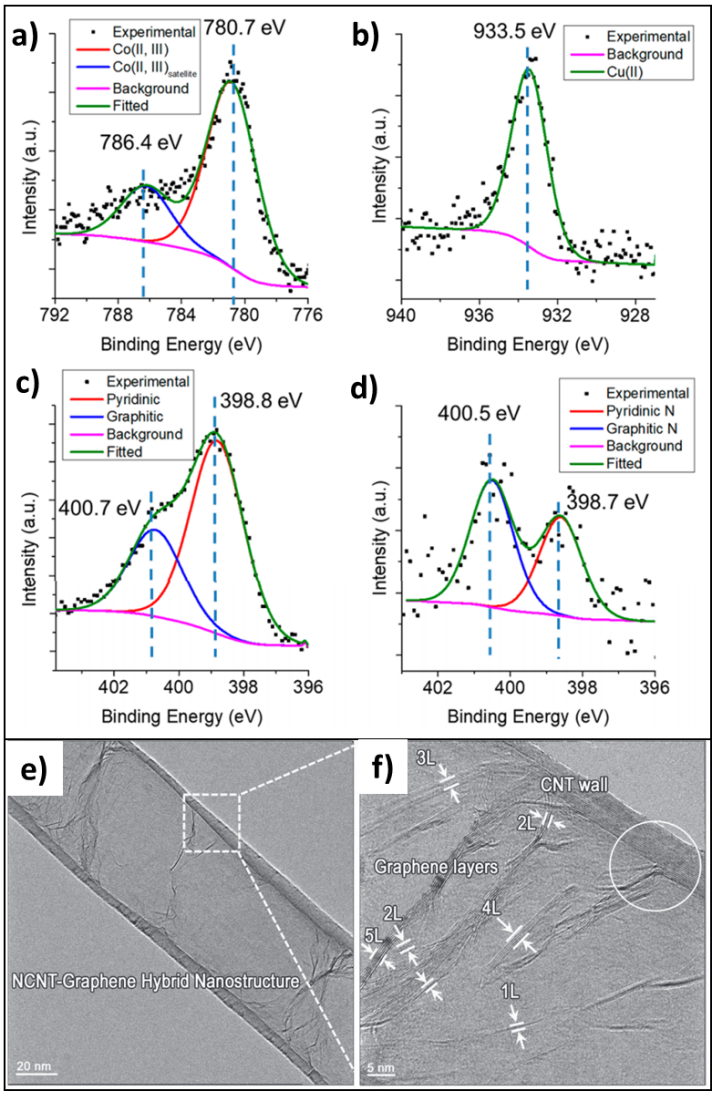

Figure 8. a) Co $2p_{3/2}$ X-ray photoelectron spectrum of Co-N-C-HCl. b) Cu $2p_{3/2}$ X-ray photoelectron spectrum of Cu-N-C. c, d) N *1s* X-ray photoelectron spectra of (c) Co-N-C-HCl and (d) Cu-N-C. Reprinted with permission from Xie, J.; *et al. ACS Catal.* **2018**, *8*, 3875-3884.[287] Copyright 2018 from the American Chemical Society. e) and f) HRTEM image of N-doped CNT-graphene hybrid, which shows 1-5 graphene layers derived from the inner walls of CNT, as pointed out in the circle part. Reprinted with permission from ref [281]. Copyright 2011 from John Wiley and Sons.

Pt NP deposition on N-,S-doped or co-doped mesoporous carbons have been investigated experimentally and theoretically.[289] Dependency on the type of heteroatom doping of the size distribution has been clearly evidenced. DFT calculations have highlighted that both N and S atoms increase the interactions between Pt and carbon support, however if the co-dopants are too close to each other's the interaction with a single Pt atom tends to be less strong. Thiophenic groups appear to be very efficient anchoring sites, making Pt NP in Pt/S-mesoporous carbon more active for electrochemical applications, than N-doped or co-doped samples.

2.2 Atom, cluster, and nanoparticle anchoring

2.2.1 Atom anchoring

Single-atom catalysts have sparked new interests in catalysis because of their high catalytic activity, stability, selectivity, and 100 % atom utilization. See ref. [290] and ref. [291] for general reviews with specific interest on innovative syntheses and characterization techniques for SAC, with a focus on their electrochemical applications in the ORR/OER, HER, and hydrocarbon conversion reactions for fuel cells (electrooxidation of methanol, ethanol, and formic acid). Rivera-Cárcamo *et al* have recently reviewed SAC on carbon-based materials,[292] focusing on the preparation of SAC on carbon materials, the comprehensive understanding of the metal-support interactions in SAC thanks to experimental and theoretical works, and how to explain their catalytic performances. As mentioned before, defects or heteroatoms usually reinforce the bonding between the TM and the carbon support. We will discuss now in more details the structures, determined experimentally as well as theoretically, of those SAC on carbon support in the most significant examples depending on the TM nature. After the seminal theoretical work of Krasheninnikov *et al*,[164] on the description of TM atoms embedded in a graphene ML, several DFT studies came out to go deeper in the description of the geometric and electronic structures, and to rationalize magnetic and electronic properties of incorporated TM atom using simple model.[293] It is based on the hybridization between the *d* states of the metal atom and the

defect levels associated with the unreconstructed D_{3h} carbon vacancy, as detailed in Figure 9. Magnetic states can thus be obtained for V, Cr, Mn, Co, Fe, Cu, Ag and Au embedded atoms. Kattel *et al*,[294] have extended the study of the electronic structures of embedded TM in the case of N-doped SV as well as DV defects. They have shown that Co-N_3, Fe-N_3, and Fe-N_4 defects are predicted to show ferromagnetic states with large magnetic moments and stabilization energies, resulting in a better stability as expressed by favorable formation energies, and high TM binding energies. In ref. [295], N_4-DV defects have been considered for various TM from groups VII-IX. The reported results have stated that the adsorption behavior of TM is not intrinsic, since it can be severely altered by changes in the local geometry of the active site, the nearest neighbors' chemical nature, and the oxidation states. To be active for ORR or OER, spin states analyses suggest that the oxidation state of those elements in the active sites should be in general +2.

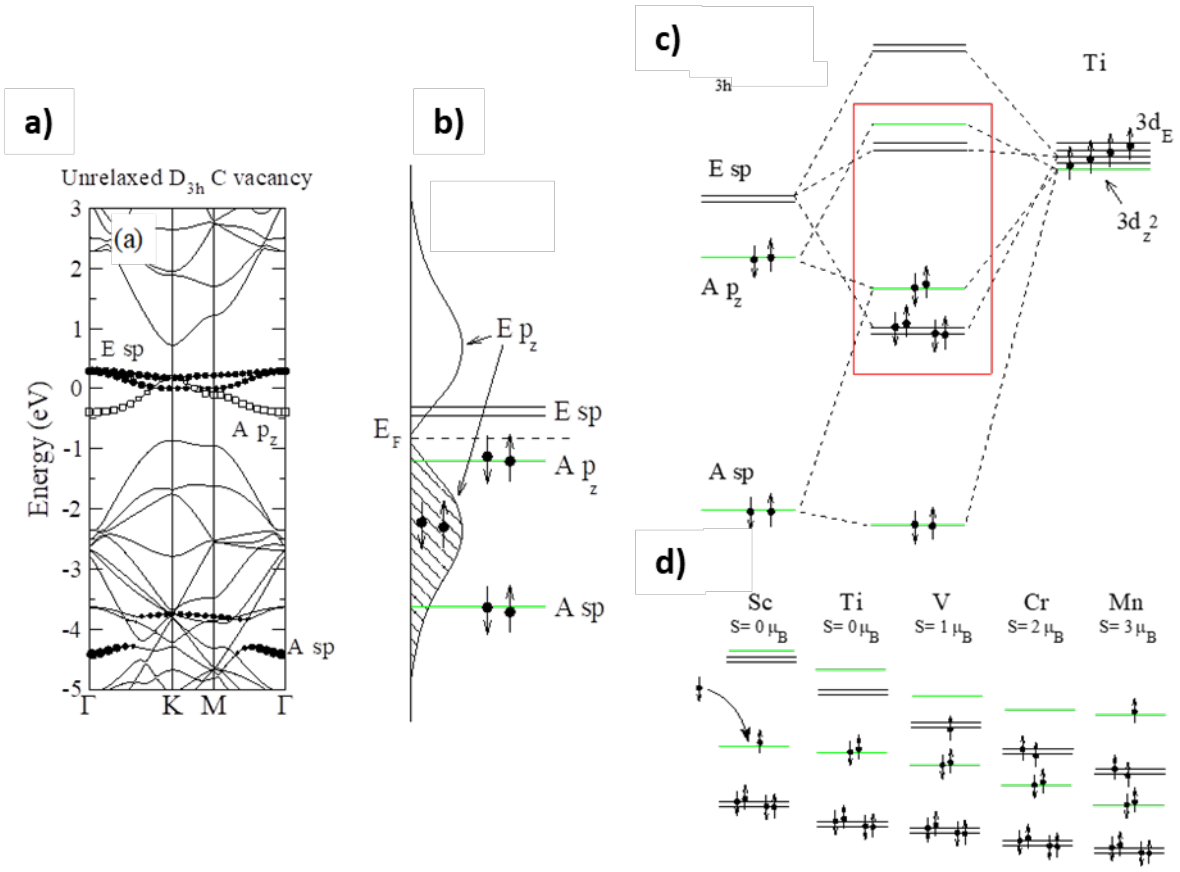

Figure 9. a) Spin-compensated calculation of the band structure of an unrelaxed carbon vacancy (D_{3h} symmetry) in a 4 × 4 supercell of graphene. The electronic structure near E_F (Fermi level) is dominated by a fully symmetric p_z level (A p_z) and two defect levels with E-symmetry and *sp* character (E *sp*). b) Approximate scheme of the electronic structure of the spin-compensated D_{3h} C vacancy indicating the character and symmetry of the different levels and their occupations. c) Schematics of the hybridization between the *3d* levels of Ti and the localized impurity levels of the D_{3h} C vacancy. d) Schematic representation of the evolution of the electronic structure near E_F for several substitutional transition metals in graphene. The spin moment (S) is also indicated. Reprinted from ref [293].

Comparisons of performance for Ag, Cu, Pd, Pt and Co SAC embedded in a SV for electrochemical reduction of CO_2 have been reported based on DFT investigations of reaction

pathways.[296] SAC show distinct differences in terms of their efficiency and selectivity in CO_2 reduction, which can be correlated with their elemental properties as a function of their group number in the periodic table. Double anchoring, in which two different TM metal layers such as a Fe-Ti couple, are absorbed on the two sides of an unique SV in a graphene, has been proposed as a promising system for hydrogen storage.[165] We recall that the energy levels of localized *d* states of TM are known to be crucial for the activation of adsorbed reactants and subsequent reactions.[297-299]

For hydrogen storage applications as for many hydrogenation reactions, the hydrogen activation is a key issue. By studying the interaction of functionalized graphene and (8,0) single-walled CNT with individual *3d* TM atoms, trends in molecular orbital analysis have been drawn.[102] Those results can be rationalized as follows: on one hand, H_2 can be dissociated by any metal site adsorbed on any surface to form a dihydride species, modifying the oxidation state of the metal in +2 units. On the other hand, the molecular adsorption mode of H is governed by back-donation, involving H_2 σ_g and σ_{g*} orbitals, bonding and antibonding orbitals respectively and $3d_{xy}$ orbitals. Occupation of MO produces a lengthening of the H−H bond, since the H−H overlap is antibonding. The amplitude of the lengthening is higher when the *d* atomic orbitals are more diffuse (on the left side of the *d* series, Sc, Ti, V). Thus, a dissociative coordination mode is favored for electropositive atom (Sc and Ti), when the stability of adsorbed molecular H_2 increases from left to right of *3d* series due to minor π back-donation, except for Cr and Mn. Similar results extended to *4d* and *5d* series have been reported.[136] Hereafter are presented some works dealing with the electronic structure investigations of single Pt, Pd, and few others TM atoms after embedding in a carbon support, for hydrogen storage, CO oxidation, electrochemical and hydrogenation reactions.

Platinum

It has been shown by first-principles-based calculations that the combination of highly reactive Pt atoms and SV over graphene makes the Pt-embedded graphene a superior mono-dispersed atomic catalyst for CO oxidation, since the strong interfacial interaction is able to tune the energy level of Pt *d*-states for the activation of O_2 (see Figure 10a). This promotes the formation and dissociation of the peroxide-like intermediate.[300] In this context, the presence of a pyridinic N-doped site close to the Pt atom enhances the CO oxidation efficiency and the resistance to poisoning, due to the combined presence of a new spin-down channel below the Fermi level, as well as a spin-up channel above the Fermi level.[301] It was also shown that the formation of Pt_1-C bond at the edges of graphene layers results in electronic strong metal-carbon interaction. As a result, the Pt atoms transfer electrons to the support to form $Pt^{\delta+}$ species, which are efficient for the 3-nitrostyrene hydrogenation.[302]

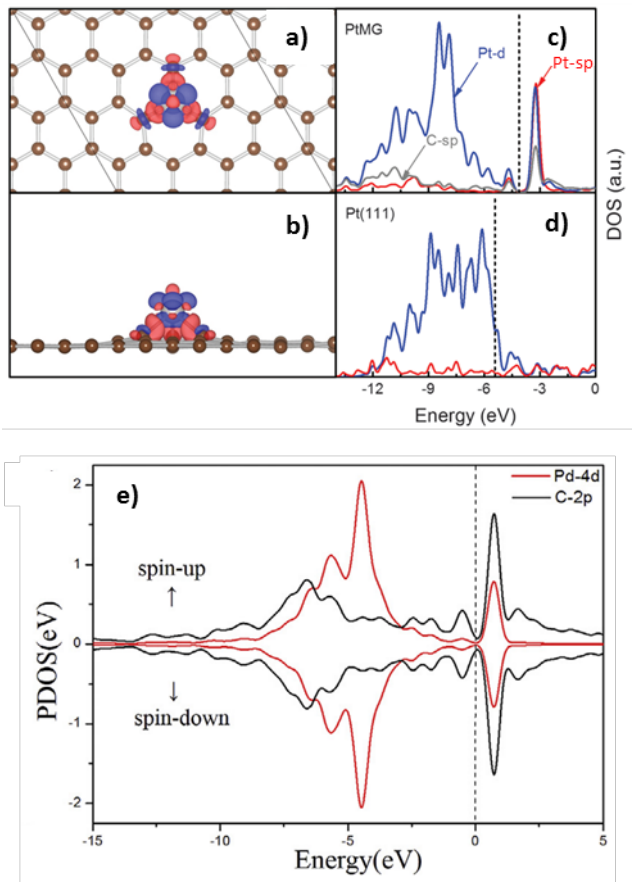

Figure 10. On the top panel, top view a); and side view b) of the contour plot of differential charge density of Pt-SV-G; density of states of Pt-SV-G c); and Pt(111) surface d). Reprinted with permission from ref [300]. Copyright 2014 from the Royal Society of Chemistry. On the bottom panel, e) spin-polarized DoS projected on Pd-*4d* orbitals (red curve) and the *2p* orbitals (black curve) of one of its neighboring carbon atoms. The Fermi level is set to zero. Reprinted with permission from ref [303]. Copyright 2017 from Elsevier.

By attempting to tune the electronic properties of single Pt atom catalysts absorbed on pristine graphene ML, thus adopting a η^2 coordination with the presence of various oxygenated groups, it was shown that the strengthening of the Pt-C interactions by the carbon support with different oxygen concentrations is more due to charge transfer than frontier-orbital hybridization. In general, the larger the concentration of oxygen containing groups is, and the closer they are to the Pt adatom, the stronger is the Pt binding energy to the carbon support. In the case of CO adsorption, by downshifting the *d*-band center of the Pt atom, due to the presence of epoxy groups, the coupling between the Pt *d*-band and the CO $2\pi^*$ state is reduced, thus decreasing the adsorption energy and at the same time the catalytic activity.[304] When comparing the adsorption states and diffusion behavior of a single Pt atom on pristine graphene and B-, N-, O-, Si-, P-, and S-doped graphene by means of DFT calculations with a thorough study of the corresponding Pt electronic structures, Hasegawa *et al,*[305] have: i) shown that localized orbitals, which can trap Pt atoms, are systematically created in the vicinity of dopants, and ii) explained the nature of the bonding and its strength. Figure 11 shows the detailed projected DoS depending on the dopants, and the position of the corresponding states available for further adsorption. O- and P-doping are particularly efficient to trap Pt atoms, preventing for desorption as well as limiting diffusion, with large (> 50 kcal.mol^{-1}) diffusion barrier compared to pristine graphene (3 kcal.mol^{-1}). The corresponding DoS has peaks associated to Pt $5dz^2$ and P sp^3

orbitals around -5 eV below the Fermi level (Figure 11i) due to their bonding characters (Figure 11l). The O-doped graphene presents dangling bonds, which allow Pt atoms bond covalently with C atoms as seen in Figure 11k).

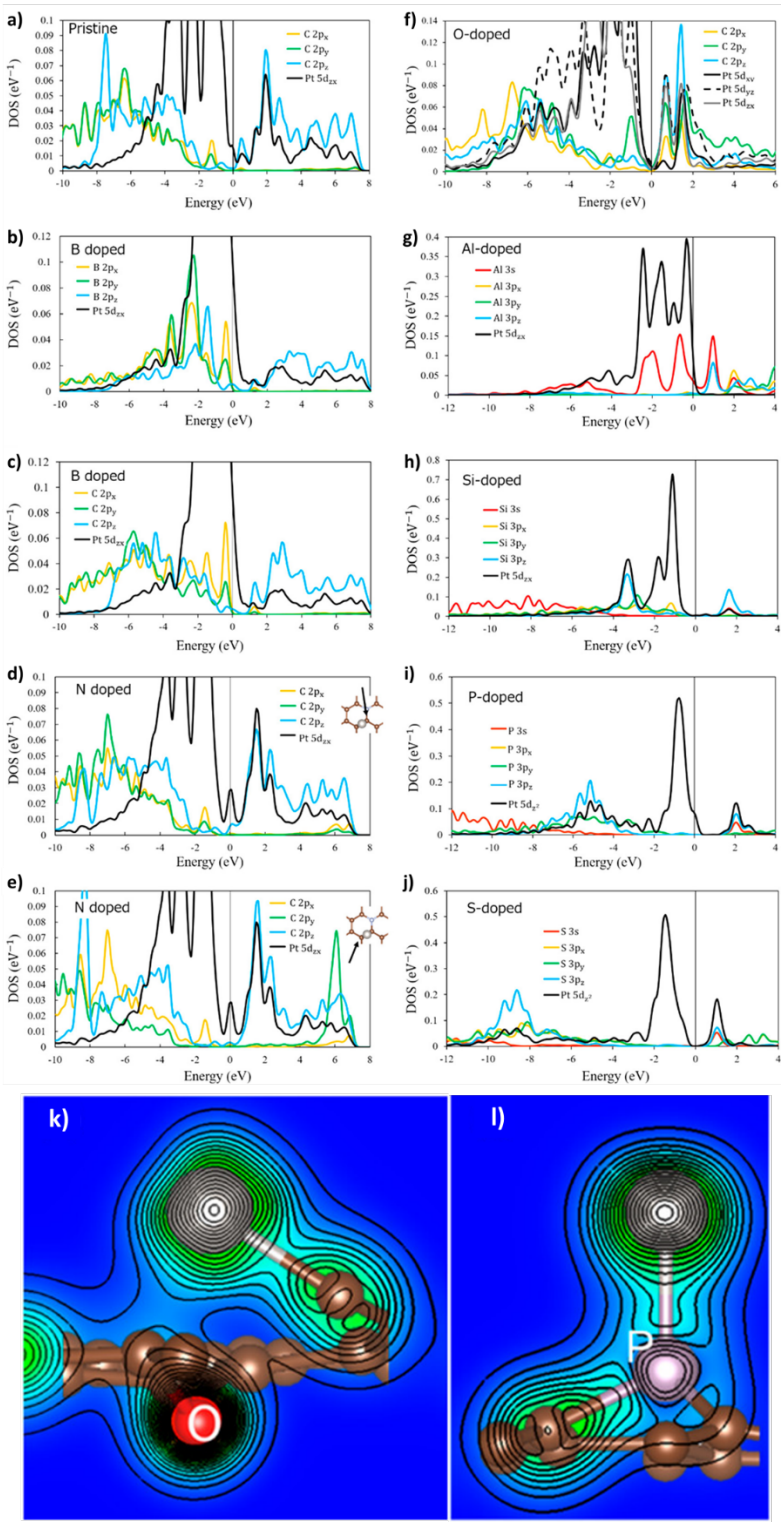

Figure 11. Projected density of states for Pt atoms adsorbed on: a) pristine graphene, b) and c) B -, d) and e) N-, f) O-, g) Al-, h) Si-, i) P-, j) S-doped graphene (the energy origin is set to the corresponding Fermi energy; and the arrows in d) and e) denote the C atoms, which are considered), and k) and l) electron density distribution in the vicinity of Pt atoms on O- and P-doped graphene, respectively. Reprinted with permission from Hasegawa, S.; *et al*. J. Phys. Chem. C **2017**, *121*, 17787-17795.[305] Copyright 2017 from the American Chemical Society.

Palladium

Recent EXAFS experiments have shown that Pd single atoms can be attached to CNF at low loading, i.e 0.2 wt%.[306] When embedded in a graphene ML, through its adsorption in a SV, the strong interaction between the Pd atom and neighboring C atoms can be confirmed by the presence of overlapping peaks in the DoS. Additionally, as it can be seen in Figure 10e, there are several Pd-*4d* and C-*2p* peaks emerging near the Fermi level, which implies the high activity of the Pd-graphene system. These states are available and ready to activate O_2 molecules, for a further CO oxidation.[303]

In ref.[307] the nature of the N-Pd interaction in N-doped CNT, with N-graphitic or pyridinic sites was investigated by XPS and NEXAFS of the N *1s* and Pd *3d* core excitations, supported by theoretical works. The interaction of those nitrogen species with a single Pd atom has been characterized and corresponds to: i) a σ-type donation from the filled π-orbital of the N atom to the empty *d*-orbital of the Pd atom, and ii) a π back-donation from the filled Pd *d*-orbital to the π* antibonding orbital of the N atom. On one hand, the interaction of Pd atom with pyridinic site is mainly covalent with a partial ionic character, consistent with the chemical shift observed in the Pd *3d* core level of divalent Pd. On the other hand, Pd on a graphitic site is covalently

bound without any charge redistribution. This electronic state of the Pd atom corresponds to metallic Pd NP electronically modified by the interaction with the support.

It has been reported that single Pd atoms anchored on exfoliated graphitic carbon nitride surpassed homogenous catalysts for Suzuki coupling.[308] This solid catalyst matches the high selectivity and broad functional group tolerance of state-of-the-art homogeneous catalysts for Suzuki couplings, and demonstrates a robust stability in flow. The adaptive coordination environment within the macro-heterocycles of exfoliated g-C_3N_4 has shown to be a facilitator for each catalytic step: the N sites in the support act as ligands in homogeneous systems that provide the electronic density required for the activation of phenylbromide. Additionally, the flexible lattice enables an almost continuous variable coordination pattern that adapts to the charge on palladium along the reaction coordinate, which gives rise to the high stability.

Decorated defective nanodiamond-graphene hybrids by single Pd atoms have shown remarkable performance for the selective hydrogenation of acetylene to ethylene, with high conversion (100%), ethylene selectivity (90%), and good stability. The Pd-C anchoring mode does not allow for unselective subsurface hydrogen species presence, and at the same time ensures the facile desorption of ethylene against the overhydrogenation to undesired ethane, which is the key for the outstanding selectivity of the catalyst.[309] Upon the adsorption of a single Pd atom on the sidewall of a single-walled CNT, the bonding character in PdH_2 has been described in details.[310] It turns out that the role of *s*, *p* and *d* orbitals on the bonding mechanism for all adsorbates and substrates have been addressed, and intermolecular donor-acceptor C-Pd and Pd-H delocalization after adsorption have been evidenced.

Others transition metals

Graphitic and pyridinic N-sites created after the pyrolysis of Metal Organic Frameworks (MOFs) followed by annealing treatment under N_2, have appeared to strongly anchor single Co atoms with very precise Co-N coordination; mainly Co-N_2 and Co-N_4 sites were evidenced by EXAFS experiments.[311] Those Co-N_2 SACs have been identified to be active sites for ORR thanks to DFT calculations. Indeed, Co-N_2 has stronger binding energies towards various ORR intermediates than Co-N_4 due to the availability of more *d*-states in the Fermi level's vicinity. Stronger O_2 binding energy allows Co-N_2 to more efficiently capture the O_2 molecules from the solution than Co-N_4, satisfying the prerequisite for the ORR in PEMFC. An extensive theoretical study to investigate the potential of TM atoms embedded in buckled g-C_3N_4 ML, has demonstrated that V, Cr, Mn, and Cu are much less susceptible to form NP than the other TM atoms under investigation, except Ti and Sc, for which clustering is thermodynamically almost impossible. In the context of CO oxidation, Cr and Mn can be considered as promising SAC since the metallic center adsorbs relatively weakly CO and O_2 and the activation of the latter is reasonable energetically ~14-17 kcal.mol^{-1}.[312] Atomic cobalt incorporated in N-G has also been identified as active sites for the reduction of water to hydrogen, thanks to EXAFS.[313] Recently, Co_1/N-G SAC has been also considered for dye-sensitized solar cells applications as counter electrode.[200] Electrochemical measurements have revealed that Co-N_4 sites embedded in N-G nanosheets are highly active, which also make the composite stable counter electrode for the interconversion of the redox couple I^-/I_3^-. Co-N_4 sites have been shown to adsorb iodine rather weakly, leading to a good balance between adsorption and desorption processes. In the electrocatalytic reduction of CO_2 to CO, both experiments and DFT calculations have shown that Ni on N-doped carbon are highly efficient catalysts due to the weak binding of CO on such catalysts that limits CO poisoning.[314]

Sahoo *et al* have investigated theoretically graphene supported single TM such as Cr, Mn, Fe, Co, and Cu atoms for activation of methane and identified catalytically active centers through

C-H bond cleavage. Low activation barriers for both TM-adsorbed and embedded systems have been obtained, compared to that of free TM-methane systems. In this study it is stated that the interaction of three d_{xz}, d_{yz} *and* d_{z2} orbitals with methane, in terms of their relative positions, and occupancies play a key role in governing the catalytic activity of supported TM systems.[315] Embedding TM has globally a negative impact, lower activation barriers are yielded for Co and Fe adsorbed on pure graphene in η^6 coordination mode.

2.2.2 Cluster (< 13 atoms, 0.5 nm) anchoring

The adsorption of small TM clusters (up to 13 atoms) of different nature on graphene has been the subject of intense theoretical works.[316-321] Usually, those systematic works rely on the report of DFT investigations of the structural, energetic, and magnetic properties of small aggregates. It is observed in most cases that when the number of atoms increases, the cluster binds more weakly to the graphene ML, while its binding energy mounts up. For Ni, Pt and Pd clusters, adsorption on pristine graphene causes minor charge redistribution: the TM atoms bound to C atoms become positively charged, while the remaining metal atoms acquire negative charge.[322]

Palladium

Anchored Pd clusters on graphene ML presenting SV have been thought to be interesting sites for hydrogen storage. Indeed, the analysis of the sequential energies and H_2 averaged bond lengths have suggested that a Pd_4 cluster is able to attach up to four molecules covalently, forming dihydrogen complexes; most importantly with moderate binding energies, within the ideal energy range for efficient cyclic adsorption/desorption at room temperature and moderate pressures.[323] If Pd atoms tend to nucleate and form small clusters around SV with strong binding energies, $E_b \approx 115$ kcal.mol^{-1}, it has been demonstrated that Pd-Pd interaction is much smaller than the Pd-SV interaction, making possible Pd dispersion on the carbon support. Moreover it

has been found that Pd binds more strongly to graphene vacancies than hydrogen does, therefore, hydrogen cannot replace Pd atoms or clusters attached to the vacancies.[324] Interestingly, on pristine graphene, hydrogenated adsorbed Pd atoms and clusters can even desorb and should compete with H_2 desorption, due to a loss of stability induced by the partial activation of H-H bond by the metallic centers. However for a Pd-H_2 complex embedded in a SV, its complete desorption is 20 times more costly than the molecular hydrogen desorption, proving that enhancing the reversible adsorption-desorption of hydrogen in porous carbon materials is possible by using Pd-SAC.[325] Pd_6 and Pd_{13} clusters adsorbed on pristine graphene have been further used to investigate H-spillover mechanism by *ab initio* molecular dynamics (MD).[326] It was shown that: i) H_2 dissociation occurs more frequently on naked Pd_{13} and generally takes place on the lateral regions of the Pd NP model, and ii) not a single dissociation event occurs on H-saturated clusters.

When using Pd clusters anchored on DV, to model cross-coupling catalytic reaction,[327] the graphene support was clearly proven to act as an electronic density reservoir, allowing for the efficient reduction of activation energy barriers of specific steps in the catalytic cycle. A strong Pd-support interaction implies an enhanced Pd_n cluster reactivity, since the bonding and antibonding orbitals that control the formation of the C-C bond are significantly stabilized by the positively charged state of the supported cluster.[328]

Increasing the size of the vacancy favors the anchorage of Pd_n (n = 3-8) clusters, since the absolute values of binding energies increase with the increasing size of the graphene nanopore.[170] Moreover the *d*-band center, the charge density difference, and charge analysis have shown that graphene with vacancies greatly changes the electronic structure of the Pd cluster because of the charge transfer from the defective support to the Pd clusters. As a result, the graphene with vacancies usually leads to a downshift of the *d*-band center. This provides interesting features for CO and O_2 adsorptions on Pd_8 adsorbed on a 6C-vacancy. Indeed, the

results show that this system has similar adsorption abilities for CO and O_2, which can enhance the CO tolerance of Pd clusters, with moderate activation barriers (~ 12 kcal.mol^{-1}) for O_2 dissociation and CO+O reaction. The catalytic decomposition of formic acid to HCO_2 + H (formate) and CO_2H + H (carboxyl) on single Pd atom embedded in SV and DV of graphene, as well as on a Pd dimer embedded in di-, tri-, and quadri-vacancy of graphene, has been theoretically investigated.[329] The former route has been proven to be kinetically more favorable, and Pd_2 embedded in DV appears to be the most active configuration with the smallest activation barrier (~ 16 kcal.mol^{-1}) corresponding to the rate-determining step, *i.e.* HCO_2 +H → CO_2+2H.

It has already been proven that energy level of the *d*-band center of small Pd NP is an efficient descriptor for their reactivity.[330] Additionally to the strong metal-substrate interaction due to the presence of vacancies, alloying Pd_{13} by substituting one single Pd atom either by Fe, Co, Ni, Cu or Zn, stabilizes the systems, tunes the averaged *d*-band center of the deposited Pd NP, and strongly interferes with O adsorption. The estimated adsorption energy of oxygen on these materials correlates well with the shift of the NP average *d*-band center. As the adsorption of these O-containing species is weakened on these systems, the ORR kinetics hindered by strong adsorption of these species will also be promoted.[331]

Platinum

The mechanisms of the ORR on defective graphene-supported Pt_{13} clusters have been investigated to understand the effect of defective graphene support on this reaction and predict possible ORR pathways.[332] The defective graphene support may provide a balance in the binding of ORR intermediates on Pt_{13} by tuning the relatively high reactivity of free Pt_{13} cluster that binds the ORR intermediates too strongly, subsequently leading to slow kinetics. The defective graphene support lowers not only the activation energy for O_2 dissociation from 9 to 4 kcal.mol^{-1}, but also the energy barrier of the rate-limiting step by reducing the stability of

HO* species. This is due to the charge transfer from the Pt_{13} aggregate to both defective graphene and the ORR intermediate species, in both scenarii involving 2 or 4 electrons pathway, see Figure 12a. DFT calculations have also shown that stronger binding of the Pt_{13} cluster to the support (vacancy sites) leads to increased charge transfer from the Pt_{13} cluster to the support, with a downshift of the cluster *d*-band center (Figure 12b-e).[318] In several cases, the *d*-band center is shifted below that of a Pt(111) surface.

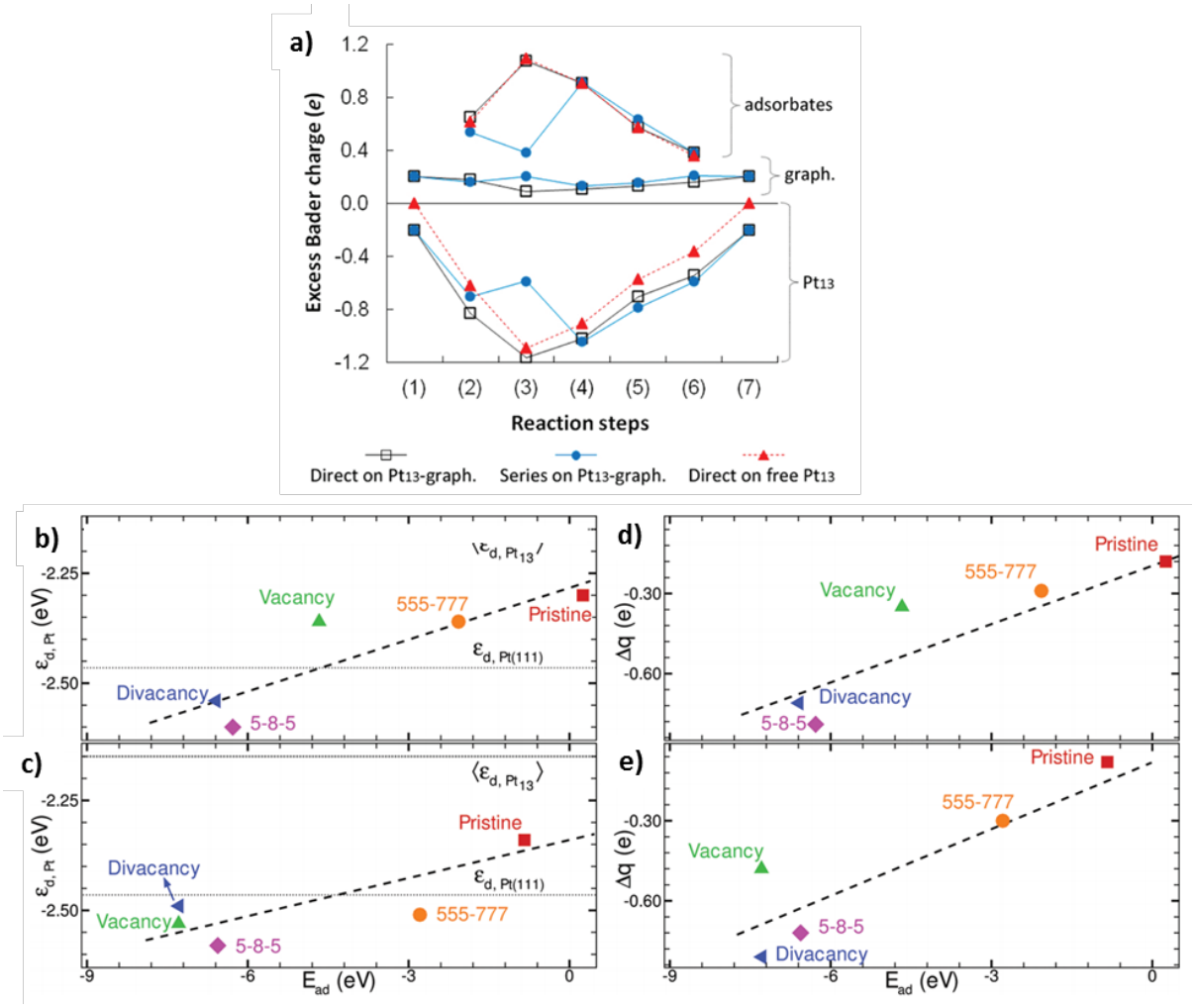

Figure 12. a) Excess Bader charges (in units of e^-) of defective graphene (graph.), Pt_{13}, and adsorbates (O_2, OOH, O, or OH) of the Pt_{13}-defective graphene and freestanding Pt_{13} systems depending on the direct and series oxygen reduction pathways. Reprinted with permission from

Lim, D.-H.; *et al*. *J. Phys. Chem. C* **2012**, *116*, 3653-3660.[332]. Copyright 2012 from the American Chemical Society. On the bottom panel, position of *d*-band center ($\varepsilon_{d,Pt}$) relative to the Fermi level for supported Pt_{13} clusters subjected to b) relaxation alone and c) annealing followed by relaxation. Horizontal dotted lines indicate the *d*-band center of the Pt(111) surface ($\varepsilon_{d,Pt(111)}$) and the average *d*-band center of the various free Pt_{13} clusters ($\langle\varepsilon_{d,Pt13}\rangle$) considered here. Charge transfer from d) relaxed and e) annealed and relaxed Pt_{13} clusters to the substrate. (The electron charge is taken to be negative here.) The dashed lines in all plots are merely guides to the eye. Reprinted with permission from Fampiou, I.; *et al*. *J. Phys. Chem. C* **2012**, *116*, 6543-6555.[318] Copyright 2012 from the American Chemical Society.

Similar effects on the electronic structures of Pt_{13} cluster[333,334] (or Pt_4[335]) in interaction with N-G have been reported. For graphitic N-sites, the enhanced binding strength of the Pt_{13} cluster is attributed to the neighboring carbon atom activation, when for pyridinic sites it involves strong hybridization of the Pt *d*-states and sp^2 N-dangling bonds. Moreover, a net charge transfer is experienced from the metallic cluster to the support, accompanied by a substantial downshift of the Pt_{13} *d*-band center, greatly weakening the interaction with adsorbed atomic species such as O,[333] or CO.[334] Thus, CO-tolerant platinum catalysts could be obtained for hydrogen oxidation reaction (HOR) on defect-engineered graphene.[334] Alloying Pt with other TMs (Fe, Co, Ni, Cu and Pd) also reinforce this downshift.[336] Gasper *et al*.[337] have found that the support-induced shifts in catalyst electronic structure correlates well with an overall change in adsorption behavior of methanol decomposition reaction intermediates, and that the reaction thermodynamics are modified in a way that suggests the potential of greater catalytic activity for Pt_{13} on graphene ML with SV. Interestingly, in the same work, it was shown that adsorption energy predictors[338-340] established for traditional heterogeneous catalysis studies of methanol

decomposition reaction on macroscopic crystalline facets are equally valid on supported nano-catalysts with irregular surface morphologies, see Figure 13.

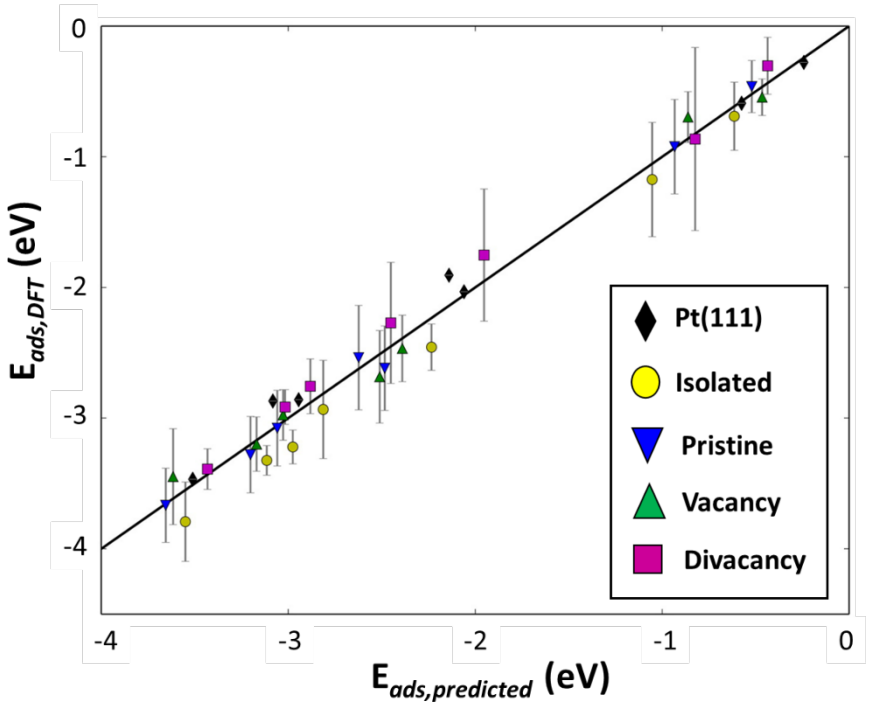

Figure 13. Adsorption energies of CH_3OH decomposition reaction intermediates on all systems predicted by fitted scaling relationships based on C and O adsorption energies versus their DFT calculated values. Error bars are Student-t 95% confidence intervals of the DFT-calculated adsorption energies. Equality line is plotted as a guide to the eye. Reprinted with permission from Gasper, R. J.; *et al*. *J. Phys. Chem. C* **2016**, *120*, 17408-17417.[337] Copyright 2016 from the American Chemical Society.

The presence of oxygenated groups (hydroxyl and epoxy) in various concentrations, as on GO, also influences Pt_{13} adsorption.[252] At low O/C ratio (< 0.125) Pt_{13} cluster weakly binds to GO support (-8 kcal.mol^{-1}) favoring cluster migration and small NP merging, or abstraction of a neighboring O atom to release more energy. At higher O/C ratio, Pt_{13} adsorption energy is larger (≤ -37 kcal.mol^{-1}) depending on the O/C ratio, thus the clusters should remain well

dispersed. The presence of oxygenated groups in the vicinity of the Pt_{13} cluster also induces a large charge transfer from the cluster to the support, which increases with the O/C ratio (from +0.93 e^- for O/C = 0.125, Figure 14a, to +1.36 e^- for O/C = 0.50, Figure 14c). These transferred electrons accumulate around the oxygen groups (the charge distribution is given in Figure 14d) and result in the destruction of epoxy groups (Figure 14e), causing the formation of a C=C bond, a C-O-Pt interface (accumulation of charges, cyan areas in Figure 14a-c) and the broken region between O and C atoms (depletion of charges, yellow areas in Figure 14a-c).

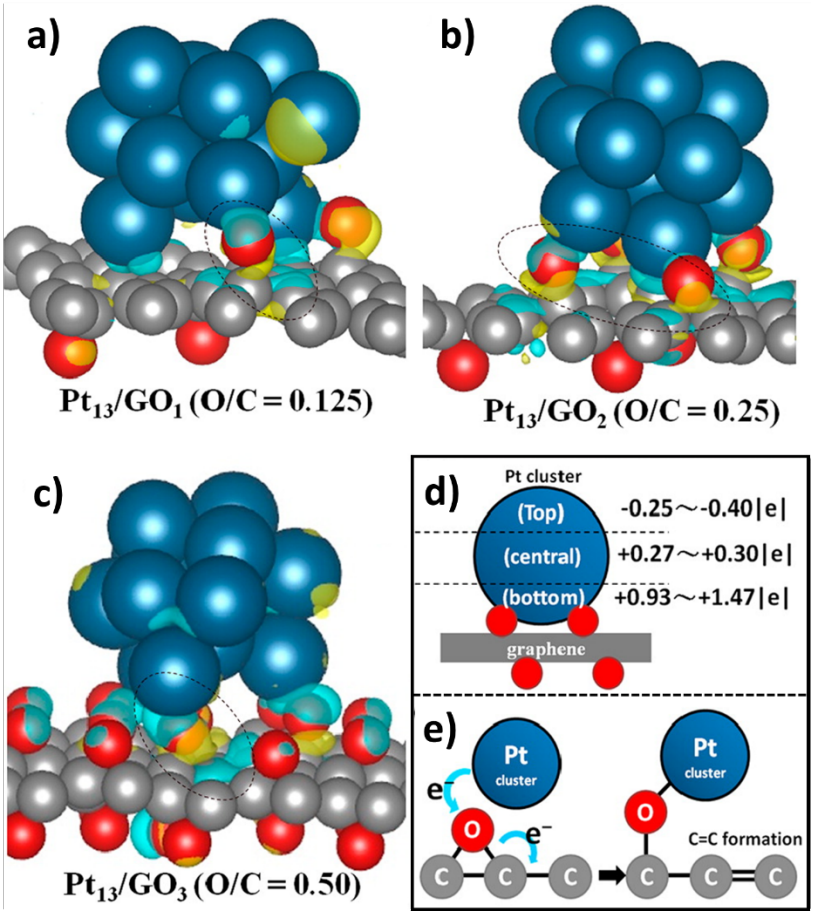

Figure 14. a-c) Charge-density difference plots of Pt_{13} on various GO models with different O/C ratios, yellow and cyan colors represent charge depletion and accumulation, respectively. d) Charge distribution of an anchored Pt_{13} cluster including top, central, and bottom areas. e) Charge-transfer scheme of a Pt_{13} cluster anchored on a GO sheet. Reprinted with permission

from Wu, S.-Y.; *et al. J. Phys. Chem. C* **2014**, *118*, 26764-26771.[252] Copyright 2014 from the American Chemical Society.

As a consequence of this charge redistribution over the cluster, which is accompanied by a downshift of the *d*-band center, CO adsorption energy is decreased (by ~4kcal.mol^{-1}), which in turn decreases the combined barriers, CO + O and CO + OH, in the water-gas shift reaction (WGSR) and thus improves the CO tolerance of this Pt catalyst. This charge redistribution has been observed experimentally in N-doped rGO by combined XPS-DFT approach.[270]

For methane to methanol conversion on Pt dimers, oxygenated groups nearby the Pt dimer, induces a d_{z2} feature well above the Fermi level, which facilitates the activation of a C-H bond of the methane, yielding moderate adsorption' for this molecule and making affordable the addition of O_2.[341]

Other transition metals

Chemical bonding of Co_{13} clusters with pristine graphene has been reported,[342] and very small charge transfer were estimates for various deposited isomers. Heteroatom doping with B or N by substitution does not disturb the strong Co-C chemical bond. When comparing Co, Fe and Ni 13-atom cluster adsorption on pristine or defective graphene ML, Co_{13} is absorbed relatively more strongly on all types of graphene-models as compared to Fe_{13} and Ni_{13} clusters,[343] with charge transfer estimates close to 0.1e$^-$ for the three clusters on SV-G.[344] The covalent character of the Cu_n (n = 4, 5, 6,7 and 13) graphene interaction for pristine and extended lineal structural defect-graphene was evidenced, when a more ionic-like interaction for SV-G was reported by García-Rodríguez *et al*.[345] These interactions appear to be rather local since only Cu/C atoms

close to the contact region are involved. The electronic contact region appears to be much larger for defective-graphene than for pristine-graphene.

DFT studies on the interaction of defective graphene-supported Fe_{13} and Al_{13} have also demonstrated that the sp^2 dangling bonds of neighboring carbons near the vacancy site significantly contribute to anchor the clusters, so that the height of the neighboring carbon atoms increases, buckling the graphene surface.[346] Electronic charges are transferred mostly from the Al cluster to the carbon atoms involved in the vacancy, when more C atoms appears to be polarized in the Fe case due to larger extend of *sp-d* orbital hybridization. The net charge accumulation on defective graphene is 1.57 and 3.08 e^- for the Fe and Al systems, respectively. Surprisingly, upon adsorption on SV-G, Fe_{13} *d*-band center is upshifted closer to the Fermi level. In ORR context, after the synthesis of N-doped carbon-supported iron catalyst, XRD, XPS and Rotating Disc Electrode experiments have revealed that Fe_3-N sites are most likely active sites, when the presence of graphitic and pyridinic N-sites was clearly identified.[347]

In a study of nickel NP supported on N-doped CNT as HOR catalyst in alkaline electrolyte,[348] DFT investigations of Ni_{13} adsorption on graphitic or pyridinic sites have been reported. The presence of a pyridinic site upshifts the *d*-band center of adjacent Ni-binding sites. As these sites originally lie in the weak binding region of H adsorption, this upshift consequently activates them for the HOR by strengthening the binding energy by 2 $kcal.mol^{-1}$. In ref. 57, Ru_{13} clusters have been adsorbed on a wide variety of defects (SV, DV and others re-constructed DV) to mimic rGO situations, which appear to be strong trapping sites. It has been shown that this interaction, which correlates with the interfacial structures and the charge transfer, tunes the averaged *d*-band center of the materials, and contributes to improve the reactivity of these catalysts. Further study reveals that the performances of the catalysts against oxygen adsorption correlate well with the *d*-band center's shift of deposited Ru NP, which originates from the

covalent interfacial Ru-C interaction and is controlled by the presence of defects on rGO support.

Comparisons of the performances of Ti_4 and Ni_4 clusters embedded in a SV-G site to store hydrogen[349] have proven that: i) both clusters should remain attached to the vacancy and will neither diffuse on the surface nor be desorbed, due to strong adsorption energies, and ii) the single absorbed H_2 molecule configuration is found to depend on the metal on which it is absorbed. The H_2 bond activation is favored by deposited Ni_4 since H 1*s* levels only interacts with the Ni 4*s* levels, forming dihydrogen-type complexes with H-H bond lengths between 0.85-0.9 Å, while the adsorption on Ti_4 exhibits a dissociative character, given that hydrogen 1*s* levels strongly interact with the Ti 3*d* levels. This results in an increase of H_2 content and favors the formation of Kubas-type complexes of $Ti_4(H_2)_n$/SV-G with n > 3. The analysis of the sequential energies and H_2 averaged bond lengths suggests that Ni_4 is able to covalently attach up to 3 molecules to form dihydrogen complexes with moderate binding energies within the ideal energy range for efficient cyclic adsorption/desorption at room temperature and moderate pressures. On the other hand, embedded Ti_4 adsorbs up to six H_2 molecules before reaching saturation, also exhibiting moderate binding energies.[349]

2.2.3 Nanoparticle anchoring

Palladium

Despite a weak bonding between Pd NP and carbon-based support, *ex-situ* preparation of Pd NP on multi-walled CNT has been proposed to be an interesting way to form efficient catalysts for cross-coupling reactions.[350] In those experiments, NP ripening appears to be strongly dependent on the CNT curvature, which is a clear manifestation of van der Waals interaction. Indeed, highly curved surfaces provide the smallest dispersion interactions between NP and

CNT, and the lowest retardation of the growth and coalescence of catalytic centers and, thus, the lowest catalyst stability.

Experimentally, one way to strongly anchor large Pd NP (8-12 nm), is to use heteroatom doping. For example, from XPS experiments performed on one-pot synthesis of Pd NP supported on N-doped carbon, anchoring of large Pd^0 NP on pyridinic and quaternary nitrogen sites has been demonstrated.[351] Similarly, the deposition of Pd NP on N-doped exfoliated graphene induces a strong enhancement of the hydrogen uptake capacity, due to the high dispersion of Pd NP over N-G sheets, and the interaction's strengthening between the N-G sheets and the NP. It originates from the carbon atoms in the vicinity of nitrogen atoms, more of pyrollic type than pyridinic in this work, which develop an increased π-electron density, making the back-donation to 5*s* orbitals of Pd easier. Moreover, anchored Pd NP can catalyze the H_2 dissociation and the subsequent migration of hydrogen atoms on the doped graphene sheets.[352] N-functionalized activated carbon was also used to stabilize Pd NP and prevent their aggregation.[353] This Pd/N-AC catalyst has shown high activity and excellent chemoselectivity for the selective hydrogenation of nitro compounds to the corresponding anilines. The presence of N-pyridinic sites is also crucial to boost the efficiency of Pd NP to dehydrogenate formic acid, due to prominent surface electronic modulation. Indeed, by combining XPS data and ATR-IR spectroscopy to monitor the absorbed linear mode of CO on the supported Pd NP, Pd atoms appears to be negatively charged.[354] Nitrogen and sulfur dual-doped graphene was also used to stabilize small Pd NP for both direct formic acid fuel cell and direct methanol fuel cell.[355]

It is important to note that if the presence of these heteroatoms on the carbon support is beneficial to stabilize the metal NP because of a strong adsorption energy; their presence as impurities in the feedstock of catalytic reactions is harmful because it can lead to poisoning and deactivation of the catalyst.[356] Pd/C catalyst poisoning has thus been reported in the presence

of sulfur-,[356] chloro-,[357] phosphorous-,[358] or amine-species.[359] The active life of Pd/C catalyst has sometimes been prolonged, and its resistance to poisoning in service increased, by selectively pre-poisoning it during its preparation.[360] In that case, the original activity is somewhat reduced, but an appreciably more stable catalyst is produced. In addition, if the addition of sulfur, nitrogen, phosphorous, or halogen containing compounds to the original catalyst often retards the reaction rate, sometimes it suppresses possible side reactions, thereby leading to high selectivity.[361]

Covalent functionalization is another possibility to improve Pd catalyst stabilization: after 1,3-dipolar cycloaddition reaction under microwave conditions on CNT sidewalls, Pd/CNT catalysts were prepared through strong electrostatic adsorption and hydrogen reduction. The enhancement of the interaction between the Pd precursors and the functionalized carbon-support yields well-dispersed small NP with an average size of 1.5 nm, avoiding the migration and coalescence of the NP.[262] Wrapping multi-walled CNT with a functional biopolymer-polydopamine by *in situ* spontaneous oxidative polymerization of dopamine, allows for the deposition of charged metal complexes, which upon reduction generate Pd NP with good dispersion and mean diameter of ~ 10 nm. The anchoring modes in this case certainly implies amine and hydroxyl surface groups.[362] XPS analyses have suggested that on rGO, with a large amount of oxygenated groups, Pd NP are suspected to be bound to carboxylate surface groups.[363] Moreover the effects of surface functionalization by HNO_3 treatment on carbon activated either by steam or phosphoric acid, investigated by means of several characterization techniques among INS,[283] in the context of Pd/C catalyst preparation have been explored.[364] It was shown that the HNO_3 treatment affects mainly the irregular borders of the graphene layers, which are decorated mainly by carboxylic and carboxylate groups. Under these conditions, the authors have noticed that the presence of these oxygen-containing groups is responsible of a general decrease of the palladium dispersion.

Platinum

On pristine carbon-support, such as graphene, dispersion forces supposedly govern Pt NP deposition. Large scale DFT calculations, by simulating the adsorption of Pt_{309} on pure graphene ML, have proven that van der Waals forces are getting more importance when increasing the NP size.[365] A charge re-organization, with an overall charge being transferred from the Pt NP to the graphene support, over the entire NP is also demonstrated, since Pt-Pt bond-lengths are increased for the closest Pt facets from the graphene sheet, when far away the interface the Pt-Pt distances are decreased. As already discussed, point defects in graphene strongly anchor Pt_n models, with n = 2-80, but also appreciably affect their morphologies.[366] From a structural analysis, it can be extracted that the fraction of potentially active surface sites in supported clusters is maximized for stable Pt clusters in the size range of 20-30 atoms. In the case of bimetallic $Pt_nFe_{(55-n)}$ (n = 0, 11, 13, 18, 28, 37, 42, 44, 55) NP on graphene SV, it was found by DFT that the NP prefer to be adsorbed on the SV through the Fe atoms (Pt and Fe atoms are both on the surface), because of the stronger interaction between Fe atoms and SV.[367] In this context, INS technique coupled with hydrogen adsorption measurements is a powerful tool to locate Pt NP on activated carbon and to observe Pt hydride formation.[368,369] EXAFS experiments have been also used to characterize *in situ* the interaction between Pt NP on CNF, in terms of Pt-C bonds.[370] The presence of oxygen-surface groups on CNF leads to the stabilization of Pt NP. After reduction, a Pt-carbon distance of 2.62 Å has been detected, and after evacuation, the distance is decreased to 2.02 Å. The 2.62 Å distance is ascribed to the presence of atomic chemisorbed hydrogen in the interface between the Pt NP and the carbon support. According to the number of interfacial Pt-C bonds (four), the Pt NP supported on CNF has been proposed to be in contact with a prismatic surface of the carbon support, on which oxygen groups have more stable bonds with carbon atoms. Six Pt-C bonds have been detected

in the metal-support interface on CB, which supports an epitaxial growth of Pt NP on the (0001) basal surface plane.

The support effect and metal particle size effect, which are often intertwined, are two critical factors influencing the activity of a supported TM catalyst. Recently, to clarify each effect on the activity of carbon-supported Pt catalysts during the dehydrogenation of decalin to release hydrogen, a series of Pt/C catalysts have been elaborately prepared from CNF and CNT, with various NP sizes (from 1 to 9 nm).[371] Great differences between Pt/CNF and Pt/CNT in both the geometric structure and electronic property of Pt clusters have been revealed, especially when the NP size is smaller than 2 nm. Pt atoms interact more strongly with the edge planes of CNF than with the basal planes of CNT, hence forming a more dispersive and simultaneously more active Pt-C boundary for further reaction of interest. The carbon support effect dominates the activity divergence in the smaller size range (< 2 nm), while the Pt particle size effect prevails on the catalysts with medium Pt particle size (2-4 nm). Both effects can fade out with continually increasing Pt particle size.

Several recent works have discussed catalytic performance of Pt NP/carbon supports systems for ORR in terms of NP size,[372] shape[373] and composition.[374] The effects of carbon support modifications have been reported too. For instance, in a recent work of Jackson *et al*,[375] it has been proven that Pt NP supported on graphite-rich boron carbide show a 50-100% increase in ORR activity in acidic media and improved cycle stability compared to commercial carbon supported Pt NP. Analyses of TEM images and XAS experiments demonstrate that similar Pt NP shapes, sizes, lattice parameters, and cluster packing on both supports are yielded, when x-ray photoelectron and absorption spectroscopy show distinctly changes in the NP's electronic structure. This shows that electronic metal-support interactions alone can significantly improve ORR activity with no further modification of shape, or size of the NP. Indeed, the Pt *4f* spectrum shifts to higher binding energies, relative to the C *1s* core levels for sample of Pt deposited on

B-doped graphite. Optimizing the electronic interaction between the catalyst and support is, therefore, a promising approach for advanced electrocatalysts where optimizing the catalytic NP themselves is constrained by other concerns. Improvement of long-term stability of ORR catalysts can be also obtained if oxygen surface groups that are effective for the anchoring of Pt NP are present on the carbon surface.[376] However, some of the oxygen surface groups, and particularly the carboxylic ones, may not be stable under the reduction conditions during catalyst preparation, and their decomposition would have negative effects on catalyst properties. Thermal treatment of the carbon support can also increase the stability of Pt/C electrocatalysts for ORR.[376] In that case, the increasing metal-support interaction is related to π-sites of the carbon basal plane, which act as anchoring centers for Pt NP.

Doping the carbon support with nitrogen has also several virtues. Pt NP deposition on CNT is clearly favored when pyridinic and quaternary surface nitrogen species are present on the sidewalls. The larger the number of available functional sites, the more the NP size is decreased.[377] Additionally, for ORR applications, incorporating nitrogen in CNT sidewalls also i) improves electronic conductivity,[378] thus favoring electron transfer to active sites for higher ORR activity, and ii) modifies the electronic structures of the Pt NP, due to the donor character of the N-doped sites. In the case of nitrogen-doped nanocage, an improve stability of the Pt catalyst for both HOR and ORR, when tested under potential conditions of practical fuel cell operation, has been evidenced.[379] Strong metal-support interactions have been also reported between the sulfur atoms in a sulfur-doped carbon support and the surface atoms of Pt NP.[380]

Metal NP stabilization on a carbon-support can also be achieved by making triple junction points by synthesizing first indium tin oxide (ITO) nanocrystals on functionalized graphene sheets, and then by depositing Pt NP.[381] The combined ITO/Pt anchoring on defective graphene implies large binding energies, and it has been suggested by DFT calculations that supported

Pt clusters prefer to bond at the interface between ITO and graphene, confirming TEM image interpretations, see Figure 15.

Atomic scale simulations of the interaction of a Pt_{38} NP model with a functionalized graphene ML by oxygenated groups such as -OH and -COOH, extend the understanding of Pt/rGO catalyst properties.[382] Again anchoring Pt NP on defective sites further decorated by functionalized groups greatly stabilizes the structure and results in net charge transfer between the two subsystems. It induces a well-localized charge redistribution within the NP and finally shifts the *d*-band center. Surprisingly, the anchoring mode is not direct, in the sense that it does not involve oxygenated groups, but C atoms neighboring them.

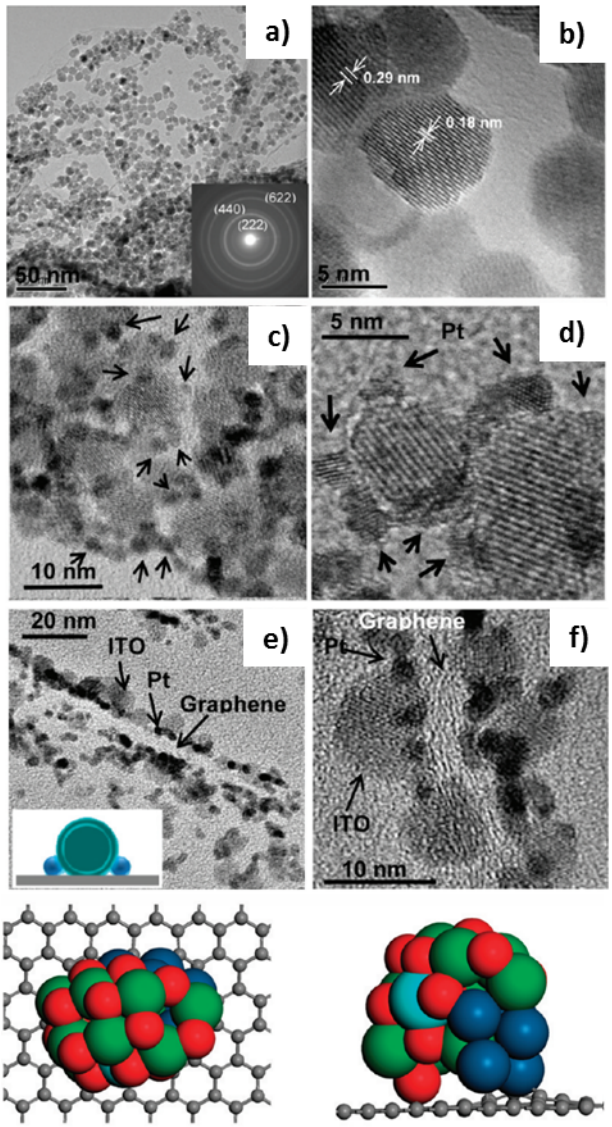

Figure 15. Top panel, TEM images of ITO nanoparticles on graphene sheets (a, b), Pt-ITO-graphene (c, d), and the cross section TEM images of Pt-ITO-graphene (e, f). Inset: The schematic structure of Pt-ITO-graphene nanocomposite. ITO content in ITO-graphene composite is 75 wt % and Pt content in Pt-ITO-graphene is 20 wt %. Bottom Panel, Pt_6-ITO-graphene triple junction model. Graphene sheet is displayed as gray balls for clarity; indium atoms are in green, oxygen atoms are in red, platinum atoms are in dark blue, and tin atoms are in light blue. Reprinted with permission from Kou, R.; *et al*. *J. Am. Chem. Soc*. **2011**, *133*, 2541-2547.[381] Copyright 2011 from the American Chemical Society.

As mentioned before Pt NP anchoring on graphene supports through surface functionalization has been already reported.[265] Interestingly, XAS and XPS experiments have shown that a strong interaction between the Pt and graphene support exists, leading to an electron density shift from the Pt to the graphene, experienced by Pt $4f_{5/2}$ and Pt $4f_{7/2}$ peaks as it can be seen in Figure 16a. When the Pt NP are deposited on graphene-SO_3H and graphene-NH_2, a further positive shift of the Pt *4f* binding energy (by 0.21 and 0.37 eV, respectively) related to the Pt/graphene is observed. These additional shifts can be attributed to the functional group presence that promoted a charge transfer from the Pt NP to graphene-SO_3H and graphene-NH_2 supports, respectively.

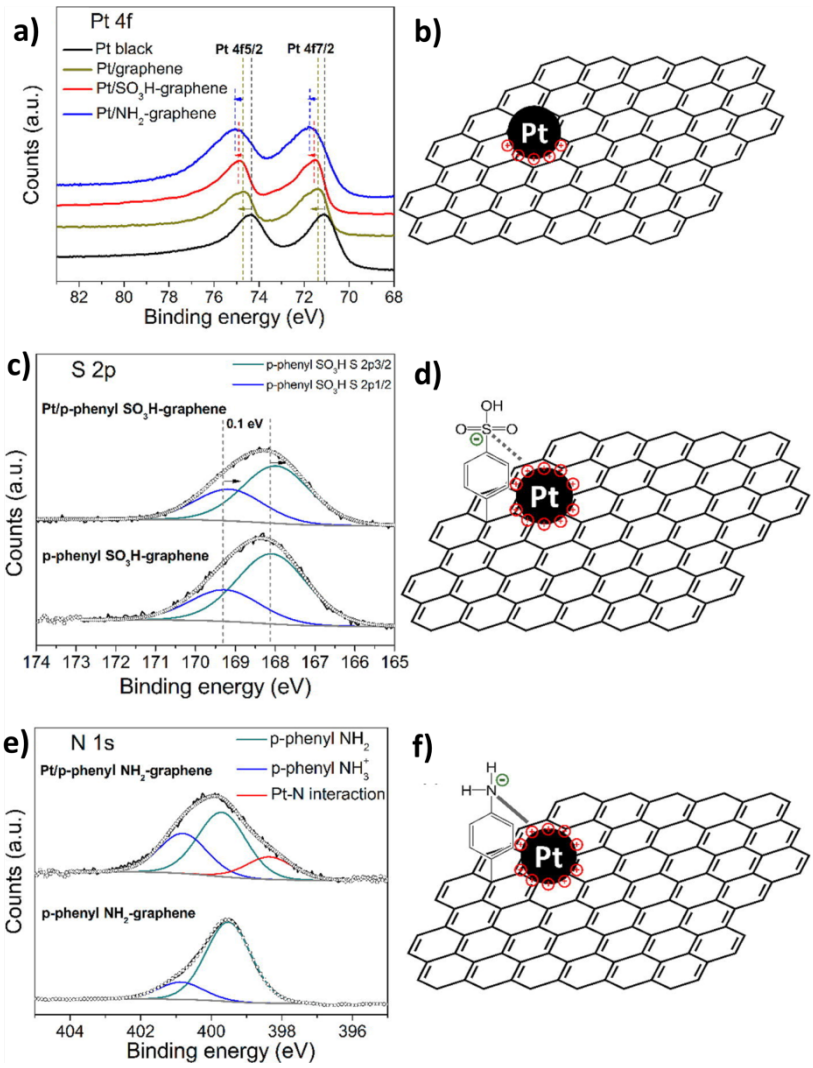

Figure 16. High-resolution XPS spectra of a) Pt *4f*, c) S *2p*, and e) N *1s*. The possible configurations of the interaction between Pt NP and functional graphene support are illustrated in b), d), and f), where dotted lines and solid lines illustrate the weak S-Pt and strong N-Pt interactions, respectively. Reprinted with permission from Xin, L.; *et al*. *ACS Catal*. **2016**, *6*, 2642-2653.[265] Copyright 2016 from the American Chemical Society.

Finally, the importance of the morphology of deposited NP with diameter around 10 nm has been recently reported, in the context of photocatalytic HER over Pt NP supported on g-C_3N_4.[383] Cubic shape NP appear to be more photoactive than octahedral or spherical ones to produce H_2. Thus the size and shape control of catalysts can be a next promising strategy for the design of future solar-to-fuel conversion photocatalysts.

Others transition metals

In the case of porous carbon-supported gold NP for ORR, the effects of the NP size on the activity have been investigated, proving that catalysts prepared from Au_{25} nanocluster precursors show the best electrocatalytic activity, yielding final NP size of 3.7 nm after pyrolysis.[384] In the same work, anchoring mode between the oxygenated carbon support and the Au NP has been elucidated. XPS measurements suggest an electron transfer from the carboxylic/carbonyl moieties to gold, and it is likely that the enhanced electron density on Au had a positive influence on the oxygen electroreduction activity. The effects on the NP morphology due to the carbon-support structure have been also studied.[275] In this work, Au NP were supported on two types of CNF with different degree of graphitization, which in turn strongly influence the deposited NP morphology, see Figure 17. When the CNF graphitic layers

are well ordered, the Au NP prefer to bind with their (111) planes and exhibits more facets areas. On the opposite, with disordered CNF surfaces, random NP orientations are obtained.

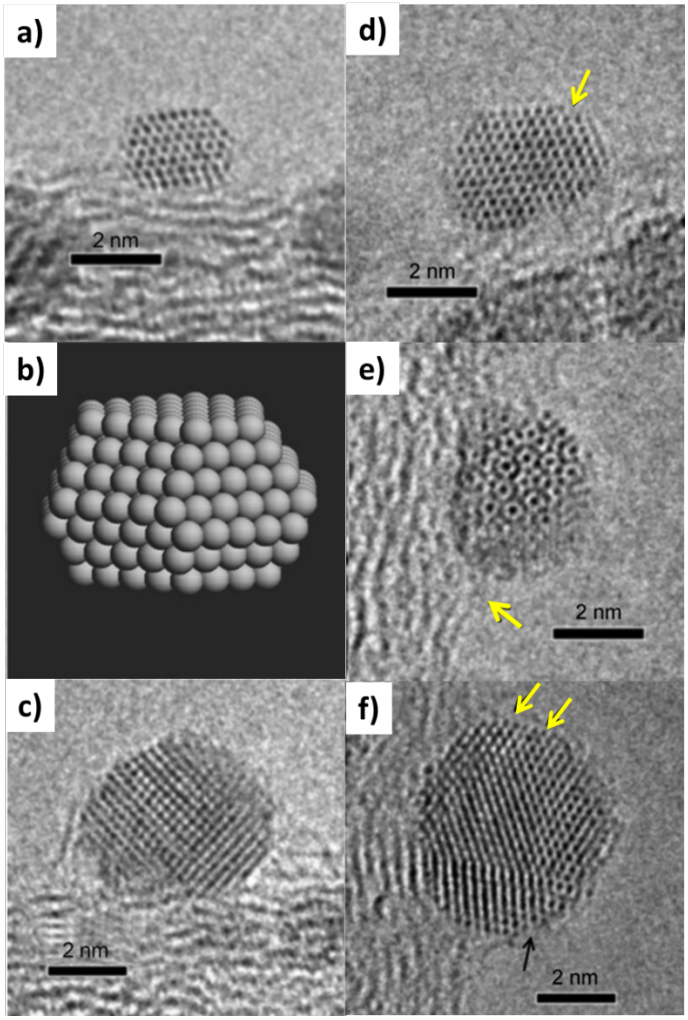

Figure 17. On the left, aberration-corrected HRTEM images of Au NP supported on ordered CNF surfaces. a) A representative 2-4 nm particle with (111) surface epitaxially parallel to the graphitic layer of CNF. b) Structure model derived from the image in part a). c) A larger particle with spherical shape showing carbon binding to the CNF surface. On the right, aberration-corrected HRTEM images of Au particles supported on disordered CNF, with d) modified cuboctahedral configuration, e) icosahedral configuration showing interaction between particle and CNF surface, and f) surface carbon decoration with uncovered windows (each indicated by arrows). Reprinted with permission from ref [275]. Copyright 2012 from the John Wiley and Sons.

The synthesis of glutathione decorated Au NP, with an average size of ~ 1.4 nm, supported on rGO at low Au loadings, with high catalytic activity for the reduction of 4-nitrophenol in an aqueous medium, has been revealed.[385] The observed Au $4f_{7/2}$ and $4f_{5/2}$ peak redshifts compared to bulk Au, consistent with $Au^{(0)}$ oxidation state, have been attributed to reduced core-hole screening in small metal particles. A controlled synthesis of carbon-supported Co catalysts from single atoms to NP has been achieved by the deposition of Co(salen) complex precursor under heat treatment.[386] The precise characterization, using TEM, XRD and *in situ* XAFS of the corresponding structural transformation are highly valuable in terms of carbon-support-TM interaction. The first decomposition of the Co(salen) complex is initiated by the dissociation of Co-O-C bonds at around 523 K, which produces isolated Co single-atom while retaining the Co-N-C bonds even up to 673 K. When the heat treatment temperature exceeds 723 K, the second decomposition of the Co-N-C bonds occurs to form Co oxide nanoclusters followed by the growth of Co NP upon further increase of the heat treatment temperature. Direct comparisons between DFT calculations of Ru NP supported on graphene and EXAFS experiments on Ru/C catalysts,[387] detail that Ru NP are very structure sensitive and stabilized on the sp^2 carbon support only in certain geometries, thus resulting in specific shapes and electronic properties, and consequently in the presence of active B5 sites. These B5 sites consist in five Ru atoms in a certain 3D arrangement exposing a 3-fold hollow site and a bridge site close together. These DFT results also suggest that for Ru clusters with more than 4 atoms, epitaxial growth of the metal on the carbon support is possible only in certain configurations.

3. Why anchoring metal nanoparticles, clusters or metal single atoms on carbon materials for catalysis?

Supported metal catalysts are among the most important solid catalysts. In general, the metal functions as the catalyst, and the function of the support is to keep the metal particles well dispersed. However, supports can play a non-innocent role in heterogeneous catalysis and are often critical for the efficiency and stability of the catalytic systems. In most applications, only the metal NP are the active centers; however, in some cases both the supported metal and the support itself function as a catalyst. The support effects on the catalytic properties of metal NP are connected to: i) changes due to metal particle charging, ii) effects related to variations in metal NP shape and crystallographic structure and, iii) appearance of specific active sites at the metal-support boundary.[388] Thus, different types of effects have been identified: i) electronic effects, ii) geometric effects, but also iii) bifunctional effects such as spillover phenomena[389] or direct involvement of the support in catalysis, and iv) confinement effects.[390] It is also worth mentioning that many of these effects are also correlated to the size of the metallic species, so that fundamental differences will be observed if large size particles or isolated single atoms are used. In this section, we will analyze these different effects in the case of carbon supports.

3.1 Metal-support interaction

The metal-support interaction may influence catalytic performances in different ways, including: i) geometric effects (changes in NP size, morphology or strain due to the presence of the support), ii) electronic effects (*e.g.* charge transfer between metal and support or 'ligand' effects due to coordination of the metal by the support), iii) interfacial reactivity (where specific sites at the metal-support interface provide a given reactivity),[391] or even iv) direct participation of the support in the catalysis (see section 3.4).[392] Electronic, geometric, and ligand effects are interrelated,[393] and it is not possible to clearly discriminate each single contribution. In the case of carbon supports, the rich surface chemistry of carbon materials as well as the broad spectrum of structurally different carbon materials offer interesting perspectives to modify the catalytic

performances. We voluntary speak about modification, and not modulation and even less of a fine tuning of the performances, since up to now such a level of control has not been achieved on carbon supports. Indeed, if the understanding and the control of the extent of metal-support interaction in carbon-supported metal catalyst opens an exciting avenue of research for the rational design of catalysts, many efforts remain to do to achieve this goal. Indeed, while the relationships between catalyst affinity and activity have been known for nearly a century, techniques to continuously and controllably tune the affinity and hence, the activity and selectivity of a catalyst are only beginning to emerge.[13,389] Recently, significant efforts have been made towards revealing metal-carbon support interactions during catalyst synthesis or catalytic reactions by XRD, electron microscopy, and spectroscopy methods.[73]

3.1.1. Geometric effects

Nørskov *et al*. have shown by DFT that surface reactivity of strained metal surfaces increases with lattice expansion, up-shifting the metal *d* states closer to the Fermi level.[394] Carbon support-induced strain in metallic NP has not been much investigated. Experimentally, strain variation within NP is usually investigated using either coherent XRD, TEM or more recently by combining high-energy resolution fluorescence detection (HERFD), XAS methods, namely, HERFD XANES and HERFD EXAFS.[395] On graphene support, local strain accumulation during the growth of Pt cluster was experimentally and theoretically evidenced.[396] The authors proposed that the local strain field in the immediate vicinity of the NP is not favorable for the growth of other NP that preferentially migrates to other pristine regions of the graphene surface. It has also been shown that strain field around the defects of graphene[397,398] or externally induced on defect-free graphene[399-401] also significantly reinforces the adsorption of the metal on graphene, by reducing the distance between the clusters and the graphene ML (Figure 18) and by increasing the adsorption energy. Consequently, charge transfer occurs between the metal and graphene, and thus its reactivity is altered. Using Au_{16} and Au_8 clusters on graphene

for CO oxidation, it was found that a small strain of 5% in graphene reverses the charge transfer between Au clusters and graphene, and thus drastically reduces the CO oxidation activation barrier from around 69 kcal.mol^{-1} (without strain) to less than 4.6 kcal.mol^{-1}.[400] An influence of strain was also noticed for the same reaction in the case of Pt_6 clusters on a graphene ML.[401]

By varying the thickness of an amorphous carbon film, strain on Ag NP can be induced, that was investigated using HRTEM by Settem *et al*.[402] It was shown that the strain increases with the thickness of the film, and that the effect is more pronounced in the case of small NP. The effect of graphene edge topology on the strain of Ag NP was also reported.[403] A +2.7% strain was found by DFT in the case of a silver-zigzag edge interface, and -1.0% in the case of the silver-armchair edges interface.

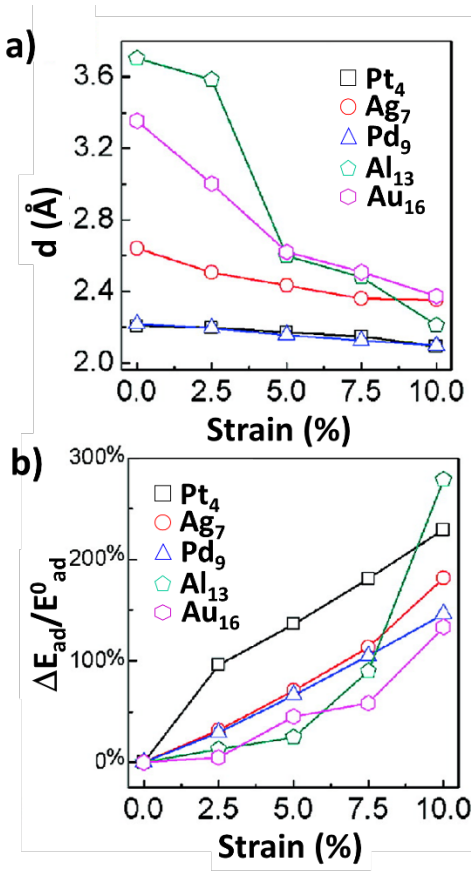

Figure 18. a) Variation of the distance between the adsorbed cluster and a graphene ML under different strains, and b) the relative change of adsorption energy of different metal clusters on graphene, where E^0_{ad} is the adsorption energy for zero strain, and ΔE_{ad} is the change of the adsorption energy under strain relative to that of zero strain. Reprinted with permission from Zhou, M.; *et al*. *J. Phys. Chem. C* **2010**, *114*, 16541-16546.[400]. Copyright 2010 from the American Chemical Society

Pt NP with thin plate-like morphologies and a (110) crystal surface parallel to the (0001) planes of graphite flakes were observed by HRTEM.[404] The Pt NP were found to be anisotropically deformed from the pristine *fcc* symmetry. Approximately two-thirds of the Pt NP were compressively strained (5.9% compared with the bulk lattice constant of Pt), and the others showed an expanded unit cells (2.8% compared with the bulk lattice constant of Pt). On CB, Pt NP (≈ 3.5 nm) were randomly oriented on the surface of the support.[405] A single Pt NP had *ca.* 70% compressive facets and *ca.* 30% expansive facets on average. The mean unit cell volume of the NP (0.386 ± 0.015 nm) was 4.2% smaller than that of bulk Pt, and no correlation was found between the monoclinic lattice parameters and Pt NP diameters. In other studies dealing with Pt NP on CB, it was shown that when decreasing the average Pt NP size down to approximately 2 nm, the unit cell parameter decreases nonlinearly (variation of 0.7% in comparison to bulk Pt) and the size effect is predominant for small Pt NP.[406,407] The origin of the bond length disorder in Pt NP on carbon was investigated from an atom-by-atom structural analysis and it was shown that it results from anisotropic distortions in the cluster arising from interactions of the bottom metal layer in contact with the graphite surface.[408] On graphitized CB, the lattice strain of Pt NP was directly observed and mapped, using aberration corrected STEM coupled with geometric phase analysis.[409] The Pt formed spheroidal NP (Figure 19) presenting Pt-Pt bond lengths varying between 2.64 Å-2.79 Å (*i.e*. by 5.7%). Slightly shorter

average bond lengths are observed at facet edges, whilst longer average bond lengths are obtained on the facet planes. Upon post-processing effects, with or without hydrogen passivation, shear instability of supported Pt NP have been addressed theoretically,[410] and it was shown that dramatic morphological change of the NP can occur even with small changes to first-shell Pt-Pt coordination number.

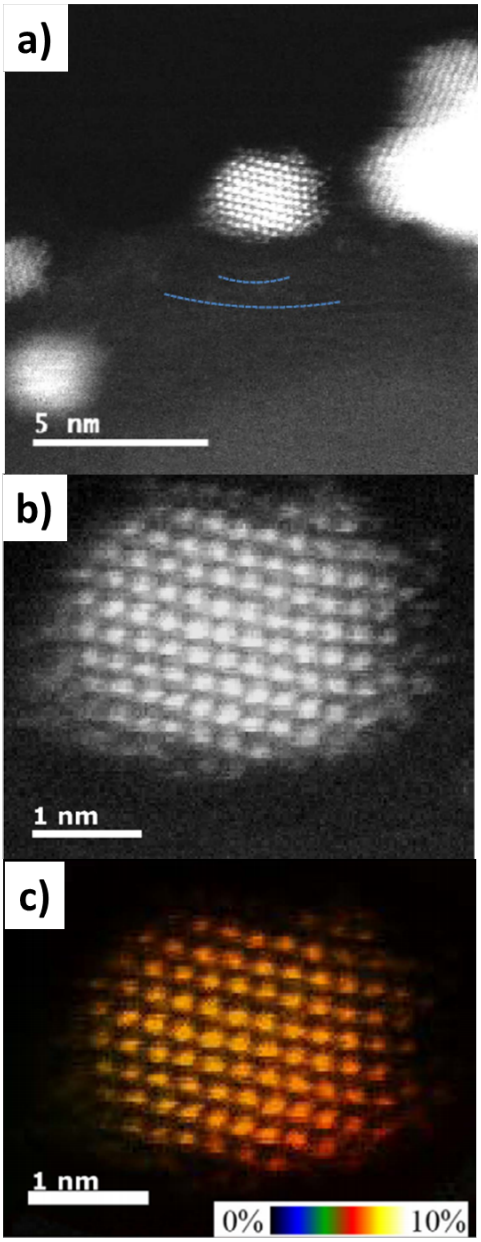

Figure 19. a) and b) atomic resolution STEM-HAADF cross-sectional images of Pt/CB; and c) false-color lattice strain amplitude map of Pt/CB obtained by geometric phase analysis of the

STEM-HAADF images. Strain maps were overlaid on the Cs-STEM image for clarity. Reprinted from ref [409].

On C_{60} nanowires, Pt NP were anisotropically strained from the *fcc* structure, with *fcc* lattice constants significantly different from those of Pt NP deposited on graphite particles (0.391 ± 0.013 nm on C_{60} and 0.388 ± 0.015 nm on graphite, 0.39231 nm for bulk Pt).[411] On CNF (platelet type) it was found from MD simulations that the initial mismatch between the atomic structure of support's edges and the adsorbed facet of a Pt_{100} cluster leads to a desorption of a few Pt atoms from the cluster and the subsequent restructuring of the cluster (flattening of the cluster).[412] Consequently, the average Pt-Pt bond length is enlarged in agreement with experimental results. This enlargement is more pronounced at the Pt/C interface than in the rest of the NP. The curvature of the carbon support has no appreciable effect on the bond-length distribution for the Pt clusters; whereas an effect is noticed for Ni clusters.[413] Simulations have shown that upon adsorption, the distribution of first-shell Pt-Pt coordination number changes significantly for Pt NP up to 2 nm, and that the restructuration of the NP decreases with particle size (Figure 20).[414] This was attributed both to the reduced binding energy per Pt atom bonded to the support and to the increased cohesive energy of the Pt NP. According to the orientation of graphene sheets, CNF are classified into three categories, platelet type, tubular type, and fishbone (or herringbone) type CNF, with their graphene sheets perpendicular, parallel, and tilted to the principal axis, respectively. For fishbone type CNF, a decrease of the apex angle decreases the binding energies of a Pt_{100} clusters to the CNF.[415] This is accompanied by a lower degree of cluster reconstruction. When more CNF edge planes are exposed, a higher Pt dispersion, lower surface first-shell Pt-Pt coordination numbers, and longer Pt-Pt surface bonds are obtained. According to the *d*-band model, the increased Pt-Pt interatomic distance results in

an upshift in the surface *d*-band center, which would eventually strengthen the binding of molecules to the supported Pt clusters.

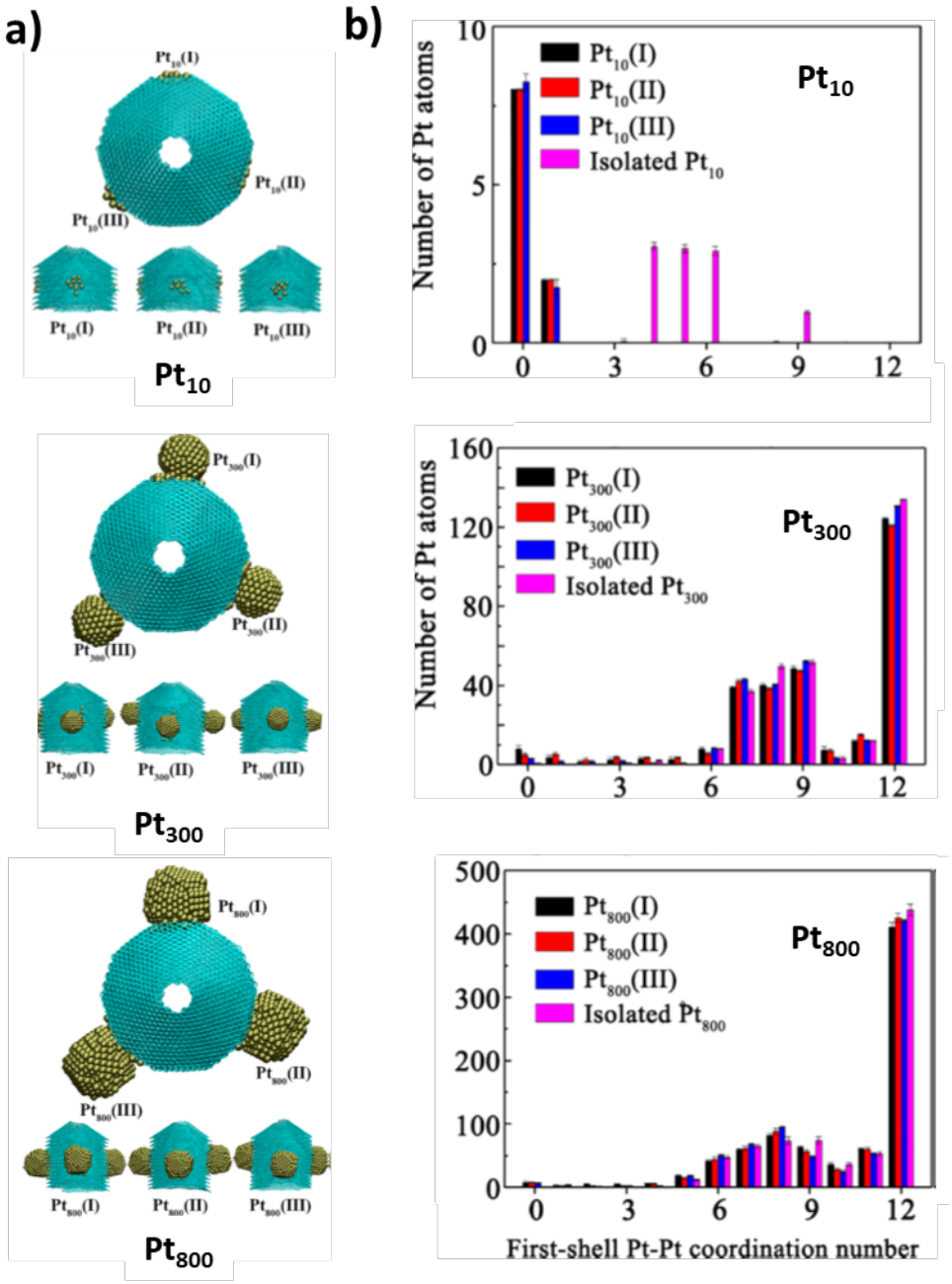

Figure 20. a) Illustrations of the equilibrium geometries of adsorbed Pt particles on CNF; and b) distributions of first-shell Pt-Pt coordination number in supported and isolated Pt NP. In each model, three Pt NP denoted as $Pt_n(I)$, $Pt_n(II)$, and $Pt_n(III)$ were initially placed over the armchair arrangement, the zigzag arrangement, and their junction, respectively, where n is the number of

atoms involved in the Pt NP. Reprinted with permission from Cheng, H.; *et al. J. Phys. Chem. C* **2014**, *118*, 23711-23722.[414]. Copyright 2014 from the American Chemical Society.

In the case of a Ni_{100} cluster adsorbed on the same support, it was reported that the Ni-Ni bond length increases as the distance to the platelet edge is enhanced, due to the strain in the region close to the platelet-cluster interface.[416] This phenomenon is even more pronounced on armchair or zigzag edges of CNF than on the basal plane of graphite (Figure 21). It was shown experimentally that the surface curvature of the CNF, and the strong interaction between the Ni NP and the graphene edges cause local deformation of the Ni NP, and thereby induce a high degree of microstrain.[417] Such lattice expansion has been shown to increase the activity of Ni NP on CNF for ethane hydrogenolysis.

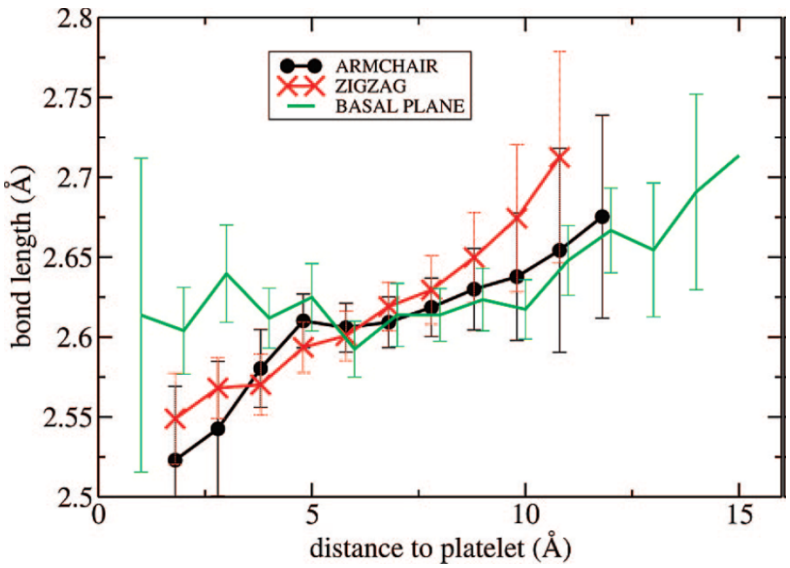

Figure 21. Mean bond-length distribution for a Ni_{100} cluster as a function of the distance to the CNF platelet edge and carbon basal plane. Reprinted with permission from Sanz-Navarro, C. F.; *et al. J. Phys. Chem. C* **2008**, *112*, 12663-12668.[416]. Copyright 2007 from the American Chemical Society.

Interfacial compressive stress was also reported in the case of $CoFe_2O_4$ NP in interaction with graphene oxide sheets.[393] These results show that the strained structure of metallic NP changes depending on the surface energy of the carbon support.

Finally, we should also mention that it is possible to take advantage of strain in multimetallic catalytic systems deposited on carbon support to control the catalytic performances. This is particularly true for electrocatalysis, as many studies have shown that tuning the surface strain of nanocatalysts is efficient for boosting the electrocatalytic performances of the ORR, including the long-term stability.[418]

3.1.2. Charge transfer

If the Fermi levels of the metal and the carbon support differ, an electron transfer occurs when the metal-support interface is created to shift the local work function at the catalytically active outer surface. This electronic transfer results from the formation of polar chemical bonds with more or less ionic character between the support surface atoms and the metal atoms. The Fermi level pinning leads to a Schottky barrier and a rectifying behavior of the contact at the junction between the metal and the support. The extent of the interaction depends on the nature of the metal, but much more on the particle size and the nature of the support.[419-421] On carbon supported catalysts, the modification of the electronic properties of metal atoms can be measured either directly or indirectly.[422] Direct methods include Raman,[423-426] XAS[423,427-429] or XPS spectroscopies.[430-435] In Raman, a shift of the G-band in graphitic materials toward higher wavenumbers is indicative of an electron-accepting metal, and a shift toward lower frequencies is indicative of an electron-donating metal (Figure 22a). For Au NP on graphene, it was reported that the shift of the 2D peak is more significant than that of the G peak.[436] For fullerene, the

$A_g(2)$ mode is particularly sensitive to charge transfer.[91] Changes in the NEXAFS intensities of π* resonance in the C K-edge and metal edge spectra are also characteristic of charge transfer.[423] XANES experiments also evidenced charge redistribution between carbon support and Pt NP (charge redistribution between C *2p*-derived states and Pt *5d* bands),[437] since during synthesis the change of oxidation state during all reaction steps can be followed.[438]

In XPS, a shift of the metal binding energy towards higher energy will result in a charge transfer from the metal to the support, when a downshift is indicative of a reverse charge transfer (Figure 22b). However, due to the dependence of binding energy with particle size (enlargement of NP size induces a positive shift in the binding energies),[439] such a conclusion should be taken with care. Indirect methods include calorimetry or infrared spectroscopy with probe molecules such as CO.[440] In FTIR, the CO band will shift toward lower frequencies if an increased back-donation to π* anti-bonding orbitals of CO occurs through a charge transfer from the support to the metal (Figure 22c). Electron microscopy equipped with energy-dispersive X-ray spectroscopy (EDS) and EELS is also a powerful tool that can be used to reveal metal-carbon interactions.[441] More sophisticated techniques combining synchrotron-radiation photoelectron spectroscopy, scanning tunneling microscopy and DFT calculations can also been used to precisely quantify the charge transfer per metal atom.[442]

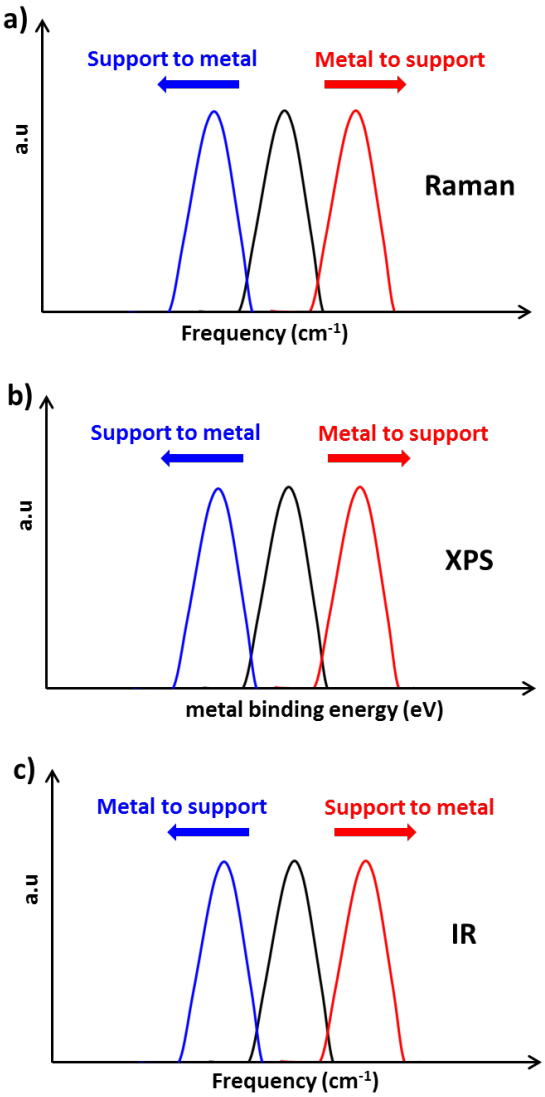

Figure 22. Different methods allowing the direct or indirect identification of charge transfer: a) Raman spectroscopy (G-band in the Raman spectra of graphitic materials); b) XPS (binding energy of core-electrons of the metal particle); and c) FTIR (ν_{CO} band of CO adsorbed on metal).

Obviously, the quantification of charge transfer on carbon-supported catalysts should take into account the possibility of metallic NP oxidation upon air exposure. This is particularly important for small NP,[443] which are very sensitive to air oxidation, even for noble metals such as platinum, and should give rise to significant charge transfer.[442] To avoid confusion related to

oxidation or NP size, comparison of charge transfer between different catalysts deposited on carbon supports should be ideally performed avoiding air oxidation and with using similar metal NP size.

It is important noting that due to strong charge screening, the excess of charge on metal NP could be expected to accumulate at the direct contact interface between the NP and the support (sub-nm short-range charge transfer), which moderately contributes to catalysis. It is thus obvious that topology of the NP should affect the extent of electron transfer, and in the case of nearly flat NP, in which most of the metal atoms are in contact with the support; they would suffer higher electron transfer. However, electrostatic considerations suggest that, in addition to the short-range charge transfer at the metal-support interface, electronic equilibration with the support leads to a long-range direct charging of the NP outer surface (at a distance up to several nanometers away from the interface) bypassing the strong charge screening of the metal particle (Figure 23).[444]

This long-range charge transfer depends on the size, shape, and proximity of the neighboring NP. If the influence of NP size and shape on catalyst performances (activity, selectivity and stability) is well documented in supported catalysis, the influence of inter-particle distance has been much less studied, particularly for carbon-supported catalysts. However, some studies on Pt/C or Pd/C electrocatalysts have clearly evidenced an influence of Pt inter-particle distances on the catalytic properties.[445-453] It has also been proposed that the NP might be polarized, with the top metal atoms bearing one type of charge and those at the interface, an opposite charge.[454]

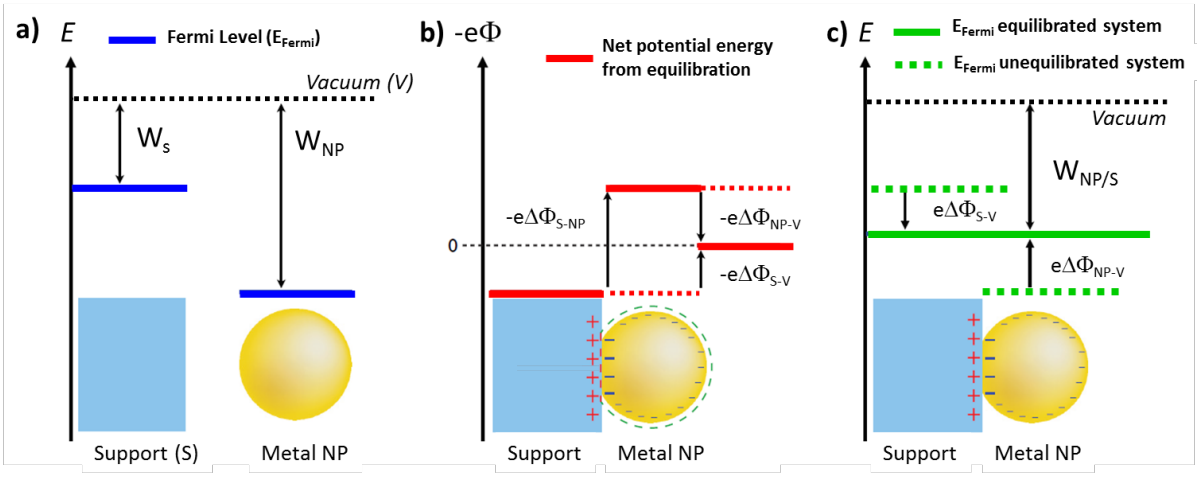

Figure 23. Schematic of energy levels, work functions (W), and electrostatic potentials during the outer surface charging of supported NP. a) Work functions of the isolated support and NP; b) illustration of the additional net electrostatic energy contribution (−e)Φ resulting from electronic equilibration. An outer surface charge on the NP is necessary to account for the difference $\Phi_{NP\text{-}V}$ of the net electrostatic potential levels in vacuum and inside the NP, respectively; and c) the equilibrated system is characterized by a common Fermi level and work function $W_{NP/S}$. Adapted from ref [444].

If the interfacial charge transfer between the metal (or semi-conductor) and the support can play a pivotal role in thermal catalysis, it is even more critical in photo-[455-457] and electro catalysis,[458,459] where metal-carbon support interactions are central. Thus, in electrocatalysis, the activity depends largely on interfacial charge transfer from the metal core to the carbon support that influences the electronic interactions between the catalyst surface and reaction intermediates, and varies with the structures and morphologies of the metal and the carbon. As far as the carbon support is concerned, the charge transfer will strongly depend on the structure of the carbon (sp^2 *vs* sp^3, orientation of the graphene layers, number of graphene layers, presence of defects) and on its surface chemistry.

Interfacial charge transfers between metals and sp^3 carbon materials (diamond-like) have been poorly studied.[460-462] Significant charge transfers were predicted between diamond and Al, Cu, Ni, Ti, V, and Zn. For fullerene and particularly C_{60} ($sp^{2.23}$ hybridization), the strong electron acceptor property of fullerene provides significant charge transfer from the metal to the C_{60}.[91,463-465] In the case of Ru NP, the electron deficient ruthenium in Ru/C_{60} catalysts shows a specific selectivity in hydrogenation of nitrobenzene[466] and cinnamaldehyde.[467] For these carbon materials, as for the sp^2 family, the direction of the charge transfer depends on the work functions of the supports and the metals. The work function of conventional carbon materials ranged between 4.15 and 6.5 eV.[468-473] These values can change significantly with the presence of defects or the introduction of heteroatoms like O, N, S, B, or P. The work function of transition metals ranged between 2 and 5.6 eV for polycrystalline surfaces.[474-476] Figure 24 shows the work functions of conventional carbon materials and selected transition metals relevant for catalysis. From this figure it appears clearly that the direction of the charge transfer will be the same (from the metal to the support) whatever the metal with fullerene C_{60}. For the other carbon materials, it will depend mainly (variations of work function with NP size exist)[477,478] on the nature of the metal. Charge density analyses are usually performed on top of DFT calculations using several partitioning schemes, the Bader analysis[479] being one of the most widely used as in ref [480]. The charge transfer estimates of a single atom in interaction with a graphene ML are reported in Table 1, and according to ref [481] they can also vary for different adsorption sites. The general trend follows that of the atom's electronegativity: for non-metallic atoms, the charge transfer is from graphene to the atoms, whereas for metals it is the opposite. For some metals, very low electron transfer was found.

H 0.15		*Electron transfer from graphene to adatom*														**He**
Li 0.86	**Be** 0.05											**B** 0.43	**C** 0.02	**N** 0.68	**O** -0.84	**F** -0.59	**Ne**
Na 0.62	**Mg** 0.10	*Electron transfer from adatom to graphene*										**Al** 0.81	**Si** 0.72	**P** 0.38	**S** -0.04	**Cl** -0.41	**Ar**
K 0.63	**Ca** 0.87	**Sc** 1.1	**Ti** 1.1	**V** 0.98	**Cr** 0.84	**Mn** 0.70	**Fe** 0.58	**Co** 0.48	**Ni** 0.45	**Cu** 0.19	**Zn** 0.03	**Ga** 0.55	**Ge** 0.43	**As** 0.22	**Se** -0.01	**Br** -0.34	**Kr**
Rb 0.60	**Sr** 0.82	**Y** 1.04	**Zr** 1.16	**Nb** 0.97	**Mo** 0.72	**Tc** 0.53	**Ru** 0.37	**Rh** 0.24	**Pd** 0.17	**Ag** 0.10	**Cd** 0.03	**In** 0.57	**Sn** 0.43	**Sb** 0.27	**Te** 0.9	**I** -0.28	**Xe**
Cs 0.61	**Ba** 0.86	**Lu** 1.23	**Hf** 0.82	**Ta** 0.83	**W** 0.72	**Re** 0.48	**Os** 0.35	**Ir** 0.22	**Pt** -0.00	**Au** -0.11	**Hg** 0.01	**Tl** 0.48	**Pb** 0.37	**Bi** 0.24	**Po**	**At**	**Rn**

greater than 0.5

lower than 0.5

Table 1. Charge density analysis of Bader for various elements of the classification period adsorbed on graphene.[480]

Basically, all TM -with the exception of Au-[482-484] transfer electron density to the graphene layer; and this charge transfer is more acute for early TM, and more attenuated for late TM due to electronegativity increase.[137] The evolution of the work function of graphene doped by different metal adatoms and at different concentrations was investigated, and in general, the work function drops significantly before reaching saturation. In the case of Cs, the work function saturates at 2.05 eV at 8% doping.[485]

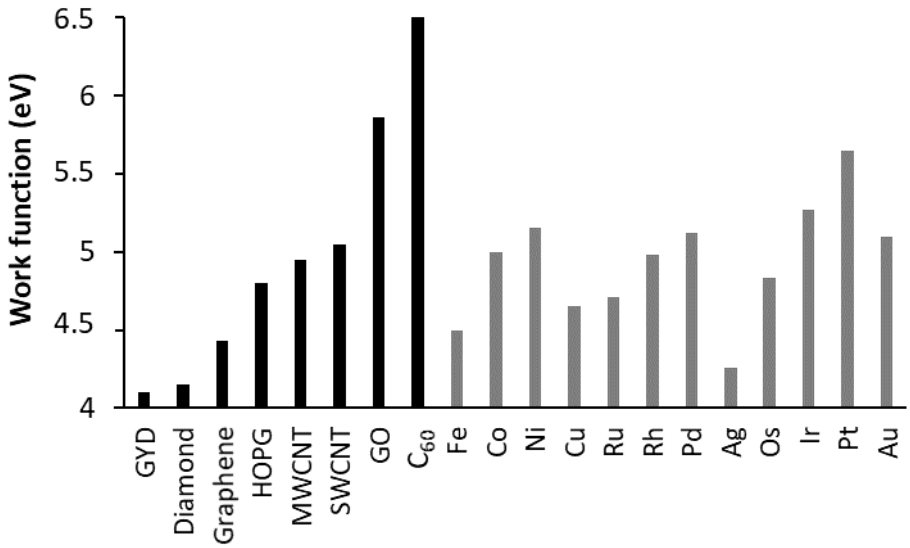

Figure 24. Work functions of conventional carbon materials (multi-walled CNT = MWCNT; single-walled CNT = SWCNT; graphdiyne = GDY) and selected 3d, 4d and 5d transition metals.

It is worth remembering that in graphite the carbon 2*p*-π electron density is symmetrically distributed with respect to the flat graphene plane, whereas the curvature of the CNT induces a re-distribution of the electron density, with most of the wave function being outside of the curved graphene layers. Thus, due to the difference in the surface electron density, interactions and charge transfer at the CNT surface are expected to be different from interaction and charge

transfer at a flat graphene layer (Figure 25). In the case of 3*d* TM atoms, a similar tendency in charge transfer variation from Sc to Cu was observed in the case of graphene and CNT, although larger charge transfer were generally observed in the case of CNT.[103] The influence of curvature on charge transfer has not been studied into details, and remains unclear. An old report proposed that, in the case of single Ni atoms, the direction of the charge transfer changed from Ni atom to carbon on graphite, to carbon to Ni in the cases of a small diameter CNT.[109] However, more recent reports have shown that for Ni atoms, the direction of the charge transfer is always from Ni atom to carbon whatever the support, graphene (0.42-0.65 e^-/Ni),[481,486] or small diameter CNT (0.21-0.73 e^-/Ni).[487,488]

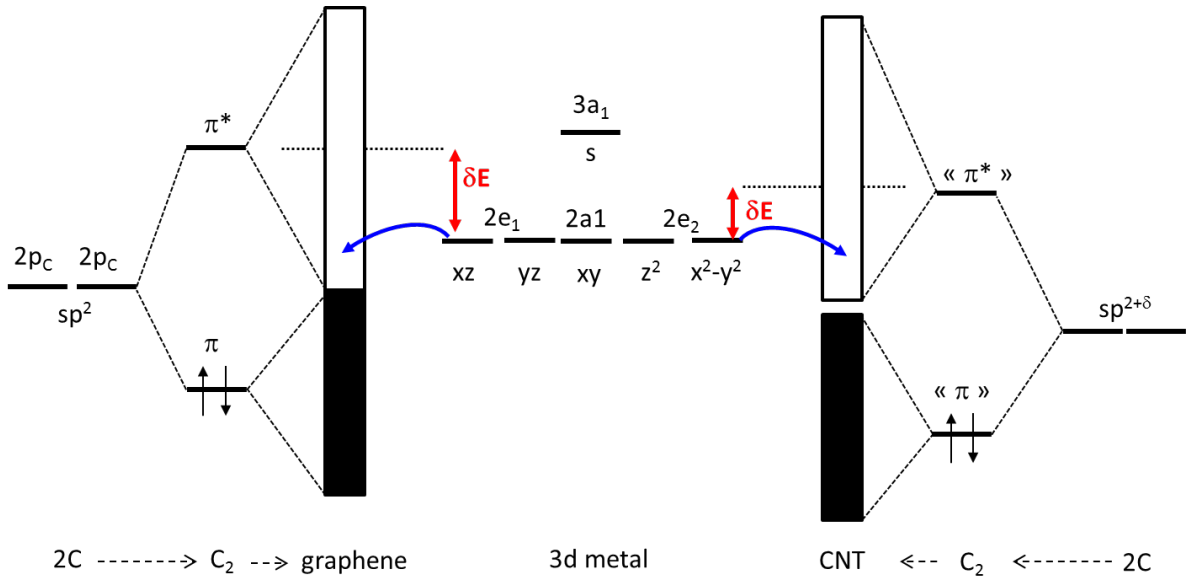

Figure 25. Schematic interaction diagrams between the graphitic surfaces and single TM adatoms. DoS are represented by boxes (black ones represented the occupied levels). The energy difference, δE (in red), is related to the interaction intensity between vacant surface π* orbitals and 3*d* metal orbitals ($2e_2$): when δE decreased, the interaction intensity increased. The curved arrows (in blue) symbolize electron transfer from the metal to the graphitic surfaces. In

the curved graphitic surface (CNT), π-like levels had sp^3 character, in contrast with the graphene levels (sp^2), and they are lower in energy.

Clearly here, computational details' choices, such as Tight-Binding approach *vs* DFT calculations scheme, as well as partitioning electronic density methods used to estimate the charge transfer, appear to be crucial. Besides, most of the studies published so far used metallic CNT, however differences in charge transfer are expected when the CNT are semi-conducting ones.[103] For a single Ru atom adsorbed in exohedral positions, the charge transfer (from the metal to the CNT) tends to increase with the tube diameter; when it is inside the tube, the charge transfer decreases with the diameter.[489] Since they are sharing the same valence electron configuration it is not surprising that Ru and Fe atoms behave similarly in terms of charge transfer with CNT, Fe atom outside the tube giving more electronic density than inside, due to a better overlap between the *d* orbitals of Fe and the *p* orbitals of the neighboring C atoms.[103,113,490]

Clusters have also been analyzed, particularly with platinum. For Pt_{38} clusters interacting with a graphene surface, small charge transfer (< 0.2 e^-) have been reported from the support to the metal but with a significant polarization effect inside the cluster.[491-493] The facet interacting with the support losses charge upon adsorption, which together with the charge obtained from the graphene layer is redistributed to the rest of the Pt atoms. Similar results were obtained on Pt_{13-147} clusters.[494] Very low charge transfers were reported for Pt_4,[495] Pt_{13},[454] and Pt_{37},[496] on graphene as well. Higher value of charge transfer were provided by Rao *et al*. for Pt_{40} clusters,[497] Auer *et al*. for Pt_{10-37} clusters[498] and by Song *et al*. for a Pt_7 cluster (~0.65 e^-).[499] Surprisingly, changes in charge transfer direction were given by Skylaris *et al*. (overall charge being transferred from Pt_{13-309} clusters to the graphene support),[500] Huang *et al*. for Pt_{4-27} clusters,[501]

and Wang *et al*. for Pt_4 clusters.[502] Again, those differences are the consequence of the wide variety of different computational settings used, which should make the reader very cautious about final statement concerning charge transfer estimate, see for instance the discrepancies obtained in the case of non-covalent doping of graphene for various electronic integration methods.[503]

Changes in charge transfer due to curvature effect compared to a graphene surface were reported by Song *et al.* in the case of a Pt_7 cluster: the higher the curvature, the higher the charge transfer is.[499] Charge transfers from CNT to Pt_{14} clusters[504] and Pt atom[505] were also reported, as expected since the value of the Pt work function is higher than CNT's one. However, for a Pt_4 cluster on CNT, the charge transfer was estimated from Pt to carbon,[506] as well for Pt_{3-13} clusters.[507,508] In that latter case, it was also shown by Mulliken charge analyses that the charge transfer amount (per Pt atom) decreases with the size of the Pt cluster (Pt_3: 0.27 e^-/Pt; Pt_7: 0.17 e^-/Pt; Pt_{13}: 0.14 e^-/Pt), in agreement with experimental observations.

For metals presenting a lower work function than Pt, like ruthenium, the charge transfer occurs from the metal to the carbon support. Such charge transfers were reported for Ru_{13} on CNT (1.1 e^-/Ru_{13})[509] and graphene (0.9 e^-/ Ru_{13}),[510] as well as for Ru_6 on CNT (1.7-2.2 e^-/Ru_6).[489] In this case, it was also shown that the charge transfer is enhanced for double-walled CNT compared to single-walled CNT. Similar charge transfers from the metal to the carbon support were reported for Mn_7/G,[142] Ti_{13}/G,[511] and Fe_{1-5}/G.[512] As expected, the metal atoms in the interfacial layer have much more positive/negative charges (according to the direction of the charge transfer) than those in the upper layer, as shown on Figure 26 for Pt_{37} and Ru_{13} clusters.

On functionalized graphene, the adsorption of Pd clusters, induces a clear signature in Raman spectra, typical of a donation from the metal to the graphene support,[513] when the *d*-band center of Pd clusters clearly shifts to closer values to the Fermi level.[514] For a single Pd adatom or a

single embedded one in a SV on graphene, the charge transfer is 0.4 and 0.2e^-, respectively from the metal to the support.[320]

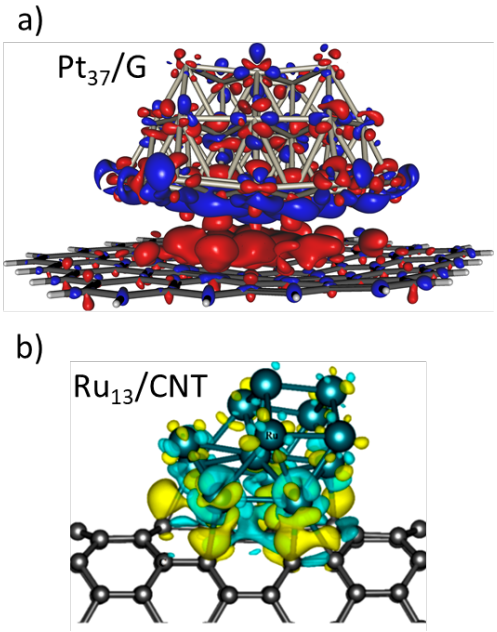

Figure 26. Contour plots of differential charge density of: a) Pt_{37}/G; in blue (red), increase (decrease) of the electron density upon interaction; reprinted with permission from ref [498] Copyright 2019 from AIP Publishing; and b) Ru_{13}/CNT. The charge accumulation region is rendered in yellow, while the charge depletion region is in blue. Reprinted with permission from Zhou, S.; *et al. J. Phys. Chem. C* **2018**, *122*, 9091-9100.[509]. Copyright 2018 from the American Chemical Society.

In the same work, polarization effect with a depletion of the electronic density at the edges of the cluster is already experienced for a Pd_6 system adsorbed on a SV-G. This phenomenon is reinforced for larger clusters, which are able to present spin-polarized edges. Considering a Pd single atom or a dimer adsorbed on CNT sidewalls, it has proposed that one type of donor-acceptor delocalization occurs: a Pd *4d* to C *2s* donation and C *2p* to Pd *5s* back-donation. For

large Pd NP deposited on stacked cup CNF, a $Pd^{\delta+}$ phase was clearly evidenced by XPS, and corroborated by DFT calculations.[430]

For oxides such as TiO_2, the charge transfer occurs from the carbon support to the TiO_2[457,515-518] Variation of work function between φ = 4.70-6.44, 4.62-6.76, and 4.51-5.62 eV have been reported for the TiO_2 anatase and rutile (001), (101) and polycrystalline surfaces, respectively.[519] Therefore, carbon support (G, CNT) enable charge transfer and inhibit the charge recombination process when combined with TiO_2-based photocatalysts.[518] Charge transfers from graphene to other oxides such as CoO and Co_3O_4 or MnO_2 were also found.[520] In the case of $CoFe_2O_4$ NP on GO sheets, a significant charge transfer from GO to the oxide NP was measured.[393] The significant change in the work function value of GO (φ = 4.60 eV), after decoration with $CoFe_2O_4$ NP (φ = 7.70 eV) confirms a shift of the highest valence bands towards the Fermi level.

As already mentioned, introduction of topological defects in carbon materials such as carbon vacancies or Stone Wales defects significantly affect their electronic properties. This results in higher binding energy of metals to the carbon[167] and in modified charge transfer. Particularly, the introduction of vacancy defects, which generates acceptor-like states will enhance the charge transfer and hence the Coulomb interaction between metal and graphene.[521] When compared to pristine carbon supports, the charge transfers are systematically higher on carbon surface presenting carbon vacancies. Thus, on a SV-G, more electrons are transferred from the Pt, Pd, Au, and Sn adatoms to the carbon atoms at the defect site.[522] Significant charge transfers from the TM to carbon supports containing SV or DV were reported for Au,[523] Rh,[524] W,[525] and Pd.[526] Higher charge transfer were also provided for clusters on defective carbon supports compared to defect-free supports, such as for Pd_{13}/SV-G (SV-G = single vacancy on G) compared to Pd_{13}/G,[527] Pt_{13}/SV-G compared to Pt_{13}/G,[501,528-530] Pt_{2-80}/SV-G compared to Pt_{2-80}/G,[531] Pt_{1-6}/SV-CNT compared to Pt_{1-6}/CNT,[502] Ru_{13}/SV-G compared to Ru_{13}/G,[510] Cu_{4-13}/SV-

G compared to Cu_{4-13}/G,[532] Au_{1-5}/SV-G and Fe_{1-5}/SV-G compared to Au_{1-5}/G and Fe_{1-5}/G.[512] In all these works, the charge transfer is from the metal to the carbon support. Similar charge transfers were reported for Fe_{13} and Al_{13} clusters on SV-G,[533] and Pd_{1-5} on SV-G[526] and DV-G.[534] For a Pd_4 cluster interacting through 3 Pd atoms on a DV-G, the three lower Pd atoms have a Mulliken charge of +0.65-0.72 e^-, while the upper atom has a Mulliken charge of -0.39 e^-.[534] With the increasing size of point defects in the carbon support, both the binding strength and charge transfer between the NP and carbon-support increase.[528,529]

The orientation of the carbon layers will also play a significant role on the charge transfer in carbon materials. A strong interaction of Pt clusters with the graphene edges of CNF was evidenced by X-ray absorption near-edge structure, EXAFS, and MD simulations.[535] In a study on graphene electrochemistry, it was shown by Pavlov *et al*. that the rate of electron transfer at graphene zigzag edges is ~4 times larger than far from edges.[536] Much faster electron transfer at graphene edges than on the basal plane was also reported by Shi *et al*.[537] Larger charge transfer could thus be anticipated on edges. A much lower charge transfer was obtained for Ag adatom adsorbed on graphene (0.022-0.029 e^- from Ag to graphene) than for Ag on armchair (0.34 e^- from Ag to graphene) or zigzag edges (0.25 e^- from Ag to graphene).[538] MD calculations were also used to compare the interaction of Pt_{100} and Pt_{400} clusters with the surface of CNT and CNF (Figure 27).[371] For Pt/CNF, the chemical attraction from the edge atoms causes Pt atoms to detach from the cluster and deposit separately on the carbon surface. This phenomenon is much more important for Pt_{100} clusters compared to Pt_{400}. On CNT, due to the poor interaction between Pt atoms and the π system, this phenomenon is not observed. For small NP (1.2-1.4 nm), a higher charge transfer from Pt to the support was experimentally evidenced from XPS analyses: Pt $4f_{7/2}$ = 72.14 eV for Pt/CNF and Pt $4f_{7/2}$ = 71.97 eV for Pt/CNT.

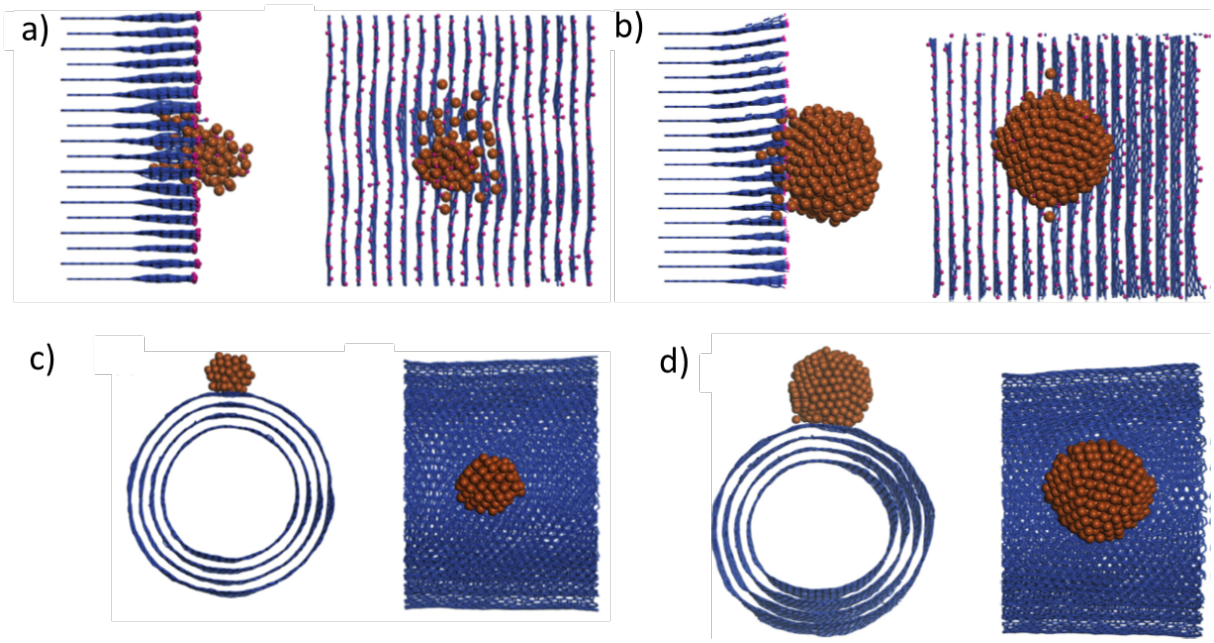

Figure 27. Snapshots of the geometries of: a) Pt_{100} cluster interacting with CNF; b) Pt_{400} cluster interacting with CNF; c) Pt_{100} cluster interacting with CNT; and d) Pt_{400} cluster interacting with CNT. Reprinted with permission from ref [371]. Copyright 2018 from Elsevier.

However, some studies, based on finite models, based on relatively large PAH molecules to mimic carbon-support, reported a charge transfer from the support to Pt.[412,498] For Pt_{37} clusters adsorbed on the basal or prismatic surface of graphite, the charge transfer observed was even higher in the case of the basal plane (0.89 e^-/Pt) compared to the prismatic surface (0.76 e^-/Pt).[498] In the case of Ni_{55} clusters interacting with small carbon surfaces, negative charges always accumulate on edge carbon atoms; on the contrary, non-edge carbon atoms have little charges.[112] Model sizes and charge transfer estimate methods should be extensively studied to leave those uncertainties for large clusters.

Heteroatom doping of the carbon support induces electron re-localization and local variations in the DoS of the support, thus producing an increase or a decrease of the work function.[472,539] This modification unavoidably influences the charge transfer, the hybridization between the

electronic states of the metal and those of the support, and definitively the metal-support interactions (Figure 28).[422]

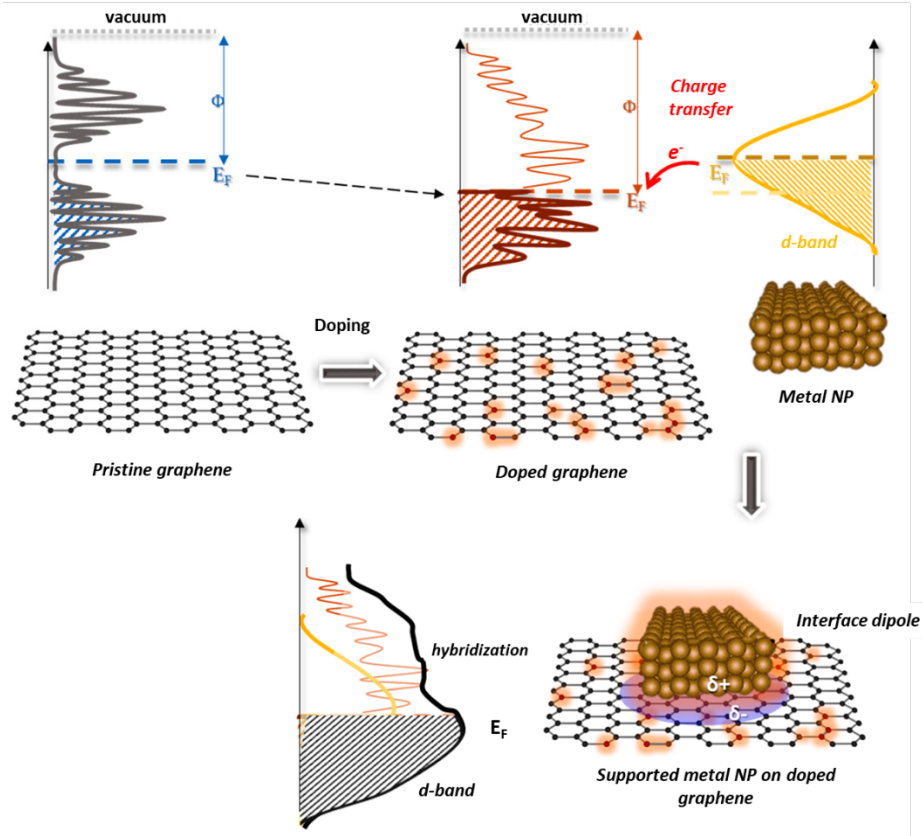

Figure 28. Effect of the introduction of heteroatoms in the carbon support on metal NP carbon support interactions. Reprinted from ref [422].

It has been shown that the work functions of heteroatom-doped graphene (doping by carbon atom substitution) obey a periodic law, except for O-doped graphene (Figure 29a).[540] The values of the work function vary with dopant concentration. Thus, the work function of B-doped graphene increases monotonically with the increase of the doping concentration, while for N-G, doping makes the work function decrease (Figure 29b). However, the type of doping for a given element also affects the work function values. If doping by atomic substitution can

provide general trends, the real doped-carbon support generally contains different types of groups for a given element. For instance, it has been shown that, in the case of O-doping of rGO, individual functional groups (carbonyl, epoxy, hydroxyl) have a different effect on the work function, with dominant effect for carbonyl groups (Figure 29c,d).[541]

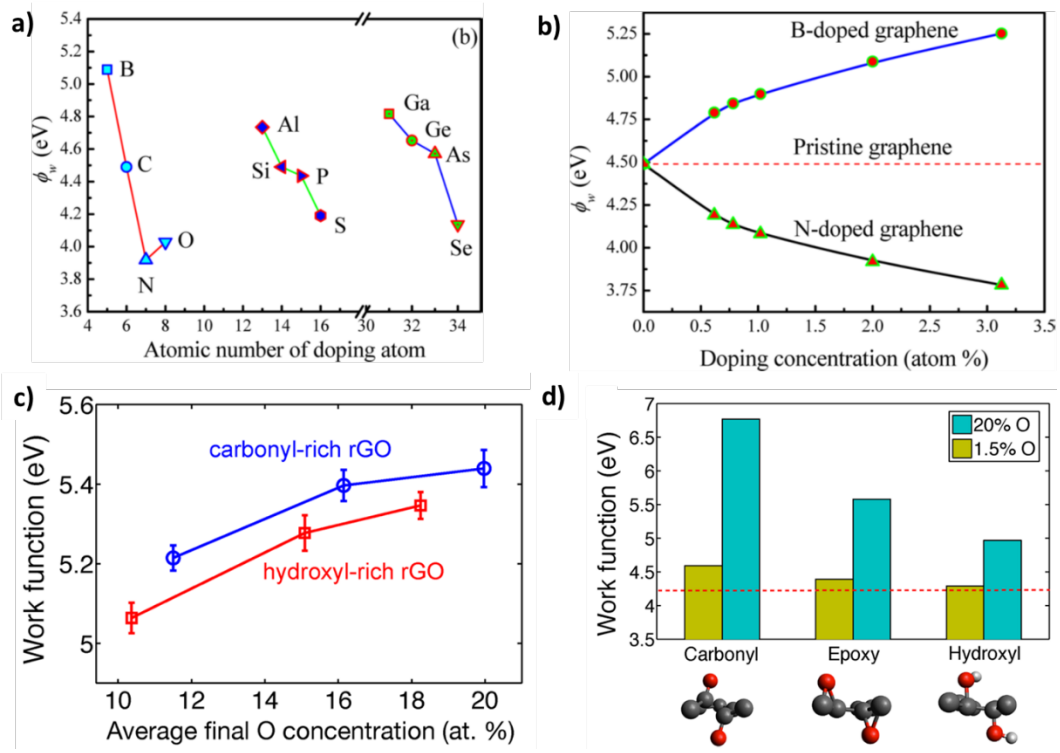

Figure 29. a) Work function *vs* the atomic number of the substituting atom for heteroatom-doped graphene, for a single substitution in 5 × 5 supercell; b) work function as a function of doping concentration for B and N-doped graphene; reprinted with permission from Gholizadeh, R.; *et al*. *J. Phys. Chem. C* **2014**, *118*, 28274-28282.[540] Copyright 2014 from the American Chemical Society; c) calculated work function of carbonyl-rich and hydroxyl-rich reduced graphene oxide structures with different oxygen content; and d) effect of individual functional groups on the work function of reduced graphene oxide, for two different total oxygen concentrations. Reprinted with permission from Kumar, P. V.; *et al*. *ACS Nano* **2013**, *7*, 1638-1645.[541]. Copyright 2013 from the American Chemical Society.

Similarly, the work function of graphene correlates strongly with the site and amount of doped nitrogen. Nitrogen atoms doped at a graphitic site lower the work function, while nitrogen atoms at a pyridinic or a pyrrolic site increase the work function.[542]

The adsorption of Cu adatoms on (defective or not) CNT functionalized with various surface functional groups, including atomic oxygen (-O), hydroxyl (-OH) and carboxyl (-COOH) groups, was investigated by DFT.[543] The oxygen functional groups can either promote charge transfer from Cu to carbon atoms, or directly interact with Cu as surface ligands. Three types of CNT were studied, pristine CNT (CNT-P), CNT with Stone-Wales defects (CNT-SW) and CNT with single vacancies (CNT-SV). Figure 30 shows the charge transfer from copper to carbon obtained on these different surfaces with or without oxygen functionalities. Among the functional groups investigated, the carboxyl functional group resulted in the largest and most consistent increase in the Cu binding energies and charge transfer on both pristine and defective CNT.

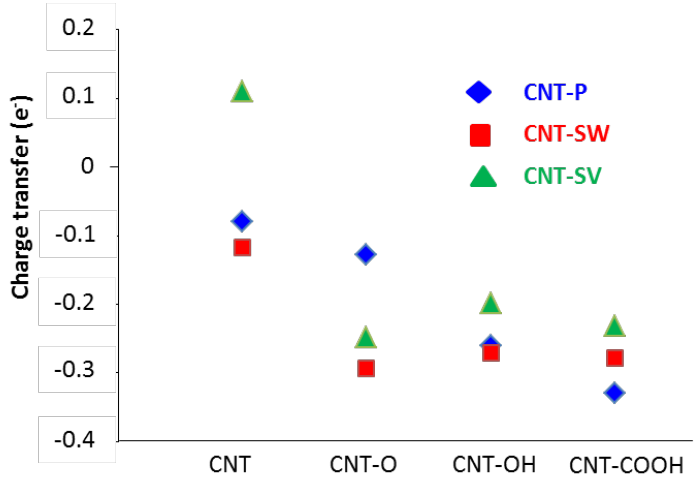

Figure 30. Charge transfer from Cu to carbon (negative sign meaning that Cu transfers electron to carbon) for a Cu adatom on various carbon surfaces.[543]

Charge transfers were also reported from Pt adatoms to oxygen functionalized carbon supports;[544] an increase concentration of oxygen containing groups leading to a shift of the *d*-band center of Pt toward lower energy. Similarly, higher charge transfer from an iron single atom to graphene was obtained if carboxylic groups were introduced on the support surface.[545] Charge transfer ($0.2e^-$) from a gold adatom to oxygen decorated double vacancy of graphene was also computed.[546] Charge transfer from 3*d* TM adatoms to a C_3N_4 support have been reported too.[547] In the case of Pd single atoms, the charge transfer was much larger in the case of Pd_1/C_3N_4 than in Pd_1/G.[548] It has also been shown by XPS analysis that the presence of nitrogen functional groups favors the reduction of Pd on CNT, suggesting an electronic promoter effect.[549]

For Pt clusters, charge transfer from the metal to the carbon support have been systematically reported for B-,[550] N-,[289,427,550] S-,[289] and O-doping.[252,492] For supports bearing oxygen containing groups it was shown that for a Pt_{38} cluster, the overall charge transfer increases slightly in the following order: $G_{\text{-COOH}} > G_{\text{-OH}} > G_{\text{pristine}}$.[492] On graphene oxide, the charge transfer from a Pt_{13} cluster to the support depends on the oxygen's concentration on the support.[252] The metal atoms in the interfacial layer have important positive charges, whereas those in the upper layer have a negative charge, as shown on Figure 14d. The overall charge tends to increase with oxygen concentration's increase of the support. Surprisingly, an inverse tendency was observed in the case of large Pd NP on CNF.[430] In the case of gold NP on GO, the electrons are better transferred from GO (higher work function) to Au NP (lower work function) when the Au NP size decreases.[421] Charge transfer from the metal to the support were reported for Pd atoms and clusters on N-G[551] or N-doped nanotubes.[431,552] For a Pd single atom, the nature of the interaction of the N-containing groups (pyridine) with the metal is of σ-type donation from the filled π-orbital of the N atom to the empty *d*-orbital of the Pd atom, and a π

back-donation from the filled Pd atomic *d*-orbital to the π* antibonding orbital of the N atom. The interaction of pyridine N with Pd is characterized by a charge transfer typical of a covalent chemical bond with partial ionic character, consistent with the chemical shift observed in the Pd *3d* core level of divalent Pd.[431] XPS and DFT results have shown that the charge may change according to the type of nitrogen functionalities present on the surface. Higher charge transfer (and binding energy) were obtained for Pd_4 clusters and Pd atoms on N-pyridinic site than on N-graphitic sites.[431,552] In the case of Pt NP, the N-graphitic sites were identified from XPS data as electron donors and the pyridinic as electron acceptor sites.[553,554] XPS analyses have clearly shown that on N-doped CNT, the charge transfer decreases with the increase of the Pt loading and thus NP size (Figure 31).[432]

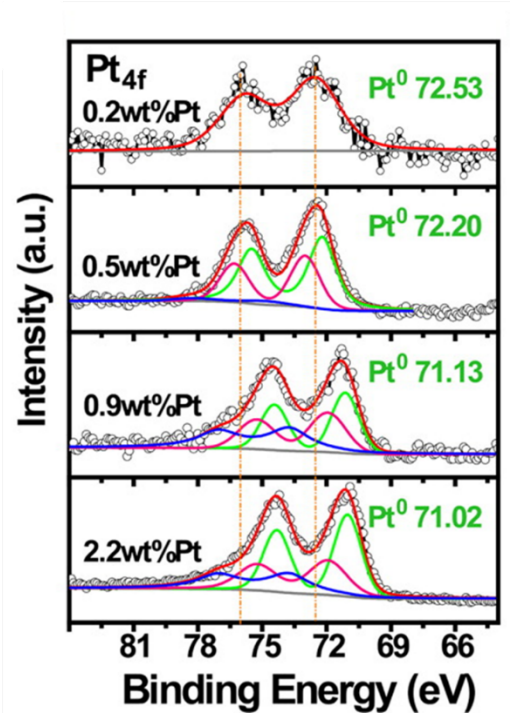

Figure 31. Pt 4f XPS spectra of Pt/N-CNT with varied Pt contents. Reprinted with permission from Shi, W.; *et al*. ACS Catal. **2016**, *6*, 7844-7854.[432]. Copyright 2016 from the American Chemical Society.

Cobalt atoms and NP were deposited on pristine graphene, B-G and N-G.[555] For Co_1/G, the junction of Co and graphene induces a charge transfer from graphene to Co due to the difference in work function between Co (ϕ = 5 eV) and graphene (ϕ = 4.5 eV). This results in an increase in the electron density of Co and a lack of electrons in graphene, as confirmed by XPS and Raman. On N-G, quaternary N incorporated into the support induced an upshift of the Fermi level and more electrons were transferred from N-G to Co. In the case of B-G, there is a downshift of the Fermi level and electron transfer occurs in the opposite direction (from Co to B-doped support). DFT was used to investigate the interaction between Rh and Ti metal adatoms and dimers with pyridinic and pyrrolic sites in graphene.[556] Charge transfer occurs from metal to substrate in all cases. Both metals prefer pyridinic defects for initial adsorption of the first atom. The charge transfer is approximately 0.68 e^- for Rh adatom, and between 1.63 and 1.76 e^- for Ti. In the case of dimers, there are around 0.85 e^- for Rh_2, and 2.57 e^- for Ti_2 being the metal atoms positively charged.

Charge transfer and catalyst preparation – Spontaneous metal reduction

If, of course, the charge transfer can influence the catalysis, it should also influence the preparation of the catalyst. Indeed, it has been shown that metal NP can form spontaneously on semiconductor and metal surfaces *via* galvanic displacement from aqueous metal salt solutions.[557] On carbon surfaces, this phenomenon can also occur, and the spontaneous reduction of metallic salts on sp^2 carbon surfaces is a well-identified phenomenon. Pd salts reduction during carbon supports' impregnation with aqueous solutions of H_2PdCl_4 is known for many years.[27,558,559] This reduction of Pd occurs because of the reductant power and the conductivity of the carbon support. Because no evolution of carbon oxides is observed upon the process, adsorption of Cl^- ions was proposed to compensate for the number of electrons

consumed from the carbon to reduce palladium.[27] The presence after the impregnation step of two forms of adsorbed Pd, metallic and ionic, determines the bimodal size distribution of the metal. The spontaneous gold or platinum NP (7-16 nm) formation on CNT sidewalls, when CNT are immersed in corresponding metal salt ($HAuCl_4$ or Na_2PtCl_4) solutions has been reported by Dai *et al*.[560] The work function of CNT has been determined to be ≈ 5 eV (Figure 24). The Fermi level of a CNT is therefore about +0.5 V above the potential of a standard hydrogen electrode (SHE), and it is well above the reduction potentials of $AuCl_4^-$ and $PtCl_4^{2-}$, which are +1.002 and +0.775 V *vs* SHE, respectively. Thus, the relative potential levels rationalize the spontaneous electron transfer from the CNT (oxidation) to the metal ions and their reduction. Interestingly, smaller Pt NP size (5 nm) were obtained when using oxidized CNT, since the oxygen-containing functional groups play a role in anchoring Pt NP.[561] Spontaneous reduction from H_2PtCl_6 aqueous solution ($E_{Pt/PtCl6}^{2-}$ (*vs* saturated calomel electrode (SCE)) = 0.68 V) at 348 K produces Pt NP (10-20 nm) on the sidewalls of oxidized CNT (E_{vsSCE} = 0.34 V).[562] Similar NP sizes were obtained from the same precursor in the inner cavity of CNT, and an EXAFS study has confirmed that the reduction of Pt^{4+} was due to the electron transfer from CNT.[428]

A broad Au NP size distribution (few nm to 200 nm) was obtained on rGO by spontaneous reduction from an aqueous solution of $HAuCl_4.3H_2O$.[563] Smaller Au particles were obtained on rGO from $AuCl_3$ in nitromethane.[564] The reduction potential of graphdiyne was estimated to be about -0.33 V *vs* SHE, which was lower than that of $PdCl_4^{2-}$ ions (+0.62 V *vs* SHE), suggesting its ability as support for the deposition of Pd NP (4 nm) from K_2PdCl_4 (Figure 32).[565] The use of oxidized graphdiyne allows the production of smaller Pd NP (1.4 nm). CNT and GO, which present reduction potentials of +0.5 V and +0.48 V *vs* SHE respectively, were also used for the spontaneous reduction of H_2PdCl_4 aqueous solutions to produce 2-3 nm Pd NP.[566] Palladium NP were obtained on CB, CNT and carbon spheres by the spontaneous reduction of $PdCl_2$ with

oxygen-functional groups on the carbon surfaces.[567] Quinone moieties have been proposed to dominate the redox property of pyrogenic carbon, both quantitatively and kinetically, although it was not possible to completely rule out the contributions of other types of redox-active groups that possess slower electron transfer kinetics.[568]

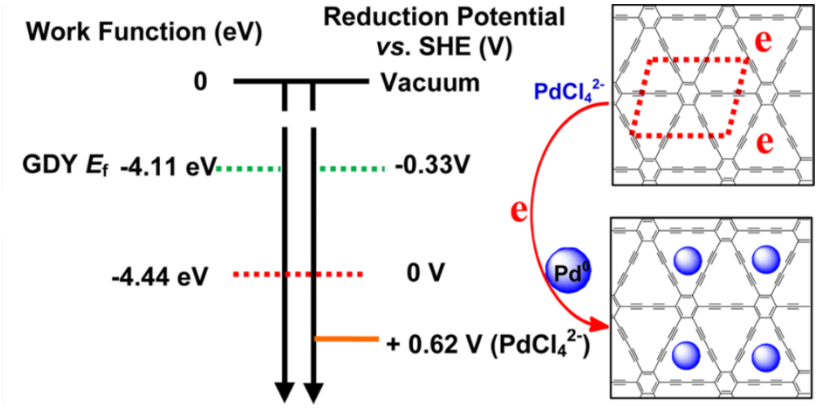

Figure 32. Schematic illustration of spontaneous reduction of $PdCl_4^{2-}$ on graphdiyne (GDY) to produce Pd NP (blues spheres). Reprinted with permission from Qi, H.; *et al*. *J. Am. Chem. Soc*. **2015**, *137*, 5260-5263.[565]. Copyright 2015 from the American Chemical Society.

$Pd(OAc)_2$ or oxime carbapalladacycle were also used as precursor for the production of 2-10 nm NP on CNT.[569] Silver NP (40-50 nm), nanocubes or Ag dendrites were also obtained by spontaneous reduction of $AgNO_3$ on GO. The geometry control was achieved by using different concentrations of silver ions, sampling orders and different reaction times at room temperature.[570] This galvanic displacement method can also be used for the preparation of oxide NP. Thus, the spontaneous redox reaction between MnO_4^- ions ($KMnO_4$ aqueous solution) and CNT provides MnO_2 NP[571] or MnO_2 coating on the CNT surface.[572] Cu_2O NP (4-5 nm) were produced on CNT from the spontaneous reduction from $[Cu(NH_3)_4]^{2+}$ aqueous solution.[573] Both the pH of the medium and the defect density on CNT influence the oxidation potential of CNT.

Spontaneous reduction of $Ru^{(VI)}$ (K_2RuO_4) was also reported for the deposition of RuO_2 NP (1-3 nm) on CNT.[574] Finally, it is interesting noting that such a phenomenon is relevant for other fields than catalysis, since electron transfer reactions are the basis of bio-geochemical cycles and govern most of geochemical and biochemical transformations.[568]

Charge transfer and catalysis – The metal-support interaction

Charge transfer also influences the adsorption of reactants on the metal surface, and can consequently influence the catalytic activity. Table 2 presents significant results obtained in various studies showing the influence of charge transfer on chemisorption of various molecules or on the catalytic activity in different reactions. For small molecules activation, it has been shown that the binding energy of H_2, [325,575,576] CO,[334,577] or O_2[578] to metallic clusters or atoms decreases when the electronic density on the metal decreases because of the charge transfer from the metal to the support (downshift of the metal *d*-band center). This phenomenon is more pronounced for small clusters, which are more sensitive to charge transfer, and should be maximal for isolated atoms. As far as H_2 dissociative chemisorption is concerned, there is a lack of theoretical study to investigate the influence of charge transfer on dihydrogen dissociation. The works carried out on Pd deposited on carbon supports have shown that small clusters, for which charge transfer from Pd to the support are generally reported, should not spontaneously dissociate H_2. In the case of small Pt clusters (for which weak charge transfers are generally obtained), spontaneous dissociation of H_2 was reported;[579] however the influence of charge transfer on this reaction, by addition of vacancies to the support, was not systematically investigated.[580]

The influence of charge transfer between the metal and the support or between the catalyst and the reactant on the catalytic activity has also been investigated for various reactions on

carbon-supported catalysts (see Table 2 for representative examples). The low-temperature oxidation of CO, has prompted broad interest due to the imperious demands of reducing CO emissions from transportation, power plants, and industrial and domestic activities. The mechanism of this reaction has been investigated by DFT for many single metal (or semi-metal) atom catalysts including: Pt,[301,581-583] Au,[523,584] Fe,[248,585-588] Co,[589,590] Ni,[591] Cu,[592,593] Pd,[303,594,595] Mn,[596] V,[597] Cr,[598] W,[525] Ti,[599] Al,[600,601] Ge,[601] and Zn[602]. According to the single atom catalyst model, the reaction for the first CO oxidation can follow a Langmuir-Hinshelwood (LH), Eley-Rideal (ER) or termolecular Eley-Rideal (TER) mechanism (Figure 33a). In the case of the LH mechanism, after the first oxidation, an oxygen atom remains on the metal, and the second CO oxidation reaction usually follows a traditional ER mechanism with low activation energy. On graphene support, the presence of vacancy or nitrogen atoms induces a charge transfer from the metal to the support, which effectively regulates O_2 and CO adsorption. The single atom catalyst transfers charge to the oxygen molecules and activates it. The charge transfer to CO (LH mechanism) is usually smaller than to O_2. For metal single atoms deposited on SV-G, DV-G, graphyne (GY) or GO that follow an ER mechanism, a correlation between the charge transferred from the metal to the O_2 molecule and the activation energy for the CO oxidation is found (Figure 33b). This activation energy is varying between 4.6 and 39.2 kcal.mol^{-1} according to the catalyst used (Figure 33a). Interestingly, very low activation energy were reported in the case of gold single atoms on CNT.[523] In the case of metallic clusters, the adsorption of the cluster on carbon vacancy allows to reduce the activation energy for CO oxidation, thanks to a significant shift of the *d*-band center. Relatively low activation energy for CO oxidation (2.3-11.5 kcal.mol^{-1}) were reported for Pt,[603,604] Au,[603] Pd[170] and bimetallic AuPd[605] clusters supported on graphene supports.

Table 2. Influence of charge transfer on adsorption of molecules or catalytic reactions on carbon-supported metal catalysts.

Reaction	System	Charge transfer influence	Ref.
Hydrogen chemisorption	M_1/G	Whatever the metal from Sc to Ni, charge transfers from M_1/G to H_2 are obtained. The dissociative chemisorption is the favored mode for the most electropositive atoms Sc and Ti. The stability for the molecular chemisorption increases from left to right, as a general trend, due to minor π back-donation.	102
	Ni_{13}/G	Dissociative chemisorption is a non-activated process on Ni_{13}, whereas an activation barrier is observed on Ni_{13}/G. The charge density depletion on the Ni_{13}/G, due to its accumulation around the Ni_{13}-graphene interface, makes H_2 dissociation electronically less favorable. When H co-adsorption is considered, a redistribution of charge density is observed, decreasing the activation barrier.	606
	Rh_2/N-G Ti_2/N-G	In both cases, there is a charge transfer from the metal to the nitrogen-doped graphene ($0.7e^-$ for Rh and 1.7 e^- for Ti). The molecular chemisorption is barrierless and the dissociative chemisorption needs a small activation energy for both systems.	556
	Ti_1/N-G	Computed electronic structures show that the charge transfer between the acceptor levels in absorbents and the Ti *d* orbitals plays a crucial role for metal dispersion and subsequence hydrogen adsorption. Upon H_2 adsorption, a certain amount of electrons are transferred from Ti *d* orbitals to the antibonding σ* of H_2.	607
	Pd_{2-4}/N-G	Positive charges were found on Pd for the Pd_{2-4}/N-G systems, with the higher charge on the Pd_2/N-G. The dissociative chemisorption needs an activation energy for all the systems; the lower activation energy was measured for the Pd_2/N-G.	608
	Pd_{1-4}/N-G	Positive charges were found on Pd for the Pd_{1-4}/N-G systems. The dissociative chemisorption needs an activation energy for all the systems.	551
	Pd_{1-6}/SV-G	The charge transfer from Pd atom to the graphene vacancy ($0.4\ e^-$) is higher than from a Pd atom to defect-free graphene ($0.16\ e^-$). In both cases, the hydrogen molecule becomes activated but the H-H bond is not broken. The H_2 molecular adsorption energy is weaker on Pd_1/SVG (4.8 $kcal.mol^{-1}$) than on Pd_1/G (22.1 $kcal.mol^{-1}$) and on free Pd atom (25.8 $kcal.mol^{-1}$). Activation energy for dissociative adsorption of H_2 on Pd_{3-6}/G have been calculated at 16.1 $kcal.mol^{-1}$ (Pd_3/G), 10.6 $kcal.mol^{-1}$ (Pd_4/G), 6 $kcal.mol^{-1}$ (Pd_5/G) and 6.9 $kcal.mol^{-1}$ (Pd_6/G).[609]	325
	Pd_9/CNT	The dissociative chemisorption is easier on the Pd_9/CNT than on the free Pd_9 cluster.	610
	Al_{4-13}/SV-G	Upon adsorption of the Al clusters on graphene SV, charge is transferred from Al to the support. The total charges on the unsaturated carbon atoms of the vacancy increase upon the adsorption of the H_2 molecule. No correlation is made between the activation energy for dissociative chemisorption and the charge transfer.	611
	Ru_1/CNT	Bader analysis reveals that Ru transfers a charge of $0.4e^-$ to single-walled CNT, allowing Ru atoms to act as adsorption center for H_2 molecules. The first H_2 molecule is dissociatively adsorbed (E_{ads} = 25.4 $kcal.mol^{-1}$) and subsequent H_2 additions (3 molecules) show that H_2 molecules are molecularly adsorbed.	612

CO chemisorption	Au_{20}/CNT	There is a charge transfer from the CNT to the gold cluster. The CO adsorption on the gold surface is accompanied by transfer of electronic density back into the CNT.	483
	Pt_2/G	The carbon support enhances the back-donation of electrons to the 2π* orbitals of the CO molecule. The high electron density and the partial negative charge on the Pt atoms not directly bonded to the support increase the repulsion between the 5σ orbital of the CO and the s-d orbitals of the metal, and consequently reduces the Pt-CO interaction.	440
	Pt_1/G_{ox}	The Pt-C bond strength is more due to charge transfer than frontier-orbital hybridization. The larger the concentration of oxygen containing groups is, the stronger is the Pt binding energy to the support. The chemisorption energy of CO to Pt is lower when increasing the concentration of oxygen containing groups (downshift of the Pt *d*-band center). This downshift suppresses the coupling between the Pt *d*-band and the CO 2π* state.	544
	Pt_1/G_{ox}	The CO-Pt binding energy is significantly lower when -COOH groups are present compared to -OH group.	613
	$Pt_{13,55,147}$/G	Low charge transfer from the support to the Pt clusters. The presence of the support induces a weaker CO adsorption, but this effect rapidly decreases with the cluster size increase and it is only significant for Pt_{13}/G.	494
	Pt_4/CNT	Charge transfer from the Pt_4 cluster to the CNT. The wide variety of dynamic reactions of CO molecules with Pt_4 clusters makes difficult to correlate charge transfer and CO binding energy.	506
	Pt_6/C	In comparison to the interaction of CO on the unsupported Pt cluster, the interaction energy is higher on the oxygen terminated sp^3 diamond-like surfaces, and lower on sp^2 and sp^3 domains of C surfaces.	614
	Pt_{13}/SV-G	A downshift of the Pt_{13} cluster *d*-band center upon immobilization on the graphene SV decreases the binding energy of CO to the cluster compared to unsupported or supported clusters on perfect graphene. Upon CO adsorption, there is a significant charge transfer from the cluster to both the graphene support and the CO.	577
O_2 chemisorption	Pt_{13}/SV-G	Upon adsorption of the Pt_{13} on graphene SV, charge is transferred from Pt to the support. With the adsorption of O_2 on Pt_{13}/SVG, strong charge depletion of the Pt atom at the interfaces of Pt-C and Pt-O_2 is observed. The Pt_{13}/SVG shows an O_2 adsorption energy (53 kcal.mol^{-1}), which is weaker than the O_2 adsorption energy on the free Pt_{13} cluster (90.4 kcal.mol^{-1}).	578
	Au_{2-7}/N-G	When O_2 is adsorbed on Au_{2-7}/N-G, the adsorption energies are largely increased compared with those on bare clusters. The increased adsorption energies significantly facilitate the electron transfer from Au *d*-orbital to π* orbital of O_2, and weaken the O-O bond.	615
	$Pt_{1,4}$/SV-G $Pt_{1,4}$/N-V-G	Charge transfer from Pt to graphene is larger for N-doped support (more positive charges on Pd, which upshift the *d*-band centers toward the Fermi level). The activation barrier for O_2 dissociation is lower on Pt_4 than on Pt_1. The positive charged sites favor the dissociation of O_2. The energy barrier for O_2 dissociation decreases almost linearly with the increase of Pt positive polarized charges.	616
CO oxidation	Pt_4/SV-G Au_8/SV-G	The reaction barrier of CO oxidation catalyzed by Au_8/G or Pt_4/G (LH mechanism) is 69 kcal.mol^{-1} and 11.5 kcal.mol^{-1}, respectively; when adsorbed on SV, the reaction barrier greatly reduced to 4.6 kcal.mol^{-1}and 3 kcal.mol^{-1}, respectively. When adsorbed on Au_8/SV-G or Pt_4/SV-G, the O-O bond of O_2 is significantly elongated (electrons transfer to the antibonding 2π* orbital of O_2) thanks to a significant charge transfer from the metal (0.7 and 0.9 e$^-$ for Au_8 and Pt_4, respectively).	603

		Pt_{13}/SV-G Pt_{13}/DV-G	The rate limiting step involves the CO*-assisted O_2 activation (ER mechanism), followed by formation of O*-O-C*-O intermediates that decompose to O* and CO_2. The strong interaction of Pt_{13} with SV and DV lowers the activation energy by more than 4.6 kcal.mol^{-1}compared to unsupported clusters. The strong charge transfer from the metal to the support is accompanied by a downshift of the Pt_{13} *d*-band center, a weakening of the Pt-CO bond, and in keeping with the Sabatier principle, lowers the barrier for CO oxidation.	604
		$Pd_{4,8}$/SV-G	The presence of vacancies on graphene (from 1 to 6) induces charge transfer from Pd to the support (from +0.10 e$^-$ for G to +0.75 e$^-$ for G with 6 vacancies); causing a substantial downshift of the *d*-band center of the Pd cluster, thus decreasing CO adsorption. For a Pd_8/6VG, the energy barrier is 11.3 kcal.mol^{-1}.	170
		Pd_mAu_n/G	The charge transfer from the metal varied between 0.01 e$^-$ for Au_7 to 0.29 e$^-$ for Pd_7. In bimetallic clusters the charge transfer increases with the Pd content up to 0.3 e$^-$. On Au-rich clusters, CO can directly react with the adsorbed O_2 with a low barrier of ~ 4.6 kcal.mol^{-1}. The Pd-rich clusters are unreactive for the reaction at low temperature.	605
		Pt_1/SV-G Pt_1N-G	Facilitating the charge transfer between Pt and O_2 increases the efficiency of the rate-limiting step in the oxidation reaction. Pt_1/SV-G and Pt_1/N-G exhibit high catalytic activity for CO oxidation with a modest energy barrier of 8.3 and 9.2 kcal.mol^{-1}, respectively. On both supports, the first CO oxidation occurs via a LH mechanism. The second CO oxidation proceeds easily *via* an ER mechanism.	301
		Mn_1/DV-G	The reaction mechanism on graphene with divacancy embedded with transition metal from Sc to Zn was studied. Mn_1/DV-G shows the best catalytic properties for CO oxidation. The charge transfer from the Mn atom to the adsorbed molecules plays an important role for the CO oxidation. The first CO oxidation occurs via a LH mechanism (E_a = 9.4 kcal.mol^{-1}). The second CO oxidation proceeds easily *via* an ER mechanism (E_a = 3.9 kcal.mol^{-1}).	596
		Fe_1/SV-G	There is about 0.27 e$^-$ charge transfer from the Fe atom to graphene, and about 0.4 e$^-$ charge transfer from Fe_1/SVG to O_2. The preferred mechanism is ER, in which the CO molecules directly react with the adsorbed and activated O_2 (E_a = 13.4 kcal.mol^{-1}).	585
		Fe_1/GO	There is a significant charge transfer from Fe to GO (1.21 e$^-$). There is also charge transfer from Fe_1/GO to O_2 (0.58 e$^-$) and CO (0.17 e$^-$). In the LH mechanism (not kinetically favorable), the reaction occurs between the co-adsorbed O_2 and CO species, while in the ER mechanism, the CO molecules directly react with the adsorbed and activated O_2 (E_a = 22.6 kcal.mol^{-1}).	248
		Fe_1/GY	There is about 0.26 e$^-$ charge transfer from the Fe atom to graphyne. There is about 0.34 e$^-$ electron transfer from Fe_1/GY to O_2 and 0.09 e$^-$ to CO. The reaction proceeds *via* the ER mechanism with an energy barrier of as low as 4.8 kcal.mol^{-1} in the rate-limiting step.	586
		Au_1/SV-CNT Au_1/DV-CNT	The defective CNT surface promotes electron transfer from the atom to O_2. For the LH mechanism, the barriers of the rate-limiting step are calculated to be 0.4 and 1.15 kcal.mol^{-1} for Au_1/SV-CNT and Au_1/DV-CNT, respectively. To regenerate the active sites, an ER-like reaction occurs to form a second CO_2 molecule.	523
Hydrogenation	1,3-butadiene	Pd/CNT Pd/CNF	The interaction of Pd with CNF edges resulted in electron transfer from the metal to the support. The strong interaction of Pd^{2+} species with the edges of graphite results in the stabilization of Pd in an ionic state. An increase in the fraction of Pd^{2+} in the catalysts was responsible for a decrease in both the activity and selectivity of Pd/C catalysts.	617

		Pd_1/SV-G	The Pd atom is located in a vacancy decorated with oxygen atoms. The Pd atom has a charge of +0.30 e^-, suggesting a significant cationic character due to charge transfer from Pd to the support. H_2 is activated by the Pd atom, but not dissociated. The activation energy on Pd SAC for hydrogenation (30.7 kcal.mol^{-1}) is higher than on Pd(111). The 1-butene desorption is dynamically driven (repulsion between the incipient 1-butene and Pd SAC).	618
		Pd_1/G-N Pd_1/G	The higher valence of Pd species (Pd^{2+} and Pd^{4+}) on G-N compared to Pd_1/G (Pd^{2+}) is likely due to a charge transfer from Pd to the support. Consequently, the Pd_1/G is much more active than Pd_1/G-N. Pd_1/G showed a higher 1-butene selectivity than that of Pd_1/G-N.	548
	Acetylene	Pd_1/G-N Pd_1/G	The Pd_1/G is much more active than Pd_1/G-N. Pd_1/G showed a lower ethylene selectivity (75%) than that of Pd_1/G-N (98%).	
		Pd_1/N-G	In-situ XPS revealed that the considerable charge transfer from the Pd NP to the support likely plays an important role in the observed high selectivity towards ethylene.	619
	Cinnamaldehyde	Pd/CNF	Support with different amount of oxygen groups were used. Higher charge transfer from Pd to the support were observed for highly defunctionalized support. Higher selectivity towards hydrocinnamaldehyde were obtained at low $Pd^0/Pd^{\delta+}$ ratio.	430
		Pd/C	Pd was deposited on graphite felt (GF) and oxygen functionalized graphite felt (OGF). The $Pd^0/Pd^{\delta+}$ ratio is higher on GF. The $Pd^{\delta+}$ metal phase, is due to the electron transfer from Pd atoms to the OGF. The higher stability of the Pd/OGF related to Pd/GF is reported. No difference in selectivity is reported.	620
		Ru@C_{60}	Significant charge transfer from Ru to C_{60} is observed. The electro-deficient Ru NP catalyzed the acetal formation from reaction of cinnamaldehyde with the alcoholic solvent.	
	Nitrobenzene	Pd/CNT Pd/N-CNT	The Pd catalysts display electron-deficiency depending on the intensity of the metal-support interaction between Pd and pyridinic nitrogens. Due to the strong adsorption of nitro-groups on electro-deficient Pd NP, it is possible to tune the catalytic activity through the charge transfer from Pd to the support (the charge transfer from Pd to the support is determined either by nitrogen content or by the distribution of nitrogen groups).	552
		Pt/CNT Pt/N-CNT	A charge transfer from N species to Pt NP is observed, generating an increased electron density on Pt. The Pt/N-CNT catalyst is more active and more selective than the Pt/CNT or than a Pt/O-CNT catalyst.	432
		Ru@C_{60}	Significant charge transfer from Ru to C_{60} is observed. Electron-deficient Ru NP supported on Ru fulleride allow the successive and chemoselective hydrogenation of nitrobenzene to aniline and then to cyclohexylamine.	466
		Ni@C_{60}	The reduced electron density of metallic Ni leads to excellent aniline selectivity.	621
	Nitrophenol	Pd/G Pd/N-G Pd/B-G	On Pd/B-G the Pd NP are electro-deficient whereas they are electron rich on Pd/N-G; Pd/G being an intermediate situation. The corresponding activity order was: Pd/B-G > 4 Pd/G > Pd/N-G. The negatively charged 4-nitrophenolate is preferentially adsorbed onto the electrophilic Pd on B-G.	555
	Levulinic acid	Ru/C	Ru NP (1.2-9 nm) were deposited on various supports. There is a progressive increase in electron-deficiency of Ru NP with the decreasing of the particle size. The smaller Ru NP have the higher TOF.	622
		Ru/AC Ru/G	Ru/G showed a lower binding energy (Ru_{3p} - 462.6 eV) and higher concentration of Ru(0) (36.8%) in comparison with Ru/AC (462.8 eV and 29.4%, respectively). The interaction of graphene and Ru NP can	623

			upshift the *d*-band center of Ru, which thus facilitates the H_2 activation, providing enhanced hydrogenation activity.	
		Ru/AC Ru/rGO	Ru/rGO showed a lower binding energy (Ru3d - 280.5 eV) in comparison with Ru/AC (280.75 eV), and a higher catalytic activity. The electron-rich state of Ru NP on rGO promotes the electron transfer from the Ru *d* orbital to the CO $2\pi^*$ antibonding orbital.	624
	CO	Co/G Co/N-G Co/B-G	On Co/G and Co/N-G the charge transfer occurs from the support to Co whereas for Co/B-G it is the opposite. The electron-rich Co in Co/N-G facilitates the back-donation, leading to an excess of charge in the CO molecule and a weakening of the intramolecular bonds compared to Co/G and Co/B-G. The weakened CO bond facilitates H-assisted CO dissociation. The opposite trend was expected with the Co/B-G system.	555
Hydro-isomerization of butene		Pd_9/CNT	The stabilizing effects produced by the presence of CNT compared to a bare Pd_9 cluster strongly increases the but-1-ene adsorption energy on palladium.	625
Acetylene hydrochlorination		Au/N-AC	Increasing the electron density of Au^{3+} *via* charge transfer from N atoms to the Au^{3+} active sites increases HCl adsorption and inhibit the of Au^{3+} to Au^0 reduction during the reaction, and hence improves the catalytic stability.	626
O_2 reduction reaction (ORR)		Pd/N-G Pd/G	The electron transfer in Pd/N-G from Pd to the support increases with the concentration of pyrrolic groups. The Pd/N-G performed 8 times better than Pd/G or commercial Pt/C for the ORR in alkaline media.	627
		Ag_8/N-G	The supported cluster is more active than the unsupported one due to significant decrease in O_2 adsorption energy and higher charge transfer to O_2. Electron transfer from Ag to O_2 leads to the elongation of the O-O bond, which facilitates the breaking of this bond.	628
		Pt/G	The ORR activity is related to the partial charge transfer from Pt to G. The extent of charge transfer can be modulated by controlling the defect concentration of the support.	629
		Pt_{13}/G	Defective graphene support lowers the activation energy for O_2 dissociation from 8.5 to 3.7 kcal.mol^{-1} by promoting charge transfer from Pt atoms to O_2, and the energy barrier of the rate-limiting step by reducing the stability of HO* species. Charge is transferred from the Pt_{13} cluster to both defective graphene and ORR intermediate species.	332
		Pt_1/G Pt_1/SV-G Pt_1/DV-G	There are 0.07, 0.27, and 0.36 e^- charge transfer from single Pt atom to graphene support in Pt_1/G, Pt_1/SV-G, and Pt_1/DV-G, respectively. Electro-deficient Pt atoms are more efficient for oxygen activation. Additionally, the oxygenated intermediates are adsorbed more strongly on Pt_1/G and Pt_1/SV-G (difficult desorption of OH*). The weaker adsorption of intermediates on the prepared Pt_1/DV-G catalyst makes all elementary steps of ORR much easier.	630
		Pt/S-G	The sulfur doping modulates the electronic properties of Pt, resulting in a downshift of the *d*-band center. This negative shift allows for improved ORR kinetics of Pt/S-G in comparison to Pt/G.	631
		Pt/O-CNT Pt/N-CNT Pt/S-CNT	The higher charge transfer from the metal to the support was measured for the Pt/O-CNT sample prepared by a non-covalent approach. The higher activity was obtained for the Pt/O-CNT catalyst.	632
		Pt-N-rGO	The interaction between Pt and N allows for an electronic transfer from Pt to the carbon support. DFT results reveal that the O-O distance is much elongated in the case of the N-doped support, which suggests lower barriers for O_2 dissociation.	493

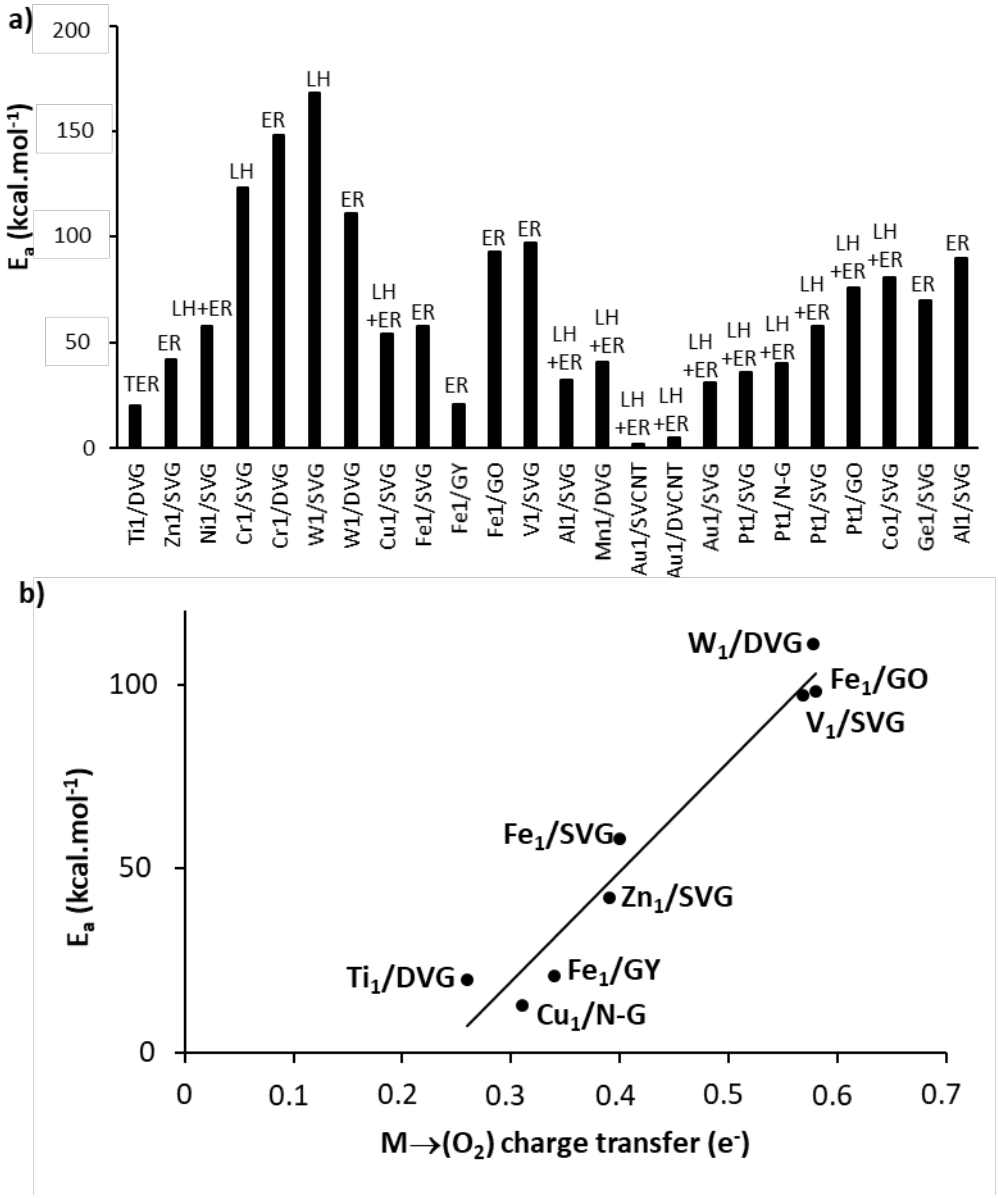

Figure 33. a) Activation barriers for the CO oxidation for various graphene-supported single atom catalysts, and the corresponding mechanisms; and b) relation between the charge transferred from the metal to O_2 and the activation barrier for CO oxidation for graphene-based metal single atoms following an ER mechanism (from refs. [248,525,585,586,593,597,599,602]).

As far as hydrogenation reactions are concerned, we have already seen that hydrogen activation is more difficult when the charge transfer leads to electro-deficient particles/atoms. The studies reported in Table 2 deal mainly with experimental works and are not systematically

combined to DFT calculations. The charge transfer is most of the time measured from XPS. For 1,3-butadiene[548,617,618,633] and acetylene hydrogenation,[548,619] the results obtained are consistent with the fact that electro-deficient NP are poorly active for the hydrogenation of these substrates. However, for acetylene hydrogenation, the use of electro-deficient Pd single atoms plays an important role in the observed high selectivity towards ethylene. For cinnamaldehyde hydrogenation, more contrasting results have been reported. Comparison between catalysts supported on graphite and activated carbon have shown that some metals present a cinnamyl alcohol (COL) selectivity that can be modulate *via* charge transfer. Thus the COL selectivity of Pt and Ru is increased on graphite or CNT because of the charge transfer to the metal, which enhances π* CO backbonding.[634-636] A poor selectivity towards COL was obtained on PtRu/CNF catalyst ($Pt^{(0)}$ = 62 at%, $Pt^{(II)}$ = 34 at%, $Pt^{(IV)}$ = 4 at%) compared to a PtRu/CNT catalyst ($Pt^{(0)}$ = 82 at%, $Pt^{(IV)}$ = 18 at%).[637] On the other hand, Ir and Pd have high intrinsic selectivity (the former to COL, the latter to HCAl), which are weakly modified by the charge transfer.[620,634] On Pd/CNF however, an influence of charge transfer was reported; a higher selectivity towards HCAL being obtained at low $Pd^{(0)}/Pd^{\delta+}$ ratio.[430] For nitrobenzene or p-chloronitrobenzene hydrogenation, electron-deficient NP are generally preferred to reach high activity and high selectivity towards the aniline.[552,638] DFT calculations performed on Ru@C_{60} catalysts have shown that in addition to an electropositive metal, the presence of hydrides on the metal is a key parameter that allows to influence the chemisorption of nitrobenzene *via* the nitro group.[466] Charge transfers between electro-deficient Ni_1/N-G single atom catalyst and the reactants (H_2 and nitrobenzene) were also evidenced by DFT, and proposed to explain the high activity and selectivity of this catalyst.[639] Interestingly, electron-deficient Pd NP deposited on highly defective carbon support were reported to be more active and more selective for the hydrogenation of 3-nitrostyrene to 3-ethylnitrobenze than Pd NP on CB.[640] For the reduction of o-nitroaniline to 1,2-benzenediamine on Au NP of different size (5-40 nm) deposited on GO,

the electrons are better transferred from GO (higher work function) to Au NP (lower work function) when the Au NP size decreases.[421] The larger charge transfer from GO to the smaller Au NP leads to a higher catalytic activity, since the enhanced electron transfer should promote the hydrogen dissociation on the Au NP surface. For levulinic acid hydrogenation to γ-valerolactone on Ru/C catalysts (a structure sensitive reaction), higher activity have been most of the time obtained on electron-rich Ru NP.[623,624,641] Higher activity were also obtained in the case of electron-rich Co NP for CO hydrogenation. Transfer hydrogenation of vanillin was studied in water phase with formic acid (FA) as hydrogen donor on Pd/C and Pd/N-C catalyst.[642] The Pd/NC catalyst shows a higher concentration of $Pd^{\delta+}$ ($Pd^0/Pd^{\delta+}$ = 34/66), a higher activity, stability and selectivity compared to Pd/C ($Pd^0/Pd^{\delta+}$ = 71/29). It was proposed that in this catalyst, the $Pd^{\delta+}$ are responsible for HCOOH decomposition, and the Pd^0 of the hydrogenation. Influence of charge transfer was also reported for Pd NP on graphitic carbon nitride, which were used for transfer hydrogenation of nitroarenes using formic acid as hydrogen source.[643] This catalyst was much more active than a commercial Pd/C catalyst. Theoretical calculations have confirmed the superiority of $Pd_{1,2}$/SV-G catalysts compared to Pd clusters or Pd(111) and Pd(211) surfaces for formic acid dehydrogenation.[644] Another study has also shown that the metal support interaction can be used to shift the *d*-band center of Pd in N-doped carbon, the smallest *d*-band center resulting in the lowest energy barrier for formic acid dehydrogenation.[645] Electro-deficient metal NP were also demonstrated to be superior in the case of dehydrogenation of ammonia borane on Pt/CNT catalysts.[646] It was proposed that on oxidized CNT (large amount of oxygen surface group) the charge transfer occurs from the CNT to Pt, whereas on defective CNT (defects and small amount of oxygen surface group), the charge transfer occurs from the Pt to the support. Large difference in activity were also reported for decalin dehydrogenation over Pt/CNT and Pt/CNF catalysts due to charge transfer.[371] For small NP (< 2nm), the larger charge transfer from Pt to CNF compared to CNT is the most significant

factor for activating the reactant while avoiding the strong adsorption of the product because of the low *d*-band center of Pt NP. When Pt NP are larger than 2 nm, the particle size effect becomes preponderant. For oxidation of 5-hydroxymethylfurfural on Au/C catalyst, better activity were obtained on electro-deficient Au NP.[647]

In the ORR, charge transfer derived from the support generates noticeable impact on the electrocatalytic activity of Pt. As for other reactions, this effect is difficult to de-correlate from other effects (size, facet, or strain effects).[648] In most studies it has been shown that the Pt-C interaction is attributed to an electron transfer from Pt to the carbon support.[391] Enhanced charge transfer have been obtained by the use of defective or functionalized carbon supports. The electro-deficient Pt NP generally allow: i) to lower the activation energy for O_2 dissociation by promoting charge transfer from Pt atoms to O_2; and ii) to lower the adsorption of OH species, which would further enhance the catalytic activity given that strongly adsorbed OH is a well-known catalyst poison. Additionally, DFT calculations have shown that the strong Pt/N-G interaction led to no changes in NP-support separation (elongation of NP-support distance) with the presence of adsorbed molecular oxygen.[493] The authors suggest that this strong interaction may be responsible for a decrease in the resistance for electron transfer between the cluster and the support, facilitating the electrochemical reactions. These tendencies have been confirmed in many studies for metal single atoms[630,649] and NP.[332] However, for small Pt_n clusters ($n < 6$), which are exceptionally dynamic and can easily change shapes upon binding different adsorbates, dynamics can break the scaling relationships for ORR.[650] For electrocatalytic oxidation reactions (methanol,[651-653] glycerol,[553] formic acid,[553] H_2[654] or CO[553,554]), several studies have reported an increase of the electron density on Pt NP, thanks to charge transfer from the carbon support to the metal, that leads to a higher activity. In that context, the use of boron-doped carbon support, which allows electron transfer from the support to Pt has been generally favored.[652-654] In the HER on carbon supported metal catalysts, charge transfer has

also been analyzed as a pivotal parameter. For Rh sheet on graphene, in the interaction region, there is a pronounced charge transfer from Rh to graphene (0.52 e^- per atom) that allows for the downshift the *d*-band center position by about 0.24 eV.[655] This downshift, resulting of a weak hybridization of Rh-*d* orbitals with H-*s* orbital, facilitates the HER activity. For single metal atoms on graphene, the high activity was attributed to a charge transfer between the metal atom and the adsorbed H atom, which significantly promotes the proton adsorption and the reduction of kinetics.[656-658] DFT calculations were used to compare the charge transfer during H adsorption on Pt_{44} and Pt_1/N-G system.[657] The electron transfer from each surface Pt atom of Pt_{44} to H is 0.1 e^-, which is much less than that of the single Pt atoms (0.421 e^-). For MoS_2[659] or CoS_2[660] nano-sheets on graphene the charge transfer was proposed to occur from the support to the sulphides.

TiO_2 photocatalysis (photo-oxidation and photo-reduction) is one of most appealing and attractive technologies for the degradation of pollutants. TiO_2 modification with carbon materials (AC, fullerene C_{60}, CNT, graphene) is a very effective route for excellent photocatalytic activity (including for water splitting[661-663]), and comprehensive reviews on the subject have already been published.[518,663-668] TiO_2 photocatalysis depends on the creation of an electron-hole pair after the light absorption with an energy equal to or greater than the band gap of TiO_2. A first problem of TiO_2 is its wide band gap (3.2 and 3.0 eV for anatase and rutile TiO_2, respectively) that makes it active only under UV-light irradiation. Another problem of TiO_2 is the fast recombination rate of photo-generated charge carriers. In that context, the combination of TiO_2 photocatalyst and carbon materials presents the opportunity to simultaneously enhance photocatalytic efficiency through a higher adsorption of pollutants, an enhanced absorption of visible light and a facile charge separation and transportation. Both ground-state charge transfer from graphene to TiO_2 and photo-induced charge transfer from graphene to TiO_2 have been demonstrated.[457] As far as (photo-induced) charge transfer is

concerned, both electron transfers from graphene to TiO_2 and from TiO_2 to graphene have been proposed, according to the energy of the incoming photons (see Figure 34).[669,670] Under visible light, electron excitation occurs from carbon-based states to both C- and Ti-based states (overall electron transfer is from graphene to TiO_2). UV photons may produce excitations from Ti-based states again to both C- and Ti-based states (overall electron transfer from TiO_2 to graphene). Thus, photo-excitations with different charge-transfer characters are possible, depending on the excitation wavelength. However, both types of photo-excitations produce charge-transfer states, thus creating electron-rich and hole-rich materials for photocatalytic applications. According to calculations, under visible light, the tunneling probability of photo-induced electrons is determined by the height and width of the Schottky barrier (Figure 34c).[671] Due to the settled electronic structure of TiO_2 and graphene, this Schottky barrier is mixed; so, decreasing its width is a reasonable approach to enhance the electron transfer at the interface. The maximum width of the Schottky barrier can be considered as the thickness of the graphene used. On the other hand, the additional control of the surface defect density (or functional group of graphene) is needed to ensure the chemical contact between the graphene basal plane and TiO_2. Therefore, a balance between the high electron transfer probability at the interface and the good intrinsic electrical property of graphene should be achieved. Several experimental and theoretical works have confirmed the role of graphene as a photosensitizer, leading to photo-induced charge transfer.[457,515,663,672-678] Photocatalytic activity of graphene composites with metal oxides other than TiO_2 has also been reviewed.[668] Graphene-TiO_2 yields superior electronic coupling compared to CNT-TiO_2, but on the other hand, CNT are more efficient TiO_2 photosensitizers.[679] For CNT-TiO_2 photocatalysts also, the charge transfer varied with the energy of the incoming photons.[680] Photoexcitation of CNT-TiO_2 with visible light results in charge transfer between TiO_2 and CNT and generation of separated charge carriers. UV light excitation can induce charge transfers in any direction from CNT to TiO_2 and from TiO_2 to

CNT, the latter process being more probable because of the higher density of initial states in TiO_2 compared to CNT. The extent of charge transfer will depend on: i) the type of CNT,[517] higher charge transfer occurring from metallic CNT to the TiO_2 surface than from semi-conducting CNT; and ii) their surface chemistry, since the electron transport is facilitated by functional groups such as -COOH, -OH, and -O- located at the edges of CNT. Thus, like for graphene, the TiO_2-CNT heterojunction can minimize recombination of photo-induced electrons and holes.

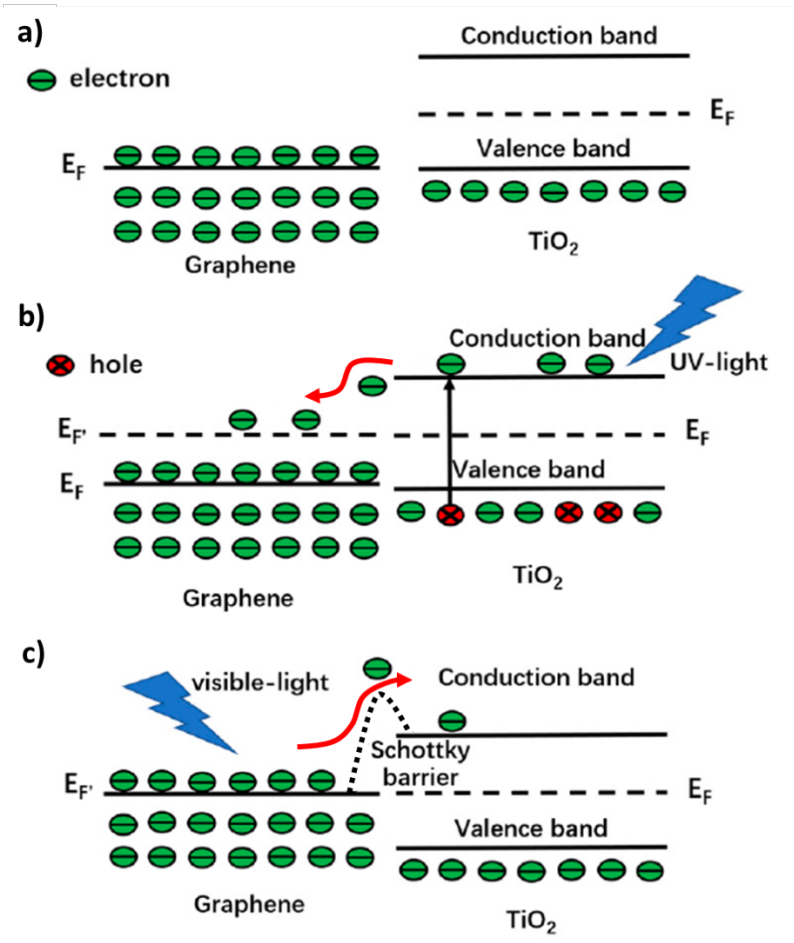

Figure 34. Band structures and interface interactions of the graphene-TiO_2: a) before combination; b) under UV-light irradiation; and c) under visible light irradiation with a close chemical contact. Reprinted from ref [667].

Fullerene C_{60} were also used in combination with TiO_2 for photocatalysis. C_{60} is an excellent electron acceptor, which can efficiently separate photo-induced charges. The performances of anatase TiO_2 NP associated to C_{60}, graphene or CNT were compared for the photocatalytic selective oxidation of benzyl alcohol to benzaldehyde under visible light irradiation.[681] No significant difference was observed on the ability of the three different carbon materials on lengthening the lifetime of photo-generated electron-hole pairs of the TiO_2/carbon catalysts. The reduction of C_{60} (one-electron process) by anatase TiO_2 NP under UV irradiation has been observed, the charge transfer between the excited TiO_2 NP and C_{60} occurs with a quantum efficiency of 24%.[682] However, the efficiency of fullerenes in combination with TiO_2 in photocatalysis needs to be nuanced as contrasting results have been published. Indeed, whereas different experimental and theoretical studies have shown the superior efficiency of C_{60}/anatase-TiO_2,[681,683] and C_{60}/P25-TiO_2[684] under UV irradiation, some works have shown that the only situation, where an effect was noticed, was by combining C_{60} with rutile-TiO_2 under visible light.[609] For rutile TiO_2 in van der Waals interaction with C_{60}, DFT calculations have shown that a charge redistribution of only 0.04 e^- from C_{60} to TiO_2 was observed, and is mostly taking place at the C_{60}/TiO_2 interface.[685] Much more efficient charge transfer occurs in boron-doped C_{60}/TiO_2 than in the C_{60}/TiO_2. Finally, in the case of C_{70}, it was proposed that the charge transfer depends on the energy of the incoming photons.[686] Under UV-light irradiation, the electrons on the valence bands of TiO_2 are excited to the conduction bands. Due to a covalent contact between C_{70} and TiO_2, the electrons on the conduction band of TiO_2 are transferred to mid-gap band and from mid-gap band to the conduction band of TiO_2.

From this analysis of the literature, it appears that charge transfer between carbon supports and metal NP might be a complicated phenomenon. More fundamental works are definitively

needed to improve our knowledge of the effect of carbon structure and functional groups on the electronic properties of the metal NP.

3.2 Confinement effects

The effects of confinement in heterogeneous catalysis have been the subject of particular attention since they can affect catalyst activity, selectivity but also stability.[390,687-692] Although the majority of the studies are dealing with confinement effects in oxides, and particularly zeolithes,[688,691,693] including 2D zeolites,[694] carbon materials have also been the subject of studies,[141] and particularly CNT. Indeed, they constitute an ideal support to study confinement effects due to: i) their specific morphology with a well-defined nanometer-size inner cavity, and ii) the possibility to deposit quite selectively the active phase either on the outer- or on the inner-surface. Besides CNT,[32,141,695-699] confinements effects have also been observed in porous carbon supports, and more recently under two-dimensional materials such as graphene.[141,700,701]

The nature of the confinement effects can be either physical or chemical. The physical effects are related to space restriction in the pores. The physical or "soft" effects can lead to shape (or inverse shape) selectivity in some reactions,[702] impact the nanofluidics and mass transport,[703-706] the phase separation and phase equilibria,[707] the freezing and melting,[708] or induce significant pressure enhancements.[709] The chemical or "hard" effects are related to interactions that involve significant electron rearrangement, including the formation and breaking of chemical bonds with the confining material. These latter effects can directly contribute to catalyst stabilization, and enhanced reductibility and/or reactivity. Thus, reaction energetics, mechanisms and dynamics could be significantly altered inside the pores of a 1D, 2D or 3D carbon material. It appears that all the above effects can affect catalytic chemical reactions to different extents, depending on the selected catalysts, the diameter and shape of the pore, and

the specific reaction carried out. The so-called confinement effect is frequently a collective result of more than just one of these effects. Although many efforts, in particular by molecular modeling,[710] have been made to evaluate the relative importance of each factor, in order to obtain fundamental information on the effects of confinement, they are still, in most cases, quite difficult to clearly identify.

3.2.1 Electronic or "hard" effects

In the *d*-band model developed by Norskov *et al*. the density of *d*-band valence electrons near the Fermi level is an important factor affecting catalytic activity, as already discussed in section 2.[711] Tuning the *d*-band center position by changing the metal-support interaction (electron transfer between support and metal catalyst particles) can lead to specific reactivity. As already mentioned in section 3.1.1, an amendment of *d*-band theory in terms of "*d*-band + work function" has been proposed to account for long-range (10-100 nm) charge transfer.[444] It is thus attractive to be able to modulate metallic NP reactivity by controlling: i) their location (inside or outside the carbon pores), ii) pore diameter, and/or iii) pore helicity in the case of CNT (metallic *vs* semi-conductor CNT).

In graphite or graphene, the π orbitals are perpendicular to the graphene layer, while in CNT or in carbon materials presenting curved surfaces as fullerenes, they are not parallel to each other due to surface bending, and locally the σ and π orbitals are no longer rigorously perpendicular. As a consequence, the π orbitals on the concave or convex surfaces rearrange in a way that the convex contribution is larger than the concave one (see Figure 35). The curvature induces a rehybridization between π orbitals and σ bonds, and introduces misalignment of π-orbitals within the carbon network (the misalignment angle, ϕ is shown on Figure 35a). This rehybridization can also be regarded as a mixture of sp^2 and sp^3 orbitals. The higher the sp^3

contribution, the higher is the reactivity. The pyramidalization angle θ, defined as the angle between the σ and π orbitals minus 90° (θ = 0° for the sp^2 hybridization), can be used (see Figure 35b) as an index for local reactivity. Indeed, the curvature induces a shift of the π electron density from the inner to the outer surface, and the occurrence of an electron potential difference across the graphene layers.[690] Additionally, as both ϕ, θ and this potential difference scale inversely with the diameter of a CNT,[690,712] there should be a correlation between the tube diameter and the chemical reactivity of the outer/inner surfaces. It has also been shown that the energy difference between the LUMO and the HOMO (bandgap) of single-walled CNT decreases when the diameter of the tube is increasing.[713]

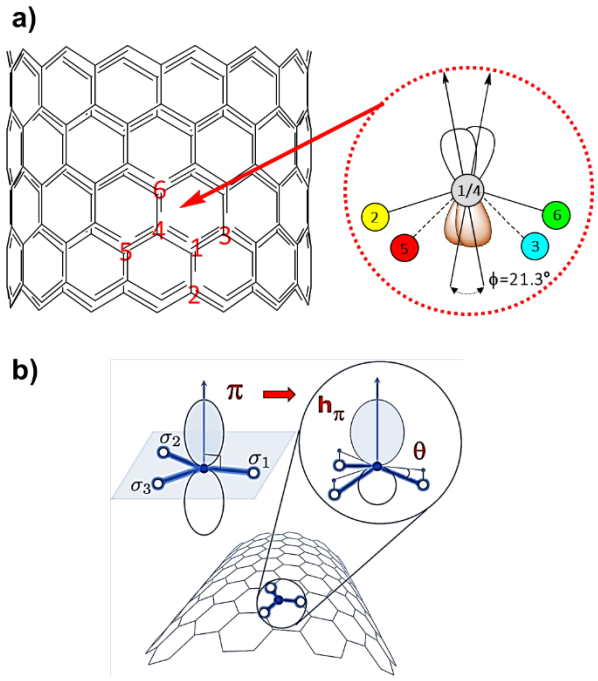

Figure 35. a) The π-orbital misalignment angles ϕ along the C_1-C_4 bond; and b) scheme showing the π orbital in planar graphene and its change into h_π under bending together with the pyramidalization angle θ.

If we now consider the interaction of a metallic NP or single atom with a curved carbon surface, the electronic structure of the metal will be affected differently if it is located on the concave or convex surface. This has been clearly demonstrated for Cs,[714] Ru[489] and Pt[715] NP and atoms adsorbed on concave/convex carbon surfaces. Figure 36 shows the DoS for Ru and Pt species adsorbed outside or inside CNT. The Ru-CNT interaction mainly comes from the coupling of *d* states of Ru atom and *sp* ones of C atoms.

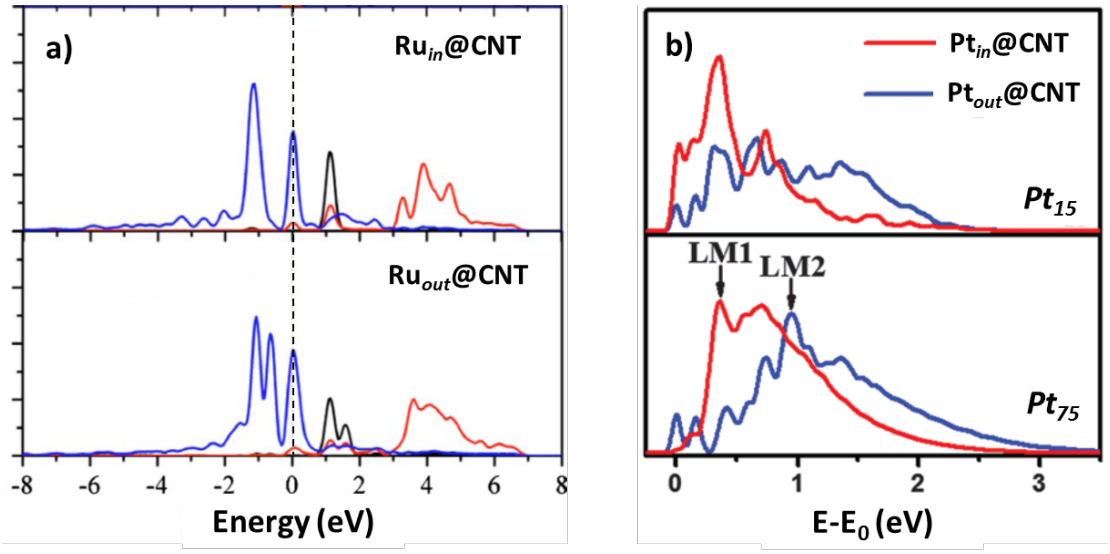

Figure 36. a) Local DoS on Ru atom for Ru inside and outside CNT. Black dashed line stands for Fermi level; black, red, and blue lines represent the *5s*, *5p*, and *4d* states, respectively. Reprinted with permission from ref [489] Copyright 2010 from AIP Publishing; and b) DoS of the minima for Pt_{15} and Pt_{75} clusters inside and outside the CNT. Reprinted with permission from ref [715]. Copyright 2015 from the Royal Society of Chemistry.

As discussed in section 2, the amount and direction of charge transfer usually show systematical trend with the electronegativity of the (semi)metal.[489] Thus for ruthenium[489] and

platinum[715] clusters encapsulated in small diameter CNTs, a net charge transfer from Ru or Pt to C atoms occurred. Interestingly despite the smaller electronegativity of aluminum compared to carbon one, encapsulated anionic Al_n clusters are expected, since transfer from C atoms to Al atoms has been reported.[716] The charge transfer from TM atoms adsorbed inside CNT is higher than that from the exohedral TM atoms by a nearly constant shift of 0.5 electrons. This reflects the higher electron density on the outer surface of CNT. It was also shown in the case of Re oxide NP that more electrons are transferred from metallic CNT to oxidized rhenium clusters, from semiconducting tubes.[717] An easier reduction under H_2 of Ru[718] and Co[719] NP confined in CNT was experimentally evidenced, compared to their counterparts deposited on the external surface.

For TM atoms or small clusters, the binding energy of TM outside CNT is generally higher than that inside CNT.[113,489,720] For large clusters and NP the opposite is often true.[715] Such differences become smaller as tube diameters increase. This can be correlated to a pronounced confinement effect on the NP structure. Indeed, the morphologies of cluster/NP under confinement turn out to be very different as compared to the free or supported cluster/NP (see Figure 37 for the case of Pt).[715,721] It has been clearly demonstrated that these structural changes of confined species has a direct impact on the properties of the NP.

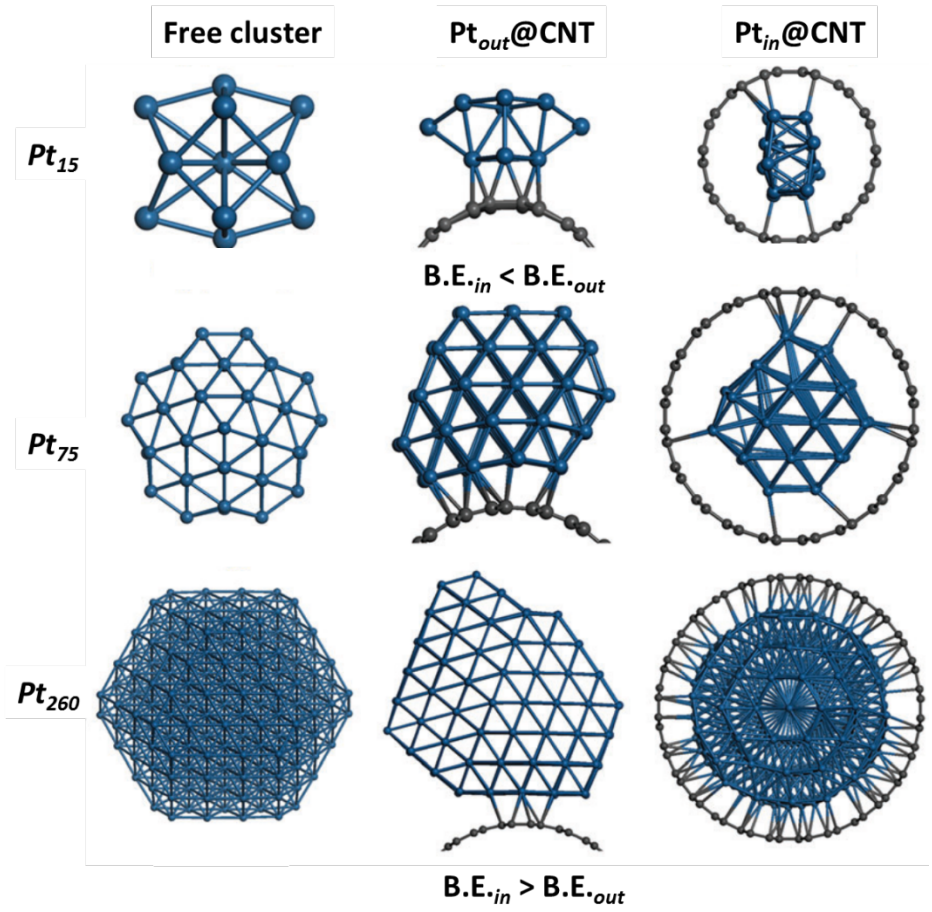

Figure 37. The ground state structures for Pt_{15}, Pt_{75}, and Pt_{260} clusters in vacuum, outside CNT and inside CNT. Reprinted with permission from ref [715]. Copyright 2015 from the Royal Society of Chemistry.

The thermal stability of Al,[722] Au,[723-725] Au-Pt,[726] Cu,[727,728] Pd,[729] Pd-Pt,[730] Pd-Au-Pt,[731] PtCo,[732] PtCu,[733] or Pt[734] clusters located in the inner cavity of CNT or carbon nanospheres has been studied by MD calculations. In the case of gold, the melting phenomenon starts from the innermost layer, when the freezing one begins from the outermost layer for confined NP. This corresponds exactly to the opposite behavior of free NP. The melting temperature of confined Au NP is lower than its bulk counterpart, and higher than that observed for free NP. The same tendency (*i.e.* a higher melting point of the confined phase related to free NP) was reported for

Au-Pd-Pt NP confined in CNT,[731] and PtCo NP confined in hollow carbon spheres.[732] For copper it was shown that the melting temperature of the NP decreases with decreasing CNT diameter. For Pd (Figure 38), contrarily to gold, it is also found that the melting temperature of the confined Pd NP is lower than that of free NP. The structural changes of the NP at high temperatures before melting, and the strength of the TM-C interaction are responsible for these observations.

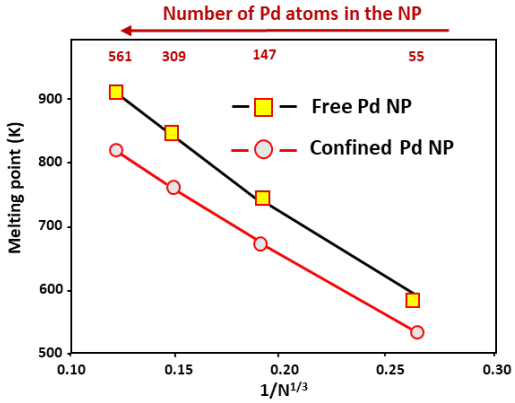

Figure 38. Melting temperatures changing with the inverse diameter of the NP for the free and CNT-confined Pd NP.[729]

Similarly, the magnetic properties of Fe,[735-739] Fe_3C,[740] Co,[736,741,742] or Ni[736] NP confined in CNT or fullerenes are modified. Except for a few cases, the total magnetic moments decrease for TM_m clusters (m = 2-6) confined in C_n fullerenes compared with free TM clusters; in particular, for large clusters (n = 5-6) inside small fullerenes (C_{60}).[736] In the case of iron clusters (Fe_{19}) or nanowires (Fe_{13}) confined in CNT, the magnetic moment of the clusters is increased in comparison with bulk *bcc* Fe. The strong interactions between the clusters and the CNT induce a reduction of the TM coordination number, and consequently an increase of the magnetic moments. Highest magnetic moments are obtained on the atoms having the lowest coordination numbers.[735]

It is also worth mentioning that if the metallic NP is confined in a carbon material, the reactivity of the outer carbon surface can itself be modified. DFT calculations have shown that Fe clusters confined in CNT significantly modify the electronic structure of the carbon surface, and significantly facilitate the activation of adsorbed O_2 molecule to produce surface epoxy groups.[743] Thus, when CNT are filled with metals, charge transfer between the sidewalls and the encapsulated metals may result in an increased electron density of the CNT outside convex surface. This strategy was followed to enhance the catalytic activity of CNT in the aerobic oxidation of cyclohexane.[744]

Theoretical works indicate that the strength of the reactants' adsorption on catalyst surfaces depends on the matching of reactants' energy levels to those of the catalyst surface (*d*-band center theory). Thus, the DoS of *d*-band valence electrons near the Fermi level is an important factor affecting adsorption and reactivity. By combining DFT calculations and experiments for Fe, FeCo, RhMn, and Ru clusters as models, Bao *et al*. observed significant strains and deformations within the CNT channels, inducing electronic structure modifications. This leads to downshifted *d*-band states, and consequently to a weaker adsorption of molecules such as CO, N_2, and O_2.[745] These authors introduced the concept of confinement energy (E_{con}): $E_{con} = E_{b(in)} - E_{b(out)}$; where $E_{b(in)}$ and $E_{b(out)}$ are the binding energies of molecules over NP adsorbed in or on CNT.[745,746] It can be anticipated that this important concept could be used to predict the effects of confinement on several catalytic reactions. This idea was used to rationalize the fact that iron oxide[747,748] or rhenium oxide[717] NP are more easily auto-reduced (carboreduction) when confined in CNT, and that Fe NP are more difficult to oxidized when confined in CNT.[749] It is also worth noting that a lower binding energy (negative E_{con}) has been reported for: i) H_2 adsorption on gold[750] and Pd[751] clusters confined in CNT and carbon nanohorns, respectively; ii) CO adsorption on Sc atom confined in CNT;[752] and iii) O_2 adsorption on Pt clusters confined in CNT.[715] In that latter study, the authors also investigated the mechanism of O_2 dissociative

chemisorption according to surface coverage. At low oxygen coverage, O_2 dissociation occurs readily on Pt_{15} NP inside and outside CNT. At high coverage, the particles inside CNT are more active for O_2 dissociation, and more resistant towards oxidation. These results were confirmed by a study of Bao's group.[746] Finally, the concept of confinement energy should also integrate CNT diameter. Thus, taking O_2 chemisorption on Pt and N_2 chemisorption on Re as probe reactions, Bao *et al*. have shown that maximum confinement effects are expected for CNT presenting an internal diameter of around 1 nm.[746] It should be also noted that the presence of defects[752] or hetero-atom dopants[720] in the CNT structure can deeply affect the adsorption energy ($E_{b(in)}$ and $E_{b(out)}$) of reactant during catalysis. Besides CNT, it was also reported that the binding energy of various molecule (CO was particularly studied) is reduced when adsorption occurs on a metallic surface covered by graphene,[753-757] graphdiyne,[758] or graphitic carbon nitride.[759]

All these results converge towards the fact that the confinement of a metallic active phase in a carbon material induces hard effects on the adsorption of molecules (potential reactants) and therefore on their potential reactivity. The trend appears to be a lower adsorption on confined NP. Of course, this confinement effect will be the most important as the adsorption energy of the molecule on the metallic NP will be large.

3.2.2 Physical or "soft" of effects

The inner surface of CNT, without defects, is atomically smoother than any known surface. As such, and considering the CNT diameter, they constitute interesting nanoreactors for catalysis. Besides the electronic effects discussed just above, additional physical or "soft" confinement effects can be expected, such as i) ultrafast mass transport, ii) an enrichment of molecules (concentration gradients), and/or iii) spatial restriction phenomena.

Fast transport and concentration gradients

Transport of confined liquids/gas/ions in CNT channels have attracted great attention in last decades due to its potential for a variety of applications such as sensing, separation, energy storage and conversion, water desalination, but also catalysis.[705,760-764] Thus, one of the most fascinating properties of CNT is their smooth surface that offers essentially resistance-free transport to small molecules in the form of gases, vapors, and liquids. Both experimental and modeling studies have established a diffusion driven mass transport of light gases and liquids inside CNT largely exceeding those of other porous materials.[765-769] Thus, increases of flow rates of gas/liquid up to one to five orders of magnitude with respect to conventional fluid-flow theory have been reported. Despite extraordinary progresses over the past few decades, efforts have to be made to understand the physical source of the non-classical phenomenon of liquid under confinement. For this, besides modeling, the development of new experimental probes that are highly sensitive to the local environment would be particularly useful. Indeed, NMR time scale is relatively long, and generally provides only an averaged time scale, while comparatively short vibrational lifetimes limit the ability of vibrational spectroscopies to probe the slow dynamics that appear upon confinement.[770]

Diffusion of gases

Gas transport through mesoporous materials is generally a combination of: i) viscous or Poiseuille flow, ii) Knudsen diffusion, and iii) surface diffusion. When the pore diameter is reduced to a size similar to the dynamic diameter of confined species, their transport behavior will change significantly. MD simulations for both self- and transport-diffusivities of light gases (Ar, Ne, H_2 and CH_4) in rigid CNT and in zeolites with similar pore sizes (ZSM-12 and silicalite) have shown that transport rates in CNT are orders of magnitude faster than in the zeolites (Figure 39).[771,772] The exceptionally high transport rates in CNT are shown to be a result of their inherent smoothness. For diatomic molecules such as O_2, molecular geometry effects have also to be taken into account to rationalize the flow physics.[773] For CO_2 in CNT (1-5 nm

diameter) transport diffusivities are roughly independent of pressure, and the observed diffusion mechanism is not Knudsen like but configurational.[774] Other MD simulations integrating the CNT flexibility have confirmed that transport diffusion of gases is also rapid in flexible CNT,[775,776] even if completely dynamic (non-rigid) CNT slowed fluids more rapidly than partially rigid ones, because the dynamic motion of the CNT walls disturbed the flow of the molecules to a greater extent.[777] However, the interfacial resistance (entrance and exit resistance) slows the diffusion of CH_4 by 2 to 3 orders of magnitude in CNT of finite length compared to infinitely long CNT.[778] The transport diffusivity in CNT of finite length increases with the length, because the inner diffusion, which increases with length, contributes the most to the overall diffusion. The introduction of defects in the CNT structure does not affect the diffusivity of gas such as Ar or CO_2 because scattering from fluid-fluid collisions dominates over the fluid-CNT collisions.[776] Extremely rapid diffusion can also occur for gas mixtures (CH_4/H_2).[779] For these binary-mixtures, the mixture-diffusion characteristics can be estimated with good accuracy from the pure-component diffusion parameters.[780] Worth to be noted is that the presence of water traces as clusters inside the tube can block the diffusion of methane because of strong hydrogen bonding.[781] However, CH_4 molecules can still replace H_2O molecules inside the CNT, and completely fill the inner cavity of CNT over a nanosecond time scale.[782] Selective gas diffusion can also be achieved by controlling gas flow channels and pores *via* different stacking methods with FLG and GO.[783] Theoretically, it has been shown that by adjusting the interlayer spacing or by chemically modifying the membrane, highly selective gas permeation can be obtained.[784]

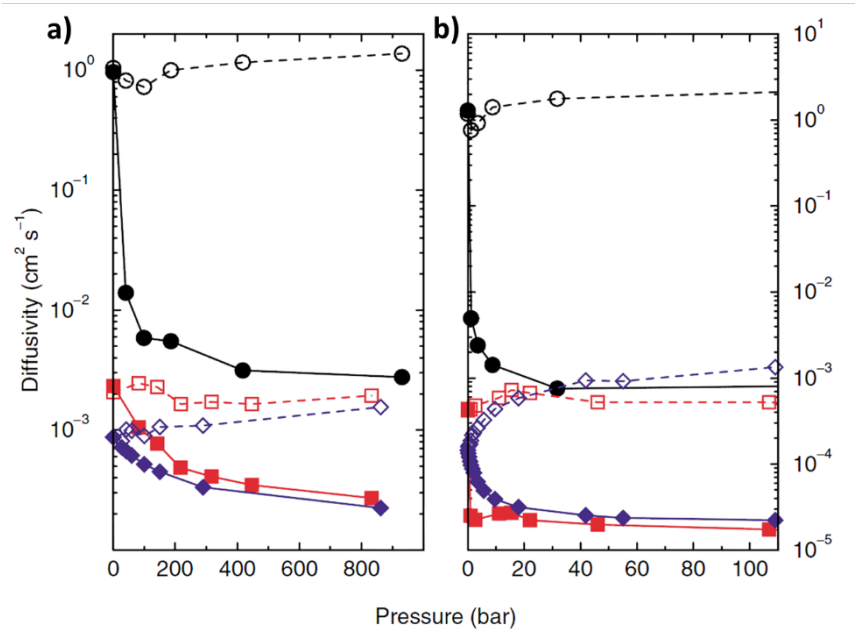

Figure 39. Diffusivities for a) H_2 and b) CH_4 in CNT (circles), ZSM-12 (squares), and silicalite (diamonds). The filled symbols and full lines represent the self-diffusivities and the open symbols and dashed lines are values for the transport diffusivities. Reprinted with permission from ref [771]. Copyright 2002 from the American Physical Society.

Molecular dynamics was used with success to compute diffusion coefficients at the single-pore level by using a pore network model for diffusion in microporous porous carbon materials.[785,786]

Diffusion of liquids

When one examines a liquid confined in nanometer pores, virtually all aspects of both the structure and dynamics are modified relative to the corresponding bulk liquid.[770] The topic of the static and dynamic behavior of liquids inside CNT includes investigation of liquid entering inside the CNT, their subsequent filling, the overall flow through CNT as well as the wetting

of the CNT walls. The understanding of the CNT filling process is still limited.[787] Numerous theoretical and experimental works have shown that the transport of water molecules through CNT is super-fast.[788,789] A unique combination of different features contribute to large flow rates in CNT, in contrast to other materials, such as: i) the fact that the water's friction at graphitic surfaces exhibits a strong curvature dependency;[790] ii) the number and distribution of hydrogen bonds per water molecule in the CNT;[791] iii) the water molecule orientations,[792] and the change of water molecules distribution in CNT caused by the variation of CNT diameter.[793] The presence of defects such as vacancies in the CNT structure causes a reduction in the confined water density, disrupts the nearly frictionless water transport, and leads to significant reduction in fluid velocity and mass flow rate.[794] The critical dimension below which confinement in CNT affects fluid transport is currently debated.[795] For water in CNT, the continuum approximation seems to break down for CNT with diameter below 10 nm, and the enhancement of flow rate decreases with increasing CNT diameter.[796] Interestingly, it has been demonstrated both experimentally and theoretically that water enters spontaneously in the inner cavity of hydrophobic CNT.[797] This phenomenon is primarily driven by an increase in the rotational entropy of H_2O inside the pore, arising from a reduction in the average number of hydrogen-bonds around a water molecule.

Beside water, which have been particularly studied, a high diffusion of various liquids (CH_3OH,[798] ethanol,[799] CH_3OH/H_2O,[800] ionic liquids,[801,802] and alkanes,[780,803]) in CNT has been reported. A grand canonical MD simulation study of the transport of a CH_3OH/H_2O mixtures in CNT functionalized (or not) with carboxyl acid groups onto the inner wall has shown that the mixture's transport through functionalized CNT is faster than through hydrophobic ones, although the mixture's diffusion is slower inside hydrophilic CNT due to the existence of a H-bond network. Thus, the transport of the liquid mixture through CNT is mainly controlled by the pore entrance effect, for which H-bonding plays an important role. Unimpeded permeation

of water have been reported in sub-micrometer-thick GO-based membranes.[804] These membranes appear to be impermeable to liquids, vapors and gases but allow easy permeation of water. Theoretical works have related this result to the presence of oxygenated functional groups.[805] There also, MD simulations have been successfully used to predict diffusion of liquids in the pores of carbon materials.[806]

In catalysis, mass transfer of reactants to and of products away from the active sites is an important step, and diffusion in microporous materials is often the dominating mechanism determining the mass transfer rates. It is thus important to keep in mind that in the case of CNT, the diffusion can be, contrarily to zeolites, MOF or activated carbons, an ultrafast process, and that it is the interfacial resistance that limits transport diffusivities.

Concentration gradients

Several experimental and modeling studies have shown that the inner cavity of CNT has stronger affinity for gas adsorption than the interstitial channels of CNT bundles.[807] This was also demonstrate for liquids, such as methanol.[808] The internal and external arrangement of molecules can differ significantly according to CNT diameter. Figure 40 shows a snapshot of benzene configuration in the presence of a (8,8) or a (10,10) single-walled CNT. Interestingly, it has been shown that benzene or methanol inside or outside CNT can be conveniently distinguished by ^{13}C MAS NMR.[808-810]

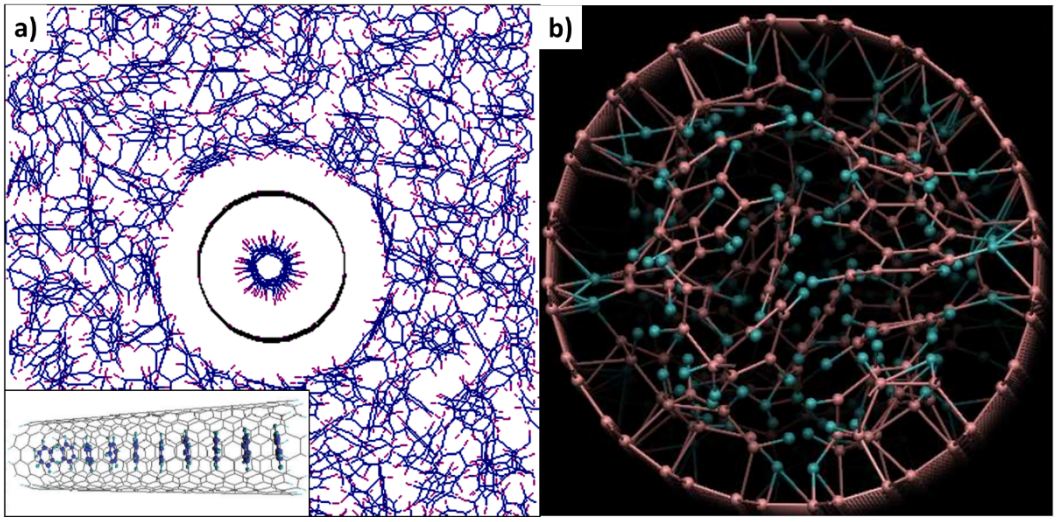

Figure 40. Snapshot of benzene molecules in: a) a (8,8) SWCNT; reprinted with permission from ref [811]; Copyright 2011 from the Royal Society of Chemistry. and b) a (10,10) single-walled CNT. Reprinted with permission from ref [812]. Copyright 2015 from the John Wiley and Sons.

The adsorption selectivity of any species inside the tube is greatly driven by its different interaction potentials with the graphitic walls. In addition to an electron-deficient environment, we recall that the internal cavity of CNT is hydrophobic. Thus, hydrophobic and/or nucleophilic species should accommodate more easily in CNT that hydrophilic and/or electrophilic ones. Adsorption and separation of binary and ternary mixtures have been investigated using different methods such as grand canonical Monte Carlo (GCMC), first-principles simulations or even classical MD calculations.

For CO_2/CH_4 mixture adsorption and diffusion in CNT, it was shown that: i) CNT show a preferential adsorption for CO_2 in the binary CO_2/CH_4 mixture;[813] ii) compared with CH_4, CO_2 prefers to stay closer to the CNT wall;[814] and iii) CNT show better performances for CO_2/CH_4 separation than disordered porous carbons.[815] For H_2/CH_4 mixtures it was evidenced that the

CNT diameter has a pronounced influence on the partition on these two gases inside or outside the CNT (Figure 41).[816] The influence of CNT diameter was also reported for ethane/ethylene mixtures, small-diameter CNT preferring ethylene to ethane.[817]

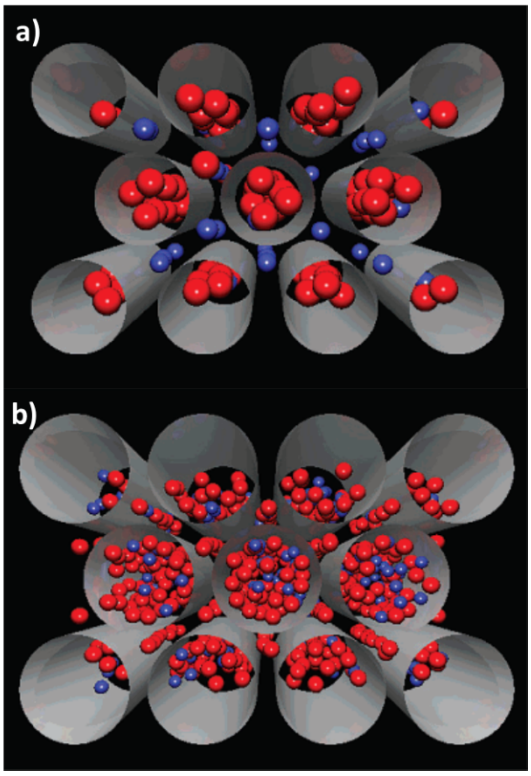

Figure 41. Equilibrium snapshot of equimolar H_2/CH_4 mixture at 293 K and 12.2 MPa in idealized bundle of a) [9,9] (left panel); and b) [18,18] SWCNT (red balls: methane; blue balls: hydrogen). Reprinted with permission from Kowalczyk, P.; *et al*. *J Phys. Chem. C* **2007**, *111*, 5250-5257.[816]. Copyright 2007 from the American Chemical Society.

Syngas was also investigated, and a stronger interaction of both H_2 and CO with the inner cavity than with the exterior surface of CNT was evidenced by GCMC, showing that CO interacts more strongly with CNT than H_2.[818] As a result, syngas molecules are enriched inside CNT and the ratio of CO/H_2 inside CNT increases with respect to the composition of syngas in the bulk gas phase. CO/O_2 enrichment in the inner cavity of CNT has been proposed to

rationalize the high activity of confined Ru NP for CO oxidation in H_2-rich streams.[819] The existence of a concentration gradient between the outside and the inside of the CNT could open the way to conduct reactions that conventionally require high pressures under much milder conditions, and contribute to selectivity shifts in some reactions involving gas mixtures.

The partition of species between the inner cavity of CNT and the outer surface or bulk phase is not limited to gas. Thus, using MD calculations, it was shown that for equimolar mixtures of water and acetonitrile, the inner CNT cavity is filled exclusively by acetonitrile for CNT of 0.55 nm radius, and that water begins to get incorporated within the inner cavities as the radius of the tube reaches ~1 nm.[820] Entropy as well as hydrogen bonding can both play important roles in determining the solute location and orientation.[821] Selective enrichment of molecules with different properties in solution was also reported for the rhenium-catalyzed hydroxylation of benzene to phenol.[822] Solid-state NMR studies have shown that benzene is enriched inside CNT while phenol is discriminatively expelled out of the cavities. The highly local concentration of benzene inside the CNT cavity and the fast desorption of phenol induces a 4-fold enhancement of the benzene conversion rate when using a Re confined catalyst compared to catalyst for which the active phase is on the CNT external surface.

There is no doubt that the existence of concentration gradients and adsorptive separation inside CNT could play a role in numerous confined catalytic reaction, but also during catalyst synthesis.

Spatial restriction and stabilization

Confining boundaries affect the spatial distribution of the hindered species and the way by which those species may dynamically evolve. These effects play an important role in the thermodynamics of the confined systems.[708,823] Thus, water molecules hindered in very narrow

CNT arrange in a single line, and exhibit a solid-like ordering at room temperature due to strong hydrogen bonding between nearest-neighbor molecules.[797] Confining boundaries also alter drastically the boiling and critical behavior of water droplets,[824] and extreme phase transition temperatures of H_2O confined inside CNT have been observed.[825] Phase transition of ionic liquids from liquid to high-melting point crystal has also been observed.[826] As in the case of water, despite CNT hydrophobic character, spontaneous filling of CNT by ionic liquids is observed.[827]

The rigid cavity of CNT can also affect the size, shape, composition and properties of confined NP. For example, it was reported in different studies on confined metallic NP synthesis that the confined NP systematically show a smaller particle size than those supported on the external surface of CNT presenting relatively large internal diameters.[828-831] Confinement effects are also responsible for major changes in the shape and composition of bimetallic systems.[832] Thus, for the preparation of confined CoPt and FePt nanostructures, a marked confinement effect has been evidenced, on both bimetallic nano-object shape and composition. In large diameter CNT, small Co- and Fe-rich NP were produced, while in small diameter CNT Pt-rich nanowires were selectively obtained (see Figure 42). Although CNT can be used as templates for the growth of metallic nanowires (MoO_2,[833] Bi,[834] FeCo,[835] $Fe_{65}Ni_{35}$,[836] PbTe,[837] Gd,[838] Au,[839,840] Ag,[841] Pt,[839] and Pd[842]) in the case of ligand stabilized FePt nanostructures, both NP or nanowires could be selectively produced in the same CNT of 4-5 nm diameter just by changing the nature of the Pt precursor (Figure 42).[832]

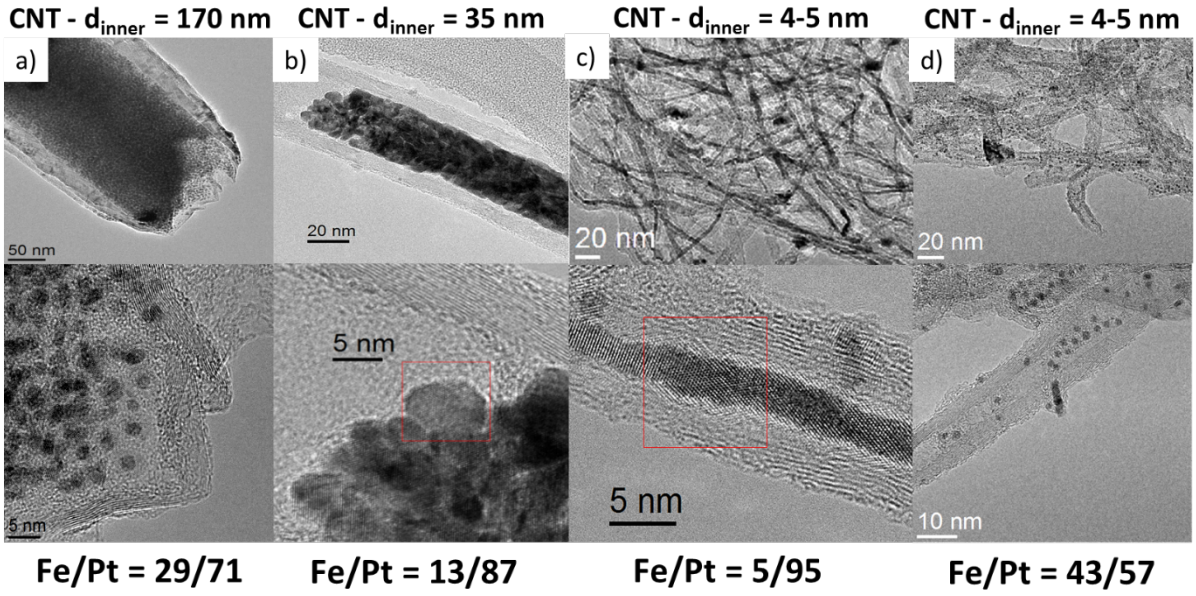

Figure 42. Evolution of PtFe nanostructures shape and composition with CNT inner diameter: a) PtFe NP in CNT of 170 nm i.d.; b) PtFe aggregated NP in CNT of 35 nm i.d.; c) PtFe nanowires in CNT of 4-5 nm i.d.; and d) PtFe NP in CNT of 4-5 nm i.d. Reprinted with permission from ref [832]. Copyright 2016 from the Royal Society of Chemistry.

Ultrathin molybdenum,[843] europium,[844] tellurium,[845] and TeSn[846] nanowires with diameters of a single atom were also selectively produced within very thin CNT by diameter-controlled polymorphism of the encapsulated materials.[847] Because the nanowires are confined and protected by the walls of the CNT, they resist oxidation and structural disintegration. The propensity to form continuous nanowires throughout the length of the CNT seems to be strongly correlated with the existence of an incomplete electronic shell in the most stable ionic state of the metal.[848] These objects however have not been investigated yet in catalysis. The stabilization of specific phases of inorganic materials inside CNT or carbon nanorods has also been reported for: lead (amorphous phase) in CNT,[849] γ-Fe phase in CNT,[850] cubic iron nitride NP in CNT,[851] new 1D allotropes of arsenic in CNT,[852] or α-NiS NP in carbon nanorods.[853]

Interestingly, for GeTe structures, amorphous to crystalline changes were evidenced under electron-beam irradiation.[854] Finally, the possibility to produce specific phase under mild condition under confinement in CNT was also reported for $CoFe_2O_4$ particles.[855-857]

Obviously, if all the effects cited above may operate independently, it is of course also possible that a combination of these primary effects leads to specific secondary confinement effects.

3.2.3 Catalytic chemical reaction confined within carbon materials

The control of chemical reaction pathways at the molecular level presents one of the most important scientific challenges to achieve fully sustainable and thermodynamically efficient chemical processes. When the space surrounding molecules becomes restricted, their reactivity and related behavior will be altered.[691,692,694,858,859] Owing to confinement effects imparted by CNT, it has been shown that novel and distinct physical and chemical properties are found for the confined species. There have been only a limited number of studies to illustrate the use of the inner space of CNT to control non-catalytic chemical reactions. Catalytic transformations however have been much more studied. The vast majority of the studies describes a positive effect of confinement, but a negative effect has also been described in rare cases. Of course, while efforts have been made in some studies to rationalize the confinement effect, in most cases it is just noted. We will limit our analysis to those studies for which an extensive study of the effects of confinement was performed, as well as to the reactions for which net trends were observed.

Fischer-Tropsch synthesis

Cobalt and iron based catalysts are both employed industrially for Fischer-Tropsch synthesis (FTS). Iron catalysts can operate under a wide range of temperature and H_2/CO ratios, with low CH_4 selectivity. They exhibit higher catalytic activity for WGSR than Co catalysts, and deactivate rapidly. Cobalt catalysts are preferred due to their high activity, high selectivity to

long-chain paraffin, low WGS activity and higher resistance to deactivation by water. Ruthenium catalysts, though presenting high performances are less studied because of the high cost of the metal. Table 3 summarized the main results obtained for Fe-, Co-, and Ru-based catalysts confined in carbon materials for FTS. Selectivity control and catalyst stability are central issue in FTS. For iron catalysts, a clear trend is that confined catalysts are more active and more selective than unconfined ones in fixed bed reactors. With regard to stability, it appears that the deactivation of the confined catalysts is slower than in the case of unconfined ones (Figure 43a).[860] For the Fe_{in}@CNT catalyst the CO conversion drops by 26.8% during 720 h FT synthesis, while in the case of Fe_{out}@CNT catalyst the decrease in CO conversion is 46.4%. Confinement also affects methane and C_{5+} liquid hydrocarbon selectivity (Figure 43b), higher selectivity to C_{5+} being obtained with the Fe_{in}@CNT catalyst. Additionally, Fe_{out}@CNT catalyst showed an increase of 11.5% in C_{5+} selectivity during 720 h FT synthesis, while the increase is only of 6.3% for the Fe_{in}@CNT catalyst. This difference could be related to the higher drop in CO conversion and the higher increase in particle sizes in the case of Fe_{out}@CNT catalyst compared to Fe_{in}@CNT catalyst. The productivity of a 10%Fe_{in}@CNT catalyst (0.336 $g_{HC}.g_{cat}^{-1}.h^{-1}$, in gram of produced hydrocarbon per gram of catalyst and per hour) is comparable to that of the commercial catalyst utilized by Sasol.

For cobalt catalysts, although a similar tendency (Figure 44) is observed in fixed bed reactors, the results are more contrasted. During long FTS tests, CH_4 selectivity decreases and C_{5+} selectivity increases with time on stream. Generally speaking, the NP (Fe or Co) confined in CNT are smaller and present a higher degree of reduction than those deposited on the external surface,[860-862] and the diameter of the confined NP decreases when decreasing CNT internal diameter.[863] Thus, small NP (5-8 nm) confined in small diameter CNT are more active than the bigger ones deposited on the external surface.

Table 3. Catalytic performances of Co, Ru and Fe based catalysts confined in carbon materials for FTS.

Catalyst	Conditions	CO conversion	Activity / TOF	C_{5+} selectivity	α	Stability	Ref
$5\%Fe_{in}0.1K@CNT$	T = 573 K, P_{syngas} = 5 bar GHSV = 21800 h^{-1}	11	-	34.7	-	-	[864]
$10\%Fe_{in}@CNT$	T = 548 K, P_{syngas} = 20 bar 1860 mL.$(h.g_{cat})^{-1}$	86	1.95 $g_{HC}.g_{cat}^{-1}.h^{-1}$	70.2	-	Stable 120 h on stream	[865]
$10\%Fe_{in}@CNT$ $10\%Fe_{out}/CNT$	T = 623 K, P_{syngas} = 10 bar GHSV=17 L/g.h	33.7 12	0.521 s^{-1} 0.288 s^{-1}	19.9 14.1	-	10 h on stream	[866]
$10\%Fe_{in}@CNT$ $10\%Fe_{out}/CNT$	T = 543 K, P_{syngas} = 10 bar	40 29	0.440 $g_{HC}.g_{cat}^{-1}.h^{-1}$ 0.210 $g_{HC}.g_{cat}.h^{-1}$	29 19	-	24 h on stream	[867]
$10\%Fe_{in}@CNT$ $10\%Fe_{out}/CNT$	T = 548 K, P_{syngas} = 20 bar	85.2 69.7	0.336 $g_{HC}.g_{cat}^{-1}.h^{-1}$ 0.272 $g_{HC}.g_{cat}^{-1}.h^{-1}$	40.5 32.9	-	48 on stream After 720 h on stream 62% CO conv. - 46% C_{5+}	[860]
$12\%Fe_{in}@CNT$ $12\%Fe_{out}/CNT$	T = 543 K, P_{syngas} = 20 bar 4000 mL.$(h.g_{cat})^{-1}$	85 79	-	36.2 23.8	-	125 on stream	[868]
$20\%Fe_{in}@CNT_{narrow}$ $20\%Fe_{in}/CNT_{large}$	T = 548 K, P_{syngas} = 20 bar 2000 mL.$(h.g_{cat})^{-1}$	25 10	-	45 12	-	Stable 120 h on stream	[863]
$13\%Fe_{in}@CNT$ $32\%Fe_{in/out}/CNT$	T = 593 K, P = 5 bar GHSV = 3500 h^{-1}	2.4 20.7	-	15.2 26	-	Stable 120 h on stream	[869]
$5.6\%FeN_{in}@CNT$ $5.2\%FeN_{in}/CNT$	T = 573 K, P_{syngas} = 5 bar GHSV = 15 000 h^{-1}	-	9.3 $mol_{CO}.\ s^{-1}.g_{Fe}^{-1}*10^{-4}$ 6.7 $mol_{CO}.\ s^{-1}.g_{Fe}^{-1}*10^{-4}$	22.9 20.9	-	24 on stream	[851]
$10\%Fe_{in}@C$	T = 543 K, P_{syngas} = 20 bar $W_{Fe}/F_{(H2+CO)}$ = 2.5 g.h.mol^{-1}	90.1	-	60.1	-	24 on stream After 100 h on stream 75% CO conv.	[870]
$Fe\text{-}FeC_{in}@C$	T = 583 K, P_{syngas} = 69 bar GHSV = 3000 h^{-1}	87.5	0.120 $g_{HC}.g_{cat}^{-1}.h^{-1}$	65	-	Stable 100 h on stream	[871]
$7.4\%Fe_xO_{yin}@C$	T = 543 K, P = 20 bar	76 (70h)	2.5 L.$g_{Fe}^{-1}.h^{-1}$	60	-	NP 7 nm fresh – 9 nm after 108 h on stream	[872]

Fe-Mn_{in}@C	T = 613 K, P = 20 bar GHSV = 5000 h^{-1}	94	5.66 $mol_{CO}.g_{Fe}^{-1}.s^{-1}*10^{-5}$	55	-	Stable 100 h on stream	[873]
10%Co_{in}@CNT	T = 493 K, P = 20 bar flow rate of = 30 mL.min^{-1}	23	0.09 $g_{HC}.g_{cat}^{-1}.h^{-1}$	72	-	48 h on stream	[874]
10%Co_{in}@CNT	T = 493 K, P = 10 bar W/F = 10 g.h.mol^{-1}	55.3	-	84.4	-	-	[875]
15%Co_{in}@CNT	T = 498 K, P = 20 bar, GHSV = 2.4 NL.$g_{cat}^{-1}.h^{-1}$	53.8	1.793 $g_{HC}.g^{-1}_{Co}.h^{-1}$	52.1	0.81	25-30 h on stream	[876]
20%Co_{in}@CNT	T = 503 K, P = 20 bar WHSV = 6750 mL.$(h.g_{cat})^{-1}$	68	0.16 s^{-1}	87.3	0.81	22 h on stream – unstable (68 to 50% conv.)	[877]
15%Co_{in}@CNT 15%$Co_{in/out}$/CNT	T = 493 K, P = 25 bar GHSV = 6000 h^{-1}	57 45	0.87 $g_{HC}.g_{cat}^{-1}.h^{-1}$ 0.81 $g_{HC}.g_{cat}^{-1}.h^{-1}$	54.8 62.2	0.82 0.87	25-30 h on stream	[862]
10%Co_{in}@CNT 10%Co_{out}/CNT	T = 493 K, P = 10 bar GHSV = 5000 h^{-1}	18.8 12.9	0.91 $g_{HC}.g^{-1}_{Co}.h^{-1}$ 0.74 $g_{HC}.g^{-1}_{Co}.h^{-1}$	83.6 79.6	-	48 h on stream	[878]
10%Co_{in}@CNT 10%Co_{out}/CNT	T = 478 K, P = 20 bar flow rate of = 33.3 mL.min^{-1}	-	-	23[a)] 26	-	-	[879]
10%Co_{in}@CNT 10%Co_{out}/CNT	T = 493 K, P_{syngas} = 10 bar 4000 mL.$(h.g_{cat})^{-1}$	29.1 24.7	4.3 $mol_{CO}.g_{Co}^{-1}.s^{-1}*10^{-5}$ 3.7 $mol_{CO}.g_{Co}^{-1}.s^{-1}*10^{-5}$	83.0 81.9	-	Stable 120 h on stream	[880]
9.5%Co_{in}@CNT 9.5%Co_{out}/CNT	T = 513 K, P = 20 bar flow rate of = 75 mL.min^{-1}	58.7 16.4	5.2 $mol_{CO}.g_{CO}^{-1}.s^{-1}*10^{-3}$ 1.4 $mol_{CO}.g_{CO}^{-1}.s^{-1}*10^{-3}$	59.1 18.9	-	Stable 130 h on stream Unstable 130 h on stream	[861]
20%Co_{in}@CNT	T = 513 K, P = 20 bar flow rate of = 52.4 mL.min^{-1}	74.6	0.42 $g_{HC}.g^{-1}_{Co}.h^{-1}$	79.7	0.86	12 h on stream After 450 h on stream 57% CO conv. - 95% C_{5+}	[881]
15%$Co_{in/out}$@CNT	T = 493 K, P_{syngas} = 20 bar 3000 mL.$(h.g_{cat})^{-1}$	30.1	0.23 $g_{HC}.g^{-1}_{Co}.h^{-1}$	81.2	0.75	20 h on stream Stable 50 h on stream	[882]
20%Co@CMK-3	T = 493 K, P_{syngas} = 20 bar GHSV = 4000 mL.$(h.g_{cat})^{-1}$	81.3	5.7 $mol_{CO}.g_{Co}^{-1}.s^{-1}*10^{-5}$	93.6	-	40 h on stream	[883]
3.5%Ru_{in}@CNT[b)]	T = 493 K, P_{syngas} = 20 bar SV = 2.0 slph.g_{cat}^{-1}	18	3.8 $mol_{CO}.g_{Ru}^{-1}.s^{-1}*10^{-5}$	67.1	0.76	Stable 300 h (slurry)	[884]
2.4%Ru_{in}@$C_{spheres}$	T = 493 K, P_{syngas} = 10 bar W/F = 15 g.h.mol^{-1}	18.5	5.5 $mol_{CO}.g_{Ru}^{-1}.s^{-1}*10^{-5}$	78.1	0.78	NP 3.2 nm fresh – 3.6 nm after 40 h on stream	[885]

a) Defined as the molar ratio of the C5+ hydrocarbons to the total of all products. b) Oxygenate selectivity ~17%.

These small NP are also less prone to sintering, mainly because of the template effect of the CNT walls. Three different deactivation steps are clearly distinguishable on Figure 44a.

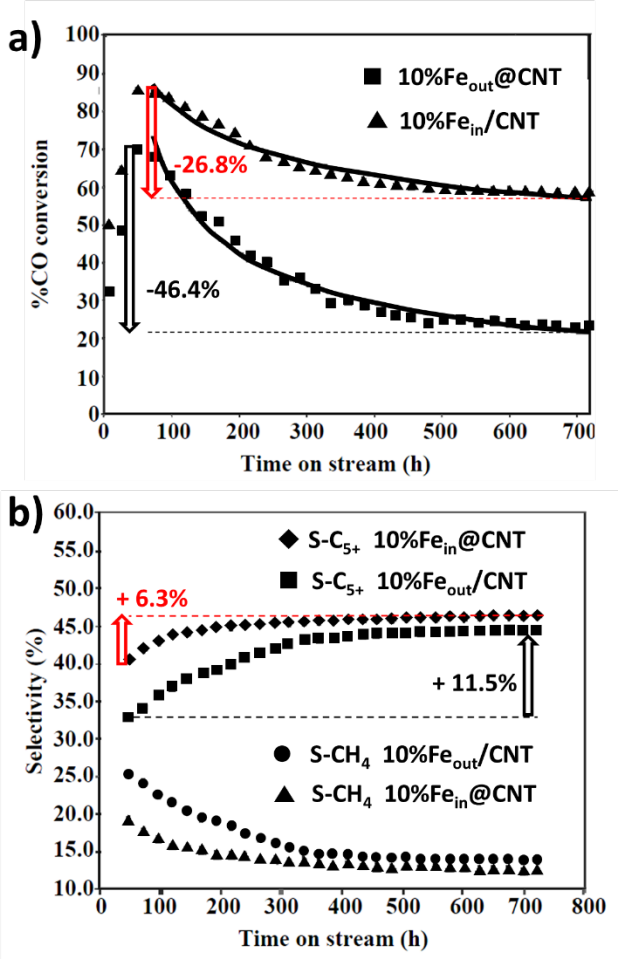

Figure 43. a) Changes in %CO conversion with time on stream for Fe_{in}@CNT and Fe_{out}/CNT catalysts; and b) changes in C_{5+} and CH_4 selectivity with time on stream for Fe_{in}@CNT and Fe_{out}/CNT catalysts.[860]

The first deactivation process has been attributed to oxidation of the smallest Co NP. The second and third deactivations have been tentatively attributed to sintering of NP outside the CNT and inside the CNT, respectively. The increase selectivity for C_{5+} upon time on stream has been correlated mainly to an increase of NP size. The higher the sintering rate, the faster is

the deactivation (conversion losses), but the faster is the selectivity gain (C_{5+} increase), as shown on Figure 44b.

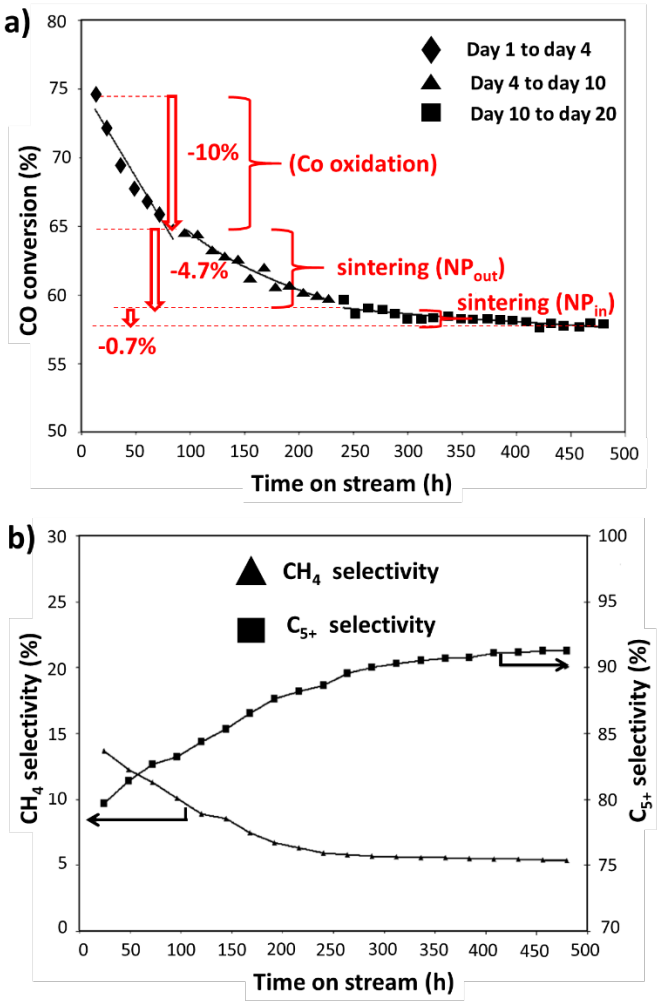

Figure 44. a) Changes in %CO conversion with time on stream for a Co_{in}@CNT catalyst; and b) changes in C_{5+} and CH_4 selectivity with time on stream for Co_{in}@CNT catalyst.[881]

Hydrogenation reactions

The confinement effects of carbon materials have been studied using mainly liquid phase hydrogenation reactions. Selective hydrogenation of α,β-unsaturated aldehydes was

particularly studied as a model reaction for evaluating chemo-selectivity issues, and few reports are dealing with asymmetric hydrogenation. Table 4 summarize the main results obtained using catalysts confined in carbon materials for hydrogenation reactions, including CO_2 hydrogenation. The analysis of these works highlights a number of clear trends. First, the confinement of NP has a net effect on the catalytic performances of the studied systems; enabling better activities but also chemo- and enantio-selectivity. With respect to confinement effects, a number of parameters are reported in a systematic way: i) the absence of transfer-related limitations in the inner cavity;[886] ii) enrichment of reagents in the internal cavity of the CNT, which directly affects the kinetics of the reaction;[830,887-892] iii) this is also true for hydrogen, and a higher H_2 pressure in the inner cavity has been reported;[890,893] iv) an easier reduction of the active phase when it is confined;[312,892,894-896] v) an easier H_2 activation and hydrogen spillover for the confined catalyst;[897-899] vi) smaller NP and higher dispersion for the confined catalyst;[312,830,893,900] vii) sometimes the presence of electro-deficient metal species within the cavity;[890,893] and viii) an improved stability of the confined phase related to sintering.[312,894,900-902] All of these experimental observations are entirely in agreement with the theoretical findings on hard and soft confinement effects reported in sections 3.2.1 and 3.2.2. Additionally, some reports have analyzed the effect of CNT diameter on the performances of the confined catalyst. The general trend is that the effects of confinement are all the stronger as the diameter of the nanotubes decreases. However, a too large reduction, as in the case of single-walled CNT, can induce transfer problem (especially for liquid phase reactions), which can be detrimental to the activity. Additionally, it was shown by DFT that within too small CNT, the binding is overly weakened, and thus activation of the reaction molecules is sluggish.[746]

Table 4. Catalytic performances of catalysts confined in carbon materials for hydrogenation reactions.

Substrate	Catalyst	Activity	Selectivity	Remark	Ref.
Acetylene	0.075%Pt_{in}@CNT 0.075%Pt_{out}/CNF	$Pt_{in} < Pt_{out}$	Ethylene $Pt_{in} > Pt_{out}$	The enhanced selectivity is due to the different electronic structure and faster Knudsen diffusion of confined acetylene in CNT channels.	903
Benzene	6%Ni_{in}@CNT 6%Ni_{out}/CNT	$Ni_{in} >> Ni_{out}$	Cyclohexane	Gas phase hydrogenation. Increased reactants concentration. Easier reduction of NiO for Ni_{in}.	892
Benzene	4%Ru_{in}/CNT 4%Ru_{out}/CNT	$Ru_{in} > Ru_{out}$		Heat treatment was performed, and XPS indicated that heat treatment made Ru NP electron rich.	904
Benzene	2%Pd_{in}@CNT	$Ni_{in} >> Ni_{out}$/AC	Cyclohexane	Absence of transfer limitations.	886
Benzene	8%Ru_{in}@C 8.5%Ru_{out}/C	$Ru_{in} >> Ru_{out}$	Cyclohexane	Enhanced hydrogen-spillover due to the intimate surface contact between the Ru NP and the carbon supports.	899
Nitrobenzene	4%Ru_{in}@CNT 4%Ru_{out}/CNT	$Ru_{in} > Ru_{out}$	Aniline	Heat treatment was performed, XPS indicated that heat treatment made Ru NP electron rich.	904
Nitrobenzene	8%Au_{in}@C	Au_{in}@C = Au/C	Aniline	Strong confinement confers stability.	901
Nitrobenzene	6%Ni_{in}@CNT 6%Ni_{out}/CNT	$Ni_{in} >> Ni_{out}$	Aniline	Efficient and reusable catalyst for the reduction of various aromatic nitro compounds.	902
Nitrobenzene	6%Pd_{in}@CNT 6%Pt_{in}@CNT	$Pd_{1in} > Pt_{in}$	Aniline $Pd_{1in} > Pt_{in}$	Magnetic NP (Fe, Co) have been grafted on CNF to improve recovery, enabling significant improvement in the reuse of the catalyst.	905
Nitrobenzene	Fe_3C_{in}@C-N-CNT Fe_3C_{out}/FLG	$Fe_3C_{in} > Fe_3C_{out}$	Aniline $Fe_3C_{in} > Fe_3C_{out}$	N-doped CNT with graphene encapsulated Fe_3C.	906
Chloronitrobenzene	10%NiB_{in}@CNT 10%NiB_{out}/CNT	$NiB_{in} >> NiB_{out}$	chloroaniline	Smaller NiB_{in} NP, and improved thermal stability in NiB_{in}. The NiB_{in} can more efficiently activate hydrogen.	900
4-nitrophenol	0.3%Pd_{1in}@C	$Pd_{1in} >> Pd_{out}$	4-aminophenol	Pd SAC formed in a confined interface between graphene and AC.	907
Hexene	12%Pt_{in}@C 10%Pt_{out}/C	Pt_{in}@C > Pt_{out}/C	-	Reaction rate constant is affected by pore confinement and changes in the following order: 2-methyl-1-peneten > 1-decene > 1-hexene.	908
Norbornene	3%Ru_{in}@CNT_{large} 3%Ru_{in}@CNT_{narrow}	Ru_{in}@CNT_{large} >> Ru_{in}@CNT_{narrow}	-	The constricted space inside the CNT_{narrow} lowers turnover numbers.	909

Acetylene	1%Pd_{in}@CNT 1%Pd_{out}/CNT	$Pd_{in} = Pd_{out}$	$Pd_{out} > Pd_{in}$	The electronic interaction between CNT and Pd weakens the adsorption strength of ethylene on Pd_{out}/CNT leading to higher ethylene selectivity.	910
Phenol	3%Pt_{in}@CNT 3%Pt_{out}/CNT	$Pt_{in} >> Pt_{out}$	$Pt_{in} > Pt_{out}$ Cyclohexanone	Smaller Pt particle size, easier reduction, and increased catalyst stability for Pt_{in}@CNT are obtained.	312
D-glucose	0.5%Ru_{in}@CNT	$Ru_{in} > Ru/AC$	-	Due to the improved transfer resistance in longer CNT, the catalytic activity increases with reducing CNT lengths. It also increases with the reduction of diameters.	911
Cellobiose	2%Ru_{in}@CNT 2%Ru_{out}/CNT	$Ru_{in} > Ru_{out}$	Sugar alcohols	Higher reducibility of Ru_{in} is yielded due to the electron-deficient of CNT interior surface. Enhanced interactions between the reactants and Ru_{in} give higher conversion. Confinement reduces the leaching and improves the stability.	894
Cellobiose	2%Ru_{in}@CNT_{large} 2%Ru_{in}@CNT_{narrow}	$Ru_{in}/CNT_{narrow} >$ Ru_{in}@CNT_{large}	Sugar alcohols	The confinement effect of CNT channel was gradually enhanced with the decrease of nanotube diameters.	912
Furfural	1%Pd_{in}@C 1%Pd_{out}/C	$Pt_{out} >> Pt_{in}$	$Pt_{out} >> Pt_{in}$ Furfuryl alcohol	1%Pd_{in}@C favors the formation of 2-methyl furan, probably due to an encapsulating effect favoring perpendicular orientation of furfural adsorbed on Pd.	913
2,5-Hydroxymethylfurfural	1%Ru_{in}@CNT 5%Ru_{in}@CNT	$Ru_{in} >> Ru/AC$	2,5-Dimethylfuran	Higher loadings result in catalysts that present lower reducibility. 1%Ru_{in}@CNT displays higher intrinsic activity than 5%Ru_{in}@CNT. The decrease in TOF by increasing Ru loading is explained by a decrease in the reducibility of the supported metal.	895
Methyl acetate	3%Cu_{in}@CNT_{large} 3%Cu_{in}/CNT_{narrow}	$Cu_{in} = Cu_{out}$	$Cu_{in} = Cu_{out}$ Methanol	Cu_{in} performed better than Cu_{out}. Cu_{in}/CNT_{narrow} exhibited stronger auto-reduction of Cu NP than Cu_{in}@CNT_{large}. Upon heat treatment the activity and selectivity of Cu_{in}/CNT_{narrow} is superior to Cu_{in}@CNT_{large}.	896
Dimethyl oxalate	8%Ag_{in}@CNT 9%Ag_{out}/CNT	$Ag_{in} > Ag_{out}$	Methyl glycolate $Ag_{in} = Ag_{out}$	Ag_{in} formed wires. The confinement effect was found to induce a geometric effect, which made the surface of Ag rough and enriched with grain boundaries and vacancies beneficial for the activation of hydrogen and diffusion of H-species.	897
Cinnamaldehyde	5%Ru_{in}@CNT	-	-	In single-walled CNT, continuous flow using *sc*CO_2. Hydrocinnamaldehyde (*ca*. 70% conversion, >99% selectivity).	914
Cinnamaldehyde	4%Ru_{in}@CNT 4%Ru_{out}/CNT	$Ru_{in} = Ru_{out}$	$Ru_{in} > Ru_{out}$	Heat treatment was performed, and XPS indicated that heat treatment made Ru NP electron rich.	904

Cinnamaldehyde	3%Ru_{in}@CNT 3.4%Ru_{out}/CNT	-	$Ru_{in} > Ru_{out}$	Different interactions between the confined Ru NP and the exterior and interior walls of the CNT were evidenced. Spatial restriction and enrichment within the CNT inner cavity likely play important roles.	887
Cinnamaldehyde	5%$PtRu_{in}$@CNF 5%$PtRu_{out}$/CNF	$PtRu_{in} > PtRu_{out}$	$PtRu_{in} > PtRu_{out}$	Enrichment within the CNT inner cavity is likely important.	830
Cinnamaldehyde	10%$PtRu_{in}$@CNF	$PtRu_{in}$ > PtRu NP	-	Higher local concentration of reactants and catalyst inside CNF.	888
Cinnamaldehyde	5%Pd_{in}@CNT	Pd_{in} > Pd/AC	$Pd_{in} >> Pd/AC$	A peculiar metal-support interaction is proposed.	915
Cinnamaldehyde	3%Pt_{in}@CNT_{large} 3%Pt_{out}/CNT_{narrow}	$Pt_{in} < Pt_{out}$	$Pt_{in} > Pt_{out}$	Complete hydrogenation on Pt_{out}, cinnamyl alcohol on Pt_{in}.	916
Cinnamaldehyde	1.6%Au_{in}@CNT 1.6%Au_{out}/CNT	$Au_{in} >> Au_{out}$	$Au_{in} = Au_{out}$	Hydrocinnamaldehyde is produced. The interaction of confined Au NP with CNT facilitates the activation of H_2, which is the rate determining state.	898
α-ketoesters	5%Pt_{in}@CNT 5%Pt_{out}/CNT	$Pt_{in} >> Pt_{out}$	$Pt_{in} > Pt_{out}$	High activity and enantioselectivity are attributed mainly to enrichment of both cinchonidine and reactants in the inner cavity of CNT.	889
α-ketoesters	5%Pt_{in}@CNT 5%Pt_{out}/CNT	$Pt_{in} >> Pt_{out}$	$Pt_{in} > Pt_{out}$	$Pt^{\delta+}$ species are stabilized in CNT when Na^+ is present. The $Pt^{\delta+}$ promoted the interaction between cinchonidine/reactant and Pt, which is crucial for high enantioselectivity. H_2 enrichment in the channels contributed to the high activity.	890
α,β-unsaturated carboxylic acid	5%Pt_{in}@CNT 5%Pt_{out}/CNT	$Pt_{in} >> Pt_{out}$	$Pt_{in} >> Pt_{out}$	Higher activity and *e.e.* on Pt_{in}. Water enhances the interaction between cinchonidine and the CNT channels, and the ability of the channels to discriminate between the reactant and product.	917
α,β-unsaturated carboxylic acid	5%Pd_{in}@CNT 5%Pd_{out}/CNT	$Pd_{in} > Pt_{out}$	$Pd_{in} > Pt_{out}$	The enhanced catalytic performances (activity and enantioselectivity) is attributed to the enrichment of reactant, chiral modifier, and additive in the channels of CNT.	891
CO_2	5%Pd_{in}@CNT 5%Pd_{out}/CNT	$Pd_{in} > Pt_{out}$	Methanol $Pd_{in} > Pt_{out}$	The channel structure and electronic density difference between the inside and outside of CNT resulted in a smaller size and more $Pd^{\delta+}$ species I Pd_{in}. The inside of CNT has a higher H_2 pressure, which is conductive to CO_2 hydrogenation.	893

Other reactions

Many reactions other than hydrogenation have been studied; the main results are reported in Table 5. It emerges from the analysis of these results that if in the majority of the published works the confinement of the active phase has a positive role on the catalytic performances (activity, selectivity and/or stability), there are reactions where the impact of confinement is negative. This is the case of the ammonia synthesis reaction,[718] for which the electron deficient Ru NP confined in CNT are less active for the dissociative adsorption of N_2 (rate determining step of the reaction) than the electron rich Ru NP deposited on the external surface of CNT, even if a selective enrichment of N_2 over H_2 has been reported in carbon micropores.[918] This electronic effect does not seem to affect the activation of dihydrogen in the same way, since as we have just seen, confined catalysts are good hydrogenation catalysts. For the rest, most of the effects of confinement reported in these studies remain the same as in the studies on FTS and hydrogenation: i) a better reducibility of the active phase, ii) a higher dispersion of the metallic phase for the confined systems, and iii) a better stability of the confined phase. MD simulations performed on a CuO_{in}@CNT catalyst for ozone decomposition and hydroxyl radical generation have shown that the effects of the confined environment of CNT included: i) more reactants into the channel; and ii) an interaction between CuO and CNT that change the electronic properties of CuO particles.[919] Another DFT study on CO oxidation over Pt_{in}@g-C_3N_4 catalyst has predicted that the energy barrier for CO oxidation over Pt_{in}@g-C_3N_4 is reduced when compared with that on pure Pt(111), suggesting a promoted reaction activity thanks to the confinement effect.[759]

Table 5. Catalytic performances of catalysts confined in carbon materials for various reactions.

Reaction	Catalyst	Activity	Selectivity	Remark	Ref.
Ethylbenzene dehydrogenation	5%CeO_{2in}@CNT 5%CeO_{2out}/CNT	CeO_{2in} > CeO_{2out}	Styrene	The confinement effect strengthens the interaction between CeO_2 NP and carbon (crystal lattice distortion). This promotes reduction of CeO_2 and activation of its surface lattice oxygen, which accelerates the ODH reaction by promoting WGSR.	920
Ethylbenzene dehydrogenation	7%$CeMn_{in}$@CNT 7%$CeMn_{out}$/CNT	$CeMn_{in}$ > $CeMn_{out}$/CNT	Styrene	Higher reduction ability, higher selectivity and reactant enrichment.	921
Ammonia synthesis	3.5%Ru_{in}@CNT 2.9%Ru_{out}/CNT	Ru_{in} < Ru_{out}	-	Ru_{out} exhibits a higher electron density than Ru_{in}. The dissociative adsorption of N_2 (electrophilic process and rate determining step) is more facile over Ru_{out} than that over Ru_{in}.	718
Ammonia decomposition	5%$FeCo_{in}$@CNT 5%$FeCo_{out}$/CNT	$FeCo_{in}$ > $FeCo_{out}$	Hydrogen	Confinement improves the thermal stability.	922
Ammonia decomposition	2%Ru_{in}@CNT 2%Ru_{out}/CNT	Ru_{in} < Ru_{out}	Hydrogen	Ru_{in} NP are smaller than Ru_{out}. Larger particles are more active in ammonia decomposition.	923
Oxidative carbonylation of methanol	9%Cu_{in}@C 9%Cu_{out}/CNT	Cu_{in} > Cu_{out}	Dimethyl carbonate	Copper species in the cavity show high auto-reduction ability in spite of poor dispersion after activation.	924
Reduction of nitrate	2%Pd-1%Cu_{in}@CNT 2%Pd-1%Cu_{out}/CNT	Pd-1%Cu_{in} < Pd-1%Cu_{out}	N_2	Pd-1%Cu_{in} NP are smaller. Superior stability of Pd-1%Cu_{in} catalyst. Electron deficient Pd-1%Cu_{in} NP are less efficient for this reaction.	925
Formic acid decomposition	2%Pd_{in}@CNT 2%Pd_{out}/CNT	Pd_{in} >> Pd_{out}	H_2	Easier reduction of Pd_{in} and Pd_{in} NP bigger than Pd_{out}. *d*-band center is shifted downward when Pd NP are confined inside the CNT.	926
Hydrodeoxygenation of guaiacol	15%Ni_{in}@CNT 15%Ni_{out}/CNT	Ni_{in} = Ni_{out}	Cyclohene/ cyclohexane	The formation of cyclohexene is favored for Ni_{in}. The differences in selectivity are attributed to steric constraints.	927
Toluene oxidation	2%Pt_{in}@CNT 2%Pt_{out}/CNT	Pt_{in} >> Pt_{out}	CO_2	Confinement allows tailoring the oxidation activity by restricting the cluster size down to around 1.0 nm and by retaining the Pt species at the active reduced state, even in the presence of O_2 up to 473 K.	928
Ethanol oxidation	2%Pt_{in}@C/CNT 2%Pt_{out}/CNT	Pt_{in}@C/CNT > Pt_{out}	Acetic acid	Carbon film encapsulated Pt NP supported on CNT. Carbon films encapsulating the Pt NP suppress the over oxidation.	929

Selective oxidation of benzyl alcohol	3%K12%Mn_{in}@C/CNT 4%K14%Mn_{out}/CNT	KMn_{in} > KMn_{out}	Benzaldehyde	Easier reducibility of MnO_2 confined in CNT.	930
CO oxidation (PROX)	1%Au_{in}@CNT 5%Au_{out}/CNT	Au_{in} < Au_{out}	-	Smaller NP in Au_{out} but not prepared by the same method than Au_{in}.	931
CO oxidation (PROX)	5%Ru_{in}@CNT 5%Ru_{out}/CNT	Ru_{in} > Ru_{out}	-	The CNT cavity can selectively increase the density of reactants and the confinement of Ru NP provides a micro-environment to increase the activity of catalytic sites.	932
CO oxidation (PROX)	5%Ru_{in}@CNT 5%Ru_{out}/CNT	Ru_{in} > Ru_{out}	-	Smaller NP and enhanced reducibility in Ru_{in} are obtained. The enrichment of CO and O_2 enhances the ratios of CO/H_2 and O_2/H_2 in the channels of CNT. Stable catalyst.	819
CO oxidation (PROX)	20%$Cu_xCe_{1-x}O_{in}$@CNT	-	-	Catalytic performance is correlated with Cu/Ce molar ratios.	933
CO oxidation	Pt@Graphene	-	-	The electronic interaction between the top graphene layer and CO helps to weaken the C–O bond in CO and promotes the formation of O–CO bond.	756
Propylene epoxidation	TiO_{2in}@CNT TiO_{2out}/CNT	TiO_{2in} > TiO_{2out}	-	Electron transfer from Ti to CNT inner surface in TiO_{2in}@CNT. In contrast, no electron transfer has been observed for TiO_{2out}/CNT.	934
Styrene epoxidation	5%Co_{in}@CNT 2%Co_{out}/CNT	Co_{in} > Co_{out}	Epoxide	Co_{in} is more active, more selective and more stable.	935
Benzene hydroxylation	4%Pd-0.3%V_{in}@CNT_{narrow} 5%Pd-0.3%V_{in}@CNT_{large}	M@CNT_{narrow} > M@CNT_{large}	-	The understanding of the confinement effects needs further systematic investigations.	936
Alkyne hydrosilylation	5%Rh_{in}@CNF 5%Rh_{out}/CNF	-	Regioselectivity Rh_{in} > Rh_{out}	Specific π-π interactions increase the local concentration of the aromatic reactant.	937
Alkyne hydrosilylation	5%Pt_{in}@CNF 5%Pt_{out}/CNF	-	Regioselectivity Pt_{in} > Pt_{out}	Increased concentration of aromatic substrates in CNT thanks to specific π-π interactions. Pt_{in}@CNT create an environment promoting the formation of aromatic over aliphatic products in the competitive hydrosilylation of phenylacetylene with mixture of triethylsilane and dimethylphenylsilane reactants.	938
Huisgen cycloaddition	5%Cu_{in}@CNF 5%Cu_{out}/CNF	Cu_{in} > Cu_{out}	-	Cu_{in}@CNT exhibits superior activity and stability in cycloaddition reactions. Sintering after recycling but activity remains high for Cu_{in}@CNT.	939
Suzuki-Miyaura reactions	8%Pd_{in}@CNF 6%Pd_{out}/CNF	Pd_{in} = Pd_{out}	Pd_{in} < Pd_{out}	Activity and selectivity of the confined reactions are sensitive to the steric congestion of the aryl iodides.	940

Suzuki-Miyaura reactions	8%Pd_{in}@CNF	-	-	Pd NP do not dissolve and re-precipitate. NP migration with coalescence is the main mechanism decreasing the active surface area under Suzuki-Miyaura reaction conditions.	941
Asymmetric oxa-Michael addition	$CoFe_2O_{4in}$@CNT $CoFe_2O_{4out}$/CNT	$CoFe_2O_{4in}$ > $CoFe_2O_{4out}$	Flavone $CoFe_2O_{4in}$ > $CoFe_2O_{4out}$	$CoFe_2O_{4in}$ is recyclable and shows excellent activity and selectivity.	942
Knoevenagel condensation-reduction cascade reaction	Pd_{in}@g-C_3N_4	-	-	Confinement in g-C_3N_4 nanotubes concentrates the reactants. The presence of N atoms stabilizes Pd NP and prevents the leaching, leading to a high stability.	943
Methane activation	Pd_{4in}@CNT Pt_{4in}@CNT	Pt > Pd	-	Higher activation energy are calculated for Pd than for Pt.	944

Electro- and photocatalytic reactions

Although several studies report an effect of confinement of the active phase in reaction such as ORR and HER,[945] few efforts have been devoted to the understanding of these effects. Nitrogen doped CNT appear to be more convenient that pure CNT to confine the active phase,[946,947] probably because of a different charge transfer. For CNT, a DFT study has shown that in the case of a confined Fe_4O_6 cluster for the OER, small diameter CNT should be used to take advantage of the electronic interaction with the CNT.[948] The inner cavity of CNT should also be beneficial for efficient molecular- and ion-diffusion.[949] Since electrocatalysis is often performed in acidic media, corrosion issues are critical. The confinement of the active phase contributes to protect the metal from sintering or leaching, providing excellent stability under accelerated degradation conditions.[947,949-952] DFT calculations have shown that it should be possible to enhance the hydrogen reactivity on Ni *via* confinement underneath graphene.[953] The graphene overlayer on the Ni surface weakens the adsorption free energy of an H adatom on Ni, shifting nickel close to the optimum of HER volcano plot. More studies are necessary to confirm potential advantages of confinement in electrocatalysis. Indeed, some experimental works in ORR have also shown that it is necessary that: i) all of the Pt NP are present on the outermost surface of the support, and ii) the ionomer covers uniformly the Pt and carbon surfaces, in order to efficiently supply large amounts of oxygen and protons at high current densities.[954]

In photocatalysis, the synergy between TiO_2 and carbon nanomaterials is well documented, and enhanced photocatalytic activity occurs through: i) minimization of electron/hole recombination, ii) band-gap tuning/photosensitization; and iii) provision of high quality highly adsorptive active sites.[664] Photocatalytic processes in spatially confined nanoreactors have also been discussed, but mainly in the case of porous oxides and hybrid photocatalysts based on molecular-organized assemblies.[955] Up to date, few works are related to the study of

confinement of photocatalytic reactions in carbon materials. The discovery of the extension of the photocatalytic activity of TiO_2 from the UV to the visible-light region upon confinement in CNT should push-up this domain of research. Table 6 shows representative results obtained with confined catalysts in electro- and photo-catalysis.

Table 6. Catalytic performances of catalysts confined in carbon materials for electro- and photocatalysis.

Reaction	Catalyst	Activity	Remark	Ref.
Confined electrocatalysis				
ORR (acidic)	Pt_{in}@CNF Pt_{out}/CNF	$Pt_{in} > Pt_{out}$	Depositing Pt NP inside GNF results in a catalyst with higher catalytic activity and stability. It also increases electrochemical active surface area.	956
ORR (acidic)	Fe_{in}@CNT Fe_{in}@N-CNT	Fe_{in}@N-CNT > Fe_{in}@CNT	DFT calculations indicate that the catalytic activity could arise from the electron transfer from Fe NP to the CNT.	946
ORR (acidic)	$PtNi_{in}$@C	-	Thanks to confinement effect, and if the threshold for significant Pt dissolution is not exceeded, the initial performance is fully retained for more than 10000 degradation cycles.	950
ORR (basic)	21%Co_{in}@N-CNT	Co_{in} = Pt/C	Great durability, and excellent tolerance for methanol crossover are reported.	952
ORR (basic)	Co_{in}@N-CNT	-	High current density and good durability capability are obtained.	957
Hydrazine oxidation	$NiFe_{in}$@CNT	-	Confined $Ni_{85}Fe_{15}$ NP have superior electrocatalytic activity for hydrazine electrocatalysis than catalysts with other compositions.	958
HER (acidic)	MoC_{xin}@CNT MoC_{xout}/CNT	$MoC_{xin} > MoC_{xout}$	Smaller NP size and more reduced states of the confined MoC_x NP are given. A weakened adsorption of hydrogen on MoC_{xin}@CNT may be another effect enhancing the HER activity.	959
HER (acidic)	Co_{in}@CNT Co_{in}@N-CNT	Co_{in}@N-CNT > Co_{in}@CNT	Fe, Co and FeCo catalysts are studied with long-term durability. Adsorption free energy of the H atom on CNT is decreased by the presence of confined metal and N dopant.	947
HER (acidic)	Co_{in}@N-CNT-rGO	-	Excellent electrocatalytic HER activity.	960
HER (basic)	$CoNi_{in}$@N-C	-	Excellent electrocatalytic HER activity.	961
HER (basic)	$FeNi_{in}$@N-C	-	Excellent electrocatalytic HER activity.	962
HER (basic)	Co_2P/CoN_{in}@N-CNT	-	Excellent electrocatalytic HER activity.	963
HER (basic)	Co_{in}@N-CNT Fe_{in}@N-CNT	$Co_{in} > Fe_{in}$	High stability.	964
HER (basic)	5%Ru_{in}@N-C 5%Ru_{out}/N-C	$Ru_{in} > Ru_{out}$	Fully confined Ru catalyst performs better than semi-confined ones. DFT calculations indicate that the confined space affects the catalytic performance by enhancing the charge transfer from Ru to C.	965
OER (basic)	Ni_{in}@CNT	-	High OER activity.	966
Methanol oxidation	Au_{in}@C	Au_{in}@C > Au_{out}/C	The electrons could transfer from the graphitic layers to the Au core.	967

Methanol oxidation	55%Pt_{in}@CNT 55%Pt_{out}/CNT	$Pt_{in} > Pt_{out}$	Pt_{in}@CNT shows higher electrocatalytic activity and stability than Pt_{out}/CNT. Well-ordered CNT channels allow a regular molecular- and ion-diffusion. No Ostwald ripening of Pt NP is observed.	949
Methanol oxidation	2.5%Pd_{in}@C 2.5%Pd_{out}/C	$Pd_{in} > Pd_{out}$	The activity improves due to the higher proximity of the NP to the reactants inside the cavity and minimal leaching of the NP over 300 cycles.	951
Glycerol oxidation	Pt_{in}@FLG	-	Pt nanosheets with a unique (100)/(111)/(100) faceted structure within FLG provide excellent catalytic activity and selectivity toward C_1 products.	968
Confined photocatalysis				
Methylene blue photodegradation	20%TiO_{2in}@CNT 20%TiO_{2out}/CNT	$TiO_{2in} > TiO_{2out}$	Large amount of unpaired electrons in TiO_{2in}@CNT, which possibly arise from oxygen vacancies are created. Ti^{3+} or oxygen vacancies generated from the modified electronic structure of TiO_2 via the confinement accounts for the extension of the photocatalytic activity from the UV to the visible-light region.	969
Methylene blue photodegradation	$ZnFe_2O_{4in}$@FLG	$ZnFe_2O_{4in}$@FLG > $ZnFe_2O_4$	The graphene is beneficial for fast transport of photon-excited electron from catalyst surface, and acts as electron reservoir that can suppress the recombination of photogenerated electron-hole pairs.	970
Methylene blue photodegradation	CdS_{in}@CNT CdS_{out}/CNT	$CdS_{in} > CdS_{out}$	Enhanced separation efficiency of photogenerated charge carriers is demonstrated. The photo-corrosion of CdS is suppressed efficiently by confinement.	971
Cyclohexane oxidation of	Au_{in}@CNT Au_{out}/CNT	$Au_{in} >> Au_{out}$	Confinement of reaction intermediates within CNT might prolong their contact time with the catalyst.	972

3.2.4 Material perspective

The confinement of metal NP in carbon (nano)material pores of nanometer scale offers significant advantages for catalysis. The controlled synthesis of such catalyst in CNT is often more delicate than a simple impregnation,[277,828,830,973] even if it has been shown that wet impregnation of oxidized CNT can allow to reach up to 80% of confinement.[829] The choice of the method depends on CNT diameters, and gas phase processes seem more adequate for small diameter CNT. We have shown in this section that confinement effects can be classified into two categories, "soft" and "hard" effects. Figure 45 summarizes the main effects observed in the studies of catalytic confinement effects in CNT. Soft effects such as reagent enrichment or rapid diffusion will directly affect the kinetics of the reaction. A hard effect like the charge transfer between the metal and the support will also affect activity/selectivity and stability. Combined hard/soft effects will also lead to better reducibility, dispersion and stability of the confined active phase.

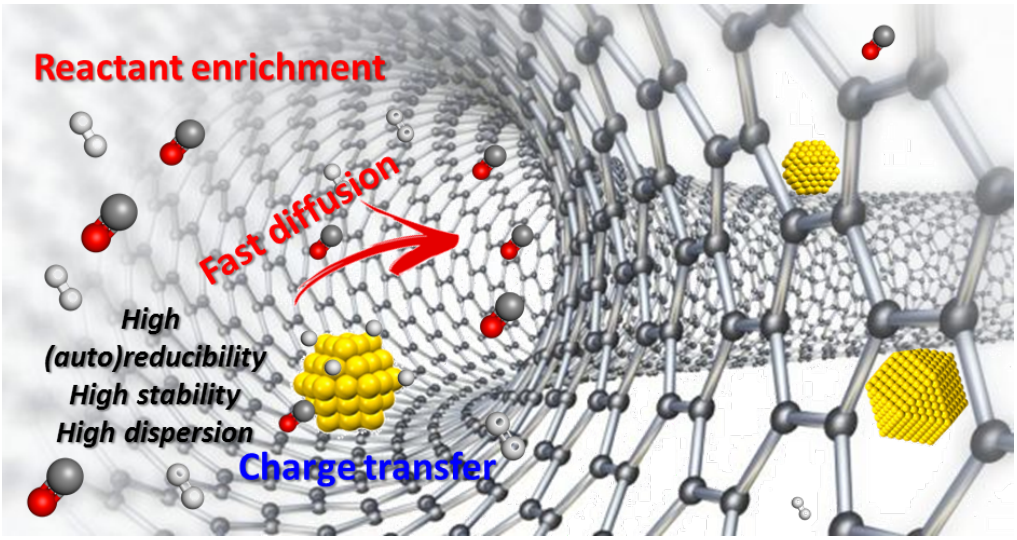

Figure 45. Main confinement effects related to catalysis observed in carbon nanotubes.

If the large majority of studies are dealing with CNT it is of course because of the peculiar morphology of these nano-objects, which present a well-defined cavity that can be easily opened. It is possible that some of the effects of Figure 45 are also operative in the porosity of other carbon materials or in metallic NP encapsulated/embedded by a graphenic or graphitic layer. However, in this latter case, the accessibility of the reactant to the metallic surface is a critical issue that is difficult to control. Indeed, even hydrogen cannot penetrate a graphene layer, so it is necessary to open a porosity in these graphenic or graphitic layers, in such a way that the confinement effects do not disappeared. Significant efforts are still to be made in this direction. As far as CNT are concerned, the confinement effects could be seen as the other properties of this material (electronic, mechanic), for which it has been shown for a long time that the reality was still far enough from the expectations because of the non-perfect structure of industrially produced CNT. However, the positive point of confinement is that it is essentially based on the perfection of the internal layer of nanotubes, which is often more perfect than the external sheets.

As far as more conventional carbon materials are concerned, such as activated carbon or carbon black with carbon slit (micro)pores, no confinement effect on catalysis has been reported. This should be linked to the defective structure of these materials, which deferred sensibly from the one of CNT or graphene. In that case, the microporosity of the materials is often a synonym of internal diffusion/mass transfer limitations in liquid[974-976] or even gas phase[977,978] catalytic reactions. The mass-transfer limitations can be evaluated experimentally using diagnostic criteria such as varying gas flow rate, stirring speed (in slurry reactors), catalyst concentration and particle size.

For the purpose of preventing these disadvantages, many attempts have been made to develop mesoporous structured supports, allowing operation in a fixed-bed reactor without significant internal diffusion limitation.

3.3 Hydrogen and oxygen spillover

Spillover is defined as the transport of a species, adsorbed or formed on a specific surface (or site), to another surface, which does not adsorb or form this species under the same conditions.[979] More specifically, Boudart *et al*. called "spillover" the migration of H atoms from metallic particles to a support.[980] In heterogeneous catalysis, only the spillover of catalytically active species is important. Spillover is involved in many surface reactions and transport phenomena, and includes other atoms than hydrogen, like oxygen or molecules as CO;[981] and sulfur spillover has also been reported on carbon materials.[982] Spillover encompasses not only adsorption but gasification of solids, creation of catalytically active sites, and reaction with adsorbed species. Hydrogen or oxygen atoms are not usually produced on a perfect graphitic surface, but can be formed on defects. Additionally, it has been shown that spillover from a metal surface to the surface of a defect-free carbon support is energetically not favorable.[983,984] Spillover of H or O atoms from metal particles to a carbon support with defects or to a contaminated support is possible. If the defects bind the H or O atoms and if the distance between the defects is not too large, then these atoms might diffuse from the metal particles to the defect sites. Spillover of hydrogen or oxygen is a fast phenomenon, which can compete with the rate of a catalytic reaction. The spillover species formed on the metal may react with the reactant adsorbed on the support. More subtle interactions are observed when the spillover species create new types of active centers on the support.[985] The catalytic activity and selectivity may be thus promoted or modified by the spillover of adsorbed species.

3.3.1 Hydrogen spillover

A hydrogen spillover mechanism should consist of several steps. In the first one, molecular hydrogen is activated and dissociated on a TM catalyst in close contact with the support. Secondly, the migration of H species from the catalyst particles to the support should occur. The last two steps consist in the diffusion and recombination of H species on the support surface. For H-spillover, different species have been considered, such as hydrogen radicals (H•), protons (H^+), hydrides (H^-) and activated hydrogen (H^*).[14] On carbon materials, the hydrogen spillover mechanism has been largely discussed because of its relevance to hydrogen storage, and to a lesser extent for its implication in catalytic reactions. Some reviews have already been published,[986-992] and we will concentrate on the most relevant results.

We will first consider the fate of dihydrogen on a bare support. Weak binding energy of molecular hydrogen on pristine graphene has been reported (1-2 kcal.mol^{-1}).[993-995] A consequence of that is the easy diffusion of H_2 on graphene with activation energy ranging between 0.2-0.4 kcal.mol^{-1}, according to the temperature.[996,997] The dissociative adsorption of dihydrogen on highly symmetric sites of graphene (or CNT) is relatively high, and ranges between 76.1 kcal.mol^{-1} and 89.9 kcal.mol^{-1}, depending on the bonding site.[983,998,999] It is associated with an endothermic heat of reaction of 43.6 kcal.mol^{-1}, making dissociation of H_2 on pure graphene a rare event.[1000] The isolated chemisorbed H species diffuses on graphite from top site to top site *via* bridge sites with an associated barrier of 22-23 kcal.mol^{-1}, and diffusion through the hollow site is unfavorable (93.4 kcal.mol^{-1}).[1000-1002] For diffusion of spiltover H in the vicinity of another H, the activation energy is lower, typically in the range 9-12 kcal.mol^{-1}.[996,1001,1003] According to the surface coverage, dimerization and clustering of atomic hydrogen on graphitic surface have also been observed both theoretically and experimentally.[1004-1008] The

existence of hydrogen-rich domain around metallic NP has thus been proposed.[1009] Calculations of diffusion distance in carbon-based spillover systems ranged from 15 nm at 298 K[1010] to 100 nm at 473 K and to 5 mm at 623 K.[1011] The stability of chemisorbed H atom(s) particularly related to desorption has been investigated. For a monomer, diffusion and desorption have similar barriers, 21.7 and 20.1 kcal.mol^{-1}, respectively. Adsorption of a second H close to the first adsorbed one does not modify the adsorption barrier, but appreciably changes the desorption of the single hydrogen.[1001,1012] Recombination of two chemisorbed H atoms (dimer) to desorb H_2 required passing an activation energy of 32.3-37.6 kcal.mol^{-1}, according to the position of the two chemisorbed H atoms on the carbon atoms.[1012] These values are in good agreement with TPD experiments for hydrogen on graphite. It is worth mentioning that much higher energy barrier have also been reported (65 kcal.mol^{-1}) depending on the model.[1001] An alternative Eley-Rideal mechanism for molecular hydrogen abstraction has also been proposed that involves an adsorbed H atom and an incoming H atom from the gas phase.[1013-1016] For this mechanism, the energy barrier is lower than for the Langmuir-Hinshelwood mechanism.[1001] The diffusion barrier is found to be curvature-dependent with a higher barrier associated with carbon atoms of higher curvature, as in single-walled CNT.[1017] Applying stress to graphene lower dramatically the barrier of H_2 dissociation and changes the process from being endothermic to exothermic, without modifying significantly the diffusion.[1000] A slight decrease of the activation energy for H_2 dissociation was reported on N-G,[1018] and for graphene bearing hydroxyl groups.[1019] DFT results thus suggest that it could be difficult for chemisorbed H atoms to move freely at near-ambient temperatures, since diffusion requires C-H bond dissociation, with a relatively high activation energy. Interestingly, it has been proposed that the use of a shuttle gas (H_2O, HF, or NH_3) can make the migration easier *via* coadsorption.[1020,1021] Without co-adsorbates a barrier of 21.7 kcal.mol^{-1} has to be passed for the diffusion barrier of H atoms on graphene, whereas with water/ammonia this barrier decreases to 19.6/2.8 kcal.mol^{-1}.[1021] The

presence of H_2S was also found to accelerate H-spillover in CoMo/C HDS catalysts.[1022] It was proposed that H_2S leads to an increase of terminal -SH groups by dissociative H_2S adsorption, which could form hydrogen bridges with the carbon support functional groups. It is worth mentioning that the addition of "co-catalysts" presenting various proton affinity to assist the spillover was already proposed in the early works of Boudart, who proposed the formation of solvated protons on the metallic surface.[1023]

It has also clearly been shown both theoretically and experimentally that the role of oxygenated surface groups is crucial to improve spillover and also decrease the H diffusion barrier,[989,1024-1028] since an energy barrier as low as 7.6 kcal.mol^{-1} has been reported for migration of a H atom from a hydroxyl group to an adjacent O (epoxide) atom. Thus, the process of H atom diffusion on oxidized carbon surfaces should happen in a similar manner to the H spillover mechanism on metal oxide surfaces. Of course, the proximity of O groups will facilitate the phenomenon; and the H diffusion barrier will depend on the type of surface functionalities. For the migration of a H between two C atoms that are both in *ortho* position to OH groups, the H diffusion barrier is 23 kcal.mol^{-1}, very similar to the one on pristine graphene.[1029] Experimental heats of adsorption, XPS analyses, and *ab initio* calculations have shown that the binding energy between the spiltover H atoms and the different groups followed the following order: lactone > semiquinone > carboxyl > basal plane.[1030] For hydrogen spillover, semiquinone are thus ideal receptors for the spiltover hydrogen. A synergistic role of oxygen surface groups and water on hydrogen spillover has also been reported.[1027] The stability of the oxygen surface groups is an important parameter to consider, since in many cases water desorption has been reported because of the poor stability of some -OH groups under attack of an H atom.[1031] Thus, H-spillover has been already used to remove oxygen surface groups of carbons,[1011] and for reduction of GO at 353 K.[1032,1033] Such a process allows to increase the C/O atomic ratio from 1.7 in GO to 22 in rGO.

Among the different intrinsic defects of graphene, the single vacancy is the one that allows the higher binding energy of dihydrogen (7-12 kcal.mol^{-1}).[993,999] The chemisorption of H_2 on such site, as well as on zigzag and armchair sites has been studied by DFT.[1034-1039] The zigzag edges are very reactive, and it is possible to dissociate H_2 on these sites without any (or very small) activation barrier.[1034,1035] There is an activation barrier hindering spontaneous H_2 dissociation at the armchair edges (13.8-39.2 kcal.mol^{-1}, according to H_2 binding site).[1036] The SV forms an intermediate level between the armchair and zigzag edges, and activation energies of 18.4-25.4 kcal.mol^{-1} have been reported.[999,1037] Lower activation energy or even barrierless profiles have also been reported.[1038,1039] On a hydrogenated vacancy, a second dihydrogen can dissociates with activation energy of 11.5-20 kcal.mol^{-1}.[999,1040] Further hydrogen incorporation is possible with an increase of the activation energy.[1040] The relative energies of C-H bonds follow the order: zigzag edge > armchair edge > basal-plane edge.[1041]

The first step in H-spillover on TM particles is to dissociate hydrogen molecules. Although several metals or semi-metals have been investigated (Ni,[349,1031] Ti,[349,556,1042] V,[1043] Rh,[97,556] Cu,[1044] Al,[611]), Pd and Pt are the most studied. The dissociative chemisorption of H_2 on Pt and Pd particles is generally easy, and is accompanied by the formation of strong M-H bonds. INS combined with H_2 adsorption measurements on Pt NP on activated carbon have detected the adsorption of H_2 on hydride-covered Pt NP, and provided evidence for the occurrence of atomic hydrogen spillover from the Pt surface to unsaturated reactive sites located at the irregular borders of the sp^2 domains on the support.[368] These binding energies are coverage dependent. Theoretical calculations on Pt clusters indicate that the binding energy of the H atoms is 56 kcal.mol^{-1} at full coverage, and 74 kcal.mol^{-1} at zero coverage.[989] On carbon supported Pt_4 clusters, the dissociative chemisorption of H_2 is barrierless, up to saturation (5 to 6 H_2).[983,1024] Strong binding energies have been reported; for example the average binding strength of H atoms on a fully saturated Pt_4 cluster (with 10 H) on graphite was calculated to be 74 kcal.mol^{-}

[1].[1024] On curved carbon surfaces such as carbon nanohorns, the binding energy is even higher: between 40 and 110 kcal.mol^{-1} according to the surface coverage.[1045] This is a very unfavorable starting point for spillover, and high-energy barriers (46-62 kcal.mol^{-1}) have been systematically predicted for migration of one H atom from the fully saturated Pt_4 cluster to the defect-free graphitic support.[188,983,984,1024] However, on curved carbon surface, DFT calculations have shown that the H atom migration from the hydrogenated Pt_4 cluster to the support surface is thermodynamically favorable at room temperature with low energy barrier and highly exothermic.[1045] A lower barrier was also measured for the migration of 2 H atoms from a physisorbed Pt_6H_{24} cluster on graphene (11 kcal.mol^{-1} per H atom).[1017] Lower energy barriers for H-migration from the fully saturated Pt_4 cluster were also reported on B-G.[188] More favorable energy barriers (≈ 35 kcal.mol^{-1}) were predicted on fullerene C_{60} for Pt_{1-13} clusters.[1046] In the presence of surface oxygen groups in the vicinity of the Pt_4 cluster, the migration of one H atom is much easier, with an energy barrier of 9.2 kcal.mol^{-1} per H atom (see Figure 46a for an epoxy group).[1024] Such a decrease was also reported for Ni_4 clusters in the vicinity of an epoxy group.[1031] Sulfonic groups present on a carbon surface can also promote the spillover process that favors H_2 adsorption in large amounts on a Pt catalyst.[1047] Tin oxide present in a PtSn/C catalyst constitutes anchoring centers for spiltover hydrogen, and the tin oxide is reduced by these H species that migrate to the particles close to the Pt atoms.[1048] In the case of supported palladium, the dissociative chemisorption barriers of H_2 is cluster-size dependent: ≈ 0, ≈ 0, 10.6, 6.0, 6.9, 2.9, and 0.7 kcal.mol^{-1} for Pd_2, Pd_3, Pd_4, Pd_5, Pd_6, Pd_9 and Pd_{13}, respectively.[326,610,1049,1050] For a single Pd atom on graphene H_2 adsorbed molecularly, with a weaker interaction and smaller binding energies than on Pt.[609,1051-1054] The adsorption energy per H_2 decreases when increasing the hydrogen concentration.[1055] If the Pd atoms or clusters are deposited on SV-G, it prevents the desorption of metal-hydrogen complexes, and lowers the Pd-hydrogen bonding energy in a more pronounced way compared to Pt on defect-free

graphene.[325,1056-1059] A different situation seems prevailing for a Pd_4 cluster on DV, since five H_2 molecules were molecularly adsorbed.[534] Nitrogen or boron doping of the support also affects significantly the Pd-H bonding energy.[551,1060-1064] The binding energy of a H_2 on Pd is thus found to depend on the cluster size and on its adsorption site (vacancy, N- or B-doping, oxygen surface groups).[263,1063] MD simulations have shown that a low energy barrier does not mean that all the molecules dissociate, and the probability for dissociation was 33% on the supported Pd_{13} cluster and only 5% on Pd_6.[326] H_2 molecules that did not find the most favorable path to dissociate are either reflected or molecularly adsorbed. On clean graphene, the energy barrier to pass for H-migration from a supported Pd_{13} cluster to the support is 60 kcal.mol^{-1},[326] so similar to the Pt system. This value decreases to 48 kcal.mol^{-1} when the Pd_{13} cluster is saturated by 10 hydrides. This barrier is further significantly reduced (15.7 kcal.mol^{-1}) if a Pd_4 cluster is in the vicinity of a fully hydrogenated graphene phase (Figure 46b).[1065] The presence of nitrogen surface groups near the Pd cluster also allows for a significant decrease of the energy barrier for H-migration. Energy barriers of 18.4 (pyridinic group) and 11.5 kcal.mol^{-1} (pyrrolic group) were estimated in the case of a fully covered Pd_4 cluster.[608]

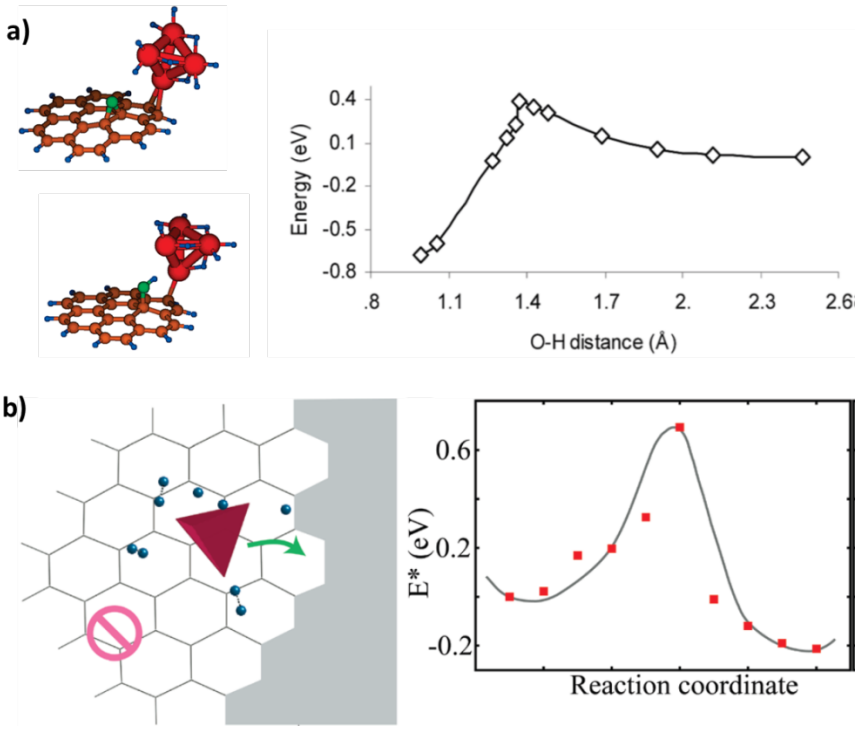

Figure 46. a) Optimized structures of the initial and final states and DFT-calculated reaction coordinate scans for the migration of H from a Pt_4 cluster to epoxide O on a model graphite surface. Reprinted with permission from Psofogiannakis, G. M.; *et al*. *J. Am. Chem. Soc*. **2009**, *131*, 15133-15135.[1024] Copyright 2009 from the American Chemical Society; and b) Fully relaxed Pd_4 cluster saturated with H, next to a hydrogenated phase (gray area), and plot of energies of intermediate images for the barrier calculation versus the reaction coordinate. Reprinted with permission from Singh, A. K.; *et al*. *ACS Nano* **2009**, *3*, 1657-1662.[1065] Copyright 2009 from the American Chemical Society.

Many experimental studies were also conducted to measure the hydrogen spillover in carbon-supported catalysts, and to identify/characterize the key involved species. Hydrogen adsorption isotherms and advanced DFT modelq can be used to obtain accurate values on physisorbed, chemisorbed and spilt-over contributions.[1066] Direct evidence for the spillover of atomic hydrogen may be studied by several techniques. Inelastic neutron scattering has been used for

the characterization of catalysts;[1067] since this technique reveals the state of hydrogen, in either atomic or molecular form, and provides a direct quantitative evaluation of the amount of hydrogen adsorbed on carbon in an atomic form *via* spillover.[368,1009,1068-1072] The existence of hydrogen-rich domains around the metal particles has been proposed from an INS study conducted on a Pt/C catalyst.[1009] Using EXAFS, Shen and coworkers have demonstrated that palladium hydride phase can be even formed, in the context of electrochemical reduction of CO_2 to synthesis gas with controlled CO/H_2 ratio,[1073] a result also confirmed by XANES under *operando* conditions when Pd/C catalysts are in the presence of hydrogen.[1074] Hydrogenation of the carbon support of a Pd/C catalyst by H-spillover was observed under harsh hydrogenation conditions (high pressure and temperature) to give a material with contributions that strongly resemble those of an amorphous hydrogenated carbon.[1072] The reactivity of defects/vacancies has also been probed by INS coupled with NMR studies.[1069] INS studies have evidenced the occurrence of atomic H-spillover from Pt or Pd surfaces to unsaturated reactive sites on the carbon support, and in particular to those located at the irregular borders (edges),[368] with the formation of C-H bond.[1075] These sites can be completely saturated during the hydrogenation process. Small-angle neutron scattering (SANS) has been used for the determination of the clustered structure and spatial distribution of hydrogen adsorbed in the porosity of carbon materials.[1076] *In situ* conductivity and *ex-situ* XPS studies have shown that spillover is responsible for molecular hydrogen hydrogenation of a Pt/CNT catalysts,[1077] and that stable C-H bonds are formed during the process.[1077,1078] *In situ* electrical studies were also performed on Pd/C to evidence that H-spillover contributes to a decrease of the electrical conductance of the carbon film.[1079] *In-situ* high-pressure Raman spectroscopy and DFT calculations were used to probe reversible spillover in Pt/C catalysts.[1080] The hydrogenation apparently occurs through H surface diffusion in a chemisorbed state, while dehydrogenation requires surface oxygen groups and the back-diffusion of the chemisorbed species to platinum. Diffuse reflectance infrared

Fourier transform spectroscopy (DRIFTS) was employed to identify the various chemical species formed during the reaction of H_2 and Ru/C.[1081] In the absence of Ru, only physisorbed H_2 was detected at room temperature. On Ru/C, in addition to the physisorbed H_2, the formation of water, surface hydroxyl groups (X-OH, where X = C or Ru), and C-H bonds was evidenced. A TPD study of nitrobenzene (coupled with CO poisoning) on Pt/N-doped-C catalyst has provided interesting information: i) the H amount is significantly higher than the chemisorption capacity of Pt; ii) the spiltover H are mobile and reverse spillover from the support to the metal can occur; and iii) the spiltover H are not active for nitrobenzene hydrogenation and thus possibly stored protons on the surface, and electrons in the bulk of the support.[1082] This later mechanism possibility, involving both protonic and electronic conductions was already proposed in 1977 by Kerren and Sofer. It could explain the positive role of surface oxygen groups and water in the diffusion step.[1083] The coexistence of strongly chemisorbed H^+ ions and weakly chemisorbed H atoms has also been proposed.[1084]

Further different parameters have been identified as affecting the spillover. First, the presence of nitrogen-[1085] or sulfur-[1086] but mostly oxygen-surface groups (such as hydroxyl groups) enhanced surface diffusion, or reversible adsorption, of the spiltover H atoms, even if surface functionalization of the support decreases its specific surface area and pore volume.[513,1027,1028,1030,1087-1093] As discussed previously, it can be due to an improved migration from the metal to the support, but also to a higher dispersion of the metallic phase on the functionalized support.[513,1030,1083,1085,1088] Based on deuterium TPD experiments, Guerrero-Ruiz *et al*. have proposed that carboxylic and/or lactonic groups should be involved in spillover, whereas phenols and carbonyls seem to be less efficient for the migration of D atoms and/or for their collection.[1090] The superiority of semiquinone groups for enhanced spillover related to phenol groups was proposed by Yang *et al*.[1030] Similar studies should be definitively encouraged to confirm these results and compared them to theoretical works. NMR and Raman

studies have also evidenced that small amounts of carboxylic groups contribute to improved spillover efficiency.[1091] A synergistic role of water and surface oxygen groups has also been reported.[1027] It has also been suggested that the removal of surface oxygen groups that may create surface defects can also improve the spillover.[1094] The addition of sodium on a Ru/C catalyst inhibits the spillover phenomenon.[1093] Beside the concentration and type or surface oxygen species, the specific surface area of the support,[1095,1096] the metal particle dispersion[1009,1097,1098] and its composition[1099] have been shown to play a role on the spillover. High surface area and dispersion provide a favorable environment. Particularly, it has been shown for Pt and Ni that when the size becomes less than 1 nm, the spillover is drastically enhanced compared to larger particles (1-2 nm).[1100,1101] EXAFS analyses have shown that for sub-nanometer Pt clusters the Pt-Pt bond is significantly contracted relative to bulk values. Interestingly, the influence of the support's dimensionality (1D - CNT, 2D - graphene, and 3D - activated carbon) on the spillover has been reported.[1102] CNT are superior to graphene, which is superior to AC. For CNT, the most significant parameters are their specific surface area and their length; higher area and shorter CNT yielding faster kinetics. The degree of metal-carbon contact contributes to enhance hydrogen spillover.[1094] The effect of temperature is also important and it has been shown that spillover is increased with increasing temperature from 273 to 353 K.[1103] Beside the diffusion of hydrogen on the surface of the support, hydrogen spillover through the gas phase was also evidenced experimentally.[1104,1105] Primary (between the metal and a first carbon material) and secondary (between the first carbon material and a second carbon material) spillover through a carbon bridge (formed with the addition of sucrose) was reported by Yang *et al* (Figure 47a).[1106,1107] This finding has to be related to the early works of Boudart, which have highlighted the importance of "carbon contaminants" on the platinum surface that provide bridges permitting surface diffusion of hydrogen atoms from Pt to the carbon support.[1108] Fullerenes C_{60} constituted excellent acceptors or bridges that promotes the

spillover, and the strength of the H-C_{60} interaction is in between physisorption and chemisorption.[1109] Primary and secondary spillovers in a Pt/CB/C_{60} composite are sketched on Figure 47b.

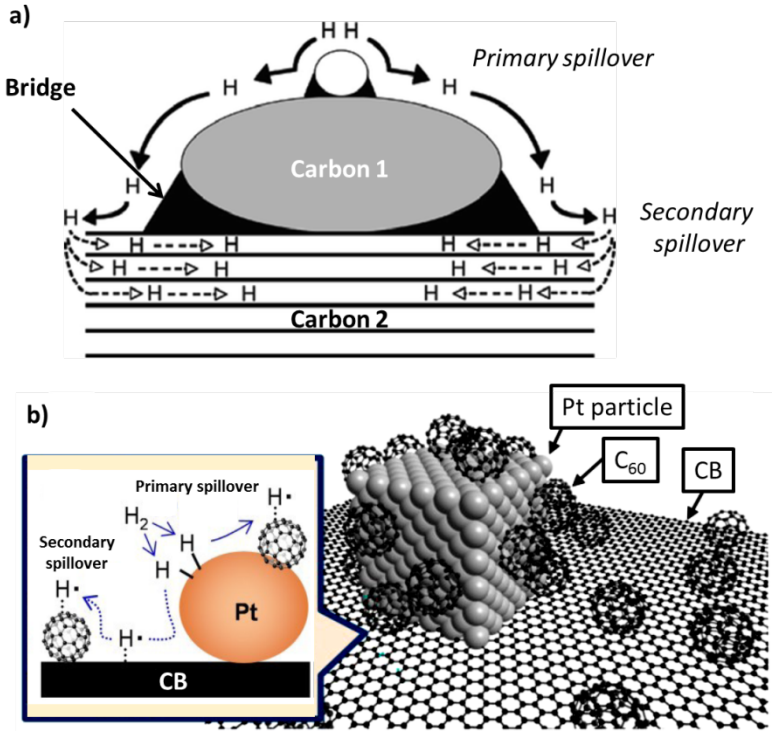

Figure 47. a) Primary and secondary spillover enhancement by improved contacts and bridges. Reprinted with permission from Lachawiec, A. J.; *et al*. *Langmuir* **2005**, *21*, 11418-11424.[1107] Copyright 2005 from the American Chemical Society; and b) A structure model describing H_2 spillover on a Pt/CB/C_{60} composite. Adapted with permission from ref [1109]. Copyright 2018 from the Royal Society of Chemistry.

Although spillover has been regularly invoked in the literature to rationalize catalytic results involving carbon-supported catalysts, particularly for hydrogenation reactions, relatively few specific studies have been published. As defective carbon materials are able to activate

hydrogen by themselves, the involvement of H-spillover in hydro-processing reactions involving carbon as catalyst has been discussed,[1110] but is out of the scope of this review. Hydrogen spillover has been detected for various reactions involving carbon-supported metal catalysts, such as but not limited to hydrogenation,[897,899,1082,1102,1111-1120] dehydrogenation,[1121-1130] isomerization,[1131-1136] and syngas conversion.[1137-1142]

The involvement of H-spiltover species in benzene hydrogenation (373-393 K) has been reported for Ru/C,[899] Pt/C[1111] and Ni/C catalysts.[1112] In these two latter studies, H_2 chemisorption and/or TPD experiments have highlighted H-spillover on these catalysts. Since spillover is often postulated when the dilution of catalyst increases its activity, this argument was proposed here. In both cases, the benzene hydrogenation activity increased upon dilution of the catalysts because of the existence of the hydrogen spillover effect. In the case of the Ru/C catalysts, Ru particles were deposited onto a porous carbon to form a sandwiched Ru/C structure. The intimate interfacial contact between Ru NP and the support supposedly favors the H-spillover, and *in fine* explains the high activity of this catalyst. For 1-hexene hydrogenation (323 K), H-spillover was also demonstrated by diluting a Pt/C catalyst with activated carbon.[1113] The initial conversion of 1-hexene was increased from 86.5% to 98.5% when the Pt/C catalyst was diluted. In the hydrogenation of anthracene (573-593 K), H-spillover was proposed for Ni/C[1118] and Pd/C catalysts.[1116] It is worth mentioning that this proposition is supported by the fact that carbon materials have been reported to be active in this reaction under similar conditions.[1119] In the gas phase hydrogenation of butyronitrile (383 K), the higher activity of Pd/C compared to Pd/Al_2O_3 has been attributed to an increase of the total surface hydrogen (chemisorbed on Pd and spiltover, from H_2 TPD) on the Pd/C catalyst.[1117] For the hydrogenation of diphenylacetylene on Pd/C catalysts (C = CNT, AC and FLG), pure catalysts and composites (1 catalyst + 1 support) were used to evidence the role of primary and secondary spillover.[1102] For primary spillover, the steps in which Pd participates are rate limiting. For

secondary spillover, the hydrogen atoms need to travel longer distances, and this step is proposed to be limiting. The authors have found that the increase kinetics in the presence of spillover agents is strongly correlated with the dimensionality of the carbon materials CNT (1D) > FLG (2D) > AC (3D). Short CNT with high surface area have been identified as the best support. Beside the dimensionality and the length of CNT, it has also been suggested that the arrangement of the graphene layer in CNT could favor spillover. In the case of Ag particles located inside herringbone and conventional (parallel-type) CNT, diffusion of spiltover H to the interplanar spaces of herringbone CNT has been proposed.[897] It was shown that these spiltover H species can contribute to the reduction of Cu particles present on the CNT, and to the activity of the Ag/CNT catalyst towards the selective hydrogenation of dimethyl oxalate. The superiority of herringbone CNT towards parallel-type CNT for H-spillover was also discussed in a study of Pd-ZnO/CNT catalysts for CO_2 hydrogenation to methanol.[1115] In that case, it was proposed that the higher concentration of dangling bonds on herringbone CNT should favor the H-spillover compared to parallel-type CNT. The authors also proposed that this spillover generates a microenvironment around the metallic particles with high concentration of active H-species, thus increasing the rate of CO_2 hydrogenation. Involvement of H-spillover has also been proposed for crotonaldehyde hydrogenation on Pt/C catalysts.[1120] In that case, the better performances in terms of selectivity towards the hydrogenation of the C=O bond obtained on oxidized supports have been rationalized in part by spillover. First, it was proposed that active centers are formed on the support upon the decomposition of oxygen surface groups during catalyst activation under dihydrogen, which can chemisorb nascent hydrogen spilt from the platinum NP. Second, the H-species on the support near Pt could polarize the C=O bond, through their interaction with the oxygen atom. This interaction would activate the C=O bond for the attack of hydrides on the Pt surface. In the case of nitrobenzene hydrogenation on Pd/C[1114] or Pt/C[1082] catalysts, if hydrogen spillover has been detected, no

evidence of an involvement of H-spiltover species in the hydrogenation performances was reported. Finally, hydrogen spillover was also reported in the case of RuCu bimetallic catalysts on carbon catalyzing the hydrogenation of alginic acid into sugar alcohols.[1143] The intimate Ru-Cu interaction facilitates hydrogen spillover from Ru to Cu, which enables Ru to maintain its hydrogenation activity in spite of a decrease in active Ru exposed due to Cu decoration.

In some dehydrogenation reactions involving C-H or O-H bond cleavage, the rate at which the adsorbed hydrogen atoms, form upon substrate activation or recombine to form dihydrogen can be rate limiting. In that case, the reverse spillover (from the support to the metal) can contribute to an enhancement of the activity. Carbon materials can catalyze the dehydrogenation of aliphatic and alicyclic hydrocarbons. In these reactions, it has been reported that the use of a carbon-supported catalyst merely accelerate the desorption of hydrogen through reverse spillover (Figure 48a).[1121,1122,1126,1129] The catalytic activity of the supported catalyst is suppressed by hydrogen molecule in the gas phase, due to the normal spillover effect. It has also been demonstrated that it is possible to use the spiltover-H for hydrogenolyzing organosulfur compounds that exist in petroleum fractions.[1126] In that case, the sulfur compounds incorporated in a hydrocarbon dehydrogenation system react with the hydrogen atoms on the metals to form hydrocarbons and hydrogen sulfide by hydrogenolysis without any consumption of gaseous hydrogen (Figure 48b). The reverse spillover was also invoked in dehydrogenation of cycloalkanes using two metals supported on carbon supports. In the case of Ag/C[1130] and Ni/C[1128] catalysts, the addition of small amounts of platinum significantly increases the activity of the catalysts for the dehydrogenation of cyclohexane. The increased catalytic activity has been tentatively attributed to the easy formation of molecular hydrogen and its rapid desorption due to the reverse spillover on Pt. Hydrogen spillover was invoked when physical mixture of Pt/C and Pd/C were used for dehydrogenation of various cycloalkanes.[1127] The catalyst mixture showed higher activities than the Pt/AC catalyst alone due to the synergistic effects of spillover,

migration, and recombination of hydrogen over Pt/C and Pd/C. Decalin dehydrogenation was studied on Pt/C and Pt/Al_2O_3 catalysts.[1123] Although the exact role of H-spillover over activity was not fully understood, it was proposed to rationalize the superior activity of Pt/C even though the Pt dispersion was similar on both supports. Finally, hydrogen spillover was also suggested to play a role in the dehydrogenation of $NaAlH_4$[1124] or $LiAlH_4$[1125] on metal-supported carbon catalysts. The metal particles can catalyze the decomposition of the hydrides, but also assist H_2 formation by recombination of H spiltover from the hydrides to the support (Figure 48c). It is also possible that part of the dihydrogen generated by catalytic decomposition of the hydride is lost in the support due to the spillover on the metallic particles.[1125]

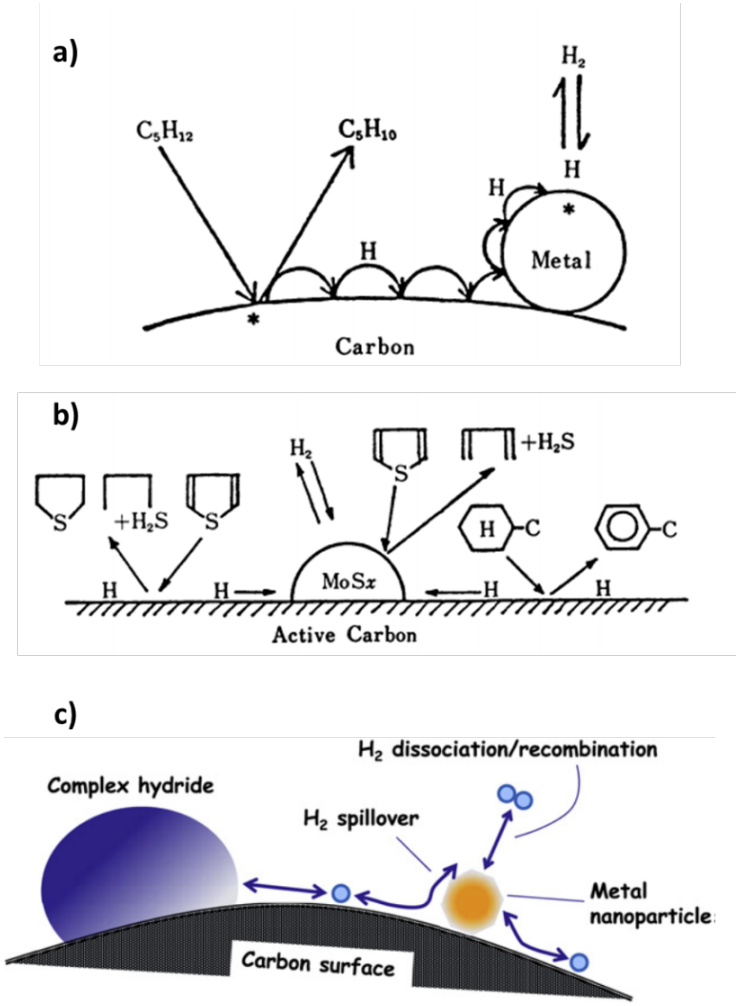

Figure 48. a) Model of hydrogen reverse spillover during cyclohexane dehydrogenation. Reprinted from ref [1126]; b) model of hydrogen transfer hydrodesulphurization of thiophene.

Reprinted from ref [1126]; and c) Schematic representation of spillover during the dehydrogenation of $NaAlH_4$. Reprinted with permission from ref [1124]. Copyright 2011 from Elsevier.

Hydrogen spillover over macroscopic distances on a combination of carbon-supported catalysts (Pd/C and a bimetallic catalyst) was evidenced in dual-bed reactor (Figure 49a) for 1-butene isomerization.[1131,1133] In this reactor, the hydrocarbon never contacted the Pd/C catalyst, and the bimetallic catalysts alone (Fe or Co, and a lanthanide metal deposited on the same carbon support that Pd) have no measurable activity for the investigated reaction at 313 K; likely because they cannot dissociate dihydrogen at this temperature. The activation energy for the reaction was found to be 1.9 kcal.mol^{-1} for the Pd/C catalyst, 10 kcal.mol^{-1} for a FeCe/C bimetallic catalyst, and 1.7 kcal.mol^{-1} for the same catalyst in the dual-bed reactor. The function of Pd/C is simply to generate H-spillover species, and the isomerization of butene occurs in the separate section of the reactor containing the bimetallic catalyst (Figure 49b). The results of this study support the fact that spillover can explain the activity synergy observed during alkene isomerization over similar trimetallic catalysts and physical mixtures of catalysts.[1144-1146]

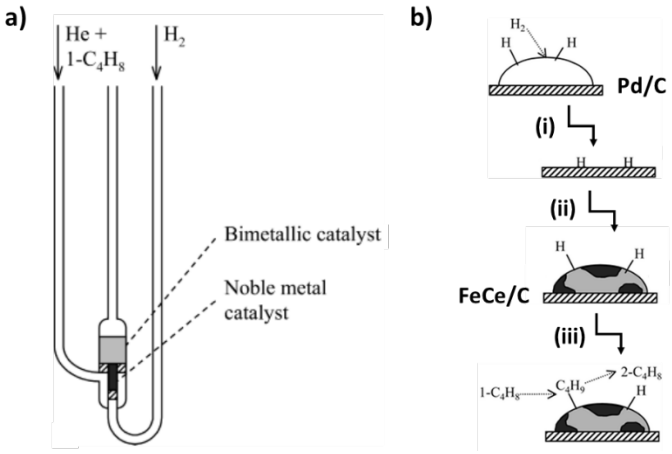

Figure 49. a) Segregated bed reactors: dual-bed, dual-feed reactor. Reprinted with permission from Weigle, J. C.; *et al*. *Langmuir* **2004**, *20*, 1189-1193..[1131] Copyright 2004 from the American Chemical Society; and b) Hydrogen dynamics within the dual-bed reactor: (i) molecular hydrogen adsorbs and dissociates over the Pd/C catalyst, (ii) atomic hydrogen diffuses along the carbon support surface to the bimetallic catalyst sites, and (iii) 1-butene adsorbs and reacts at a bimetallic site, forming 2-butene. Adapted with permission from Weigle, J. C.; *et al*. *AIChE J*. **2004**, *50*, 821-828.[1133]. Copyright 2016 from John Wiley and Sons.

The n-hexane skeletal isomerization was studied on Pt/CNF and Pt/SiO_2 catalysts.[1135] The Pt/CNF catalyst can activate n-hexane at lower temperatures than Pt/SiO_2, with a high selectivity. These performances have been attributed to a higher abundance of surface H at the active Pt sites thanks to reverse spillover of hydrogen retained by the CNF.[1132,1135] It was pointed there also that Pt on herringbone CNF shows higher spillover capacity compared to Pt on parallel-type CNF.[1132] Hydrogen spillover has also been proposed as an important factor determining the lower deactivation *via* carbon deposition of Pt/CNF catalyst compared to Pt/SiO_2.[1134] A similar observation (lower fragmentation of the substrate compared to Pt/SiO_2) was made for Rh/CNF catalysts involved in the ring-opening reactions of methylcyclopentane; and there also this was attributed to the highest reverse spillover supplying H to the metallic sites.[1136]

Hydrogen spillover was also reported to be involved in reactions with syngas such as FTS[1138] or higher alcohol synthesis (HAS).[1137,1139] In FTS, the H-spillover effect has been proposed to be involved in the improvement of the reduction of Co-based catalysts on carbon supports, thanks to their functionalization with oxygen surface groups.[1140-1142] The same phenomenon was proposed to take place when the Co catalyst was doped with a minute amount of noble metal (Ru) to assist the cobalt reduction (Figure 50).[1138] In the case of HAS, the excellent

performances of a CoMo-K/CNT catalyst were attributed to its ability in adsorbing and activating H_2, and in promoting H-spillover.[1137,1139] Based on TPD analyses, it was proposed that large amounts of reversibly adsorbed H-species on the catalyst surface would generate surface microenvironments with high stationary-state concentrations of H-species on the catalyst. Beside these reactions, H-spillover was also proposed to play a significant role in other thermally activated reactions involving carbon-supported catalysts.[992,1147-1153] Table 7 summarized the main findings reported in these studies.

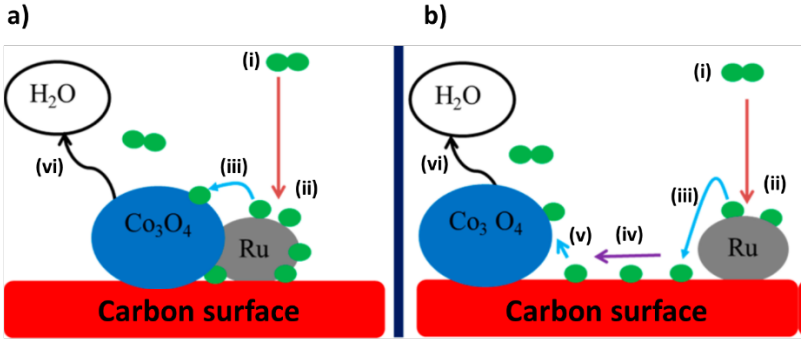

Figure 50. Pathways for spillover-assisted Co reduction on Ru-Co/C catalyst, a) primary; and b) secondary spillover. (i) Molecular hydrogen; (ii) dissociative adsorption; (iii) spillover; (iv) hydrogen atom surface migration; (v) spillover; and (vi) reduction and water removal. Reprinted with permission from Phaahlamohlaka, T. N.; *et al*. *ACS Catal.* **2017**, *7*, 1568-1578.[1138] Copyright 2017 from the American Chemical Society.

Finally, H-spillover is also a phenomenon that is relevant in electrocatalysis. In PEMFC, catalysts typically consist of Pt NP dispersed on carbon black. H-spillover in such catalysts has been evidenced in various studies, and the importance of specific surface functional groups (-COOH, $-SO_3H$) of the support on the diffusion processes has been evidenced.[1047,1154-1156] Although this effect could contribute to the electrochemical characteristics of the systems,

further works are needed to investigate the potential impact of H-spillover on these electrocatalysts, both for accurate characterization of catalytic systems and for the rational design of innovative functionalized carbon supports, allowing alternative routes of proton transfer. It is also worth mentioning that pre-treating Pt/C catalysts in H_2 allows the removal of oxygen functional groups *via* H-spillover.[1033,1157] This treatment produces more robust catalysts for PEMFC. Although no clear explanation has been given to explain this latter result, it is possible that the vacancies created upon functional groups removal contribute to Pt stabilization.

Table 7. Examples of reactions in which hydrogen spillover plays a role.

Reaction	Catalyst	H-spillover involvement	Ref.
Hydrodechlorination (HDC)	Pd/C and Ni/C (CNF, AC, graphite)	Presence of chemisorbed-H (on Pd), spillover-H (on the carbon support), and hydride (associated with Pd) are reported. Spillover hydrogen can contribute to the catalytic activity of the supported metal. The HDC rate increases with decreasing metal surface area, where spillover-H allows enhancing HDC performances.	1147-1149
Ammonia borane hydrolysis	Ru/CNT	The high reaction rate is attributed to a combination of H-spillover and strong interface interaction between metal and multi-walled CNT.	1151
Glycerol hydrogenolysis	Cu-Ru/CNT	Ru clusters are in contact with the Cu NP. The Ru clusters are inactive for hydrogenolysis, but generate and transfer *via* hydrogen spillover H-species to the Cu surface. The Cu-Ru/CNT catalyst show similar selectivity for 1,2-propanediol than Cu metal, and much higher activity than Cu metal because of the H-spillover effect.	1150
Benzylic alcohol hydrogenolysis	Rh/C	The higher activity of Rh/C compared to Rh/Al_2O_3 is due to the formation of a better leaving group (OH_2^+) from the benzyl hydroxy group on the carbon support followed by the scission of the C-O bond with spillover hydrogen.	1152
H_2O_2 synthesis from H_2/O_2	C-coated-Pt/SiO_2	Competing reactions such as H_2O formation and consecutive decomposition/hydrogenation of the produced H_2O_2 into H_2O are suppressed when an amorphous carbon layer that can selectively allow the diffusion of H_2 over O_2 covers Pt. H_2 diffuses through the carbon layer, dissociates on the Pt surface. Then the activated hydrogen diffuses to the outer surface of the carbon layers through H-spillover. The spiltover H can further react with O_2 on the carbon surface without O-O dissociation to selectively form H_2O_2 (Figure 51).	992,1153

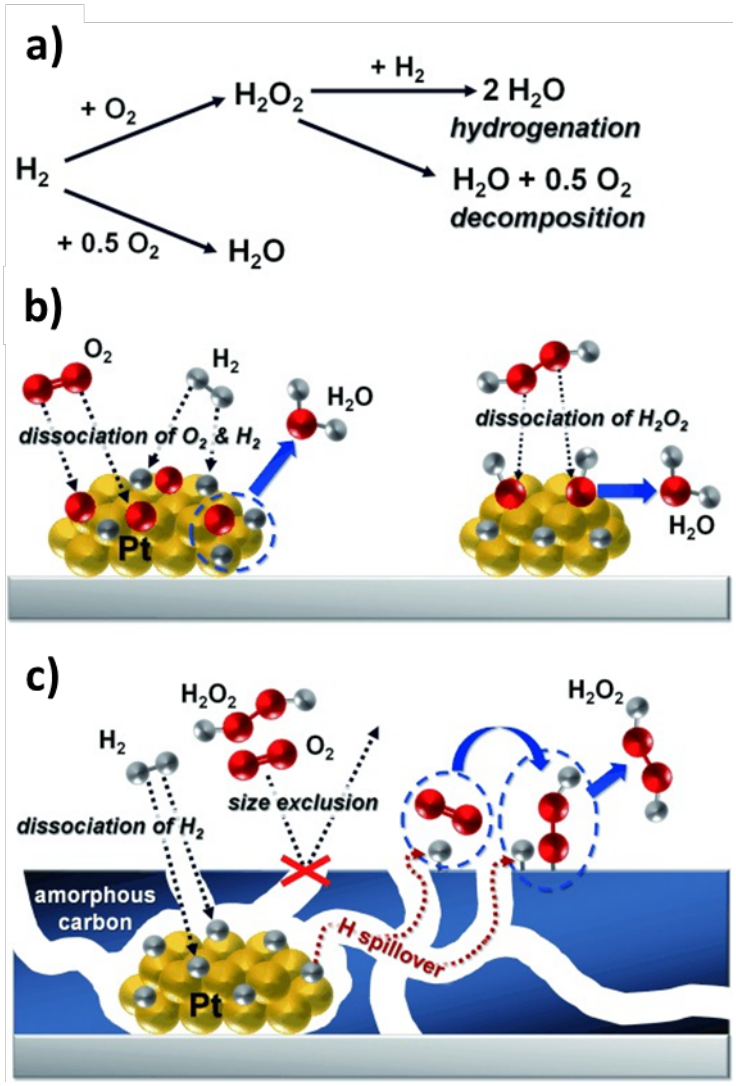

Figure 51. a) Reaction pathways involved in the direct synthesis of H_2O_2; b) schematic representation for the reaction pathways in conventional Pt catalyst on open porous supports; and c) in Pt catalyst covered by amorphous carbon layers that allow selective diffusion of H_2 over O_2. Reprinted with permission from ref [1153]. Copyright 2014 from John Wiley and Sons.

It appears obvious from the analysis of the modeling literature that the "imperfections" of the carbon support such as oxygen surface groups, lattice dopants and defects will play a crucial, and most of the time positive, role on the spillover mechanism. These imperfections will affect the bonding of the cluster on the support, the binding energy of hydrogen molecules or atoms

on the metal, the migration energy of H atoms from the metal to the support, and finally the diffusion of hydrogen on the support. The exact role of these imperfections needs definitively further works, since it can be at the origin of the discrepancies often observed between theoretical and experimental studies, but also between different experimental investigations.[1158] Experimental studies have clearly shown that H-spillover can occur on carbon-supported catalysts, even at room temperature, depending on the metal and support natures. The exact nature of the H-species involved in spillover (radicals, protons, hydride, and activated hydrogen) remains unclear, and further works are necessary to gain further information on that issue. Direct or reverse, primary or secondary spillover have been observed, depending on the type of reaction. Gas phase and surface spillover have also been evidenced in different studies. The involvement of H-species arising from spillover in catalytic reactions has been also proved in many catalytic reactions. The role of these H-species can be direct (direct reaction with a reactant) or indirect. In that latter case the H-species can: i) create a favorable microenvironment in the vicinity of the metallic NP with high concentration of active H-species that will positively affect the reaction rate, ii) assist the reduction of a hardly reducible metal under the condition of the reaction, or iii) provide hydrogen to a (reduced) metal that is not able to dissociate hydrogen under the condition of the reaction, and give to him the opportunity to perform the aimed catalytic transformation. Finally, experimental studies have also shown that the H-spiltover species can contribute to improve the activity the catalysts, but also their selectivity and even their stability.

3.3.2 Oxygen spillover

If hydrogen spillover on carbon materials is well documented, the literature on oxygen spillover, especially the comparison between theory and experiment, is quite limited for carbon surfaces. Its implication is most of the time limited to the creation of surface functional

groups,[1159,1160] or related to the oxidation of the carbon support;[1161-1163] although its implication in other reactions should also be envisaged. One particularity of oxygen spillover on carbon surfaces is that the presence of a metal is not a prerequisite, since experimental and theoretical works have shown that some specific sites can easily activate the dioxygen molecule.[1164-1167] Spillover involves interaction and mobility of reactant species over the support and the catalyst surface, and may occur in either direction, from the support to the catalyst edge and vice versa. Jiang et *al*. have proposed that oxygen spillover from the carbon support to Pt particles explains the increase in Pt utilization with catalyst layer thickness in a fuel cell electrode.[1168] The adsorption energy of dioxygen changes from physisorption on perfect graphitic surfaces (E_a = 6 kcal.mol^{-1})[1169] to chemisorption for oxygen-containing functional groups on the edge of a graphite surface.[1170] In that case, the O_2 is strongly adsorbed onto the surface to form a four-membered ring structure, in which the O-O bond is greatly weakened. The adsorption energy of O_2 depends on the type of oxygen-containing functional groups. In the case of N-doped carbon materials, a chemisorption of O_2 was also evidenced, with an adsorption energy of 14.7 kcal.mol^{-1} close to a graphitic N.[1169] Higher nitrogen concentration reduces the energy barrier efficiently for graphitic N.[268,1171] This mechanism is relevant to the N-doped carbon catalyzed ORR in electrocatalysis. The adsorption and dissociation of O_2 on N-G was followed experimentally with multiple *in situ* synchrotron spectroscopy experiments.[1172] The interaction leads to O_2 dissociation and formation of C-O single bonds on graphene. Change in the chemical environment of graphitic N upon oxidation is consistent with the adsorption of two oxygen atoms on the nearest carbon atom neighbors of the graphitic N (epoxy position), as predicted theoretically. The interaction of dioxygen with vacancies or Stone-Wales defects was also investigated by DFT.[1173] Dioxygen was chemisorbed on SV in CNT, but physisorbed on perfect and SW-defected CNT. Radovic *et al*. have demonstrated by DFT that epoxide groups present on a graphitic surface are formed on the basal plane *via* spillover of atomic oxygen from

graphene edges.[1159] The carbene-type sites on zigzag edges are susceptible to non-dissociative adsorption of O_2 followed by its dissociation to a semiquinone oxygen (in the graphene plane) combined with an out-of-plane epoxy-type oxygen. The likely subsequent fate of the epoxy-type oxygen is surface diffusion on the basal plane. The mobility of these groups, and how it is affected by the geometric/electronic properties of the graphene support has been studied by DFT.[1174-1178] The adsorption energy of an isolated oxygen atom on graphene to form an epoxide is 53 kcal.mol^{-1}, indicating a strong adsorption with small variations according to the surface coverage.[1175] However, the migration barrier of these oxygen atoms on graphene is only 17-18 kcal.mol^{-1} (inclusion of van der Waals correction in DFT reduces the value by 10.4 kcal.mol^{-1}) and makes oxygen diffusion possible.[1175,1177] Thus, although a single oxygen atom is very difficult to desorb,[1174] cooperative desorption of two oxygen atoms should be feasible.[1175] DFT calculations have also shown that a correlation exists between the strength of the "leaving" epoxide group and the epoxy oxygen-hopping barrier. Under the most favorable conditions, oxygen mobility is of the same order as that of gas-phase O_2 in micropores.[1174] Both geometric and electronic properties of graphene affect this energy barrier.[1174,1177] DFT calculations on diffusion of oxygen on the surface of a defective graphene sheet have shown that atomic oxygen diffuses at different rates depending on the local environment; however with relatively low barriers (mostly < 23 kcal.mol^{-1}), and in some cases lower than on pristine graphene.[1177] The effect of strain on graphene on oxygen diffusion has also been studied, and it appears that the energy barrier for atomic oxygen diffusion increases with strain, from 16 kcal.mol^{-1} for pristine graphene to 20.2 kcal.mol^{-1} on strained graphene.[1176] The importance of electronic properties and the carrier density (modified with an external gate voltage) on the atomic oxygen diffusion has also been evidenced.[1178] For pristine graphene, a barrier of 16 kcal.mol^{-1} was calculated; however, upon electron doping the barrier decreases almost linearly to reach values as low as 3.4 kcal.mol^{-1} for densities of -7.6.10^{13} cm^{-2} (corresponding to one electron added to the

calculation cell). Interestingly, *ab initio* calculations have shown a strong tendency of epoxy groups to form tightly packed structures (clusters).[1179] Indeed, O atoms added in close proximity to another O have a greater binding energy than O atoms separated by larger distances.[1180] This clustering can further induce an easier desorption of O_2,[1181] and changes in the material's conductivity.[1182] It has been also shown that it is energetically favorable for the epoxide groups, if combined with hydroxyl groups, to aggregate together and to form specific types of strips with sp^2 carbon regions in between.[1183]

The adsorption and dissociation of molecular oxygen was also studied on metals (atoms or clusters) deposited on graphene, which is a key step in the ORR.[493,578,616,1184-1193] Unfortunately, most of these studies concentrate on the dissociation of O_2 on the metal, but do not treat the possible hopping of oxygen atoms on the support. Compared to carbon vacancy in graphene, the introduction of TM single atoms may increase the dissociation barriers of the O_2 molecule, and, depending on the metal, the O=O bond is not necessarily broken.[1185-1187,1193] The possible involvement of the carbon support on this process has been suggested, and in that case an epoxy group can be formed (Figure 52a,b).[1187,1193] For Pt, the energy barrier for all the process is 27.7 $kcal.mol^{-1}$,[1193] whereas it is only of 9.2 $kcal.mol^{-1}$ for a Ni single atom.[1187] Compared to N-graphitic carbon in N-G, the introduction of TM single atoms ($M-N_4$ environment) may decrease the dissociation barriers of O_2, and the O=O bond is generally broken.[1184,1188,1190,1191] In that case also, involvement of the carbon support and formation of an epoxy group has been proposed (Figure 52c), with energy barriers of 16-35 $kcal.mol^{-1}$ for the overall process, depending on the metal (Fe, Co or Mn).[1190] For an iron-based system, the energy barrier to pass from the species where O_2 is dissociatively adsorbed on the iron center to the [Fe-O + epoxy] system is only of 11.5 $kcal.mol^{-1}$.

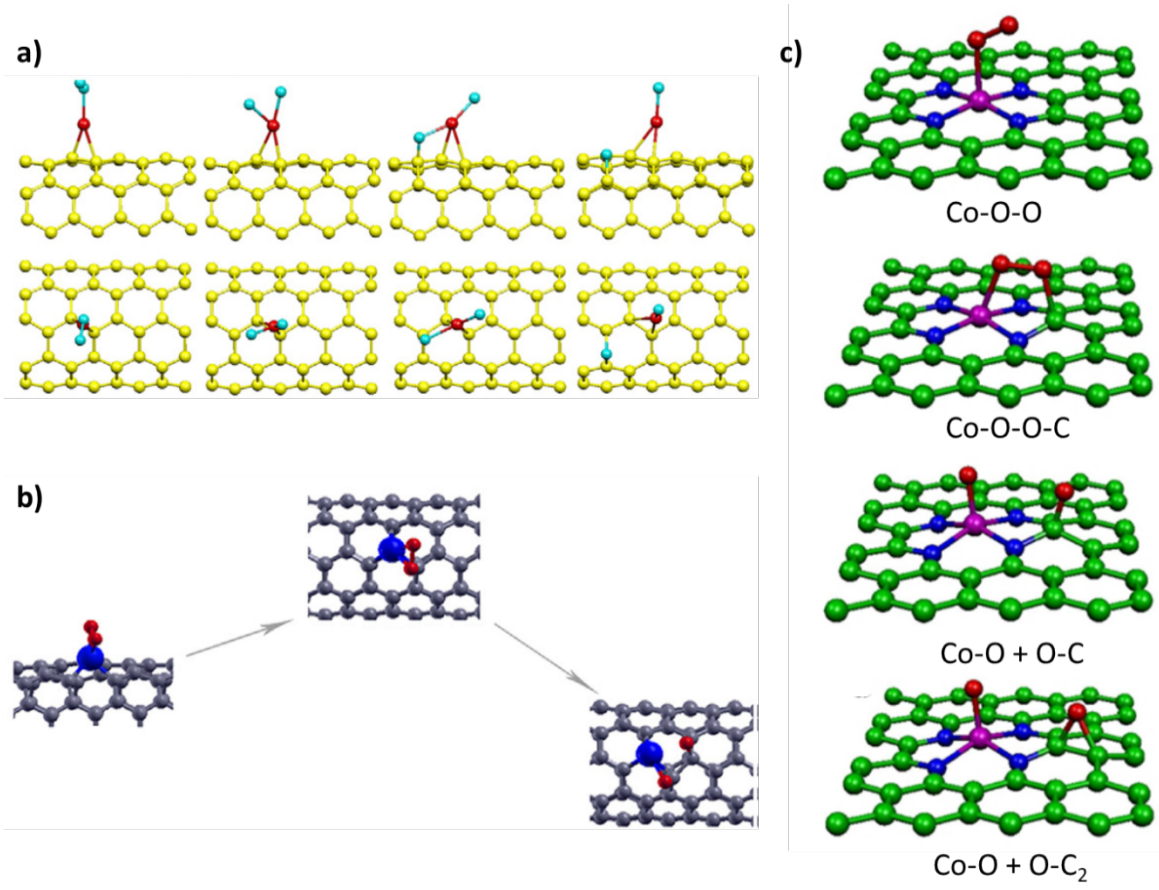

Figure 52. a) Side and top views of the optimized structures of O_2-Pt_1/CNT systems along the minimum energy path to the dissociative adsorption of O_2. Reprinted with permission from ref [1193]. b) Dissociation paths of O_2 on a Ni_1/CNT single atom. Reprinted with permission from ref [1187]. c) Minimum energy path for the O_2 dissociation after the adsorption on the metal of the Co−N_4 center in graphene. Reprinted from Orellana, W. *J. Phys. Chem. C* **2013**, *117*, 9812-9818.[1190]. Copyright 2013 American Chemical Society.

On Pt_n clusters (n = 4,[493,616] 13[578] or 38[493]) deposited on various graphene (vacancy, N-doped), O_2 is first adsorbed molecularly with adsorption energy ranging between 34.5 and 53 kcal.mol^{-1} according to the cluster size and the nature of the support. Then, on Pt_4 cluster, low energy barriers have been reported for O_2 dissociation (7 to 8 kcal.mol^{-1}), according to the nature of the support,[616] since the supports induce positive polarized charges on Pt that favor the O_2

dissociation. However, in that case, a direct implication of the support and the formation of epoxy groups was not discussed. Using scanning tunneling microscopy and Auger electron spectroscopy, Novotny *et al*. investigated O_2 interactions with easily reducible CeO_x clusters on a graphene ML-covered Ru(0001) surface.[1192] In the presence of molecular oxygen, the clusters promote the intercalation of oxygen under the graphene layer. The authors proposed that the mechanism for the intercalation includes the formation of holes in the graphene layer directly below the CeO_x clusters, and oxygen atoms are released from the CeO_x clusters.

Oxygen spillover is an important phenomenon related to carbon material oxidation, which is relevant for soot oxidation or electrode deterioration in fuel cells. In many studies, spillover is proposed to occur on the surface of an oxide, which can be the support of Pt (Al_2O_3 or SiO_2) or the catalyst itself (transition metal oxides or CeO_2).[1160,1161,1194-1196] However, experimental studies dealing with catalytic soot oxidation have shown that activated oxygen atoms (oxygen spillover) can migrate from the metal (Pt) to the carbon *via* the gas phase.[1162,1197-1199] In particular, Zeng *et al*. have stated that activated oxygen is mainly transported *via* the gas phase and that the generally accepted surface transport is indeed negligible.[1199] A direct spillover of atomic oxygen on the carbon support has been first proposed by Baumgarten *et al*.[1161] When the Pt catalyst is in direct contact with the carbon support, a dissociative adsorption of O_2 on the metal followed by the spillover of atomic O to the carbon at the Pt/C interface.[1163] Spillover of atomic O from Pt NP to graphite has also been proposed in a combined XPS and STM study by Kalinkin *et al*,[1200] in which the authors find that the supported platinum greatly enhance the graphite oxidation. Pd catalysts supported on FLG, CNT and AC have been used in the aerobic oxidation of aromatic alcohols using molecular oxygen.[1201] Based on O_2-TPD analyses, the superior performances of the Pd/FLG catalyst have been attributed to an enhanced oxygen spillover from Pd to the adjacent bridge sites of graphene.

3.4 Effects of surface functional groups on catalysis

We have seen in section 2 that the surface functional groups of carbon materials play a crucial role in the anchoring of the active phase. We also saw in sections 3.1 and 3.3 that their presence could have a significant impact on charge transfer and spillover. To be complete we have to discuss the direct influence of the presence (or absence) of these functional groups on metal-catalyzed reactions. Indeed, the surface functional groups may be involved either in the adsorption/desorption step, or directly during the chemical transformation (Figure 53). As far as adsorption/desorption modification is concerned it is mainly an effect of the support's polarity. When considering chemical reactivity, we can distinguish between: i) bifunctional catalysis, where the surface functional groups ensure one catalytic function (most of the time acid catalysis) and the metal another one; and ii) cooperative catalysis where the functional groups and the metal operate concertedly during a single chemical transformation.

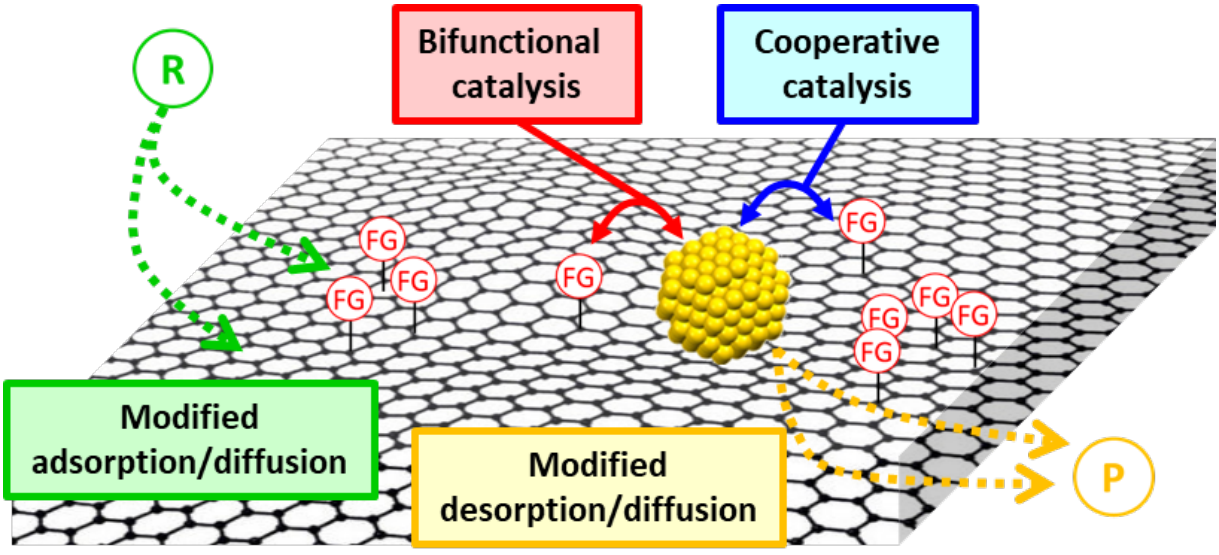

Figure 53. Direct effects of surface functional groups on catalysis.

3.4.1 Effect of support polarity

Different studies, dealing with the selective hydrogenation of cinnamaldehyde, have reported that the presence/absence of the surface oxygen groups of carbon supports, plays a role on the performances of metal supported catalysts. Thus, for Pt/CNF,[1202-1204] Ru/CNF,[1204,1205] Pt/CNT,[1206,1207] Ir/CNT[1207] and PtRu/CNT[108,637] it was shown that the removal of oxygen surface groups by a heat-treatment under inert atmosphere at 973 K significantly affects the catalytic activity. For all the investigated systems, a significant increase in activity is observed upon oxygen surface group removal, while particle size effect is unlikely to bring about such changes in catalytic performance. For Pt/CNF, the intrinsic reaction rate is increased up to a factor of 120 by the removal of the oxygen surface groups. Additionally, adsorption constants increase significantly, suggesting that the hydrogenation is assisted by adsorption of the aromatic ring of cinnamaldehyde on the non-polar CNF support surface after removal of the oxygen-containing groups.[1203] The adsorption of aromatic rings enables the periphery of the metal NP to participate in the hydrogenation. This adsorption may result in the preferential orientation of the C=O bond towards the metal surface, which could explain the higher selectivity towards cinnamyl alcohol observed for the support with low amount of surface oxygen groups.[1204]

For the selective hydrogenation of resorcinol (RES) to 1,3-cyclohexanedione on Pd/rGO catalysts, the high selectivity obtained in apolar solvents is attributed to: i) the strong π-π and p-π interactions between the non-functionalized graphene surface and the aromatic ring and hydroxyl group in RES molecule; and ii) the weak interaction between 1,3-cyclohexanedione and the graphene surface (easy desorption). Similar effects and explanations were proposed for the same reaction with Pd/AC catalysts.[1208] In the case of phenol and derivatives hydrogenation, the use of a polar and protic solvent (water) in combination with a hydrophilic support (g-C_3N_4) allows to reach very high selectivity towards cyclohexanone on Pd/g-C_3N_4 catalysts.[1209] In this

system, phenol can interact with the surface through hydroxyl groups to form strong O-H···N or O-H···π interactions. Although an interaction of the phenol's aromatic ring with the π electrons of the carbon nitride is not excluded, it is expected that such a π···π interaction is rather weak, and that the phenol therefore adsorbs in a non-planar fashion over the basic sites of the support (Figure 54a). The benzene ring of phenol is then partially hydrogenated to the enol (Figure 54b), which can isomerize rapidly to give cyclohexanone. Once formed on Pd, the cyclohexanone leaves the surface of the catalyst quickly, being replaced by a more strongly bound new phenol molecule (Figure 54c). A similar explanation was proposed to explain the high selectivity obtained in water towards cyclohexanone on palladium NP supported on hydrophilic (containing -OH, C=O and -COOH surface species) carbon supports.[1210]

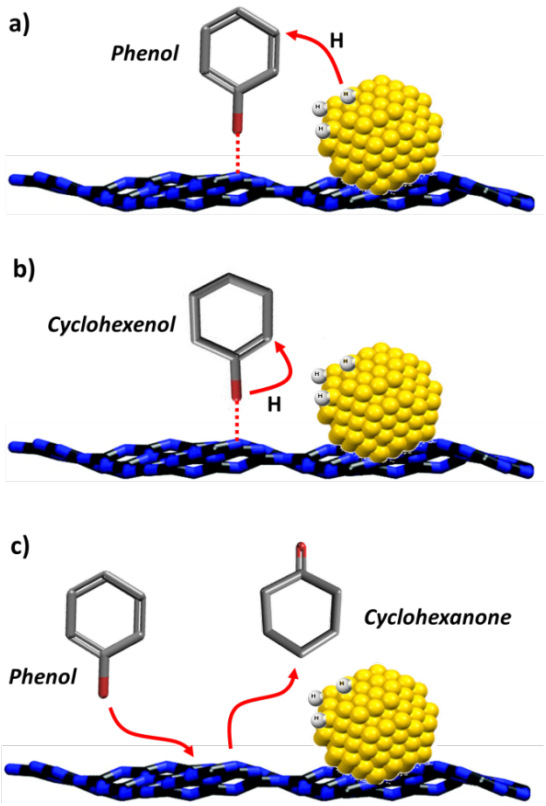

Figure 54. Proposed reaction mechanism of phenol hydrogenation to cyclohexanone over Pd/g-C_3N_4 catalyst.[1209]

For selective hydrogenation of aromatic carboxylic acids over Pd/N-C, it was clearly demonstrated that the introduction of nitrogen surface groups (predominantly pyridinic groups) notably improves the surface hydrophilicity and the adsorption of acid molecules.[1211] Pd/N-C catalysts show an enhanced activity in water for the selective ring hydrogenation of benzoic acid (and also benzamide or removal of phenol) in comparison to undoped catalysts. In the case of benzene hydrogenation over Pt/AC[1212] and Ru/AC[1213] catalysts, a positive effect of the presence of surface carboxylic groups on activity was reported. Ru/AC catalysts were used in liquid phase with water for the selective hydrogenation to cyclohexene. The main role of water is to withdraw cyclohexene from the surface of the more hydrophilic catalyst, reducing its undesired hydrogenation. As far as activity is concerned, it was further proposed an stronger adsorption on benzene on acidic surface sites (-COOH). The rate enhancement could be associated with an additional contribution from the benzene molecules that adsorb on surface support acidic sites and then react either with chemisorbed hydrogen on the particle surface or with spiltover hydrogen.[1111,1214] An influence of the hydrophilicity of the support was also reported in the enantioselective hydrogenation of methyl pyruvate over Pt/C catalysts.[1215] The authors proposed that: i) the surface oxygen groups (whatever their nature) facilitate the reactant transport; and ii) hydrogen bond interactions exist between the oxygen atom from the substrate (C=O bond) and hydrogen species chemisorbed on the support (located on the active sites created after the thermal decomposition of the surface groups). Enantioselectivity is neither affected by the surface content nor by the chemical nature of the functional groups. Oxidation of benzyl alcohol with molecular oxygen has been investigated on Ru/CNF catalysts.[1216] After partial removal of surface -COOH groups by annealing under N_2, the catalytic activity is significantly reduced. It is proposed that the benzyl alcohol's adsorption on the support through hydrogen bond could activate the alcohol group. Moreover, when the activated alcohol group

is close enough to oxygen atoms dissociated on Ru NP surface, benzyl alcohol is easily converted into benzaldehyde. A similar effect of oxygen surface group was also noticed for the same reaction on Co_3O_4/C catalysts.[1217]

Interestingly, in the aqueous phase reforming (APR) of glycerol over Pt/CNT[1218] and PtCo/CNT,[1219] a negative impact of -COOH surface groups was reported. Compared to as-received CNT support, if the Pt NP dispersion was improved on oxidized CNT due to the presence of surface -COOH groups, the TOF of APR was decreased by half. The TOF was recovered by removing the carboxylic groups *via* high temperature annealing. These results were rationalized by considering a competitive adsorption of water and ethylene glycol on the support. The introduction of -COOH groups increases the hydrophilicity of the CNT support and, therefore, the local concentration of water around the support. The decrease in the local concentration of ethylene glycol around the catalytic component (lower than that in the bulk liquid) leads to lower activity in terms of TOF. The effect of CNT functionalization (-COOH surface groups) on Pt particle size and catalytic activity has been explored by Haller *et al*. *via* different probe reactions.[1218] The oxidized CNT supported catalyst have lower activity in reactions with a binary mixture (APR, 10 wt% ethylene glycol in water), both in aqueous and gas phase, where competitive adsorption does occur. However, for alkane dehydrogenation with a pure hydrocarbon reactant, the Pt particle size effect is more important. For the hydrodechlorination of chlorobenzenes over Pd/C, Pd/CB and Pd/CNF, a negative impact of surface -COOH groups was also evidenced.[1220] Hydrodechlorination inhibition was attributed to chloroarene interactions with the surface -COOH groups that renders the reactant less susceptible to hydrogenolytic attack.

In electrocatalysis, the use of sulfuric acid or chlorosulfuric acid functionalized carbon materials can improve the electrocatalytic performances thanks to an easier access for protons (higher ionic transport), and better wettability (higher water uptake).[1221,1222] Electrochemical

characterizations have shown that catalysts supported on sulfonated carbons present better performances for alcohol electro-oxidation,[1221,1223,1224] formic acid electro-oxidation,[1225,1226] ethylene glycol electro-oxidation[1227] and ORR[1228-1233] as compared to un-sulfonated supports. The basic sites of nitrogen-doped carbon were also used to improve the efficiency of Pt catalysts in the direct electroreduction and carboxylation of CO_2 with halides.[1234] It was proposed that the basic nitrogen sites of the support could adsorb CO_2 molecules and increase the local CO_2 concentration around the Pt NP, which might account for the much higher yields obtained with Pt/N-C compared to the pure Pt NP.

It was shown that it is possible to produce amphiphilic partially N-doped CNT containing in the same nanotube two different sections: a hydrophobic undoped part connected to a hydrophilic N-doped segment.[1235] These CNT interact very well with aqueous media due to the hydrophilic N-doped section, whereas the undoped hydrophobic one has strong affinity for organic molecules. They have been used as pickering interfacial catalysts for oxidation of 2-heptanol with molecular oxygen on Ru and Pd.

3.4.2 Bifunctional catalysis

It is first important to remind that carbon materials can be used as metal-free (electro)catalysts, and that their activity is related to the presence of surface groups or defects.[46,1236-1239] Thus, diverse defects and chemical functionalities on graphene layers can catalyze reactions, including oxygenated functional groups, carbon vacancies and holes, edge effects, and the presence of dopant elements.[1240] Although bifunctional catalysis with carbon materials is limited to metal-acid functionalities, since some carbon materials behave as a strong protonic acids,[1241,1242] other functionalities could be exploited such as quinone groups as nucleophilic sites,[1243] or pyridinic groups as basic sites.[1244]

Skeletal isomerization of alkanes into the corresponding branched isomers has attracted much attention as a catalytic process able to produce clean fuel with high-octane quality. The reaction is commonly carried out over bifunctional catalysts, with a hydrogenation/dehydrogenation function performed by a noble metal (often Pt or Pd) and acid sites for skeletal isomerization reaction involving carbenium ions.[1245] Catalysts presenting a high degree of hydrogenation activity and a low degree of acidity are the best for maximizing hydro-isomerization versus hydrocracking. Generally, acidic oxide supports (zeolites, silico-alumino-phosphates, amorphous mixed oxides and mesoporous molecular sieves) are used as a support, but carbon materials have been also investigated. A Pt/AC catalyst showing an optimized acidity (-COOH surface groups) have shown similar performances than a commercial Pt/SAPO-11 catalyst for the hydro-isomerization of n-decane.[1246] For the hydrogenation on myrcene on Pd/C catalysts, the better performances of catalysts prepared on oxidized supports bearing -COOH groups were tentatively attributed to an involvement of the carboxylic groups in the isomerization of the hard to reduce internal C=C bond of myrcene into an easy to hydrogenate terminal C=C bond.[1247] Indeed, alkene isomerization on carbon materials bearing -COOH functionalities has already been reported elsewhere.[1248,1249] Pristine, N-doped, and O-doped ordered mesoporous carbons were used as supports to prepare Pt catalysts for the hydro-conversion of n-heptane.[1250] The best performances have been achieved on the Pt/N-doped-C catalyst that shows a proper balance between the metal dispersion and the weak acid sites density, which is essential for n-heptane activation.

Tire oil hydro-processing (hydrodesulphurization, hydrocracking) has also been studied on bifunctional NiMo/AC[1251] and PtPd/AC catalysts.[1252] For NiMo/AC catalysts, it has been reported that the increase of the acidity of the support could yield faster isomerization rates, combined to those of hydrodesulphurization, and could significantly increase the removal of substituted dibenzothiophene species. In order to produce stable acidic sites, chemical

activation with H_3PO_4 has been performed on an AC; such a treatment produces oxygen-phosphorus surface groups (mainly C-O-PO_3 and C-PO_3).[1252] These phosphate groups are stable hydrocracking sites, with comparable performance to that of the acid sites present in amorphous SiO_2-Al_2O_3. The PtPd/AC bifunctional catalyst is capable of removing 97.3% of the original sulfur and up to 97 wt% of the heavy gasoil molecules in the pretreated tire oil.

Bifunctional catalysts present the advantage of integrating several catalytic processes (hydrogenation, oxidation, hydrolysis, or dehydration, etc.) that are usually tandem or parallel in the transformations of biomass. Thus, metal/acid bifunctional catalysts are also used for biomass valorization in various reactions of a biorefinery[45] such as: cellulose hydrolytic hydrogenation towards C_2-C_6 sugar alcohols (Ru/C and Pt/C),[1253-1256] conversion of levulinic acid to γ-valerolactone (Ru/C),[1257] or sugar conversion to alkyl lactate and lactic acid (Sn/AC-SiO_2).[1258]

The mechanism of the heterogeneous metal/acid-catalyzed direct conversion of cellulose to sorbitol consists first in cellulose proton-catalyzed hydrolytic depolymerization at the glycoside bond by the acid sites of the support,[1259] followed by the metal-catalyzed hydrogenation of the so-formed glucose.[1260] On Pt/CB catalyst without acidic sites it is proposed that both reaction can occur on Pt, but that the rate-determining step is the hydrolysis one.[1261] On Ru/C catalyst without acidic sites, supposedly the reaction proceeds through two steps: cellulose hydrolysis to glucose by acids, that are reversibly formed *in situ* from hot water, and subsequent glucose hydrogenation by supported Ru NP.[1262] It is also known that carbon materials presenting acidic surface functional groups (-SO_3H, -COOH, and -OH) are active for the hydrolysis of cellulose into saccharides.[45,1263-1268] Ru/C catalysts are also reported to be active for cellulose hydrolysis to glucose.[1269,1270] In that case, a synergistic effect between the support and Ru is observed, in which the main role of the carbon support is the hydrolysis of cellulose to oligosaccharides, while Ru promotes the conversion of oligosaccharides into glucose. Generally, high sorbitol

yields are achieved only if the hydrolysis is the rate-determining step, and a fast hydrogenation reaction prevents the degradation of the thermolabile glucose. In that context, the use of bifunctional metal/acid catalysts combining a hydrogenating metallic center and an acidic site of the carbon support has been investigated (Table 8). Some important findings are summarized below. First, it is found that ball-milling of cellulose and catalyst (mix-milling) drastically improves the yield of glucose and oligosaccharides, due to better contacts between the solid cellulose and solid catalyst.[1264] It was also proposed that acids necessary for the hydrolysis can be reversibly formed *in situ* from hot water,[1262] although the role of the support or the metal in this process was not discussed. Thus, the same Ru/C catalyst is active in water and inactive in either protic (ethanol) or aprotic (dioxane) solvents. However, other authors have shown that, even in hot water, acidic groups of the support are mandatory to have an activity on Ru/AC catalysts.[1255] Indeed, AC, AC-SO_3H and Ru/AC are found not to be active for sorbitol production, whereas the Ru/AC-SO_3H catalyst is very active. As far as surface functional groups are concerned, a synergistic effect between surface -OH or -COOH and -SO_3H groups was reported.[1271,1272] The carbon material is capable of adsorbing β-1,4-glucan thanks to the -OH or -COOH surface groups, and -SO_3H groups function as active sites for both decomposing the hydrogen bonds and hydrolyzing the β-1,4-glycosidic bonds. In the case of a Pt/rGO catalyst it is proposed that the acidity is maintained throughout the reaction thanks to hydrogen spillover from the metal to the support.[1273] In the same study, the authors have compared different carbon materials for the catalytic conversions of cellobiose (a diholoside produced by the degradation of cellulose) into sorbitol. The best performances follow the order: rGO > GO ≈ CNT >> AC > G. As far as the choice of the metal to reach high sorbitol selectivity is concerned, different results are obtained according to the nature of the support. On carbon black, the order follows: Pt > Ru >> Ir >> Rh > Pd.[1261] On CNT the order is: Ru >> Ir > Rh > Pt >> Pt > Fe >> Co ≈ Ni ≈ Ag ≈ Au.[1256]

Table 8. Bifunctional metal/acid catalysts for direct conversion of cellulose to sorbitol.

Catalyst	Conditions	Cellulose conversion (%)	Sorbitol selectivity (%)	Ref.
10 wt.% Ru/AC-SO_3H	Ball-milled cellulose 50 mg, catalyst 20 mg, water 12 mL, 438 K, 50 bar H_2, 24 h	81	58.7	[1255]
5%Pt/AC-SO_3H	1.12 g microcrystalline cellulose, 0.48 g cat., 40 mL water, 453 K, 20 bar H_2, 24 h	46.9	40.2[a)]	[1253]
5%Ru/AC-SO_3H		38.3	31.7[a)]	
3%Pt/AC-SO_3H	1.12 g ball-milled cellulose, 0.48 g cat., 40 mL water, 453 K, 20 bar H_2, 24 h	88.6	49.4[a)]	
3%Ru/AC-SO_3H		94.8	41.7[a)]	
5%Ru/CB-SO_3H	Cellulose (500 mg), catalyst (125 mg), distilled H_2O (25 g), 463 K, 50 bar H_2, 3 h	68.8	43.5	[1254]
1%Ru/CNT-COOH	Cellulose (crystallinity, 33%) 0.16 g; catalyst 50 mg; H_2O 20 mL, 458 K, 50 bar H_2, 24 h	-	69[b)]	[1256]
2%Ru/AC[c)]	Milled cellulose 324 mg, catalyst 50 mg, water 30 mL, 2-propanol 10 mL, 463 K, 18 h	80.2	36.8	[1274]
2%Ru/AC[c)]	324 mg of cellulose oligomers, catalyst 100 mg, 20 mL of water, 20 mL of 2-propanol, 15 bar Ar at room temperature, 20 min.	75	35.3[a),b)]	[1275]
5%Pt/rGO	Cellulose 171 mg, catalyst 50 mg, 20 mL of water, 463 K, 50 bar H_2, 24 h	84	54	[1273]
1%Rh-5%Ni/C	0.5 g cellulose (Merck, microcrystalline), 0.15 g catalyst, 50 mL water, 518 K, 60 bar H_2, 30 min.	100	51.5	[1276]
7.5%Ni/CNF	Ball-milled cellulose 1 g, 0.5 g catalyst, 50 mL water, 463 K, 60 bar H_2, 24 h.	93	76[d)]	[1277]

a) Sorbitol and mannitol, with an average ratio of 50-60% sorbitol and 40-50% mannitol based on ion chromatography measurements. b) Sorbitol yield. c) Transfer hydrogenation. d) Hexitol yield.

It is also evidenced that a minimal metal (Pt or Ru) loading (*ca.* 3-5 wt.%) is necessary to promote the hydrogenation of glucose to sorbitol *versus* other acid-catalyzed reactions.[1253] The same observation is made for Ni/CNF catalysts, and in that case the optimum Ni loading is 7.5% w/w.[1277] For the same catalyst, the balance between the hydrogenation and the acid functions has been also examined, and it is found that a relatively high amount of Ni surface atoms and a low density of Brønsted acid sites show the highest hexitol yields. Finally, transfer hydrogenation with 2-propanol has been also investigated as an alternative to H_2 pressure for this reaction on Ru/C catalysts.[1274,1275] Experiences with deuterium (D_2 and D_2O) have allowed to establish that the direct transfer of hydrides from 2-propanol to glucose occurs through a dihydride mechanism in which both hydrogen atoms are transferred to the ruthenium surface.

The catalytic hydrogenation of levulinic acid (LA) involves a two-step sequence: a metal-catalyzed hydrogenation of LA to 4-hydroxyvaleric acid (4-HVA), followed by an acid-catalyzed intra-molecular esterification to γ-valerolactone (GVL) (Scheme 1).

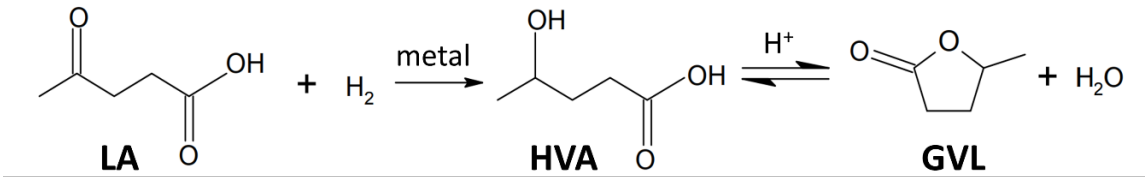

Scheme 1. Reaction scheme for the catalytic hydrogenation of LA (levulinic acid) to GVL (γ-valerolactone).

Regarding the intramolecular esterification reaction of 4-HVA to GVL, it is assumed that the reaction is an equilibrium reaction catalyzed by a Brønsted acid. Two acids, LA and 4-HVA, are present in the reaction mixture and it is assumed that both catalyze this reaction. Thus, this

reaction was reported to proceed in water on Ru/C,[1278-1281] Pt/C[1282], Ir/C,[1282] Ir/CNT,[1283] Fe@C,[1284] Re/C,[1282], Ni/C[1282,1285] Pd/CNT[1286] and Pd/C[1280,1287] catalysts without the need of acid functions on carbon material. The best selectivity to GVL is obtained on Ru catalysts.[1282] However, it has been shown that in water, surface hydroxyl groups are formed on a Ru/C catalyst, and that the formation of these groups coincides with the emergence of Brønsted acid sites on the catalyst.[1288] Moreover, the performances of a Ru/C catalyst are improved by the addition of a heterogeneous acid co-catalyst, such as the ion exchange resins Amberlyst-15.[1289,1290] A Ru/polyethersulfone catalyst is also active for LA hydrogenation to GVA in aqueous solution.[1291] The high reactivity is ascribed to the fact that acid and metal sites are both operating in this bifunctional catalyst. Support with high point of zero charge (PZC) favors the reversible deactivation of Ru catalyst during LA hydrogenation.[1292] Thus, the use of a carbon support with acidic sites, combining an activity for acid-catalyzed intra-molecular esterification, and a low PZC is potentially interesting. Surprisingly, there is only one report concerning the use of an acidic carbon support for this important reaction. A Ru/rGO-SO_3H catalyst has been prepared, presenting excellent activity (522 h^{-1}) and selectivity towards GVA (82%) at 323 K and 20 bar H_2,[1257] whereas a Ru/rGO catalyst yields only 18 % for similar Ru NP sizes. Compared to catalyst deposited on other acidic supports or even to a Ru/AC-Amberlyst catalysts, the Ru/rGO-SO_3H shows lower selectivity but significantly higher activity.

A bifunctional carbon-silica composite (CSM) catalysts containing grafted $Sn^{(IV)}$ species on SiO_2 has been used for trioses, glyceraldehyde and dihydroxyacetone conversion to ethyl lactate in ethanol.[1258] For this catalyst, Lewis acidity is provided by $Sn^{(IV)}$, while weak Brønsted acidity originates from surface oxygen groups on the carbon. In the investigated reactions, strong Brønsted acidity should be avoided as it favors competitive reactions. The presence of weak

Brønsted acid sites is crucial in accelerating the rate-determining dehydration reaction, that is, the first step in the reaction mechanism from triose to lactate.

Finally, acid-base bifunctional catalysis over WO_x/N-doped carbon has been used for one-pot cascade reactions comprising sequential acetal hydrolysis and Knoevenagel condensation from dimethoxymethylbenzene.[1293] The reaction proceeds through a two-step mechanism involving acid-catalyzed hydrolysis of dimethoxymethyl benzene to benzaldehyde, which undergoes a base-catalyzed Knoevenagel condensation in the presence of ethyl cyanoacetate (Scheme 2).

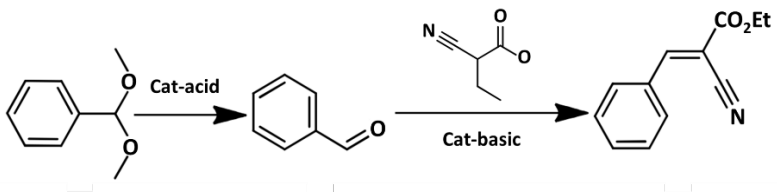

Scheme 2. Reaction pathway for Knoevenagel reaction of dimethoxymethyl benzene over bifunctional WO_x/N-C catalyst.

3.4.3 Cooperative catalysis

The basic properties of N-doped carbon materials have been exploited for cooperative catalysis. Indeed, the introduction of N atoms alters the acid-base properties of the support surface, which is beneficial for transfer hydrogenation, dehydrogenation, and oxidation reactions (Scheme 3).[75] In that case, the presence of N species acting as basic sites, are able of improving the interactions of the carbon surface with acidic molecules though dipole-dipole, hydrogen bonding, and/or covalent bonding.

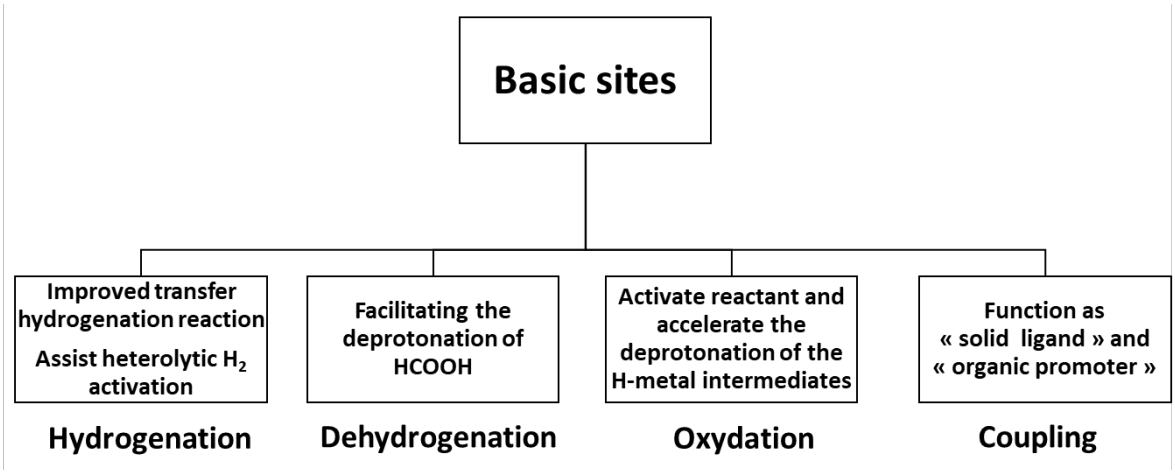

Scheme 3. Promotional effect of N-doping on carbon-supported bifunctional catalysts.

On SAC deposited on carbon materials, the hydrogen activation during hydrogenation reactions is often difficult because the single atom is electro-deficient. Several works have shown that on SAC deposited on N-doped carbon materials, a heterolytic activation of dihydrogen occurs.[1294,1295] On such catalysts, the metal is in close proximity with nitrogen groups of the support. Thus, on isolated Pd atoms, the hydrogen activation occurs first by the coordination of molecular hydrogen on the metal, which undergoes heterolytic dissociation, leaving one of the hydrogen atoms bound to a nitrogen atom of the support and the second one on the Pd atom.[1294] A similar reactivity was observed on Ni_1/N-C catalysts.[1295] This type of reactivity is not limited to nitrogen-doped carbon materials, since for Pd atoms it is also shown that the proximity of oxygen atoms is found to be crucial for facilitating heterolytic H_2 dissociation.[1296] This dissociation is reminiscent of that of frustrated Lewis pairs in homogeneous catalysts, where H_2 is heterolytically dissociated at the sterically encumbered Lewis acids and bases. In supported SAC, the single metal atoms are usually positively charged,[292] and therefore act as a Lewis acid, while the nearby nitrogen atoms from the support can act as a Lewis base; the combination of the two facilitates the dissociation of hydrogen *via* a heterolytic pathway. A similar cooperation between the metal and the nitrogen-doped carbon

is also proposed for the activation of molecular oxygen on Co/N-C catalysts occurring during the oxidative dehydrogenation of 1,2,3,4-tetrahydroquinoline.[1297]

Nitrogen surface groups and particularly pyridinic groups of carbon material can function as Lewis-base sites, which can be used to adsorb the alcohol (hydrogen-donor) and thus enhance metal hydrides' formation in transfer hydrogenation reactions. Thus, a bifunctional Co/N-C catalysts has been used for base-free transfer hydrogenations of nitriles.[1298] Under base-free conditions with 2-propanol as both proton donor and solvent, the Co/N-C catalyst could convert nitriles into primary amines or imines with high selectivity. It is proposed that the N-basic sites play a role similar to that of the base additives, which not only inhibit the formation of polyamine, but also effectively promote the transfer hydrogenation. Similar conclusions were obtained in the case of a Fe/N-C catalyst for the catalytic transfer hydrogenation of furfural to furfuryl alcohol.[1299] In that case, the authors propose that the transfer hydrogenation mechanism requires both basic and acidic active centers. The alcohol (hydrogen donor) is adsorbed on the basic site and the ketone on an adjacent acidic site and hydrogen is transferred as hydride. The pyridinic basic sites may also have a positive impact on the dehydrogenation of formic acid. For this reaction, the crucial role of amines is to promote the O-H bond cleavage, leading to the formation of a metal-formate species. Pt catalysts on N-CNF have been investigated for this reaction,[1300] suggesting that the pyridinic surface groups induce both the formation of electro-deficient Pt centers, and the dissociation of the O-H bond in formic acid, hence leading to improved catalytic activity.

In the aerobic oxidation of alcohols, a sacrificial base as NaOH is generally needed to initiate the reaction by capturing H^+ from hydroxyl groups of reactants. Additionally, the base can contribute to prolong the catalyst lifetime by removing from the catalyst surface strongly adsorbed reactions products such as organic acids. Pt/N-C catalysts were used for the base-free oxidation of 5-hydroxymethylfurfural (HMF) to 2,5-furandicarboxylic acid.[1301] It was shown

that the pyridine surface groups played a key role in the selective oxidation of HMF, which was attributed to their medium strength basicity that could promote the activation of hydroxyl and the formation of hemiacetal intermediates in this reaction. Similar observation (acceleration of the deprotonation process) was made in the case of the aerobic oxidation of several alcohols under base-free conditions on Co/N-C,[1302-1304] Pd/N-C,[1305] and Pt/N-C[1306] catalysts.

The reductive Ullmann homo-coupling of aryl halides using Pd/N-G catalysts without any external reductant was also investigated. Although bases have been needed for this reaction, the Pd catalyst on N-G performs much better than on graphene or rGO. It was proposed that N-doped graphene acts as both catalyst support and electron source (reducing agent) in this reaction.

Although to a lesser extent, the acidic properties of O-doped carbon materials (-OH and -COOH groups) have also been exploited for cooperative catalysis. For the hydrogenolysis of hydroxymatairesinol to oxomatairesinol over Pd/C and Pd/CNF catalysts, an active role of the Brønsted acid sites present on the catalyst support (-COOH groups) is noticed, and higher activities are achieved over Pd catalysts on more acidic supports.[1307,1308] Quantum chemical calculations have been performed as an attempt to understand the role of acid sites.[1308] The Brønsted acid sites have been suspected to be involved in the protonation of hydroxymatairesinol, which has been identified as the first step in the formation of oxomatairesinol. Finally, DFT calculations were used to investigate the synthesis mechanism of vinyl acetate from acetylene and acetic acid catalyzed by carbon-supported zinc acetate containing different types of surface oxygen groups.[1309] It has been found that carboxyl groups can reduce the activation barrier of the rate-limiting step ($CH{\equiv}CH + CH_3COOH^* \rightarrow CH_2{=}CH{-}OCOCH_3^*$) dramatically, while hydroxyl groups increases it. Carbonyl groups shift into epoxy group and as such do not improve the kinetics.

4. Conclusions and perspectives

"*Carbon is often described as one of the most long-established, and yet newest material to be used in technology*." This statement of E. Fitzer, although dating from 1967,[1310] is still relevant in 2020, proving the richness of chemistry and physics centered around this element. Research on carbon materials dates from the mid-nineteenth century,[1311] and for a long period, the study of carbon materials remained a story of specialists. Inagaki identified three periods for the development of carbon materials: i) before 1960, *period I* for the *classic carbons* (artificial graphite, activated carbons, carbon blacks and natural diamond); ii) 1960-1985, *period II* for the *new carbons* (carbon fibers, glass-like carbons, pyrolytic carbons, intercalation compounds, composites, and synthetic diamond); and after 1985, *period III* for the *carbon nanomaterials* (fullerenes, carbon nanotubes, and graphene).[1312] It has to be emphasized that carbon materials from *period I* are currently the principal products and principal incomes for carbon industries worldwide. The structural characteristics in each family are relatively broad, and each carbon family shows various possibilities for accepting foreign atoms (doping, substitution, and intercalation). Although the study of chemistry and physics of carbon was largely initiated during *period II*, as exemplified by the book series "Chemistry and Physics of Carbon" initiated in 1965 by P.L. Walker; it is during *period III* that the domain became really multidisciplinary and that scientist from different horizons were interested in these materials. However, still today, and because of the large family of carbon materials, the field is still relatively partitioned.

In this respect, catalysis constitutes a specific field, in the sense that the spectrum of carbon materials used is very wide. In fact, almost all the materials of the three periods have been used in catalysis, either as support or as catalyst. If, as in the other fields, the materials of the *period I* are still today those which are used in industrial catalytic processes, the materials of *period*

III constitute excellent model materials, which make it possible to better apprehend the chemistry and the physics of structurally more complex materials like activated carbon or carbon black. The use of carbon materials as catalyst support requires a good knowledge of many characteristics, such as the surface chemistry, the electronic, mechanical, structural and textural properties, which will all affect the final catalyst. Due to the complexity of the structure and surface chemistry of some carbon materials (as stated in the introduction of this review, still today, the precise atomic structure of activated carbon remains unknown), more efforts have to be devoted to the study of model systems, and establishing correlations between these model systems and the more complex ones. It is noted that studies on model catalysts comprising carbon supports are relatively rare compared to oxides.[1313-1315]

In this review article, we were interested in compiling and discussing the most significant experimental and theoretical results allowing a better understanding of key phenomena in catalysis as: i) the anchoring of the metal; ii) the metal-support interactions (geometric effects, charge transfer); iii) confinement; iv) spillover; or v) surface functional group effects. Undeniable advances in modeling and advanced analytical techniques have allowed, as in the case of other catalyst support, a better understanding of these phenomena. It appears that in a sp^2 or $sp^{2+\delta}$ carbon material, the regular arrangement of carbon atoms allows mainly the control of: i) the morphology, which can play on the confinement, and ii) the electronic properties that can play on the charge transfer. Next to that, the ratio of prismatic to basal surface is an important parameter that affects the surface charge and bonding strength with metal particles. The presence of vacancies and the exact nature of the edges is also a crucial point that definitively requires more attention, since these sites are theoretically highly reactive and can strongly affect many properties, it was suggested that they are at the origin of the magnetic properties of some carbon materials.[63,153] If the existence of these sites does not seem to be a problem for theoreticians, the experimenters must be circumspect because: i) their generation

is not simple and requires special conditions,[1316,1317] and ii) the stability of the more reactive sites is questionable.[1318]

The introduction of heteroatoms into the carbon matrix constitutes also a possibility to modulate its properties. There is still little work involving side-by-side comparisons among doping of different elements in carbon materials. Controlling the doping selectivity of carbon materials is also a point that requires more effort on the part of synthetic chemists. In particular, the control of the type of functional group introduced for a given heteroatom is mostly not achieved, although it is often a key point towards better activity, selectivity and even stability. In that prospect, new materials like graphdiyne[1319] or graphitic carbon nitride[1320] are particularly interesting.

All the limitations mentioned above contribute to the fact that the study of certain phenomena, such as charge transfer or spillover on carbon materials is particularly difficult. Combined experimental and theoretical approach will be essential to deeply understand these phenomena and to identify the structure, mechanism and kinetics of the catalytic center.

AUTHOR INFORMATION

Corresponding Authors

*E-mails: igerber@insa-toulouse.fr; philippe.serp@ensiacet.fr

ORCID

Iann Gerber: 0000-0001-5091-2655

Philippe Serp: 0000-0003-1424-2724

Notes

The authors declare no competing financial interest.

Biographies

Iann C. Gerber has been an Assistant Professor of Condensed Matter Physics at the Institut National des Sciences Appliquées de Toulouse, since 2007. He received his Ph.D. degree from the Henri Poincaré Nancy-I Université in 2005 and pursued his research career in the Department of Physics of the Aalto University, Helsinki. His current research interests include studying nanostructure electronic structure properties based on DFT calculations as well as theoretical nanocatalysis. He has published over 60 articles and 1 book chapter.

Philippe Serp is a Professor of Inorganic Chemistry at the Toulouse National Polytecnic Institute. He received his Ph.D. degree from the University Paul Sabatier in 1994 and engaged in postdoctoral research at the University of Porto and Louvain-la-Neuve from 1995 to 1997. His research interests in the Laboratory of Coordination Chemistry include the preparation of nanostructured catalytic materials, nanocatalysis, and molecular approaches to understand heterogeneous catalysis; fields in which with co-workers he has published over 200 papers among them twenty European and U.S. patents. His research has been recognized by the Catalysis (2004) and Industrial Chemistry (2012) Division Awards of the French Chemical Society.

DEDICATION

We sadly learned during the writing of this review the untimely death of our colleague Dang Sheng Su (Chinese Academy of Sciences), who has greatly contributed to the study of carbon materials for catalysis since the beginning of the century (see *Chem. Rev*. **2013**, *113*, 5782-5816), and who has really invested a lot in forming a living community around the world. We dedicate this review article to his memory.

References

(1) Bender, H. L.; US1355299A, Ed., 1920.
(2) Wilson, R. E.; Whetzel, J. C.; US1519470A, Ed., 1921.
(3) Reimerink, W. M. T. M. In *Stud. Surf. Sci. Catal.*; Dąbrowski, A., Ed.; Elsevier, 1999; Vol. 120.
(4) Arunajatesan, V.; Chen, B.; Möbus, K.; Ostgard, D. J.; Tacke, T.; Wolf, D. In *Carbon Materials for Catalysis*; Serp, P.;Figueiredo, J. L., Eds.; Wiley, 2008, DOI:doi:10.1002/9780470403709.ch15 doi:10.1002/9780470403709.ch15.
(5) Auer, E.; Freund, A.; Pietsch, J.; Tacke, T. Carbons as Supports for Industrial Precious Metal Catalysts. *Applied Catalysis A: General* **1998,** *173*, 259-271.
(6) Johnston, P.; Carthey, N.; Hutchings, G. J. Discovery, Development, and Commercialization of Gold Catalysts for Acetylene Hydrochlorination. *J. Am. Chem. Soc.* **2015,** *137*, 14548-14557.
(7) Malta, G.; Kondrat, S. A.; Freakley, S. J.; Davies, C. J.; Lu, L.; Dawson, S.; Thetford, A.; Gibson, E. K.; Morgan, D. J.; Jones, W.et al. Identification of Single-Site Gold Catalysis in Acetylene Hydrochlorination. *Science* **2017,** *355*, 1399-1403.
(8) Serp, P. In *Comprehensive Inorganic Chemistry Ii (Second Edition)*; Reedijk, J.;Poeppelmeier, K., Eds.; Elsevier: Amsterdam, 2013, DOI:https://doi.org/10.1016/B978-0-08-097774-4.00731-2 https://doi.org/10.1016/B978-0-08-097774-4.00731-2.
(9) Larsen, E. C.; Walton, J. H. Activated Carbon as a Catalyst in Certain Oxidation-Reduction Reactions. *The Journal of Physical Chemistry* **1940,** *44*, 70-85.
(10) Coughlin, R. W. Carbon as Adsorbent and Catalyst. *Product R&D* **1969,** *8*, 12-23.
(11) Hillenbrand, L. J.; Lacksonen, J. W. The Platinum-on-Carbon Catalyst System for Hydrogen Anodes: Ii . Chemical Requirements of the Carbon Surface. *J. Electrochem. Soc.* **1965,** *112*, 249-252.
(12) Singh, H.; Prasad, M.; Srivastava, R. D. Metal Support Interactions in the Palladium-Catalysed Decomposition of Furfural to Furan. *J. Chem. Technol. Biotechnol.* **1980,** *30*, 293-296.
(13) Acres, G. J. K.; Cooper, B. J. Carbon-Supported Platinum Metal Catalysts for Hydrogenation Reactions. Mass Transport Effects in Liquid Phase Hydrogenation over Pd/C. *Journal of Applied Chemistry and Biotechnology* **1972,** *22*, 769-785.
(14) McMichael, B. D.; Kmetko, E. A.; Mrozowski, S. An Aromatic Detector for the Infrared*. *Journal of the Optical Society of America* **1954,** *44*, 26-30.
(15) Franklin, R. E. Crystallite Growth in Graphitizing and Non-Graphitizing Carbons. *Proceedings of the Royal Society of London. Series A. Mathematical and Physical Sciences* **1951,** *209*, 196-218.
(16) Peter, J. F. H.; Zheng, L.; Kazu, S. Imaging the Atomic Structure of Activated carbon. *J. Phys.: Condens. Matter* **2008,** *20*, 362201.

(17) Derbyshire, F. J.; de Beer, V. H. J.; Abotsi, G. M. K.; Scaroni, A. W.; Solar, J. M.; Skrovanek, D. J. The Influence of Surface Functionality on the Activity of Carbon-Supported Catalysts. *Applied Catalysis* **1986,** *27*, 117-131.
(18) Prado-Burguete, C.; Linares-Solano, A.; Rodríguez-Reinoso, F.; de Lecea, C. S.-M. The Effect of Oxygen Surface Groups of the Support on Platinum Dispersion in Pt/Carbon Catalysts. *J. Catal.* **1989,** *115*, 98-106.
(19) Jüntgen, H. Activated Carbon as Catalyst Support: A Review of New Research Results. *Fuel* **1986,** *65*, 1436-1446.
(20) Rhead, T. F. E.; Wheeler, R. V. Liii.—the Mode of Combustion of Carbon. *Journal of the Chemical Society, Transactions* **1913,** *103*, 461-489.
(21) Boehm, H.-P.; Diehl, E.; Heck, W.; Sappok, R. Surface Oxides of Carbon. *Angewandte Chemie International Edition in English* **1964,** *3*, 669-677.
(22) Coltharp, M. T.; Hackerman, N. Surface of a Carbon with Sorbed Oxygen on Pyrolysis. *The Journal of Physical Chemistry* **1968,** *72*, 1171-1177.
(23) Yuchen, M.; Lehtinen, P. O.; Foster, A. S.; Nieminen, R. M. Magnetic Properties of Vacancies in Graphene and Single-Walled Carbon Nanotubes. *New Journal of Physics* **2004,** *6*, 68.
(24) Binford, J. S. In *Literature of the Combustion of Petroleum*; AMERICAN CHEMICAL SOCIETY, 1958; Vol. 20.
(25) Walker, P. L. Carbon - an Old but New Material. *American Scientist* **1962,** *50*, 259-293.
(26) Walker, P. L. Carbon: An Old but New Material Revisited. *Carbon* **1990,** *28*, 261-279.
(27) Simonov, P. A.; Romanenko, A. V.; Prosvirin, I. P.; Moroz, E. M.; Boronin, A. I.; Chuvilin, A. L.; Likholobov, V. A. On the Nature of the Interaction of H2pdcl4 with the Surface of Graphite-Like Carbon Materials. *Carbon* **1997,** *35*, 73-82.
(28) Rodríguez-reinoso, F. The Role of Carbon Materials in Heterogeneous Catalysis. *Carbon* **1998,** *36*, 159-175.
(29) Serp, P.; Corrias, M.; Kalck, P. Carbon Nanotubes and Nanofibers in Catalysis. *Applied Catalysis A: General* **2003,** *253*, 337-358.
(30) Wildgoose, G. G.; Banks, C. E.; Compton, R. G. Metal Nanoparticles and Related Materials Supported on Carbon Nanotubes: Methods and Applications. *Small* **2006,** *2*, 182-193.
(31) Antolini, E. Carbon Supports for Low-Temperature Fuel Cell Catalysts. *Applied Catalysis B: Environmental* **2009,** *88*, 1-24.
(32) Serp, P.; Castillejos, E. Catalysis in Carbon Nanotubes. *ChemCatChem* **2010,** *2*, 41-47.
(33) Machado, B. F.; Serp, P. Graphene-Based Materials for Catalysis. *Catalysis Science & Technology* **2012,** *2*, 54-75.
(34) De Jong, K. P.; Geus, J. W. Carbon Nanofibers: Catalytic Synthesis and Applications. *Catalysis Reviews* **2000,** *42*, 481-510.
(35) Hu, M.; Yao, Z.; Wang, X. Graphene-Based Nanomaterials for Catalysis. *Industrial & Engineering Chemistry Research* **2017,** *56*, 3477-3502.
(36) Mabena, L. F.; Sinha Ray, S.; Mhlanga, S. D.; Coville, N. J. Nitrogen-Doped Carbon Nanotubes as a Metal Catalyst Support. *Applied Nanoscience* **2011,** *1*, 67-77.
(37) Moreno-Castilla, C.; Maldonado-Hódar, F. J. Carbon Aerogels for Catalysis Applications: An Overview. *Carbon* **2005,** *43*, 455-465.
(38) Zhu, J.; Xiao, P.; Li, H.; Carabineiro, S. A. C. Graphitic Carbon Nitride: Synthesis, Properties, and Applications in Catalysis. *ACS Applied Materials & Interfaces* **2014,** *6*, 16449-16465.
(39) Furimsky, E. *Carbons and Carbon Supported Catalysts in Hydroprocessing*; RSC, 2008.
(40) Serp, P.; Figueiredo, J. L. *Carbon Materials for Catalysis*; John Wiley & Sons, Inc.: Hoboken, New Jersey, 2008.
(41) Serp, P.; Machado, B. *Nanostructured Carbon Materials for Catalysis*; RSC: Cambridge, 2015.
(42) Villa, A.; Dimitratos, N. *Metal-Free Functionalized Carbons in Catalysis: Synthesis, Characterization and Applications*; RSC, 2018.
(43) Yang, Y.; Chiang, K.; Burke, N. Porous Carbon-Supported Catalysts for Energy and Environmental Applications: A Short Review. *Catal. Today* **2011,** *178*, 197-205.

(44) Yang, Z.; Ren, J.; Zhang, Z.; Chen, X.; Guan, G.; Qiu, L.; Zhang, Y.; Peng, H. Recent Advancement of Nanostructured Carbon for Energy Applications. *Chem. Rev.* **2015,** *115*, 5159-5223.
(45) Lam, E.; Luong, J. H. T. Carbon Materials as Catalyst Supports and Catalysts in the Transformation of Biomass to Fuels and Chemicals. *ACS Catalysis* **2014,** *4*, 3393-3410.
(46) Dai, L.; Xue, Y.; Qu, L.; Choi, H.-J.; Baek, J.-B. Metal-Free Catalysts for Oxygen Reduction Reaction. *Chem. Rev.* **2015,** *115*, 4823-4892.
(47) Ong, W.-J.; Tan, L.-L.; Ng, Y. H.; Yong, S.-T.; Chai, S.-P. Graphitic Carbon Nitride (G-C3n4)-Based Photocatalysts for Artificial Photosynthesis and Environmental Remediation: Are We a Step Closer to Achieving Sustainability? *Chem. Rev.* **2016,** *116*, 7159-7329.
(48) Jin, H.; Guo, C.; Liu, X.; Liu, J.; Vasileff, A.; Jiao, Y.; Zheng, Y.; Qiao, S.-Z. Emerging Two-Dimensional Nanomaterials for Electrocatalysis. *Chem. Rev.* **2018,** *118*, 6337-6408.
(49) Fang, B.; Chaudhari, N. K.; Kim, M.-S.; Kim, J. H.; Yu, J.-S. Homogeneous Deposition of Platinum Nanoparticles on Carbon Black for Proton Exchange Membrane Fuel Cell. *J. Am. Chem. Soc.* **2009,** *131*, 15330-15338.
(50) Reier, T.; Oezaslan, M.; Strasser, P. Electrocatalytic Oxygen Evolution Reaction (Oer) on Ru, Ir, and Pt Catalysts: A Comparative Study of Nanoparticles and Bulk Materials. *ACS Catalysis* **2012,** *2*, 1765-1772.
(51) Bulushev, D. A.; Yuranov, I.; Suvorova, E. I.; Buffat, P. A.; Kiwi-Minsker, L. Highly Dispersed Gold on Activated Carbon Fibers for Low-Temperature Co Oxidation. *J. Catal.* **2004,** *224*, 8-17.
(52) Wu, G.; More, K. L.; Johnston, C. M.; Zelenay, P. High-Performance Electrocatalysts for Oxygen Reduction Derived from Polyaniline, Iron, and Cobalt. *Science* **2011,** *332*, 443-447.
(53) Li, W.; Liang, C.; Zhou, W.; Qiu, J.; Zhou; Sun, G.; Xin, Q. Preparation and Characterization of Multiwalled Carbon Nanotube-Supported Platinum for Cathode Catalysts of Direct Methanol Fuel Cells. *The Journal of Physical Chemistry B* **2003,** *107*, 6292-6299.
(54) Li, Y.; Zhou, W.; Wang, H.; Xie, L.; Liang, Y.; Wei, F.; Idrobo, J.-C.; Pennycook, S. J.; Dai, H. An Oxygen Reduction Electrocatalyst Based on Carbon Nanotube–Graphene Complexes. *Nature Nanotechnology* **2012,** *7*, 394.
(55) Liang, Y.; Li, Y.; Wang, H.; Zhou, J.; Wang, J.; Regier, T.; Dai, H. Co3o4 Nanocrystals on Graphene as a Synergistic Catalyst for Oxygen Reduction Reaction. *Nature Materials* **2011,** *10*, 780.
(56) Yoo, E.; Okata, T.; Akita, T.; Kohyama, M.; Nakamura, J.; Honma, I. Enhanced Electrocatalytic Activity of Pt Subnanoclusters on Graphene Nanosheet Surface. *Nano Lett.* **2009,** *9*, 2255-2259.
(57) Liu, X.; Sui, Y.; Meng, C.; Han, Y. Tuning the Reactivity of Ru Nanoparticles by Defect Engineering of the Reduced Graphene Oxide Support. *RSC Advances* **2014,** *4*, 22230-22240.
(58) Harris, P. J. F. Fullerene-Like Models for Microporous Carbon. *Journal of Materials Science* **2013,** *48*, 565-577.
(59) Sarkisov, L.; Centineo, A.; Brandani, S. Molecular Simulation and Experiments of Water Adsorption in a High Surface Area Activated Carbon: Hysteresis, Scanning Curves and Spatial Organization of Water Clusters. *Carbon* **2017,** *118*, 127-138.
(60) Machado, B. F.; Oubenali, M.; Rosa Axet, M.; Trang Nguyen, T.; Tunckol, M.; Girleanu, M.; Ersen, O.; Gerber, I. C.; Serp, P. Understanding the Surface Chemistry of Carbon Nanotubes: Toward a Rational Design of Ru Nanocatalysts. *J. Catal.* **2014,** *309*, 185-198.
(61) Yazyev, O. V.; Helm, L. Defect-Induced Magnetism in Graphene. *Physical Review B* **2007,** *75*, 125408.
(62) Acik, M.; Chabal, Y. J. Nature of Graphene Edges: A Review. *Japanese Journal of Applied Physics* **2011,** *50*, 070101.
(63) Radovic, L. R.; Bockrath, B. On the Chemical Nature of Graphene Edges: Origin of Stability and Potential for Magnetism in Carbon Materials. *J. Am. Chem. Soc.* **2005,** *127*, 5917-5927.
(64) Banhart, F.; Kotakoski, J.; Krasheninnikov, A. V. Structural Defects in Graphene. *ACS Nano* **2011,** *5*, 26-41.
(65) Ayala, P.; Arenal, R.; Rümmeli, M.; Rubio, A.; Pichler, T. The Doping of Carbon Nanotubes with Nitrogen and Their Potential Applications. *Carbon* **2010,** *48*, 575-586.

(66) Lee, W. J.; Maiti, U. N.; Lee, J. M.; Lim, J.; Han, T. H.; Kim, S. O. Nitrogen-Doped Carbon Nanotubes and Graphene Composite Structures for Energy and Catalytic Applications. *Chem. Commun.* **2014,** *50*, 6818-6830.
(67) Wang, H.; Maiyalagan, T.; Wang, X. Review on Recent Progress in Nitrogen-Doped Graphene: Synthesis, Characterization, and Its Potential Applications. *ACS Catalysis* **2012,** *2*, 781-794.
(68) Axet, M. R.; Dechy-Cabaret, O.; Durand, J.; Gouygou, M.; Serp, P. Coordination Chemistry on Carbon Surfaces. *Coord. Chem. Rev.* **2016,** *308*, 236-345.
(69) Hughes, Z. E.; Walsh, T. R. Computational Chemistry for Graphene-Based Energy Applications: Progress and Challenges. *Nanoscale* **2015,** *7*, 6883–6908.
(70) Zhou, M.; Wang, H.-L.; Guo, S. Towards High-Efficiency Nanoelectrocatalysts for Oxygen Reduction through Engineering Advanced Carbon Nanomaterials. *Chem. Soc. Rev.* **2015**, 1–35.
(71) Zhou, Y.; Neyerlin, K.; Olson, T. S.; Pylypenko, S.; Bult, J.; Dinh, H. N.; Gennett, T.; Shao, Z.; O'Hayre, R. Enhancement of Pt and Pt-Alloy Fuel Cell Catalyst Activity and Durability Via Nitrogen-Modified Carbon Supports. *Energy Environ. Sci.* **2010,** *3*, 1437–1410.
(72) Shrestha, S.; Liu, Y.; Mustain, W. E. Electrocatalytic Activity and Stability of Pt Clusters on State-of-the-Art Supports: A Review. *Catalysis Reviews* **2011,** *53*, 256–336.
(73) Zhang, B.; Su, D. S. Probing the Metal-Support Interaction in Carbon-Supported Catalysts by Using Electron Microscopy. *ChemCatChem* **2015,** *7*, 3639–3645.
(74) Campisi, S.; Chan-Thaw, C.; Villa, A. Understanding Heteroatom-Mediated Metal–Support Interactions in Functionalized Carbons: A Perspective Review. *Applied Sciences* **2018,** *8*, 1159–1125.
(75) Cao, Y.; Mao, S.; Li, M.; Chen, Y.; Wang, Y. Metal/Porous Carbon Composites for Heterogeneous Catalysis: Old Catalysts with Improved Performance Promoted by N-Doping. *ACS Catalysis* **2017,** *7*, 8090–8112.
(76) Yildirim, T.; Íñiguez, J.; Ciraci, S. Molecular and Dissociative Adsorption of Multiple Hydrogen Molecules on Transition Metal Decorated ${\Mathrm{C}}_{60}$. *Physical Review B* **2005,** *72*, 153403.
(77) Giacalone, F.; Martn, N.; Wudl, F. In *Fullerene Polymers*; Wiley-VCH Verlag GmbH & Co. KGaA, 2009.
(78) Rosseinsky, M. J. Recent Developments in the Chemistry and Physics of Metal Fullerides. *Chem. Mater.* **1998,** *10*, 2665-2685.
(79) Ivanova, V. N. Fullerene Compounds with Transition Metals Mnc60: Preparation, Structure, and Properties. *J. Struct. Chem.* **2000,** *41*, 135-148.
(80) Nagashima, H.; Nakaoka, A.; Saito, Y.; Kato, M.; Kawanishi, T.; Itoh, K. C60pd: The First Organometallic Polymer of Buckminsterfullerene. *J. Chem. Soc., Chem. Commun.* **1992**, DOI:10.1039/c39920000377 10.1039/c39920000377, 377-379.
(81) Lavrentiev, V.; Abe, H.; Yamamoto, S.; Naramotoand, H.; Narumi, K. Co and C60 Interaction under Conditions of Mixture. *Molecular Crystals and Liquid Crystals* **2002,** *386*, 139-143.
(82) Wohlers, M.; Herzog, B.; Belz, T.; Bauer, A.; Braun, T.; Rühle, T.; Schlögl, R. Ruthenium-C60 Compounds: Properties and Catalytic Potential. *Synth. Met.* **1996,** *77*, 55-58.
(83) Gurav, A. S.; Duan, Z.; Wang, L.; Hampden-Smith, M. J.; Kodas, T. T. Synthesis of Fullerene-Rhodium Nanocomposites Via Aerosol Decomposition. *Chem. Mater.* **1993,** *5*, 214-216.
(84) Norin, L.; Jansson, U.; Dyer, C.; Jacobsson, P.; McGinnis, S. On the Existence of Transition-Metal Fullerides: Deposition and Characterization of Tixc60. *Chem. Mater.* **1998,** *10*, 1184-1190.
(85) Saha, D.; Deng, S. Hydrogen Adsorption on Pd- and Ru-Doped C60 Fullerene at an Ambient Temperature. *Langmuir* **2011,** *27*, 6780-6786.
(86) Soto, D.; Salcedo, R. Coordination Modes and Different Hapticities for Fullerene Organometallic Complexes. *Molecules* **2012,** *17*.
(87) Lavrentiev, V.; Abe, H.; Naramoto, H.; Sakai, S.; Narumi, K. Polymeric Chains in C60 and Co Mixture. *Chem. Phys. Lett.* **2006,** *424*, 101-104.
(88) Mendez-Camacho, R.; Guirado-Lopez, R. A. Adsorption and Diffusion of Hydrogen on C-60-Supported Pt-N Clusters. *JOURNAL OF PHYSICAL CHEMISTRY C* **2013,** *117*, 10059-10069.

(89) Pham, N. N. T.; Le, H. M. A Density Functional Theory Investigation of Nin, Pdn, and Ptn Clusters (N=1–4) Adsorbed on Buckminsterfullerene. *ChemPhysChem* **2017,** *18*, 1376-1384.
(90) Konarev, D. V.; Khasanov, S. S.; Nakano, Y.; Otsuka, A.; Yamochi, H.; Saito, G.; Lyubovskaya, R. N. Linear Coordination Fullerene C60 Polymer [{Ni(Me3p)2}(M-H2,H2-C60)]∞ Bridged by Zerovalent Nickel Atoms. *Inorg. Chem.* **2014,** *53*, 11960-11965.
(91) Leng, F.; Gerber, I. C.; Lecante, P.; Bacsa, W.; Miller, J.; Gallagher, J. R.; Moldovan, S.; Girleanu, M.; Axet, M. R.; Serp, P. Synthesis and Structure of Ruthenium-Fullerides. *RSC Advances* **2016,** *6*, 69135-69148.
(92) de Groot, F. M. F. Site-Selective Xafs: A New Tool for Catalysis Research. *Top. Catal.* **2000,** *10*, 179-186.
(93) Goclon, J.; Winkler, K.; Margraf, J. T. Theoretical Investigation of Interactions between Palladium and Fullerene in Polymer. *RSC Advances* **2017,** *7*, 2202-2210.
(94) Yan, W.; Seifermann, S. M.; Pierrat, P.; Bräse, S. Synthesis of Highly Functionalized C60 Fullerene Derivatives and Their Applications in Material and Life Sciences. *Organic & Biomolecular Chemistry* **2015,** *13*, 25-54.
(95) Leng, F.; Gerber, I. C.; Lecante, P.; Bentaleb, A.; Muñoz, A.; Illescas, B. M.; Martín, N.; Melinte, G.; Ersen, O.; Martinez, H.et al. Hexakis [60]Fullerene Adduct-Mediated Covalent Assembly of Ruthenium Nanoparticles and Their Catalytic Properties. *Chemistry – A European Journal* **2017,** *23*, 13379-13386.
(96) Campisciano, V.; Gruttadauria, M.; Giacalone, F. Modified Nanocarbons for Catalysis. *ChemCatChem* **2018,** *11*, 90–133.
(97) Dutta, A.; Mondal, P. Density Functional Approach toward the Adsorption of Molecular Hydrogen as Well as the Formation of Metal Hydride on Bare and Activated Carbon-Supported Rhodium Clusters. *The Journal of Physical Chemistry C* **2018,** *122*, 16925-16939.
(98) Sathe, B. R. Rhodium Nanoparticle–Carbon Nanosphere Hybrid Material as an Electrochemical Hydrogen Sensor. *RSC Advances* **2013,** *3*, 5361-5365.
(99) Liu, B.; Jin, L.; Zhong, W.; Lopes, A.; Suib, S. L.; He, J. Ultrafine and Ligand-Free Precious Metal (Ru, Ag, Au, Rh and Pd) Nanoclusters Supported on Phosphorus-Doped Carbon. *Chemistry - A European Journal* **2018,** *24*, 2565–2569.
(100) Umadevi, D.; Sastry, G. N. Metal Ion Binding with Carbon Nanotubes and Graphene: Effect of Chirality and Curvature. *Chem. Phys. Lett.* **2012,** *549*, 39-43.
(101) Durgun, E.; Dag, S.; Ciraci, S.; Gülseren, O. Energetics and Electronic Structures of Individual Atoms Adsorbed on Carbon Nanotubes. *The Journal of Physical Chemistry B* **2004,** *108*, 575-582.
(102) Valencia, H.; Gil, A.; Frapper, G. Trends in the Hydrogen Activation and Storage by Adsorbed 3d Transition Metal Atoms onto Graphene and Nanotube Surfaces: A Dft Study and Molecular Orbital Analysis. *The Journal of Physical Chemistry C* **2015,** *119*, 5506-5522.
(103) Valencia, H.; Gil, A.; Frapper, G. Trends in the Adsorption of 3d Transition Metal Atoms onto Graphene and Nanotube Surfaces: A Dft Study and Molecular Orbital Analysis. *The Journal of Physical Chemistry C* **2010,** *114*, 14141-14153.
(104) Yildirim, T.; Ciraci, S. Titanium-Decorated Carbon Nanotubes as a Potential High-Capacity Hydrogen Storage Medium. *Phys. Rev. Lett.* **2005,** *94*, 175501.
(105) Durgun, E.; Ciraci, S.; Yildirim, T. Functionalization of Carbon-Based Nanostructures with Light Transition-Metal Atoms for Hydrogen Storage. *Physical Review B* **2008,** *77*, 085405.
(106) Wu, M.-C.; Li, C.-L.; Hu, C.-K.; Chang, Y.-C.; Liaw, Y.-H.; Huang, L.-W.; Chang, C.-S.; Tsong, T.-T.; Hsu, T. Curvature Effect on the Surface Diffusion of Silver Adatoms on Carbon Nanotubes: Deposition Experiments and Numerical Simulations. *Physical Review B* **2006,** *74*, 125424.
(107) Shu, D. J.; Gong, X. G. Curvature Effect on Surface Diffusion: The Nanotube. *The Journal of Chemical Physics* **2001,** *114*, 10922-10926.
(108) Teddy, J.; Falqui, A.; Corrias, A.; Carta, D.; Lecante, P.; Gerber, I.; Serp, P. Influence of Particles Alloying on the Performances of Pt–Ru/Cnt Catalysts for Selective Hydrogenation. *J. Catal.* **2011,** *278*, 59-70.

(109) Menon, M.; Andriotis, A. N.; Froudakis, G. E. Curvature Dependence of the Metal Catalyst Atom Interaction with Carbon Nanotubes Walls. *Chem. Phys. Lett.* **2000,** *320*, 425-434.
(110) Chen, G.; Kawazoe, Y. Interaction between a Single Pt Atom and a Carbon Nanotube Studied by Density Functional Theory. *Physical Review B* **2006,** *73*, 125410.
(111) Zhuang, H. L.; Zheng, G. P.; Soh, A. K. Interactions between Transition Metals and Defective Carbon Nanotubes. *Computational Materials Science* **2008,** *43*, 823-828.
(112) Chen, Y. K.; Liu, L. V.; Tian, W. Q.; Wang, Y. A. Theoretical Studies of Transition-Metal-Doped Single-Walled Carbon Nanotubes. *The Journal of Physical Chemistry C* **2011,** *115*, 9306-9311.
(113) Yu, L.; Li, W.-X.; Pan, X.; Bao, X. In- and out-Dependent Interactions of Iron with Carbon Nanotubes. *The Journal of Physical Chemistry C* **2012,** *116*, 16461-16466.
(114) Zoberbier, T.; Chamberlain, T. W.; Biskupek, J.; Kuganathan, N.; Eyhusen, S.; Bichoutskaia, E.; Kaiser, U.; Khlobystov, A. N. Interactions and Reactions of Transition Metal Clusters with the Interior of Single-Walled Carbon Nanotubes Imaged at the Atomic Scale. *J. Am. Chem. Soc.* **2012,** *134*, 3073-3079.
(115) Staykov, A.; Ooishi, Y.; Ishihara, T. Immobilizing Metal Nanoparticles on Single Wall Nanotubes. Effect of Surface Curvature. *The Journal of Physical Chemistry C* **2014,** *118*, 8907–8916.
(116) Du, G.; Zhang, J.; Chen, Q.; Kuang, Q.; Xie, Z. Morphology Led High Dispersion of Pt Icosahedral Nanocrystals on Carbon Nanotubes for Enhanced Electro-Catalytic Activity and Stability. *Chem. Commun.* **2018,** *54*, 10855–10858.
(117) Tavakkoli, M.; Holmberg, N.; Kronberg, R.; Jiang, H.; Sainio, J.; Kauppinen, E. I.; Kallio, T.; Laasonen, K. Electrochemical Activation of Single-Walled Carbon Nanotubes with Pseudo-Atomic-Scale Platinum for the Hydrogen Evolution Reaction. *ACS Catalysis* **2017,** *7*, 3121-3130.
(118) Karousis, N.; Tagmatarchis, N.; Tasis, D. Current Progress on the Chemical Modification of Carbon Nanotubes. *Chem. Rev.* **2010,** *110*, 5366-5397.
(119) Su, D. S. In *Nanomaterials in Catalysis*; John Wiley & Sons, Ltd, 2012.
(120) Kundu, S.; Wang, Y.; Xia, W.; Muhler, M. Thermal Stability and Reducibility of Oxygen-Containing Functional Groups on Multiwalled Carbon Nanotube Surfaces: A Quantitative High-Resolution Xps and Tpd/Tpr Study. *The Journal of Physical Chemistry C* **2008,** *112*, 16869-16878.
(121) Gerber, I.; Oubenali, M.; Bacsa, R.; Durand, J.; Gonçalves, A.; Pereira, M. F. R.; Jolibois, F.; Perrin, L.; Poteau, R.; Serp, P. Theoretical and Experimental Studies on the Carbon-Nanotube Surface Oxidation by Nitric Acid: Interplay between Functionalization and Vacancy Enlargement. *Chemistry - A European Journal* **2011,** *17*, 11467–11477.
(122) Datsyuk, V.; Kalyva, M.; Papagelis, K.; Parthenios, J.; Tasis, D.; Siokou, A.; Kallitsis, I.; Galiotis, C. Chemical Oxidation of Multiwalled Carbon Nanotubes. *Carbon* **2008,** *46*, 833–840.
(123) Chiang, Y.-C.; Ciou, J.-R. Effects of Surface Chemical States of Carbon Nanotubes Supported Pt Nanoparticles on Performance of Proton Exchange Membrane Fuel Cells. *Int. J. Hydrogen Energy* **2011,** *36*, 6826-6831.
(124) Qian, Z.; Ma, J.; Zhou, J.; Lin, P.; Chen, C.; Chen, J.; Feng, H. Facile Synthesis of Halogenated Multi-Walled Carbon Nanotubes and Their Unusual Photoluminescence. *J. Mater. Chem.* **2012,** *22*, 22113-22119.
(125) Bulusheva, L. G.; Okotrub, A. V.; Flahaut, E.; Asanov, I. P.; Gevko, P. N.; Koroteev, V. O.; Fedoseeva, Y. V.; Yaya, A.; Ewels, C. P. Bromination of Double-Walled Carbon Nanotubes. *Chem. Mater.* **2012,** *24*, 2708-2715.
(126) Yu, H.; Jin, Y.; Li, Z.; Peng, F.; Wang, H. Synthesis and Characterization of Sulfonated Single-Walled Carbon Nanotubes and Their Performance as Solid Acid Catalyst. *J. Solid State Chem.* **2008,** *181*, 432-438.
(127) Simmons, T. J.; Bult, J.; Hashim, D. P.; Linhardt, R. J.; Ajayan, P. M. Noncovalent Functionalization as an Alternative to Oxidative Acid Treatment of Single Wall Carbon Nanotubes with Applications for Polymer Composites. *ACS Nano* **2009,** *3*, 865-870.

(128) Labulo, A. H.; Martincigh, B. S.; Omondi, B.; Nyamori, V. O. Advances in Carbon Nanotubes as Efficacious Supports for Palladium-Catalysed Carbon–Carbon Cross-Coupling Reactions. *Journal of Materials Science* **2017,** *52*, 9225–9248.
(129) Stamatin, S. N.; Borghei, M.; Dhiman, R.; Andersen, S. M.; Ruiz, V.; Kauppinen, E.; Skou, E. M. Activity and Stability Studies of Platinized Multi-Walled Carbon Nanotubes as Fuel Cell Electrocatalysts. *Applied Catalysis B: Environmental* **2015,** *162*, 289-299.
(130) Fan, J.-J.; Fan, Y.-J.; Wang, R.-X.; Xiang, S.; Tang, H.-G.; Sun, S.-G. A Novel Strategy for the Synthesis of Sulfur-Doped Carbon Nanotubes as a Highly Efficient Pt Catalyst Support toward the Methanol Oxidation Reaction. *Journal of Materials Chemistry A* **2017,** *5*, 19467-19475.
(131) Chizari, K.; Janowska, I.; Houllé, M.; Florea, I.; Ersen, O.; Romero, T.; Bernhardt, P.; Ledoux, M. J.; Pham-Huu, C. Tuning of Nitrogen-Doped Carbon Nanotubes as Catalyst Support for Liquid-Phase Reaction. *Applied Catalysis A: General* **2010,** *380*, 72-80.
(132) Shi, W.; Wu, K.-H.; Xu, J.; Zhang, Q.; Zhang, B.; Su, D. S. Enhanced Stability of Immobilized Platinum Nanoparticles through Nitrogen Heteroatoms on Doped Carbon Supports. *Chem. Mater.* **2017,** *29*, 8670–8678.
(133) Xia, W. Interactions between Metal Species and Nitrogen-Functionalized Carbon Nanotubes. *Catalysis Science & Technology* **2016,** *6*, 630–644.
(134) Ruffino, F.; Giannazzo, F. A Review on Metal Nanoparticles Nucleation and Growth on/in Graphene. *Crystals* **2017,** *7*, 219–240.
(135) Liu, X.; Wang, C.-Z.; Hupalo, M.; Lin, H.-Q.; Ho, K.-M.; Tringides, C. M. Metals on Graphene: Interactions, Growth Morphology, and Thermal Stability. *Crystals* **2013,** *3*.
(136) Manadé, M.; Viñes, F.; Gil, A.; Illas, F. On the H 2interactions with Transition Metal Adatoms Supported on Graphene: A Systematic Density Functional Study. *PCCP* **2018,** *20*, 3819–3830.
(137) Manadé, M.; Viñes, F.; Illas, F. Transition Metal Adatoms on Graphene: A Systematic Density Functional Study. *Carbon* **2015,** *95*, 525-534.
(138) Chan, K. T.; Neaton, J. B.; Cohen, M. L. First-Principles Study of Metal Adatom Adsorption on Graphene. *Physical Review B* **2008,** *77*, 235430.
(139) Donati, F.; Dubout, Q.; Autès, G.; Patthey, F.; Calleja, F.; Gambardella, P.; Yazyev, O. V.; Brune, H. Magnetic Moment and Anisotropy of Individual Co Atoms on Graphene. *Phys. Rev. Lett.* **2013,** *111*, 236801.
(140) Rudenko, A. N.; Keil, F. J.; Katsnelson, M. I.; Lichtenstein, A. I. Adsorption of Cobalt on Graphene: Electron Correlation Effects from a Quantum Chemical Perspective. *Physical Review B* **2012,** *86*, 075422-075411.
(141) Tang, Y.; Zhang, H.; Shen, Z.; Zhao, M.; Li, Y.; Dai, X. The Electronic and Diffusion Properties of Metal Adatoms on Graphene Sheets: A First-Principles Study. *RSC Advances* **2017,** *7*, 33208-33218.
(142) Appy, D.; Lei, H.; Wang, C.-Z.; Tringides, M. C.; Liu, D.-J.; Evans, J. W.; Thiel, P. A. Transition Metals on the (0001) Surface of Graphite: Fundamental Aspects of Adsorption, Diffusion, and Morphology. *Prog. Surf. Sci.* **2014,** *89*, 219-238.
(143) Hardcastle, T. P.; Seabourne, C. R.; Zan, R.; Brydson, R. M. D.; Bangert, U.; Ramasse, Q. M.; Novoselov, K. S.; Scott, A. J. Mobile Metal Adatoms on Single Layer, Bilayer, and Trilayer Graphene: An Ab Initio Dft Study with Van Der Waals Corrections Correlated with Electron Microscopy Data. *Physical Review B* **2013,** *87*, 195430.
(144) Wang, H.; Li, K.; Cheng, Y.; Wang, Q.; Yao, Y.; Schwingenschlögl, U.; Zhang, X.; Yang, W. Interaction between Single Gold Atom and the Graphene Edge: A Study Via Aberration-Corrected Transmission Electron Microscopy. *Nanoscale* **2012,** *4*, 2920-2925.
(145) Zhao, J.; Deng, Q.; Avdoshenko, S. M.; Fu, L.; Eckert, J.; Rümmeli, M. H. Direct in Situ Observations of Single Fe Atom Catalytic Processes and Anomalous Diffusion at Graphene Edges. *Proceedings of the National Academy of Sciences* **2014,** *111*, 15641.
(146) Yamazaki, K.; Maehara, Y.; Lee, C.-C.; Yoshinobu, J.; Ozaki, T.; Gohara, K. Atomic Structure and Local Electronic States of Single Pt Atoms Dispersed on Graphene. *The Journal of Physical Chemistry C* **2018,** *122*, 27292–27300.

(147) Yang, Y.-E.; Xiao, Y.; Yan, X.-H.; Dai, C.-J. Transport Properties of Zigzag Graphene Nanoribbons Adsorbed with Single Iron Atom. *Chinese Physics B* **2015,** *24*, 117204.
(148) Terrones, H.; Lv, R.; Terrones, M.; Dresselhaus, M. S. The Role of Defects and Doping in 2d Graphene Sheets and 1d Nanoribbons. *Rep. Prog. Phys.* **2012,** *75*, 062501.
(149) Martinazzo, R.; Casolo, S.; Tantardini, G. F. GraphITA 2011, Berlin, Heidelberg, 2012; p 137-145.
(150) Skowron, S. T.; Lebedeva, I. V.; Popov, A. M.; Bichoutskaia, E. Energetics of Atomic Scale Structure Changes in Graphene. *Chem. Soc. Rev.* **2015,** *44*, 3143-3176.
(151) Hashimoto, A.; Suenaga, K.; Gloter, A.; Urita, K.; Iijima, S. Direct Evidence for Atomic Defects in Graphene Layers. *Nature* **2004,** *430*, 870.
(152) Meyer, J. C.; Geim, A. K.; Katsnelson, M. I.; Novoselov, K. S.; Booth, T. J.; Roth, S. The Structure of Suspended Graphene Sheets. *Nature* **2007,** *446*, 60.
(153) Ugeda, M. M.; Brihuega, I.; Guinea, F.; Gómez-Rodríguez, J. M. Missing Atom as a Source of Carbon Magnetism. *Phys. Rev. Lett.* **2010,** *104*, 096804.
(154) El-Barbary, A. A.; Telling, R. H.; Ewels, C. P.; Heggie, M. I.; Briddon, P. R. Structure and Energetics of the Vacancy in Graphite. *Physical Review B* **2003,** *68*, 144107.
(155) Krasheninnikov, A. V.; Lehtinen, P. O.; Foster, A. S.; Nieminen, R. M. Bending the Rules: Contrasting Vacancy Energetics and Migration in Graphite and Carbon Nanotubes. *Chem. Phys. Lett.* **2006,** *418*, 132-136.
(156) Lehtinen, P. O.; Foster, A. S.; Ma, Y.; Krasheninnikov, A. V.; Nieminen, R. M. Irradiation-Induced Magnetism in Graphite: A Density Functional Study. *Phys. Rev. Lett.* **2004,** *93*, 187202.
(157) Valencia, A. M.; Caldas, M. J. Single Vacancy Defect in Graphene: Insights into Its Magnetic Properties from Theoretical Modeling. *Physical Review B* **2017,** *96*, 125431.
(158) Berber, S.; Oshiyama, A. Reconstruction of Mono-Vacancies in Carbon Nanotubes: Atomic Relaxation Vs. Spin Polarization. *Physica B: Condensed Matter* **2006,** *376-377*, 272-275.
(159) Grayfer, E. D.; Kibis, L. S.; Stadnichenko, A. I.; Vilkov, O. Y.; Boronin, A. I.; Slavinskaya, E. M.; Stonkus, O. A.; Fedorov, V. E. Ultradisperse Pt Nanoparticles Anchored on Defect Sites in Oxygen-Free Few-Layer Graphene and Their Catalytic Properties in Co Oxidation. *Carbon* **2015,** *89*, 290–299.
(160) Lee, G.-D.; Wang, C. Z.; Yoon, E.; Hwang, N.-M.; Kim, D.-Y.; Ho, K. M. Diffusion, Coalescence, and Reconstruction of Vacancy Defects in Graphene Layers. *Phys. Rev. Lett.* **2005,** *95*, 205501.
(161) Wu, L.; Hou, T.; Li, Y.; Chan, K. S.; Lee, S.-T. First-Principles Study on Migration and Coalescence of Point Defects in Monolayer Graphene. *The Journal of Physical Chemistry C* **2013,** *117*, 17066-17072.
(162) Kim, G.; Jhi, S.-H.; Lim, S.; Park, N. Effect of Vacancy Defects in Graphene on Metal Anchoring and Hydrogen Adsorption. *Applied Physics Letters* **2009,** *94*, 173102-173104.
(163) Cretu, O.; Krasheninnikov, A. V.; Rodríguez-Manzo, J. A.; Sun, L.; Nieminen, R. M.; Banhart, F. Migration and Localization of Metal Atoms on Strained Graphene. *Phys. Rev. Lett.* **2010,** *105*, 113-115.
(164) Krasheninnikov, A. V.; Lehtinen, P. O.; Foster, A. S.; Pyykkö, P.; Nieminen, R. M. Embedding Transition-Metal Atoms in Graphene: Structure, Bonding, and Magnetism. *Phys. Rev. Lett.* **2009,** *102*, 126807.
(165) Bhattacharya, A.; Bhattacharya, S.; Majumder, C.; Das, G. P. Transition-Metal Decoration Enhanced Room-Temperature Hydrogen Storage in a Defect-Modulated Graphene Sheet. *The Journal of Physical Chemistry C* **2010,** *114*, 10297-10301.
(166) Wang, H.; Wang, Q.; Cheng, Y.; Li, K.; Yao, Y.; Zhang, Q.; Dong, C.; Wang, P.; Schwingenschlögl, U.; Yang, W.et al. Doping Monolayer Graphene with Single Atom Substitutions. *Nano Lett.* **2012,** *12*, 141-144.
(167) Pašti, I. A.; Jovanović, A.; Dobrota, A. S.; Mentus, S. V.; Johansson, B.; Skorodumova, N. V. Atomic Adsorption on Graphene with a Single Vacancy: Systematic Dft Study through the Periodic Table of Elements. *PCCP* **2018,** *20*, 858-865.

(168) Robertson, A. W.; Montanari, B.; He, K.; Kim, J.; Allen, C. S.; Wu, Y. A.; Olivier, J.; Neethling, J.; Harrison, N.; Kirkland, A. I.et al. Dynamics of Single Fe Atoms in Graphene Vacancies. *Nano Letters* **2013,** *13*, 1468-1475.
(169) Krasheninnikov, A. V.; Nieminen, R. M. Attractive Interaction between Transition-Metal Atom Impurities and Vacancies in Graphene: A First-Principles Study. *Theor. Chem. Acc.* **2011,** *129*, 625-630.
(170) Zhou, H.; Chen, X.; Wang, L.; Zhong, X.; Zhuang, G.; Li, X.; Mei, D.; Wang, J. Effect of Graphene with Nanopores on Metal Clusters. *PCCP* **2015,** *17*, 24420-24426.
(171) Holme, T.; Zhou, Y.; Pasquarelli, R.; O'Hayre, R. First Principles Study of Doped Carbon Supports for Enhanced Platinum Catalysts. *PCCP* **2010,** *12*, 9461-9468.
(172) Stone, A. J.; Wales, D. J. Theoretical Studies of Icosahedral C60 and Some Related Species. *Chem. Phys. Lett.* **1986,** *128*, 501-503.
(173) Zhou, L. G.; Shi, S.-Q. Formation Energy of Stone–Wales Defects in Carbon Nanotubes. *Appl. Phys. Lett.* **2003,** *83*, 1222-1224.
(174) Li, L.; Reich, S.; Robertson, J. Defect Energies of Graphite: Density-Functional Calculations. *Physical Review B* **2005,** *72*, 184109.
(175) Ertekin, E.; Chrzan, D. C.; Daw, M. S. Topological Description of the Stone-Wales Defect Formation Energy in Carbon Nanotubes and Graphene. *Physical Review B* **2009,** *79*, 155421.
(176) Ma, J.; Alfè, D.; Michaelides, A.; Wang, E. Stone-Wales Defects in Graphene and Other Planar $S{P}^{2}$-Bonded Materials. *Physical Review B* **2009,** *80*, 033407.
(177) Meyer, J. C.; Kisielowski, C.; Erni, R.; Rossell, M. D.; Crommie, M. F.; Zettl, A. Direct Imaging of Lattice Atoms and Topological Defects in Graphene Membranes. *Nano Lett.* **2008,** *8*, 3582-3586.
(178) Kotakoski, J.; Krasheninnikov, A. V.; Kaiser, U.; Meyer, J. C. From Point Defects in Graphene to Two-Dimensional Amorphous Carbon. *Phys. Rev. Lett.* **2011,** *106*, 105505-105504.
(179) Kotakoski, J.; Meyer, J. C.; Kurasch, S.; Santos-Cottin, D.; Kaiser, U.; Krasheninnikov, A. V. Stone-Wales-Type Transformations in Carbon Nanostructures Driven by Electron Irradiation. *Physical Review B* **2011,** *83*, 245420.
(180) Harman, A. J.; Raelynn, L. Density Functional Theory Study of Metal Adatoms at or near a Stone-Wales Defect in Graphene. *Procedia Engineering* **2014,** *93*, 2-7.
(181) Yang, S. H.; Shin, W. H.; Kang, J. K. Ni Adsorption on Stone-Wales Defect Sites in Single-Wall Carbon Nanotubes. *The Journal of Chemical Physics* **2006,** *125*, 084705-084706.
(182) Yang, S. H.; Shin, W. H.; Lee, J. W.; Kim, S. Y.; Woo, S. I.; Kang, J. K. Interaction of a Transition Metal Atom with Intrinsic Defects in Single-Walled Carbon Nanotubes. *The Journal of Physical Chemistry B* **2006,** *110*, 13941-13946.
(183) Baldez, R. N. L.; Piquini, P.; Schmidt, A. A.; Kuroda, M. A. Tunable Interaction between Metal Clusters and Graphene. *PCCP* **2017,** *19*, 22153-22160.
(184) Liu, H.; Liu, Y.; Zhu, D. Chemical Doping of Graphene. *J. Mater. Chem.* **2011,** *21*, 3335-3345.
(185) Panchakarla, L. S.; Subrahmanyam, K. S.; Saha, S. K.; Govindaraj, A.; Krishnamurthy, H. R.; Waghmare, U. V.; Rao, C. N. R. Synthesis, Structure, and Properties of Boron- and Nitrogen-Doped Graphene. *Adv. Mater.* **2009,** *6*, NA-NA.
(186) Paraknowitsch, J. P.; Thomas, A. Doping Carbons Beyond Nitrogen: An Overview of Advanced Heteroatom Doped Carbons with Boron, Sulphur and Phosphorus for Energy Applications. *Energy & Environmental Science* **2013,** *6*, 2839-2855.
(187) Faccio, R.; Fernández-Werner, L.; Pardo, H.; Goyenola, C.; Ventura, O. N.; Mombrú, Á. W. Electronic and Structural Distortions in Graphene Induced by Carbon Vacancies and Boron Doping. *The Journal of Physical Chemistry C* **2010,** *114*, 18961-18971.
(188) Wu, H.-Y.; Fan, X.; Kuo, J.-L.; Deng, W.-Q. Dft Study of Hydrogen Storage by Spillover on Graphene with Boron Substitution. *The Journal of Physical Chemistry C* **2011,** *115*, 9241-9249.
(189) Batzill, M. The Surface Science of Graphene: Metal Interfaces, Cvd Synthesis, Nanoribbons, Chemical Modifications, and Defects. *Surf. Sci. Rep.* **2012,** *67*, 83-115.

(190) Deng, Y.; Xie, Y.; Zou, K.; Ji, X. Review on Recent Advances in Nitrogen-Doped Carbons: Preparations and Applications in Supercapacitors. *Journal of Materials Chemistry A* **2016,** *4*, 1144-1173.
(191) Shao, M.; Chang, Q.; Dodelet, J.-P.; Chenitz, R. Recent Advances in Electrocatalysts for Oxygen Reduction Reaction. *Chem. Rev.* **2016,** *116*, 3594-3657.
(192) Shao, Y.; Sui, J.; Yin, G.; Gao, Y. Nitrogen-Doped Carbon Nanostructures and Their Composites as Catalytic Materials for Proton Exchange Membrane Fuel Cell. *Applied Catalysis B: Environmental* **2008,** *79*, 89-99.
(193) Wei, D.; Liu, Y.; Wang, Y.; Zhang, H.; Huang, L.; Yu, G. Synthesis of N-Doped Graphene by Chemical Vapor Deposition and Its Electrical Properties. *Nano Lett.* **2009,** *9*, 1752-1758.
(194) Lin, Y.-C.; Teng, P.-Y.; Yeh, C.-H.; Koshino, M.; Chiu, P.-W.; Suenaga, K. Structural and Chemical Dynamics of Pyridinic-Nitrogen Defects in Graphene. *Nano Lett.* **2015,** *15*, 7408-7413.
(195) Artyushkova, K.; Kiefer, B.; Halevi, B.; Knop-Gericke, A.; Schlogl, R.; Atanassov, P. Density Functional Theory Calculations of Xps Binding Energy Shift for Nitrogen-Containing Graphene-Like Structures. *Chem. Commun.* **2013,** *49*, 2539-2533.
(196) Feng, H.; Ma, J.; Hu, Z. Nitrogen-Doped Carbon Nanotubes Functionalized by Transition Metal Atoms: A Density Functional Study. *J. Mater. Chem.* **2010,** *20*, 1702-1707.
(197) Yang, M.; Wang, L.; Li, M.; Hou, T.; Li, Y. Structural Stability and O 2dissociation on Nitrogen-Doped Graphene with Transition Metal Atoms Embedded: A First-Principles Study. *AIP Advances* **2015,** *5*, 067136-067110.
(198) Tison, Y.; Lagoute, J.; Repain, V.; Chacon, C.; Girard, Y.; Rousset, S.; Joucken, F.; Sharma, D.; Henrard, L.; Amara, H.et al. Electronic Interaction between Nitrogen Atoms in Doped Graphene. *ACS Nano* **2015,** *9*, 670-678.
(199) Zhao, L.; He, R.; Rim, K. T.; Schiros, T.; Kim, K. S.; Zhou, H.; Gutiérrez, C.; Chockalingam, S. P.; Arguello, C. J.; Pálová, L.et al. Visualizing Individual Nitrogen Dopants in Monolayer Graphene. *Science* **2011,** *333*, 999.
(200) Cui, X.; Xiao, J.; Wu, Y.; Du, P.; Si, R.; Yang, H.; Tian, H.; Li, J.; Zhang, W.-H.; Deng, D.et al. A Graphene Composite Material with Single Cobalt Active Sites: A Highly Efficient Counter Electrode for Dye-Sensitized Solar Cells. *Angewandte Chemie* **2016,** *128*, 6820-6824.
(201) Lu, Z.; Xu, G.; He, C.; Wang, T.; Yang, L.; Yang, Z.; Ma, D. Novel Catalytic Activity for Oxygen Reduction Reaction on Mnn4 Embedded Graphene: A Dispersion-Corrected Density Functional Theory Study. *Carbon* **2015,** *84*, 500-508.
(202) Srinivasu, K.; Modak, B.; Ghosh, S. K. Porous Graphitic Carbon Nitride: A Possible Metal-Free Photocatalyst for Water Splitting. *The Journal of Physical Chemistry C* **2014,** *118*, 26479-26484.
(203) Li, J.; Cao, C.; Hao, J.; Qiu, H.; Xu, Y.; Zhu, H. Self-Assembled One-Dimensional Carbon Nitride Architectures. *Diamond Relat. Mater.* **2006,** *15*, 1593-1600.
(204) Cao, C.; Huang, F.; Cao, C.; Li, J.; Zhu, H. Synthesis of Carbon Nitride Nanotubes Via a Catalytic-Assembly Solvothermal Route. *Chemistry of Materials* **2004,** *16*, 5213-5215.
(205) Chen, Z.; Mitchell, S.; Vorobyeva, E.; Leary, R. K.; Hauert, R.; Furnival, T.; Ramasse, Q. M.; Thomas, J. M.; Midgley, P. A.; Dontsova, D.et al. Stabilization of Single Metal Atoms on Graphitic Carbon Nitride. *Adv. Funct. Mater.* **2017,** *27*, 1605785.
(206) Yang, D.-S.; Chaudhari, S.; Rajesh, K. P.; Yu, J.-S. Preparation of Nitrogen-Doped Porous Carbon Nanofibers and the Effect of Porosity, Electrical Conductivity, and Nitrogen Content on Their Oxygen Reduction Performance. *ChemCatChem* **2014,** *11*, n/a–n/a.
(207) Ghosh, D.; Periyasamy, G.; Pandey, B.; Pati, S. K. Computational Studies on Magnetism and the Optical Properties of Transition Metal Embedded Graphitic Carbon Nitride Sheets. *Journal of Materials Chemistry C* **2014,** *2*, 7943-7951.
(208) Du, J.; Xia, C.; Xiong, W.; Zhao, X.; Wang, T.; Jia, Y. Tuning the Electronic Structures and Magnetism of Two-Dimensional Porous C2n Via Transition Metal Embedding. *PCCP* **2016,** *18*, 22678-22686.
(209) Zhang, Y.; Wang, Z.; Cao, J. Prediction of Magnetic Anisotropy of 5d Transition Metal-Doped G-C3n4. *Journal of Materials Chemistry C* **2014,** *2*, 8817-8821.

(210) Zheng, Y.; Jiao, Y.; Zhu, Y.; Cai, Q.; Vasileff, A.; Li, L. H.; Han, Y.; Chen, Y.; Qiao, S.-Z. Molecule-Level G-C3n4 Coordinated Transition Metals as a New Class of Electrocatalysts for Oxygen Electrode Reactions. *J. Am. Chem. Soc.* **2017,** *139*, 3336-3339.
(211) Wang, X.; Li, X.; Zhang, L.; Yoon, Y.; Weber, P. K.; Wang, H.; Guo, J.; Dai, H. N-Doping of Graphene through Electrothermal Reactions with Ammonia. *Science* **2009,** *324*, 768.
(212) Li, X.-H.; Antonietti, M. Metal Nanoparticles at Mesoporous N-Doped Carbons and Carbon Nitrides: Functional Mott–Schottky Heterojunctions for Catalysis. *Chem. Soc. Rev.* **2013,** *42*, 6593-6604.
(213) Coraux, J.; N'Diaye, A. T.; Busse, C.; Michely, T. Structural Coherency of Graphene on Ir(111). *Nano Lett.* **2008,** *8*, 565-570.
(214) Červenka, J.; Katsnelson, M. I.; Flipse, C. F. J. Room-Temperature Ferromagnetism in Graphite Driven by Two-Dimensional Networks of Point defects. *Nature Physics* **2009,** *5*, 840.
(215) Lahiri, J.; Lin, Y.; Bozkurt, P.; Oleynik, I. I.; Batzill, M. An Extended Defect in Graphene as a Metallic Wire. *Nature Nanotechnology* **2010,** *5*, 326.
(216) Robertson, A. W.; Bachmatiuk, A.; Wu, Y. A.; Schäffel, F.; Rellinghaus, B.; Büchner, B.; Rümmeli, M. H.; Warner, J. H. Atomic Structure of Interconnected Few-Layer Graphene Domains. *ACS Nano* **2011,** *5*, 6610-6618.
(217) Liu, Y.; Yakobson, B. I. Cones, Pringles, and Grain Boundary Landscapes in Graphene Topology. *Nano Lett.* **2010,** *10*, 2178-2183.
(218) Huang, P. Y.; Ruiz-Vargas, C. S.; van der Zande, A. M.; Whitney, W. S.; Levendorf, M. P.; Kevek, J. W.; Garg, S.; Alden, J. S.; Hustedt, C. J.; Zhu, Y.et al. Grains and Grain Boundaries in Single-Layer Graphene Atomic Patchwork Quilts. *Nature* **2011,** *469*, 389.
(219) Červenka, J.; Flipse, C. F. J. Structural and Electronic Properties of Grain Boundaries in Graphite: Planes of Periodically Distributed Point Defects. *Physical Review B* **2009,** *79*, 195429.
(220) Yazyev, O. V.; Louie, S. G. Electronic Transport in Polycrystalline Graphene. *Nature Materials* **2010,** *9*, 806.
(221) Kou, L.; Tang, C.; Guo, W.; Chen, C. Tunable Magnetism in Strained Graphene with Topological Line Defect. *ACS Nano* **2011,** *5*, 1012-1017.
(222) Malola, S.; Häkkinen, H.; Koskinen, P. Structural, Chemical, and Dynamical Trends in Graphene Grain Boundaries. *Physical Review B* **2010,** *81*, 165447.
(223) Kim, K.; Lee, H.-B.-R.; Johnson, R. W.; Tanskanen, J. T.; Liu, N.; Kim, M.-G.; Pang, C.; Ahn, C.; Bent, S. F.; Bao, Z. Selective Metal Deposition at Graphene Line Defects by Atomic Layer Deposition. *Nature Communications* **2014,** *5*, 4781.
(224) Bissett, M. A.; Konabe, S.; Okada, S.; Tsuji, M.; Ago, H. Enhanced Chemical Reactivity of Graphene Induced by Mechanical Strain. *ACS Nano* **2013,** *7*, 10335-10343.
(225) de Souza, F. A. L.; Amorim, R. G.; Prasongkit, J.; Scopel, W. L.; Scheicher, R. H.; Rocha, A. R. Topological Line Defects in Graphene for Applications in Gas Sensing. *Carbon* **2018,** *129*, 803-808.
(226) Zhang, L.; Xu, Q.; Niu, J.; Xia, Z. Role of Lattice Defects in Catalytic Activities of Graphene Clusters for Fuel Cells. *PCCP* **2015,** *17*, 16733-16743.
(227) Helgee, E. E.; Isacsson, A. Adsorption of Metal Atoms at a Buckled Graphene Grain Boundary Using Model Potentials. *AIP Advances* **2016,** *6*, 015210.
(228) Zhou, L.-J.; Hou, Z. F.; Wu, L.-M.; Zhang, Y.-F. First-Principles Studies of Lithium Adsorption and Diffusion on Graphene with Grain Boundaries. *The Journal of Physical Chemistry C* **2014,** *118*, 28055-28062.
(229) de Lima, F. D. C.; Miwa, R. H. Nanolines of Transition Metals Ruled by Grain Boundaries in Graphene: An Ab Initio Study. *Mater. Chem. Phys.* **2017,** *194*, 118-127.
(230) Chen, D.; Feng, H.; Li, J. Graphene Oxide: Preparation, Functionalization, and Electrochemical Applications. *Chem. Rev.* **2012,** *112*, 6027-6053.
(231) Singh, R. K.; Kumar, R.; Singh, D. P. Graphene Oxide: Strategies for Synthesis, Reduction and Frontier Applications. *RSC Advances* **2016,** *6*, 64993-65011.

(232) Eigler, S.; Hirsch, A. Chemistry with Graphene and Graphene Oxide—Challenges for Synthetic Chemists. *Angew. Chem. Int. Ed.* **2014,** *53*, 7720-7738.
(233) Navalon, S.; Dhakshinamoorthy, A.; Alvaro, M.; Garcia, H. Metal Nanoparticles Supported on Two-Dimensional Graphenes as Heterogeneous Catalysts. *Coord. Chem. Rev.* **2016,** *312*, 99–148.
(234) Wang, C.; Astruc, D. Recent Developments of Metallic Nanoparticle-Graphene Nanocatalysts. *Prog. Mater Sci.* **2018,** *94*, 306–383.
(235) Xie, G.; Zhang, K.; Guo, B.; Liu, Q.; Fang, L.; Gong, J. R. Graphene-Based Materials for Hydrogen Generation from Light-Driven Water Splitting. *Adv. Mater.* **2013,** *25*, 3820–3839.
(236) Dongxing, Y.; Aruna, V.; Gülay, B.; Sungjin, P.; Meryl, S.; Richard, D. P.; Sasha, S.; Inhwa, J.; Daniel, A. F.; Carl, A. V.et al. Chemical Analysis of Graphene Oxide Films after Heat and Chemical Treatments by X-Ray Photoelectron and Micro-Raman Spectroscopy. *Carbon* **2009,** *47*, 145-152.
(237) Krishnamoorthy, K.; Veerapandian, M.; Yun, K.; Kim, S. J. The Chemical and Structural Analysis of Graphene Oxide with Different Degrees of Oxidation. *Carbon* **2013,** *53*, 38-49.
(238) Zhou, S.; Bongiorno, A. Density Functional Theory Modeling of Multilayer "Epitaxial" Graphene Oxide. *Accounts of Chemical Research* **2014,** *47*, 3331-3339.
(239) Saxena, S.; Tyson, T. A.; Negusse, E. Investigation of the Local Structure of Graphene Oxide. *The Journal of Physical Chemistry Letters* **2010,** *1*, 3433-3437.
(240) Boukhvalov, D. W.; Dreyer, D. R.; Bielawski, C. W.; Son, Y.-W. A Computational Investigation of the Catalytic Properties of Graphene Oxide: Exploring Mechanisms by Using Dft Methods. *ChemCatChem* **2012,** *4*, 1844-1849.
(241) Lahaye, R. J. W. E.; Jeong, H. K.; Park, C. Y.; Lee, Y. H. Density Functional Theory Study of Graphite Oxide for Different Oxidation Levels. *Physical Review B* **2009,** *79*, 125435-125438.
(242) Sun, Y.; Yang, S.; Chen, Y.; Ding, C.; Cheng, W.; Wang, X. Adsorption and Desorption of U(Vi) on Functionalized Graphene Oxides: A Combined Experimental and Theoretical Study. *Environmental Science & Technology* **2015,** *49*, 4255-4262.
(243) Dimiev, A. M.; Alemany, L. B.; Tour, J. M. Graphene Oxide. Origin of Acidity, Its Instability in Water, and a New Dynamic Structural Model. *ACS Nano* **2012,** *7*, 576-588.
(244) Wang, L.; Lee, K.; Sun, Y.-Y.; Lucking, M.; Chen, Z.; Zhao, J. J.; Zhang, S. B. Graphene Oxide as an Ideal Substrate for Hydrogen Storage. *ACS Nano* **2009,** *3*, 2995-3000.
(245) Yang, M.; Zhou, M.; Zhang, A.; Zhang, C. Graphene Oxide: An Ideal Support for Gold Nanocatalysts. *The Journal of Physical Chemistry C* **2012,** *116*, 22336-22340.
(246) Pei, S.; Cheng, H.-M. The Reduction of Graphene Oxide. *Carbon* **2012,** *50*, 3210-3228.
(247) Tung, V. C.; Allen, M. J.; Yang, Y.; Kaner, R. B. High-Throughput Solution Processing of Large-Scale Graphene. *Nature Nanotechnology* **2008,** *4*, 25.
(248) Li, F.; Zhao, J.; Chen, Z. Fe-Anchored Graphene Oxide: A Low-Cost and Easily Accessible Catalyst for Low-Temperature Co Oxidation. *The Journal of Physical Chemistry C* **2012,** *116*, 2507-2514.
(249) Esrafili, M. D.; Sharifi, F.; Nematollahi, P. Al- or Si-Decorated Graphene Oxide: A Favorable Metal-Free Catalyst for the N2o Reduction. *Applied Surface Science* **2016,** *387*, 454-460.
(250) Pašti, I. A.; Skorodumova, N. V. Oxidized Graphene as an Electrode Material for Rechargeable Metal-Ion Batteries – a Dft Point of View. *Electrochimica Acta* **2015,** *176*, 1092-1099.
(251) Groves, M. N.; Malardier-Jugroot, C.; Jugroot, M. Improving Platinum Catalyst Durability with a Doped Graphene Support. *The Journal of Physical Chemistry C* **2012,** *116*, 10548–10556.
(252) Wu, S.-Y.; Ho, J.-J. Adsorption of a Pt13 Cluster on Graphene Oxides at Varied Ratios of Oxygen to Carbon and Its Catalytic Reactions for Co Removal Investigated with Quantum-Chemical Calculations. *The Journal of Physical Chemistry C* **2014,** *118*, 26764-26771.
(253) Dobrota, A. S.; Pašti, I. A.; Mentus, S. V.; Skorodumova, N. V. A General View on the Reactivity of the Oxygen-Functionalized Graphene Basal Plane. *PCCP* **2016,** *18*, 6580–6586.
(254) Zhou, C.; Szpunar, J. A. Hydrogen Storage Performance in Pd/Graphene Nanocomposites. *ACS Applied Materials & Interfaces* **2016,** *8*, 25933–25940.

(255) Zhao, G.; Li, X.; Huang, M.; Zhen, Z.; Zhong, Y.; Chen, Q.; Zhao, X.; He, Y.; Hu, R.; Yang, T.et al. The Physics and Chemistry of Graphene-on-Surfaces. *Chem. Soc. Rev.* **2017,** *46*, 4417–4449.
(256) Georgakilas, V.; Otyepka, M.; Bourlinos, A. B.; Chandra, V.; Kim, N.; Kemp, K. C.; Hobza, P.; Zboril, R.; Kim, K. S. Functionalization of Graphene: Covalent and Non-Covalent Approaches, Derivatives and Applications. *Chem. Rev.* **2012,** *112*, 6156-6214.
(257) Bottari, G.; Herranz, M. Á.; Wibmer, L.; Volland, M.; Rodríguez-Pérez, L.; Guldi, D. M.; Hirsch, A.; Martín, N.; D'Souza, F.; Torres, T. Chemical Functionalization and Characterization of Graphene-Based Materials. *Chem. Soc. Rev.* **2017,** *46*, 4464-4500.
(258) Tang, Q.; Zhou, Z.; Chen, Z. Graphene-Related Nanomaterials: Tuning Properties by Functionalization. *Nanoscale* **2013,** *5*, 4541–4544.
(259) Pykal, M.; Jurečka, P.; Karlický, F.; Otyepka, M. Modelling of Graphene Functionalization. *PCCP* **2016,** *18*, 6351-6372.
(260) Liu, M.; Zhang, R.; Chen, W. Graphene-Supported Nanoelectrocatalysts for Fuel Cells: Synthesis, Properties, and Applications. *Chem. Rev.* **2014,** *114*, 5117–5160.
(261) Stambula, S.; Gauquelin, N.; Bugnet, M.; Gorantla, S.; Turner, S.; Sun, S.; Liu, J.; Zhang, G.; Sun, X.; Botton, G. A. Chemical Structure of Nitrogen-Doped Graphene with Single Platinum Atoms and Atomic Clusters as a Platform for the Pemfc Electrode. *The Journal of Physical Chemistry C* **2014,** *118*, 3890–3900.
(262) Gu, X.; Qi, W.; Xu, X.; Sun, Z.; Zhang, L.; Liu, W.; Pan, X.; Su, D. Covalently Functionalized Carbon Nanotube Supported Pd Nanoparticles for Catalytic Reduction of 4-Nitrophenol. *Nanoscale* **2014,** *6*, 6609-6616.
(263) Fan, X.; Zhang, G.; Zhang, F. Multiple Roles of Graphene in Heterogeneous Catalysis. *Chem. Soc. Rev.* **2015**, 1–13.
(264) Perivoliotis, D. K.; Tagmatarchis, N. Recent Advancements in Metal-Based Hybrid Electrocatalysts Supported on Graphene and Related 2d Materials for the Oxygen Reduction Reaction. *Carbon* **2017,** *118*, 493–510.
(265) Xin, L.; Yang, F.; Rasouli, S.; Qiu, Y.; Li, Z.-F.; Uzunoglu, A.; Sun, C.-J.; Liu, Y.; Ferreira, P.; Li, W.et al. Understanding Pt Nanoparticle Anchoring on Graphene Supports through Surface Functionalization. *Acs Catalysis* **2016,** *6*, 2642-2653.
(266) Zhang, L.; Niu, J.; Dai, L.; Xia, Z. Effect of Microstructure of Nitrogen-Doped Graphene on Oxygen Reduction Activity in Fuel Cells. *Langmuir* **2012,** *28*, 7542-7550.
(267) Chai, G.-L.; Hou, Z.; Shu, D.-J.; Ikeda, T.; Terakura, K. Active Sites and Mechanisms for Oxygen Reduction Reaction on Nitrogen-Doped Carbon Alloy Catalysts: Stone–Wales Defect and Curvature Effect. *J. Am. Chem. Soc.* **2014,** *136*, 13629-13640.
(268) Ni, S.; Li, Z.; Yang, J. Oxygen Molecule Dissociation on Carbon Nanostructures with Different Types of Nitrogen Doping. *Nanoscale* **2012,** *4*, 1184-1189.
(269) Yan, J.-M.; Li, S.-J.; Yi, S.-S.; Wulan, B.-R.; Zheng, W.-T.; Jiang, Q. Anchoring and Upgrading Ultrafine Nipd on Room-Temperature-Synthesized Bifunctional Nh 2-N-Rgo toward Low-Cost and Highly Efficient Catalysts for Selective Formic Acid Dehydrogenation. *Adv. Mater.* **2018,** *30*, 1703038–1703038.
(270) Ma, J.; Habrioux, A.; Luo, Y.; Ramos-Sanchez, G.; Calvillo, L.; Granozzi, G.; Balbuena, P. B.; Alonso-Vante, N. Electronic Interaction between Platinum Nanoparticles and Nitrogen-Doped Reduced Graphene Oxide: Effect on the Oxygen Reduction Reaction. *Journal of Materials Chemistry A* **2015,** *3*, 11891–11904.
(271) Zhang, L.; Niu, J.; Li, M.; Xia, Z. Catalytic Mechanisms of Sulfur-Doped Graphene as Efficient Oxygen Reduction Reaction Catalysts for Fuel Cells. *The Journal of Physical Chemistry C* **2014,** *118*, 3545-3553.
(272) Berger, D.; Ratsch, C. Line Defects in Graphene: How Doping Affects the Electronic and Mechanical Properties. *Physical Review B* **2016,** *93*, 235441.
(273) Zhao, L.; Wang, Z.-B.; Li, J.-L.; Zhang, J.-J.; Sui, X.-L.; Zhang, L.-M. A Newly-Designed Sandwich-Structured Graphene–Pt–Graphene Catalyst with Improved Electrocatalytic Performance for

Fuel Cells. *Journal of Materials Chemistry A: Materials for energy and sustainability* **2015,** *3*, 5313–5320.

(274) Melke, J.; Peter, B.; Habereder, A.; Ziegler, J.; Fasel, C.; Nefedov, A.; Sezen, H.; Wöll, C.; Ehrenberg, H.; Roth, C. Metal–Support Interactions of Platinum Nanoparticles Decorated N-Doped Carbon Nanofibers for the Oxygen Reduction Reaction. *ACS Applied Materials & Interfaces* **2016,** *8*, 82–90.

(275) Wang, D.; Villa, A.; Su, D.; Prati, L.; Schloegl, R. Carbon-Supported Gold Nanocatalysts: Shape Effect in the Selective Glycerol Oxidation. *Chemcatchem* **2013,** *5*, 2717-2723.

(276) Wang, H.; Ming, M.; Hu, M.; Xu, C.; Wang, Y.; Zhang, Y.; Gao, D.; Bi, J.; Fan, G.; Hu, J.-S. Size and Electronic Modulation of Iridium Nanoparticles on Nitrogen-Functionalized Carbon toward Advanced Electrocatalysts for Alkaline Water Splitting. *ACS Applied Materials & Interfaces* **2018,** *10*, 22340–22347.

(277) La Torre, A.; Giménez-López, M. d. C.; Fay, M. W.; Rance, G. A.; Solomonsz, W. A.; Chamberlain, T. W.; Brown, P. D.; Khlobystov, A. N. Assembly, Growth, and Catalytic Activity of Gold Nanoparticles in Hollow Carbon Nanofibers. *ACS Nano* **2012,** *6*, 2000-2007.

(278) La Torre, A.; Fay, M. W.; Rance, G. A.; del Carmen Gimenez-Lopez, M.; Solomonsz, W. A.; Brown, P. D.; Khlobystov, A. N. Interactions of Gold Nanoparticles with the Interior of Hollow Graphitized Carbon Nanofibers. *Small* **2012,** *8*, 1222-1228.

(279) Cornelio, B.; Saunders, A. R.; Solomonsz, W. A.; Laronze-Cochard, M.; Fontana, A.; Sapi, J.; Khlobystov, A. N.; Rance, G. A. Palladium Nanoparticles in Catalytic Carbon Nanoreactors: The Effect of Confinement on Suzuki–Miyaura Reactions. *Journal of Materials Chemistry A* **2015,** *3*, 3918–3927.

(280) Vijwani, H.; Mukhopadhyay, S. M. Palladium Nanoparticles on Hierarchical Carbon Surfaces: A New Architecture for Robust Nano-Catalysts. *Appl. Surf. Sci.* **2012,** *263*, 712-721.

(281) Lv, R.; Cui, T.; Jun, M.-S.; Zhang, Q.; Cao, A.; Su, D. S.; Zhang, Z.; Yoon, S.-H.; Miyawaki, J.; Mochida, I.et al. Open-Ended, N-Doped Carbon Nanotube-Graphene Hybrid Nanostructures as High-Performance Catalyst Support. *Advanced Functional Materials* **2011,** *21*, 999-1006.

(282) Fortunato, G. V.; Pizzutilo, E.; Mingers, A. M.; Kasian, O.; Cherevko, S.; Cardoso, E. S. F.; Mayrhofer, K. J. J.; Maia, G.; Ledendecker, M. Impact of Palladium Loading and Interparticle Distance on the Selectivity for the Oxygen Reduction Reaction toward Hydrogen Peroxide. *The Journal of Physical Chemistry C* **2018,** *122*, 15878–15885.

(283) Albers, P.; Auer, E.; Ruth, K.; Parker, S. F. Inelastic Neutron Scattering Investigation of the Nature of Surface Sites Occupied by Hydrogen on Highly Dispersed Platinum on Commercial Carbon Black Supports. *J. Catal.* **2000,** *196*, 174-179.

(284) O'Malley, A. J.; Parker, S. F.; Catlow, C. R. A. Neutron Spectroscopy as a Tool in Catalytic Science. *Chem. Commun.* **2017,** *53*, 12164-12176.

(285) Jones, D. R.; Iqbal, S.; Kondrat, S. A.; Lari, G. M.; Miedziak, P. J.; Morgan, D. J.; Parker, S. F.; Hutchings, G. J. An Investigation of the Effect of Carbon Support on Ruthenium/Carbon Catalysts for Lactic Acid and Butanone Hydrogenation. *PCCP* **2016,** *18*, 17259-17264.

(286) Xie, J.; Yin, K.; Serov, A.; Artyushkova, K.; Pham, H. N.; Sang, X.; Unocic, R. R.; Atanassov, P.; Datye, A. K.; Davis, R. J. Selective Aerobic Oxidation of Alcohols over Atomically-Dispersed Non-Precious Metal Catalysts. *ChemSusChem* **2016,** *10*, 359-362.

(287) Xie, J.; Kammert, J. D.; Kaylor, N.; Zheng, J. W.; Choi, E.; Pham, H. N.; Sang, X.; Stavitski, E.; Attenkofer, K.; Unocic, R. R.et al. Atomically Dispersed Co and Cu on N-Doped Carbon for Reactions Involving C–H Activation. *ACS Catalysis* **2018,** *8*, 3875–3884.

(288) Sahoo, B.; Kreyenschulte, C.; Agostini, G.; Lund, H.; Bachmann, S.; Scalone, M.; Junge, K.; Beller, M. A Robust Iron Catalyst for the Selective Hydrogenation of Substituted (Iso)Quinolones. *Chemical Science* **2018,** *9*, 8134–8141.

(289) Perazzolo, V.; Brandiele, R.; Durante, C.; Zerbetto, M.; Causin, V.; Rizzi, G. A.; Cerri, I.; Granozzi, G.; Gennaro, A. Density Functional Theory (Dft) and Experimental Evidences of Metal–Support Interaction in Platinum Nanoparticles Supported on Nitrogen- and Sulfur-Doped Mesoporous Carbons: Synthesis, Activity, and Stability. *ACS Catalysis* **2018,** *8*, 1122-1137.

(290) Zhu, C.; Fu, S.; Shi, Q.; Du, D.; Lin, Y. Single-Atom Electrocatalysts. *Angew. Chem. Int. Ed.* **2017,** *56*, 13944–13960.
(291) Kim, J.; Kim, H.-E.; Lee, H. Single-Atom Catalysts of Precious Metals for Electrochemical Reactions. *Chemsuschem* **2018,** *11*, 104-113.
(292) Rivera-Cárcamo, C.; Serp, P. Single Atom Catalysts on Carbon-Based Materials. *ChemCatChem* **2018,** *10*, 5058-5091.
(293) Santos, E. J. G.; Ayuela, A.; Sánchez-Portal, D. First-Principles Study of Substitutional Metal Impurities in Graphene: Structural, Electronic and Magnetic Properties. *New Journal of Physics* **2010,** *12*, 053012.
(294) Kattel, S.; Atanassov, P.; Kiefer, B. Stability, Electronic and Magnetic Properties of in-Plane Defects in Graphene: A First-Principles Study. *The Journal of Physical Chemistry C* **2012,** *116*, 8161-8166.
(295) Calle-Vallejo, F.; Martínez, J. I.; Rossmeisl, J. Density Functional Studies of Functionalized Graphitic Materials with Late Transition Metals for Oxygen Reduction Reactions. *PCCP* **2011,** *13*, 15639-15635.
(296) He, H.; Jagvaral, Y. Electrochemical Reduction of Co 2on Graphene Supported Transition Metals – Towards Single Atom Catalysts. *PCCP* **2017,** *19*, 11436–11446.
(297) Hammer, B.; Nørskov, J. K. Electronic Factors Determining the Reactivity of Metal Surfaces. *Surf. Sci.* **1995,** *343*, 211-220.
(298) Hammer, B.; Nørskov, J. K. In *Advances in Catalysis*; Academic Press, 2000; Vol. 45.
(299) Gerber, I. C.; Poteau, R. In *Nanomaterials in Catalysis*; Wiley-VCH Verlag GmbH & Co. KGaA John Wiley & Sons, Ltd, 2012, DOI:papers3://publication/doi/10.1002/9783527656875.ch12 papers3://publication/doi/10.1002/9783527656875.ch12.
(300) Liu, X.; Sui, Y.; Duan, T.; Meng, C.; Han, Y. Co Oxidation Catalyzed by Pt-Embedded Graphene: A First-Principles Investigation. *PCCP* **2014,** *16*, 23584–23593.
(301) Wang, C. S.; Wang, H.; Wu, R.; Ragan, R. Evaluating the Stability of Single-Atom Catalysts with High Chemical Activity. *The Journal of Physical Chemistry C* **2018,** *122*, 21919-21926.
(302) Lou, Y.; Wu, H.; Liu, J. Nanocarbon-Edge-Anchored High-Density Pt Atoms for 3-Nitrostyrene Hydrogenation: Strong Metal-Carbon Interaction. *iScience* **2019,** *13*, 190-198.
(303) Xu, G.; Wang, R.; Yang, F.; Ma, D.; Yang, Z.; Lu, Z. Co Oxidation on Single Pd Atom Embedded Defect-Graphene Via a New Termolecular Eley-Rideal Mechanism. *Carbon* **2017,** *118*, 35-42.
(304) Mahmoodinia, M.; \AAstrand, P.-O.; Chen, D. Tuning the Electronic Properties of Single-Atom Pt Catalysts by Functionalization of the Carbon Support Material. *The Journal of Physical Chemistry C* **2017,** *121*, 20802–20812.
(305) Hasegawa, S.; Kunisada, Y.; Sakaguchi, N. Diffusion of a Single Platinum Atom on Light-Element-Doped Graphene. *The Journal of Physical Chemistry C* **2017,** *121*, 17787–17795.
(306) Kochubey, D. I.; Chesnokov, V. V.; Malykhin, S. E. Evidence for Atomically Dispersed Pd in Catalysts Supported on Carbon Nanofibers. *Carbon* **2012,** *50*, 2782-2787.
(307) Arrigo, R.; Schuster, M. E.; Xie, Z.; Yi, Y.; Wowsnick, G.; Sun, L. L.; Hermann, K. E.; Friedrich, M.; Kast, P.; Hävecker, M.et al. Nature of the N–Pd Interaction in Nitrogen-Doped Carbon Nanotube Catalysts. *ACS Catalysis* **2015,** *5*, 2740–2753.
(308) Chen, Z.; Vorobyeva, E.; Mitchell, S.; Fako, E.; Ortuño, M. A.; Lopez, N.; Collins, S. M.; Midgley, P. A.; Richard, S.; Vilé, G.et al. A Heterogeneous Single-Atom Palladium Catalyst Surpassing Homogeneous Systems for Suzuki Coupling. *Nature Nanotechnology* **2018,** *13*, 702-707.
(309) Huang, F.; Deng, Y.; Chen, Y.; Cai, X.; Peng, M.; Jia, Z.; Ren, P.; Xiao, D.; Wen, X.; Wang, N.et al. Atomically Dispersed Pd on Nanodiamond/Graphene Hybrid for Selective Hydrogenation of Acetylene. *J. Am. Chem. Soc.* **2018,** *140*, 13142–13146.
(310) López-Corral, I.; Irigoyen, B.; Juan, A. Bonding in Pdh2 and Pd2h2 Systems Adsorbed on Carbon Nanotubes: Implications for Hydrogen Storage. *International Journal of Hydrogen Energy* **2014,** *39*, 8780-8790.

(311) Yin, P.; Yao, T.; Wu, Y.; Zheng, L.; Lin, Y.; Liu, W.; Ju, H.; Zhu, J.; Hong, X.; Deng, Z.et al. Single Cobalt Atoms with Precise N-Coordination as Superior Oxygen Reduction Reaction Catalysts. *Angew. Chem.* **2016,** *128*, 10958–10963.
(312) Li, S.-L.; Yin, H.; Kan, X.; Gan, L.-Y.; Schwingenschlogl, U.; Zhao, Y. Potential of Transition Metal Atoms Embedded in Buckled Monolayer G-C 3n 4as Single-Atom Catalysts. *PCCP* **2017,** *19*, 30069–30077.
(313) Fei, H.; Dong, J.; nez, M. J. A.-J. e.; Ye, G.; Kim, N. D.; Samuel, E. L. G.; Peng, Z.; Zhu, Z.; Qin, F.; Bao, J.et al. Atomic Cobalt on Nitrogen-Doped Graphene for Hydrogen Generation. *Nature Communications* **2015,** *6*, 1-8.
(314) Möller, T.; Ju, W.; Bagger, A.; Wang, X.; Luo, F.; Ngo Thanh, T.; Varela, A. S.; Rossmeisl, J.; Strasser, P. Efficient Co2 to Co Electrolysis on Solid Ni–N–C Catalysts at Industrial Current Densities. *Energy & Environmental Science* **2019,** *12*, 640-647.
(315) Sahoo, S.; Suib, S. L.; Alpay, S. P. Graphene Supported Single Atom Transition Metal Catalysts for Methane Activation. *ChemCatChem* **2018,** *10*, 3229–3235.
(316) Amft, M.; Sanyal, B.; Eriksson, O.; Skorodumova, N. V. Small Gold Clusters on Graphene, Their Mobility and Clustering: A Dft Study. *J. Phys.: Condens. Matter* **2011,** *23*, 205301.
(317) Błoński, P.; Hafner, J. r. Geometric and Magnetic Properties of Pt Clusters Supported on Graphene: Relativistic Density-Functional Calculations. *The Journal of Chemical Physics* **2011,** *134*, 154705-154713.
(318) Fampiou, I.; Ramasubramaniam, A. Binding of Pt Nanoclusters to Point Defects in Graphene: Adsorption, Morphology, and Electronic Structure. *Journal of Physical Chemistry C* **2012,** *116*, 6543-6555.
(319) Cabria, I.; López, M. J.; Alonso, J. A. Theoretical Study of the Transition from Planar to Three-Dimensional Structures of Palladium Clusters Supported on Graphene. *Physical Review B* **2010,** *81*, 035403.
(320) López, M. J.; Cabria, I.; Alonso, J. A. Palladium Clusters Anchored on Graphene Vacancies and Their Effect on the Reversible Adsorption of Hydrogen. *The Journal of Physical Chemistry C* **2014,** *118*, 5081–5090.
(321) Porter, C. D.; Stroud, D. Clustering and Magnetic Anisotropy of Fe Adatoms on Graphene. *Physical Review B* **2012,** *85*, 235452.
(322) Rêgo, C. R. C.; Tereshchuk, P.; Oliveira, L. N.; Da Silva, J. L. F. Graphene-Supported Small Transition-Metal Clusters: A Density Functional Theory Investigation within Van Der Waals Corrections. *Physical Review B* **2017,** *95*, 235422–235411.
(323) Ramos-Castillo, C. M.; Reveles, J. U.; Zope, R. R.; de Coss, R. Palladium Clusters Supported on Graphene Monovacancies for Hydrogen Storage. *The Journal of Physical Chemistry C* **2015,** *119*, 8402–8409.
(324) Granja-DelRio, A.; Alonso, J. A.; Lopez, M. J. Competition between Palladium Clusters and Hydrogen to Saturate Graphene Vacancies. *JOURNAL OF PHYSICAL CHEMISTRY C* **2017,** *121*, 10843-10850.
(325) López, M. J.; Cabria, I.; Alonso, J. A. Palladium Clusters Anchored on Graphene Vacancies and Their Effect on the Reversible Adsorption of Hydrogen. *The Journal of Physical Chemistry C* **2014,** *118*, 5081-5090.
(326) Blanco-Rey, M.; Juaristi, J. I.; Alducin, M.; López, M. J.; Alonso, J. A. Is Spillover Relevant for Hydrogen Adsorption and Storage in Porous Carbons Doped with Palladium Nanoparticles? *The Journal of Physical Chemistry C* **2016,** *120*, 17357–17364.
(327) Yang, Y.; Castano, C. E.; Gupton, B. F.; Reber, A. C.; Khanna, S. N. A Fundamental Analysis of Enhanced Cross-Coupling Catalytic Activity for Palladium Clusters on Graphene Supports. *Nanoscale* **2016,** *8*, 19564-19572.
(328) Yang, Y.; Reber, A. C.; Gilliland III, S. E.; Castano, C. E.; Gupton, B. F.; Khanna, S. N. More Than Just a Support: Graphene as a Solid-State Ligand for Palladium-Catalyzed Cross-Coupling Reactions. *J. Catal.* **2018,** *360*, 20–26.

(329) Luo, Q.; Zhang, W.; Fu, C.-F.; Yang, J. Single Pd Atom and Pd Dimer Embedded Graphene Catalyzed Formic Acid Dehydrogenation: A First-Principles Study. *Int. J. Hydrogen Energy* **2018,** *43*, 6997–7006.
(330) Piotrowski, M. J.; Piquini, P.; Zeng, Z.; Da Silva, J. L. F. Adsorption of No on the Rh13, Pd13, Ir13, and Pt13 Clusters: A Density Functional Theory Investigation. *The Journal of Physical Chemistry C* **2012,** *116*, 20540-20549.
(331) Liu, X.; Meng, C.; Han, Y. Defective Graphene Supported Mpd 12(M = Fe, Co, Ni, Cu, Zn, Pd) Nanoparticles as Potential Oxygen Reduction Electrocatalysts: A First-Principles Study. *The Journal of Physical Chemistry C* **2013,** *117*, 1350–1357.
(332) Lim, D.-H.; Wilcox, J. Mechanisms of the Oxygen Reduction Reaction on Defective Graphene-Supported Pt Nanoparticles from First-Principles. *The Journal of Physical Chemistry C* **2012,** *116*, 3653–3660.
(333) Tian, Y.; Liu, Y.-j.; Zhao, J.-x.; Ding, Y.-h. High Stability and Superior Catalytic Reactivity of Nitrogen-Doped Graphene Supporting Pt Nanoparticles as a Catalyst for the Oxygen Reduction Reaction: A Density Functional Theory Study. *RSC Advances* **2015,** *5*, 34070–34077.
(334) Kim, G.; Jhi, S.-H. Carbon Monoxide-Tolerant Platinum Nanoparticle Catalysts on Defect-Engineered Graphene. *ACS Nano* **2011,** *5*, 805-810.
(335) Chen, I.-N.; Wu, S.-Y.; Chen, H.-T. Hydrogen Storage in N- and B-Doped Graphene Decorated by Small Platinum Clusters: A Computational Study. *Appl. Surf. Sci.* **2018,** *441*, 607–612.
(336) Wang, Q.; Tian, Y.; Chen, G.; Zhao, J. Theoretical Insights into the Energetics and Electronic Properties of Mpt12 (M=Fe, Co, Ni, Cu, and Pd) Nanoparticles Supported by N-Doped Defective Graphene. *Appl. Surf. Sci.* **2017,** *397*, 199–205.
(337) Gasper, R. J.; Ramasubramaniam, A. Density Functional Theory Studies of the Methanol Decomposition Reaction on Graphene-Supported Pt 13nanoclusters. *The Journal of Physical Chemistry C* **2016,** *120*, 17408–17417.
(338) Yang, B.; Burch, R.; Hardacre, C.; Headdock, G.; Hu, P. Understanding the Optimal Adsorption Energies for Catalyst Screening in Heterogeneous Catalysis. *ACS Catalysis* **2014,** *4*, 182-186.
(339) Logadottir, A.; Rod, T. H.; Nørskov, J. K.; Hammer, B.; Dahl, S.; Jacobsen, C. J. H. The Brønsted–Evans–Polanyi Relation and the Volcano Plot for Ammonia Synthesis over Transition Metal Catalysts. *J. Catal.* **2001,** *197*, 229-231.
(340) Nørskov, J. K.; Bligaard, T.; Hvolbæk, B.; Abild-Pedersen, F.; Chorkendorff, I.; Christensen, C. H. The Nature of the Active Site in Heterogeneous Metal Catalysis. *Chem. Soc. Rev.* **2008,** *37*, 2163-2171.
(341) Wu, S.-Y.; Lin, C.-H.; Ho, J.-J. Density-Functional Calculations of the Conversion of Methane to Methanol on Platinum-Decorated Sheets of Graphene Oxide. *PCCP* **2015**, 1–7.
(342) Alonso-Lanza, T.; Ayuela, A.; Aguilera-Granja, F. Chemical Bonding of Transition-Metal Co 13clusters with Graphene. *ChemPhysChem* **2015,** *16*, 3700–3710.
(343) Song, W.; Jiao, M.; Li, K.; Wang, Y.; Wu, Z. Theoretical Study on the Interaction of Pristine, Defective and Strained Graphene with Fen and Nin (N=13, 38, 55) Clusters. *Chem. Phys. Lett.* **2013,** *588*, 203–207.
(344) Sahoo, S.; Gruner, M. E.; Khanna, S. N.; Entel, P. First-Principles Studies on Graphene-Supported Transition Metal Clusters. *The Journal of Chemical Physics* **2014,** *141*, 074707–074710.
(345) García-Rodríguez, D. E.; Mendoza-Huizar, L. H.; Díaz, C. A Dft Study of Cu Nanoparticles Adsorbed on Defective Graphene. *Appl. Surf. Sci.* **2017,** *412*, 146–151.
(346) Lim, D.-H.; Negreira, A. S.; Wilcox, J. Dft Studies on the Interaction of Defective Graphene-Supported Fe and Al Nanoparticles. *Journal of Physical Chemistry C* **2011,** *115*, 8961-8970.
(347) Qian, Y.; Du, P.; Wu, P.; Cai, C.; Gervasio, D. F. Chemical Nature of Catalytic Active Sites for the Oxygen Reduction Reaction on Nitrogen-Doped Carbon-Supported Non-Noble Metal Catalysts. *The Journal of Physical Chemistry C* **2016,** *120*, 9884–9896.

(348) Zhuang, Z.; Giles, S. A.; Zheng, J.; Jenness, G. R.; Caratzoulas, S.; Vlachos, D. G.; Yan, Y. Nickel Supported on Nitrogen-Doped Carbon Nanotubes as Hydrogen Oxidation Reaction Catalyst in Alkaline Electrolyte. *Nature Communications* **2016,** *7*, 10141.

(349) Ramos-Castillo, C. M.; Reveles, J. U.; Cifuentes-Quintal, M. E.; Zope, R. R.; de Coss, R. Ti4- and Ni4-Doped Defective Graphene Nanoplatelets as Efficient Materials for Hydrogen Storage. *The Journal of Physical Chemistry C* **2016,** *120*, 5001-5009.

(350) Cornelio, B.; Rance, G. A.; Laronze-Cochard, M.; Fontana, A.; Sapi, J.; Khlobystov, A. N. Palladium Nanoparticles on Carbon Nanotubes as Catalysts of Cross-Coupling Reactions. *Journal of Materials Chemistry A* **2013,** *1*, 8737-8744.

(351) Li, Z.; Liu, J.; Huang, Z.; Yang, Y.; Xia, C.; Li, F. One-Pot Synthesis of Pd Nanoparticle Catalysts Supported on N-Doped Carbon and Application in the Domino Carbonylation. *Acs Catalysis* **2013,** *3*, 839-845.

(352) Parambhath, V. B.; Nagar, R.; Ramaprabhu, S. Effect of Nitrogen Doping on Hydrogen Storage Capacity of Palladium Decorated Graphene. *Langmuir* **2012,** *28*, 7826-7833.

(353) Li, Z.; Li, J.; Liu, J.; Zhao, Z.; Xia, C.; Li, F. Palladium Nanoparticles Supported on Nitrogen-Functionalized Active Carbon: A Stable and Highly Efficient Catalyst for the Selective Hydrogenation of Nitroarenes. *ChemCatChem* **2014,** *6*, 1333-1339.

(354) Bi, Q.-Y.; Lin, J.-D.; Liu, Y.-M.; He, H.-Y.; Huang, F.-Q.; Cao, Y. Dehydrogenation of Formic Acid at Room Temperature: Boosting Palladium Nanoparticle Efficiency by Coupling with Pyridinic-Nitrogen-Doped Carbon. *Angewandte Chemie-International Edition* **2016,** *55*, 11849-11853.

(355) Zhang, X.; Zhu, J.; Tiwary, C. S.; Ma, Z.; Huang, H.; Zhang, J.; Lu, Z.; Huang, W.; Wu, Y. Palladium Nanoparticles Supported on Nitrogen and Sulfur Dual-Doped Graphene as Highly Active Electrocatalysts for Formic Acid and Methanol Oxidation. *ACS Applied Materials & Interfaces* **2016,** *8*, 10858-10865.

(356) Zhang, Q.; LÜ, J.; Ma, L.; Lu, C.; Liu, W.; Li, X. Study on Deactivation by Sulfur and Regeneration of Pd/C Catalyst in Hydrogenation of N-(3-Nitro-4-Methoxyphenyl) Acetamide. *Chin. J. Chem. Eng.* **2013,** *21*, 622-626.

(357) Choudhary, V. R.; Sane, M. G. Poisoning of Pd–Carbon Catalysts by Sulphur, Chloro and Heavy Metal Compounds in Liquid Phase Hydrogenation of O-Nitrophenol to O-Aminophenol. *Journal of Chemical Technology & Biotechnology* **1998,** *73*, 336-340.

(358) Simakova, I.; Simakova, O.; Mäki-Arvela, P.; Murzin, D. Y. Decarboxylation of Fatty Acids over Pd Supported on Mesoporous Carbon. *Catal. Today* **2010,** *150*, 28-31.

(359) Sajiki, H.; Hirota, K. Pd/C-Catalyzed Chemoselective Hydrogenation in the Presence of a Phenolic Mpm Protective Group Using Pyridine as a Catalyst Poison. *Chem. Pharm. Bull.* **2003,** *51*, 320-324.

(360) Chaston, J. C. Palladium-on-Charcoal Catalysts. *Platinum Metals Rev., 1961, 5, (4), 122* **1961,** *5*, 122-125.

(361) Motoyama, Y.; Lee, Y.; Tsuji, K.; Yoon, S.-H.; Mochida, I.; Nagashima, H. Platinum Nanoparticles Supported on Nitrogen-Doped Carbon Nanofibers as Efficient Poisoning Catalysts for the Hydrogenation of Nitroarenes. *ChemCatChem* **2011,** *3*, 1578-1581.

(362) Ye, W.; Hu, H.; Zhang, H.; Zhou, F.; Liu, W. Multi-Walled Carbon Nanotube Supported Pd and Pt Nanoparticles with High Solution Affinity for Effective Electrocatalysis. *Appl. Surf. Sci.* **2010,** *256*, 6723-6728.

(363) Szőri, K.; Puskás, R.; Szőllősi, G.; Bertóti, I.; Szépvölgyi, J.; Bartók, M. Palladium Nanoparticle–Graphene Catalysts for Asymmetric Hydrogenation. *Catal. Lett.* **2013,** *143*, 539–546.

(364) Lazzarini, A.; Pellegrini, R.; Piovano, A.; Rudić, S.; Castan-Guerrero, C.; Torelli, P.; Chierotti, M. R.; Gobetto, R.; Lamberti, C.; Groppo, E. The Effect of Surface Chemistry on the Performances of Pd-Based Catalysts Supported on Activated Carbons. *Catalysis Science & Technology* **2017,** *7*, 4162-4172.

(365) Verga, L. G.; Aarons, J.; Sarwar, M.; Thompsett, D.; Russell, A. E.; Skylaris, C. K. Effect of Graphene Support on Large Pt Nanoparticles. *Physical Chemistry Chemical Physics* **2016,** *18*, 32713–32722.

(366) Shi, H.; Auerbach, S. M.; Ramasubramaniam, A. First-Principles Predictions of Structure–Function Relationships of Graphene-Supported Platinum Nanoclusters. *The Journal of Physical Chemistry C* **2016,** *120*, 11899–11909.
(367) Yang, Y.; Cheng, P.; Huang, S. Unraveling the Roles of Iron in Stabilizing the Defective Graphene-Supported Ptfe Bimetallic Nanoparticles. *J. Alloys Compd.* **2016,** *688*, 1172-1180.
(368) Carosso, M.; Lazzarini, A.; Piovano, A.; Pellegrini, R.; Morandi, S.; Manzoli, M.; Vitillo, J. G.; Ruiz, M. J.; Lamberti, C.; Groppo, E. Looking for the Active Hydrogen Species in a 5 wt% Pt/C Catalyst: A Challenge for Inelastic Neutron Scattering. *Faraday Discuss.* **2018,** *208*, 227-242.
(369) Arrigo, R.; Badmus, K.; Baletto, F.; Boeije, M.; Bowker, M.; Brinkert, K.; Bugaev, A.; Bukhtiyarov, V.; Carosso, M.; Catlow, R.et al. The Challenges of Characterising Nanoparticulate Catalysts: General Discussion. *Faraday Discuss.* **2018,** *208*, 339-394.
(370) Zhang, Y.; Toebes, M. L.; van der Eerden, A.; O'Grady, W. E.; de Jong, K. P.; Koningsberger, D. C. Metal Particle Size and Structure of the Metal−Support Interface of Carbon-Supported Platinum Catalysts as Determined with Exafs Spectroscopy. *The Journal of Physical Chemistry B* **2004,** *108*, 18509-18519.
(371) Tuo, Y.-X.; Shi, L.-J.; Cheng, H.-Y.; Zhu, Y.-A.; Yang, M.-L.; Xu, J.; Han, Y.-F.; Li, P.; Yuan, W.-K. Insight into the Support Effect on the Particle Size Effect of Pt/C Catalysts in Dehydrogenation. *J. Catal.* **2018,** *360*, 175-186.
(372) Leontyev, I. N.; Belenov, S. V.; Guterman, V. E.; Haghi-Ashtiani, P.; Shaganov, A. P.; Dkhil, B. Catalytic Activity of Carbon-Supported Pt Nanoelectrocatalysts. Why Reducing the Size of Pt Nanoparticles Is Not Always Beneficial. *The Journal of Physical Chemistry C* **2011,** *115*, 5429-5434.
(373) Sui, S.; Wang, X.; Zhou, X.; Su, Y.; Riffat, S.; Liu, C.-j. A Comprehensive Review of Pt Electrocatalysts for the Oxygen Reduction Reaction: Nanostructure, Activity, Mechanism and Carbon Support in Pem Fuel Cells. *Journal of Materials Chemistry A* **2017,** *5*, 1808-1825.
(374) Wang, Y.-J.; Zhao, N.; Fang, B.; Li, H.; Bi, X. T.; Wang, H. Carbon-Supported Pt-Based Alloy Electrocatalysts for the Oxygen Reduction Reaction in Polymer Electrolyte Membrane Fuel Cells: Particle Size, Shape, and Composition Manipulation and Their Impact to Activity. *Chem. Rev.* **2015,** *115*, 3433–3467.
(375) Jackson, C.; Smith, G. T.; Inwood, D. W.; Leach, A. S.; Whalley, P. S.; Callisti, M.; Polcar, T.; Russell, A. E.; Levecque, P.; Kramer, D. Electronic Metal-Support Interaction Enhanced Oxygen Reduction Activity and Stability of Boron Carbide Supported Platinum. *Nature Communications* **2017,** *8*, 15802.
(376) Yu, X.; Ye, S. Recent Advances in Activity and Durability Enhancement of Pt/C Catalytic Cathode in Pemfc: Part Ii: Degradation Mechanism and Durability Enhancement of Carbon Supported Platinum Catalyst. *J. Power Sources* **2007,** *172*, 145-154.
(377) Higgins, D. C.; Meza, D.; Chen, Z. Nitrogen-Doped Carbon Nanotubes as Platinum Catalyst Supports for Oxygen Reduction Reaction in Proton Exchange Membrane Fuel Cells. *Journal of Physical Chemistry C* **2010,** *114*, 21982-21988.
(378) Panchakarla, L. S.; Govindaraj, A.; Rao, C. N. R. Nitrogen- and Boron-Doped Double-Walled Carbon Nanotubes. *ACS Nano* **2007,** *1*, 494-500.
(379) Wang, X. X.; Tan, Z. H.; Zeng, M.; Wang, J. N. Carbon Nanocages: A New Support Material for Pt Catalyst with Remarkably High Durability. *Scientific Reports* **2014,** *4*, 4437.
(380) Lee, H. I.; Joo, S. H.; Kim, J. H.; You, D. J.; Kim, J. M.; Park, J.-N.; Chang, H.; Pak, C. Ultrastable Pt Nanoparticles Supported on Sulfur-Containing Ordered Mesoporous Carbonvia Strong Metal-Support Interaction. *J. Mater. Chem.* **2009,** *19*, 5934-5939.
(381) Kou, R.; Shao, Y.; Mei, D.; Nie, Z.; Wang, D.; Wang, C.; Viswanathan, V. V.; Park, S.; Aksay, I. A.; Lin, Y.et al. Stabilization of Electrocatalytic Metal Nanoparticles at Metal−Metal Oxide−Graphene Triple Junction Points. *J. Am. Chem. Soc.* **2011,** *133*, 2541-2547.
(382) Matsutsu, M.; Petersen, M. A.; van Steen, E. Pt 38cluster on Oh- and Cooh-Functionalised Graphene as a Model for Pt/C-Catalysts. *Physical Chemistry Chemical Physics* **2016,** *18*, 25693–25704.

(383) Cao, S.; Jiang, J.; Zhu, B.; Yu, J. Shape-Dependent Photocatalytic Hydrogen Evolution Activity over a Pt Nanoparticle Coupled G-C 3n 4photocatalyst. *PCCP* **2016,** *18*, 19457–19463.
(384) Wang, L.; Tang, Z.; Yan, W.; Yang, H.; Wang, Q.; Chen, S. Porous Carbon-Supported Gold Nanoparticles for Oxygen Reduction Reaction: Effects of Nanoparticle Size. *Acs Applied Materials & Interfaces* **2016,** *8*, 20635-20641.
(385) Song, Z.; Li, W.; Niu, F.; Xu, Y.; Niu, L.; Yang, W.; Wang, Y.; Liu, J. A Novel Method to Decorate Au Clusters onto Graphene Via a Mild Co-Reduction Process for Ultrahigh Catalytic Activity. *Journal of Materials Chemistry A* **2017,** *5*, 230-239.
(386) Nakatsuka, K.; Yoshii, T.; Kuwahara, Y.; Mori, K.; Yamashita, H. Controlled Synthesis of Carbon-Supported Co Catalysts from Single-Sites to Nanoparticles: Characterization of the Structural Transformation and Investigation of Their Oxidation Catalysis. *PCCP* **2017,** *19*, 4967-4974.
(387) Czekaj, I.; Pin, S.; Wambach, J. Ru/Active Carbon Catalyst: Improved Spectroscopic Data Analysis by Density Functional Theory. *The Journal of Physical Chemistry C* **2013,** *117*, 26588-26597.
(388) Stakheev, A. Y.; Kustov, L. M. Effects of the Support on the Morphology and Electronic Properties of Supported Metal Clusters: Modern Concepts and Progress in 1990s. *Applied Catalysis A: General* **1999,** *188*, 3-35.
(389) Pan, C.-J.; Tsai, M.-C.; Su, W.-N.; Rick, J.; Akalework, N. G.; Agegnehu, A. K.; Cheng, S.-Y.; Hwang, B.-J. Tuning/Exploiting Strong Metal-Support Interaction (Smsi) in Heterogeneous Catalysis. *Journal of the Taiwan Institute of Chemical Engineers* **2017,** *74*, 154-186.
(390) Goettmann, F.; Sanchez, C. How Does Confinement Affect the Catalytic Activity of Mesoporous Materials? *J. Mater. Chem.* **2007,** *17*, 24-30.
(391) Yu, X.; Ye, S. Recent Advances in Activity and Durability Enhancement of Pt/C Catalytic Cathode in Pemfc: Part I. Physico-Chemical and Electronic Interaction between Pt and Carbon Support, and Activity Enhancement of Pt/C Catalyst. *J. Power Sources* **2007,** *172*, 133-144.
(392) Coq, B. In *Metal-Ligand Interactions in Chemistry, Physics and Biology*; Russo, N.;Salahub, D. R., Eds.; Springer Netherlands: Dordrecht, 2000, DOI:10.1007/978-94-011-4245-8_3 10.1007/978-94-011-4245-8_3.
(393) Mishra, A.; Singh, V. K.; Mohanty, T. Coexistence of Interfacial Stress and Charge Transfer in Graphene Oxide-Based Magnetic Nanocomposites. *Journal of Materials Science* **2017,** *52*, 7677-7687.
(394) Mavrikakis, M.; Hammer, B.; Nørskov, J. K. Effect of Strain on the Reactivity of Metal Surfaces. *Phys. Rev. Lett.* **1998,** *81*, 2819-2822.
(395) Frenkel, A. I.; Small, M. W.; Smith, J. G.; Nuzzo, R. G.; Kvashnina, K. O.; Tromp, M. An in Situ Study of Bond Strains in 1 Nm Pt Catalysts and Their Sensitivities to Cluster–Support and Cluster–Adsorbate Interactions. *The Journal of Physical Chemistry C* **2013,** *117*, 23286-23294.
(396) Xu, P.; Dong, L.; Neek-Amal, M.; Ackerman, M. L.; Yu, J.; Barber, S. D.; Schoelz, J. K.; Qi, D.; Xu, F.; Thibado, P. M.et al. Self-Organized Platinum Nanoparticles on Freestanding Graphene. *ACS Nano* **2014,** *8*, 2697-2703.
(397) Cretu, O.; Krasheninnikov, A. V.; Rodríguez-Manzo, J. A.; Sun, L.; Nieminen, R. M.; Banhart, F. Migration and Localization of Metal Atoms on Strained Graphene. *Physical Review Letters* **2010,** *105*, 196102.
(398) Moldovan, M. S.; Bulou, H.; Dappe, Y. J.; Janowska, I.; Bégin, D.; Pham-Huu, C.; Ersen, O. On the Evolution of Pt Nanoparticles on Few-Layer Graphene Supports in the High-Temperature Range. *The Journal of Physical Chemistry C* **2012,** *116*, 9274-9282.
(399) Zhou, M.; Lu, Y.; Zhang, C.; Feng, Y. P. Strain Effects on Hydrogen Storage Capability of Metal-Decorated Graphene: A First-Principles Study. *Appl. Phys. Lett.* **2010,** *97*, 103109.
(400) Zhou, M.; Zhang, A.; Dai, Z.; Feng, Y. P.; Zhang, C. Strain-Enhanced Stabilization and Catalytic Activity of Metal Nanoclusters on Graphene. *The Journal of Physical Chemistry C* **2010,** *114*, 16541-16546.
(401) Kim, G.; Kawazoe, Y.; Lee, K.-R. Controlled Catalytic Properties of Platinum Clusters on Strained Graphene. *The Journal of Physical Chemistry Letters* **2012,** *3*, 1989-1996.

(402) Settem, M.; Rajak, P.; Islam, M.; Bhattacharyya, S. Influence of Supporting Amorphous Carbon Film Thickness on Measured Strain Variation within a Nanoparticle. *Nanoscale* **2017,** *9*, 17054-17062.
(403) Pizzocchero, F.; Vanin, M.; Kling, J.; Hansen, T. W.; Jacobsen, K. W.; Bøggild, P.; Booth, T. J. Graphene Edges Dictate the Morphology of Nanoparticles During Catalytic Channeling. *The Journal of Physical Chemistry C* **2014,** *118*, 4296-4302.
(404) Miyazawa, K. i.; Yoshitake, M.; Tanaka, Y. Hrtem Analyses of the Platinum Nanoparticles Prepared on Graphite Particles Using Coaxial Arc Plasma Deposition. *J. Nanopart. Res.* **2017,** *19*, 191.
(405) Miyazawa, K. i.; Shimomura, S.; Yoshitake, M.; Tanaka, Y. Hrtem Structural Characterization of Platinum Nanoparticles Loaded on Carbon Black Particles Using Focused Ion Beam Milling. *Mater. Lett.* **2019,** *237*, 96-100.
(406) Leontyev, I. N.; Kuriganova, A. B.; Leontyev, N. G.; Hennet, L.; Rakhmatullin, A.; Smirnova, N. V.; Dmitriev, V. Size Dependence of the Lattice Parameters of Carbon Supported Platinum Nanoparticles: X-Ray Diffraction Analysis and Theoretical Considerations. *RSC Advances* **2014,** *4*, 35959-35965.
(407) Frenkel, A. I.; Hills, C. W.; Nuzzo, R. G. A View from the Inside: Complexity in the Atomic Scale Ordering of Supported Metal Nanoparticles. *The Journal of Physical Chemistry B* **2001,** *105*, 12689-12703.
(408) Wang, L.-L.; Khare, S. V.; Chirita, V.; Johnson, D. D.; Rockett, A. A.; Frenkel, A. I.; Mack, N. H.; Nuzzo, R. G. Origin of Bulklike Structure and Bond Length Disorder of Pt37 and Pt6ru31 Clusters on Carbon: Comparison of Theory and Experiment. *J. Am. Chem. Soc.* **2006,** *128*, 131-142.
(409) Daio, T.; Staykov, A.; Guo, L.; Liu, J.; Tanaka, M.; Matthew Lyth, S.; Sasaki, K. Lattice Strain Mapping of Platinum Nanoparticles on Carbon and Sno2 Supports. *Scientific Reports* **2015,** *5*, 13126.
(410) Wang, L.-L.; Johnson, D. D. Shear Instabilities in Metallic Nanoparticles: Hydrogen-Stabilized Structure of Pt37 on Carbon. *J. Am. Chem. Soc.* **2007,** *129*, 3658-3664.
(411) Yoshitake, M.; Tanaka, Y. Characterisation of Platinum Nanoparticles Deposited on C60 Fullerene Nanowhiskers Au - Miyazawa, Kun'ichi. *Surf. Eng.* **2018,** *34*, 846-851.
(412) Sanz-Navarro, C. F.; Åstrand, P.-O.; Chen, D.; Rønning, M.; van Duin, A. C. T.; Jacob, T.; Goddard, W. A. Molecular Dynamics Simulations of the Interactions between Platinum Clusters and Carbon Platelets. *The Journal of Physical Chemistry A* **2008,** *112*, 1392-1402.
(413) Sanz-Navarro, C. F.; Åstrand, P.-O.; Chen, D.; Rønning, M.; van Duin, A. C. T.; Goddard, W. A. Molecular Dynamics Simulations of Metal Clusters Supported on Fishbone Carbon Nanofibers. *The Journal of Physical Chemistry C* **2010,** *114*, 3522-3530.
(414) Cheng, H.; Zhu, Y.-A.; Chen, D.; Åstrand, P.-O.; Li, P.; Qi, Z.; Zhou, X.-G. Evolution of Carbon Nanofiber-Supported Pt Nanoparticles of Different Particle Sizes: A Molecular Dynamics Study. *The Journal of Physical Chemistry C* **2014,** *118*, 23711-23722.
(415) Cheng, H.-Y.; Zhu, Y.-A.; Åstrand, P.-O.; Chen, D.; Li, P.; Zhou, X.-G. Evolution of Pt Nanoparticles Supported on Fishbone-Type Carbon Nanofibers with Cone–Helix Structures: A Molecular Dynamics Study. *The Journal of Physical Chemistry C* **2013,** *117*, 14261-14271.
(416) Sanz-Navarro, C. F.; Åstrand, P.-O.; Chen, D.; Rønning, M.; Duin, A. C. T. v.; Mueller, J. E.; Goddard Iii, W. A. Molecular Dynamics Simulations of Carbon-Supported Ni Clusters Using the Reax Reactive Force Field. *The Journal of Physical Chemistry C* **2008,** *112*, 12663-12668.
(417) Ochoa-Fernández, E.; Chen, D.; Yu, Z.; Tøtdal, B.; Rønning, M.; Holmen, A. Effect of Carbon Nanofiber-Induced Microstrain on the Catalytic Activity of Ni Crystals. *Surf. Sci.* **2004,** *554*, L107-L112.
(418) Luo, M.; Guo, S. Strain-Controlled Electrocatalysis on Multimetallic Nanomaterials. *Nature Reviews Materials* **2017,** *2*, 17059.
(419) Pacchioni, G. Electronic Interactions and Charge Transfers of Metal Atoms and Clusters on Oxide Surfaces. *PCCP* **2013,** *15*, 1737-1757.

(420) Pacchioni, G.; Freund, H.-J. Controlling the Charge State of Supported Nanoparticles in Catalysis: Lessons from Model Systems. *Chem. Soc. Rev.* **2018,** *47*, 8474-8502.
(421) Khoa, N. T.; Kim, S. W.; Yoo, D.-H.; Kim, E. J.; Hahn, S. H. Size-Dependent Work Function and Catalytic Performance of Gold Nanoparticles Decorated Graphene Oxide Sheets. *Applied Catalysis A: General* **2014,** *469*, 159-164.
(422) Campisi, S.; Chan-Thaw, C. E.; Villa, A. Understanding Heteroatom-Mediated Metal–Support Interactions in Functionalized Carbons: A Perspective Review. *Applied Sciences* **2018,** *8*, 1159.
(423) Wang, L.; Han, J.; Zhu, Y.; Zhou, R.; Jaye, C.; Liu, H.; Li, Z.-Q.; Taylor, G. T.; Fischer, D. A.; Appenzeller, J.et al. Probing the Dependence of Electron Transfer on Size and Coverage in Carbon Nanotube–Quantum Dot Heterostructures. *The Journal of Physical Chemistry C* **2015,** *119*, 26327-26338.
(424) Schroeder, V.; Savagatrup, S.; He, M.; Lin, S.; Swager, T. M. Carbon Nanotube Chemical Sensors. *Chem. Rev.* **2019,** *119*, 599-663.
(425) Strauss, V.; Roth, A.; Sekita, M.; Guldi, Dirk M. Efficient Energy-Conversion Materials for the Future: Understanding and Tailoring Charge-Transfer Processes in Carbon Nanostructures. *Chem* **2016,** *1*, 531-556.
(426) Rakesh, V.; Barun, D.; Chandra Sekhar, R.; Rao, C. N. R. Effects of Charge Transfer Interaction of Graphene with Electron Donor And acceptor Molecules Examined Using Raman Spectroscopy and Cognate Techniques. *J. Phys.: Condens. Matter* **2008,** *20*, 472204.
(427) Sun, C.-L.; Pao, C.-W.; Tsai, H.-M.; Chiou, J.-W.; Ray, S. C.; Wang, H.-W.; Hayashi, M.; Chen, L.-C.; Lin, H.-J.; Lee, J.-F.et al. Atomistic Nucleation Sites of Pt Nanoparticles on N-Doped Carbon Nanotubes. *Nanoscale* **2013,** *5*, 6812-6818.
(428) Jiang, F.; Li, C.; Fu, H.; Guo, X.; Wu, G.; Chen, S. Probing the Spontaneous Reduction Mechanism of Platinum Ions Confined in the Nanospace by X-Ray Absorption Fine Structure Spectroscopy. *PCCP* **2016,** *18*, 19259-19266.
(429) Liu, C.; Pfefferle, L. D.; Haller, G. L. The Electronic Structure or Charge Delocalization of Sulfated Zirconia (Supported on Multi-Walled Carbon Nanotubes): Acid Sites Probed by X-Ray Absorption Spectroscopy. *Top. Catal.* **2014,** *57*, 774-784.
(430) Rao, R. G.; Blume, R.; Hansen, T. W.; Fuentes, E.; Dreyer, K.; Moldovan, S.; Ersen, O.; Hibbitts, D. D.; Chabal, Y. J.; Schlögl, R.et al. Interfacial Charge Distributions in Carbon-Supported Palladium Catalysts. *Nature communications* **2017,** *8*, 340-340.
(431) Arrigo, R.; Schuster, M. E.; Xie, Z.; Yi, Y.; Wowsnick, G.; Sun, L. L.; Hermann, K. E.; Friedrich, M.; Kast, P.; Hävecker, M.et al. Nature of the N–Pd Interaction in Nitrogen-Doped Carbon Nanotube Catalysts. *ACS Catalysis* **2015,** *5*, 2740-2753.
(432) Shi, W.; Zhang, B.; Lin, Y.; Wang, Q.; Zhang, Q.; Su, D. S. Enhanced Chemoselective Hydrogenation through Tuning the Interaction between Pt Nanoparticles and Carbon Supports: Insights from Identical Location Transmission Electron Microscopy and X-Ray Photoelectron Spectroscopy. *ACS Catalysis* **2016,** *6*, 7844-7854.
(433) Bastl, Z.; Přibyl, O.; Mikušík, P. X-Ray Photoelectron Spectroscopic Study of Palladium Particles on Carbon Surfaces. *Czechoslovak Journal of Physics B* **1984,** *34*, 981-988.
(434) Zhang, G.; Yang, D.; Sacher, E. X-Ray Photoelectron Spectroscopic Analysis of Pt Nanoparticles on Highly Oriented Pyrolytic Graphite, Using Symmetric Component Line Shapes. *The Journal of Physical Chemistry C* **2007,** *111*, 565-570.
(435) Marcus, P.; Hinnen, C. Xps Study of the Early Stages of Deposition of Ni, Cu and Pt on Hopg. *Surf. Sci.* **1997,** *392*, 134-142.
(436) Zheng, X.; Chen, W.; Wang, G.; Yu, Y.; Qin, S.; Fang, J.; Wang, F.; Zhang, X.-A. The Raman Redshift of Graphene Impacted by Gold Nanoparticles. *AIP Advances* **2015,** *5*, 057133.
(437) Zhou, J.; Zhou, X.; Sun, X.; Li, R.; Murphy, M.; Ding, Z.; Sun, X.; Sham, T.-K. Interaction between Pt Nanoparticles and Carbon Nanotubes – an X-Ray Absorption near Edge Structures (Xanes) Study. *Chem. Phys. Lett.* **2007,** *437*, 229-232.
(438) Hwang, B. J.; Chen, C.-H.; Sarma, L. S.; Chen, J.-M.; Wang, G.-R.; Tang, M.-T.; Liu, D.-G.; Lee, J.-F. Probing the Formation Mechanism and Chemical States of Carbon-Supported Pt−Ru

Nanoparticles by in Situ X-Ray Absorption Spectroscopy. *The Journal of Physical Chemistry B* **2006,** *110*, 6475-6482.
(439) Şen, F.; Gökağaç, G. Different Sized Platinum Nanoparticles Supported on Carbon: An Xps Study on These Methanol Oxidation Catalysts. *The Journal of Physical Chemistry C* **2007,** *111*, 5715-5720.
(440) Mahmoodinia, M.; Åstrand, P.-O.; Chen, D. Influence of Carbon Support on Electronic Structure and Catalytic Activity of Pt Catalysts: Binding to the Co Molecule. *The Journal of Physical Chemistry C* **2016,** *120*, 12452-12462.
(441) Zhang, B.; Su, D. S. Probing the Metal–Support Interaction in Carbon-Supported Catalysts by Using Electron Microscopy. *ChemCatChem* **2015,** *7*, 3639-3645.
(442) Lykhach, Y.; Kozlov, S. M.; Skála, T.; Tovt, A.; Stetsovych, V.; Tsud, N.; Dvořák, F.; Johánek, V.; Neitzel, A.; Mysliveček, J.et al. Counting Electrons on Supported Nanoparticles. *Nature Materials* **2015,** *15*, 284.
(443) Banerjee, R.; Chen, D. A.; Karakalos, S.; Piedboeuf, M.-L. C.; Job, N.; Regalbuto, J. R. Ambient Oxidation of Ultrasmall Platinum Nanoparticles on Microporous Carbon Catalyst Supports. *ACS Applied Nano Materials* **2018,** *1*, 5876-5884.
(444) Binninger, T.; Schmidt, T. J.; Kramer, D. Capacitive Electronic Metal-Support Interactions: Outer Surface Charging of Supported Catalyst Particles. *Physical Review B* **2017,** *96*, 165405.
(445) Watanabe, M.; Sei, H.; Stonehart, P. The Influence of Platinum Crystallite Size on the Electroreduction of Oxygen. *Journal of Electroanalytical Chemistry and Interfacial Electrochemistry* **1989,** *261*, 375-387.
(446) Lindström, R. W.; Seidel, Y. E.; Jusys, Z.; Gustavsson, M.; Wickman, B.; Kasemo, B.; Behm, R. J. Electrocatalysis and Transport Effects on Nanostructured Pt/Gc Electrodes. *J. Electroanal. Chem.* **2010,** *644*, 90-102.
(447) Yano, H.; Akiyama, T.; Watanabe, M.; Uchida, H. High Durability of Pt/Graphitized Carbon Catalysts for Polymer Electrolyte Fuel Cells Prepared by the Nanocapsule Method. *J. Electroanal. Chem.* **2013,** *688*, 137-142.
(448) Watanabe, M.; Yano, H.; Uchida, H.; Tryk, D. A. Achievement of Distinctively High Durability at Nanosized Pt Catalysts Supported on Carbon Black for Fuel Cell Cathodes. *J. Electroanal. Chem.* **2018,** *819*, 359-364.
(449) Fortunato, G. V.; Pizzutilo, E.; Mingers, A. M.; Kasian, O.; Cherevko, S.; Cardoso, E. S. F.; Mayrhofer, K. J. J.; Maia, G.; Ledendecker, M. Impact of Palladium Loading and Interparticle Distance on the Selectivity for the Oxygen Reduction Reaction toward Hydrogen Peroxide. *The Journal of Physical Chemistry C* **2018,** *122*, 15878-15885.
(450) Yano, H.; Akiyama, T.; Bele, P.; Uchida, H.; Watanabe, M. Durability of Pt/Graphitized Carbon Catalysts for the Oxygen Reduction Reaction Prepared by the Nanocapsule Method. *PCCP* **2010,** *12*, 3806-3814.
(451) Yano, H.; Akiyama, T.; Uchida, H.; Watanabe, M. Temperature Dependence of Oxygen Reduction Activity at Nafion-Coated Pt/Graphitized Carbon Black Catalysts Prepared by the Nanocapsule Method. *Energy & Environmental Science* **2010,** *3*, 1511-1514.
(452) Speder, J.; Altmann, L.; Bäumer, M.; Kirkensgaard, J. J. K.; Mortensen, K.; Arenz, M. The Particle Proximity Effect: From Model to High Surface Area Fuel Cell Catalysts. *RSC Advances* **2014,** *4*, 14971-14978.
(453) Corradini, P. G.; Pires, F. I.; Paganin, V. A.; Perez, J.; Antolini, E. Effect of the Relationship between Particle Size, Inter-Particle Distance, and Metal Loading of Carbon Supported Fuel Cell Catalysts on Their Catalytic Activity. *J. Nanopart. Res.* **2012,** *14*, 1080.
(454) Ma, J.; Habrioux, A.; Morais, C.; Lewera, A.; Vogel, W.; Verde-Gómez, Y.; Ramos-Sanchez, G.; Balbuena, P. B.; Alonso-Vante, N. Spectroelectrochemical Probing of the Strong Interaction between Platinum Nanoparticles and Graphitic Domains of Carbon. *ACS Catalysis* **2013,** *3*, 1940-1950.
(455) Li, X.; Yu, J.; Wageh, S.; Al-Ghamdi, A. A.; Xie, J. Graphene in Photocatalysis: A Review. *Small* **2016,** *12*, 6640-6696.

(456) Gangu, K. K.; Maddila, S.; Jonnalagadda, S. B. A Review on Novel Composites of Mwcnts Mediated Semiconducting Materials as Photocatalysts in Water Treatment. *Sci. Total Environ.* **2019,** *646*, 1398-1412.
(457) Du, A.; Ng, Y. H.; Bell, N. J.; Zhu, Z.; Amal, R.; Smith, S. C. Hybrid Graphene/Titania Nanocomposite: Interface Charge Transfer, Hole Doping, and Sensitization for Visible Light Response. *The Journal of Physical Chemistry Letters* **2011,** *2*, 894-899.
(458) Peng, Y.; Lu, B.; Wang, N.; Li, L.; Chen, S. Impacts of Interfacial Charge Transfer on Nanoparticle Electrocatalytic Activity Towards Oxygen Reduction. *PCCP* **2017,** *19*, 9336-9348.
(459) Peng, Y.; Chen, S. Electrocatalysts Based on Metal@Carbon Core@Shell Nanocomposites: An overview. *Green Energy & Environment* **2018,** *3*, 335-351.
(460) Guo, H.; Qi, Y.; Li, X. Adhesion at Diamond/Metal Interfaces: A Density Functional Theory Study. *J. Appl. Phys.* **2010,** *107*, 033722.
(461) Tiwari, A. K.; Goss, J. P.; Briddon, P. R.; Wright, N. G.; Horsfall, A. B.; Rayson, M. J. Electronic and Structural Properties of Diamond (001) Surfaces Terminated by Selected Transition Metals. *Physical Review B* **2012,** *86*, 155301.
(462) Amit, K. T.; Goss, J. P.; Briddon, P. R.; Horsfall, A. B.; Wright, N. G.; Jones, R.; Rayson, M. J. Unexpected Change in the Electron Affinity of Diamond Caused by the Ultra-Thin Transition Metal Oxide Films. *EPL (Europhysics Letters)* **2014,** *108*, 46005.
(463) Loboda, O. In *Quantum-Chemical Studies on Porphyrins, Fullerenes and Carbon Nanostructures*; Springer Berlin Heidelberg: Berlin, Heidelberg, 2013, DOI:10.1007/978-3-642-31845-0_2 10.1007/978-3-642-31845-0_2.
(464) Akimov, A. V.; Williams, C.; Kolomeisky, A. B. Charge Transfer and Chemisorption of Fullerene Molecules on Metal Surfaces: Application to Dynamics of Nanocars. *The Journal of Physical Chemistry C* **2012,** *116*, 13816-13826.
(465) Mahdy, A. M. E. Dft Study of Hydrogen Storage in Pd-Decorated C60 Fullerene. *Mol. Phys.* **2015,** *113*, 3531-3544.
(466) Leng, F.; Gerber, I. C.; Lecante, P.; Moldovan, S.; Girleanu, M.; Axet, M. R.; Serp, P. Controlled and Chemoselective Hydrogenation of Nitrobenzene over Ru@C60 Catalysts. *ACS Catalysis* **2016,** *6*, 6018-6024.
(467) Leng, F.; Gerber, I. C.; Axet, M. R.; Serp, P. Selectivity Shifts in Hydrogenation of Cinnamaldehyde on Electron-Deficient Ruthenium Nanoparticles. *Comptes Rendus Chimie* **2018,** *21*, 346-353.
(468) Mackie, W. A.; Plumlee, J. E.; Bell, A. E. Work Function Measurements of Diamond Film Surfaces. *Journal of Vacuum Science & Technology B: Microelectronics and Nanometer Structures Processing, Measurement, and Phenomena* **1996,** *14*, 2041-2045.
(469) Liu, P.; Sun, Q.; Zhu, F.; Liu, K.; Jiang, K.; Liu, L.; Li, Q.; Fan, S. Measuring the Work Function of Carbon Nanotubes with Thermionic Method. *Nano Lett.* **2008,** *8*, 647-651.
(470) Shiraishi, M.; Ata, M. Work Function of Carbon Nanotubes. *MRS Proceedings* **2011,** *633*, A4.4.
(471) Shiraishi, M.; Hinokuma, K.; Ata, M. The Measurement of Work Function of Carbon Nanotubes. *AIP Conference Proceedings* **2000,** *544*, 359-362.
(472) Garg, R.; Dutta, N. K.; Choudhury, N. R. Work Function Engineering of Graphene. *Nanomaterials (Basel, Switzerland)* **2014,** *4*, 267-300.
(473) Leenaerts, O.; Partoens, B.; Peeters, F. M.; Volodin, A.; Haesendonck, C. V. The Work Function of Few-Layer Graphene. *J. Phys.: Condens. Matter* **2017,** *29*, 035003.
(474) Skriver, H. L.; Rosengaard, N. M. Surface Energy and Work Function of Elemental Metals. *Physical Review B* **1992,** *46*, 7157-7168.
(475) Trasatti, S. Work Function, Electronegativity, and Electrochemical Behaviour of Metals: Iii. Electrolytic Hydrogen Evolution in Acid Solutions. *Journal of Electroanalytical Chemistry and Interfacial Electrochemistry* **1972,** *39*, 163-184.
(476) Michaelson, H. B. The Work Function of the Elements and Its Periodicity. *J. Appl. Phys.* **1977,** *48*, 4729-4733.

(477) Zhou, L.; Zachariah, M. R. Size Resolved Particle Work Function Measurement of Free Nanoparticles: Aggregates Vs. Spheres. *Chem. Phys. Lett.* **2012,** *525-526*, 77-81.
(478) Meiwes-Broer, K. H. Work Functions of Metal Clusters. *Hyperfine Interact.* **1994,** *89*, 263-269.
(479) Bader, R. F. W. *Atoms in Molecules. A Quantum Theory.* ; Oxford University press: Oxford, 1990.
(480) Nakada, K. I., Akira In *Graphene Simulation*; Gong, J. R., Ed.; IntechOpen, 2011, DOI:10.5772/20477 10.5772/20477.
(481) Sigal, A.; Rojas, M. I.; Leiva, E. P. M. Interferents for Hydrogen Storage on a Graphene Sheet Decorated with Nickel: A Dft Study. *Int. J. Hydrogen Energy* **2011,** *36*, 3537-3546.
(482) Ding, M.; Tang, Y.; Star, A. Understanding Interfaces in Metal–Graphitic Hybrid Nanostructures. *The Journal of Physical Chemistry Letters* **2013,** *4*, 147-160.
(483) Kauffman, D. R.; Sorescu, D. C.; Schofield, D. P.; Allen, B. L.; Jordan, K. D.; Star, A. Understanding the Sensor Response of Metal-Decorated Carbon Nanotubes. *Nano Lett.* **2010,** *10*, 958-963.
(484) Lopez-Salido, I.; Lim, D. C.; Dietsche, R.; Bertram, N.; Kim, Y. D. Electronic and Geometric Properties of Au Nanoparticles on Highly Ordered Pyrolytic Graphite (Hopg) Studied Using X-Ray Photoelectron Spectroscopy (Xps) and Scanning Tunneling Microscopy (Stm). *The Journal of Physical Chemistry B* **2006,** *110*, 1128-1136.
(485) Legesse, M.; Mellouhi, F. E.; Bentria, E. T.; Madjet, M. E.; Fisher, T. S.; Kais, S.; Alharbi, F. H. Reduced Work Function of Graphene by Metal Adatoms. *Appl. Surf. Sci.* **2017,** *394*, 98-107.
(486) Johll, H.; Kang, H. C.; Tok, E. S. Density Functional Theory Study of Fe, Co, and Ni Adatoms and Dimers Adsorbed on Graphene. *Physical Review B* **2009,** *79*, 245416.
(487) Tabtimsai, C.; Ruangpornvisuti, V.; Wanno, B. Density Functional Theory Investigation of the Viiib Transition Metal Atoms Deposited on (5,5) Single-Walled Carbon Nanotubes. *Physica E: Low-dimensional Systems and Nanostructures* **2013,** *49*, 61-67.
(488) Seenithurai, S.; Kodi Pandyan, R.; Vinodh Kumar, S.; Mahendran, M. H2 Adsorption in Ni and Passivated Ni Doped 4 å Single Walled Carbon Nanotube. *Int. J. Hydrogen Energy* **2013,** *38*, 7376-7381.
(489) Gao, H.; Zhao, J. First-Principles Study of Ru Atoms and Clusters Adsorbed Outside and inside Carbon Nanotubes. *The Journal of Chemical Physics* **2010,** *132*, 234704.
(490) Vo, T.; Wu, Y.-D.; Car, R.; Robert, M. Structures, Interactions, and Ferromagnetism of Fe−Carbon Nanotube Systems. *The Journal of Physical Chemistry C* **2008,** *112*, 8400-8407.
(491) Ramos-Sanchez, G.; Balbuena, P. B. Interactions of Platinum Clusters with a Graphite Substrate. *PCCP* **2013,** *15*, 11950-11959.
(492) Matsutsu, M.; Petersen, M. A.; van Steen, E. Pt38 Cluster on Oh- and Cooh-Functionalised Graphene as a Model for Pt/C-Catalysts. *PCCP* **2016,** *18*, 25693-25704.
(493) Ma, J.; Habrioux, A.; Luo, Y.; Ramos-Sanchez, G.; Calvillo, L.; Granozzi, G.; Balbuena, P. B.; Alonso-Vante, N. Electronic Interaction between Platinum Nanoparticles and Nitrogen-Doped Reduced Graphene Oxide: Effect on the Oxygen Reduction Reaction. *Journal of Materials Chemistry A* **2015,** *3*, 11891-11904.
(494) G. Verga, L.; Russell, A. E.; Skylaris, C. K. Ethanol, O, and Co Adsorption on Pt Nanoparticles: Effects of Nanoparticle Size and Graphene Support. *PCCP* **2018,** *20*, 25918-25930.
(495) Adjizian, J. J.; De Marco, P.; Suarez-Martinez, I.; El Mel, A. A.; Snyders, R.; Gengler, R. Y. N.; Rudolf, P.; Ke, X.; Van Tendeloo, G.; Bittencourt, C.et al. Platinum and Palladium on Carbon Nanotubes: Experimental and Theoretical Studies. *Chem. Phys. Lett.* **2013,** *571*, 44-48.
(496) Schneider, W. B.; Benedikt, U.; Auer, A. A. Interaction of Platinum Nanoparticles with Graphitic Carbon Structures: A Computational Study. *ChemPhysChem* **2013,** *14*, 2984-2989.
(497) Subrahmanyam, K. S.; Manna, A. K.; Pati, S. K.; Rao, C. N. R. A Study of Graphene Decorated with Metal Nanoparticles. *Chem. Phys. Lett.* **2010,** *497*, 70-75.
(498) Poidevin, C.; Paciok, P.; Heggen, M.; Auer, A. A. High Resolution Transmission Electron Microscopy and Electronic Structure Theory Investigation of Platinum Nanoparticles on Carbon Black. *The Journal of Chemical Physics* **2019,** *150*, 041705.

(499) Yang, J.; Kim, S. H.; Kwak, S. K.; Song, H.-K. Curvature-Induced Metal–Support Interaction of an Islands-by-Islands Composite of Platinum Catalyst and Carbon Nano-Onion for Durable Oxygen Reduction. *ACS Applied Materials & Interfaces* **2017,** *9*, 23302-23308.
(500) Verga, L. G.; Aarons, J.; Sarwar, M.; Thompsett, D.; Russell, A. E.; Skylaris, C. K. Effect of Graphene Support on Large Pt Nanoparticles. *PCCP* **2016,** *18*, 32713-32722.
(501) Qi, Q.; Liu, H.; Feng, W.; Tian, H.; Xu, H.; Huang, X. Theoretical Investigation on the Interaction of Subnano Platinum Clusters with Graphene Using Dft Methods. *Computational Materials Science* **2015,** *96*, 268-276.
(502) Wang, J.-g.; Lv, Y.-a.; Li, X.-n.; Dong, M. Point-Defect Mediated Bonding of Pt Clusters on (5,5) Carbon Nanotubes. *The Journal of Physical Chemistry C* **2009,** *113*, 890-893.
(503) Gerber, I. C.; Poteau, R. Critical Assessment of Charge Transfer Estimates in Non-Covalent Graphene Doping. *Theoretical Chemistry Accounts* **2018,** *137*, 156.
(504) Ritz, B.; Heller, H.; Myalitsin, A.; Kornowski, A.; Martin-Martinez, F. J.; Melchor, S.; Dobado, J. A.; Juárez, B. H.; Weller, H.; Klinke, C. Reversible Attachment of Platinum Alloy Nanoparticles to Nonfunctionalized Carbon Nanotubes. *ACS Nano* **2010,** *4*, 2438-2444.
(505) Zhang, X.; Dai, Z.; Wei, L.; Liang, N.; Wu, X. Theoretical Calculation of the Gas-Sensing Properties of Pt-Decorated Carbon Nanotubes. *Sensors* **2013,** *13*, 15159.
(506) Cuong, N. T.; Sugiyama, A.; Fujiwara, A.; Mitani, T.; Chi, D. H. Density Functional Study of ${\Text{Pt}}_{4}$ Clusters Adsorbed on a Carbon Nanotube Support. *Physical Review B* **2009,** *79*, 235417.
(507) Chi, D. H.; Cuong, N. T.; Tuan, N. A.; Kim, Y.-T.; Bao, H. T.; Mitani, T.; Ozaki, T.; Nagao, H. Electronic Structures of Pt Clusters Adsorbed on (5,5) Single Wall Carbon Nanotube. *Chem. Phys. Lett.* **2006,** *432*, 213-217.
(508) Cuong, N. T.; Chi, D. H.; Kim, Y.-T.; Mitani, T. Structural and Electronic Properties of Ptn (N = 3, 7, 13) Clusters on Metallic Single Wall Carbon Nanotube. *physica status solidi (b)* **2006,** *243*, 3472-3475.
(509) Zhou, S.; Lin, S.; Guo, H. First-Principles Insights into Ammonia Decomposition Catalyzed by Ru Clusters Anchored on Carbon Nanotubes: Size Dependence and Interfacial Effects. *The Journal of Physical Chemistry C* **2018,** *122*, 9091-9100.
(510) Liu, X.; Yao, K. X.; Meng, C.; Han, Y. Graphene Substrate-Mediated Catalytic Performance Enhancement of Ru Nanoparticles: A First-Principles Study. *Dalton Transactions* **2012,** *41*, 1289-1296.
(511) Gialampouki, M. A.; Lekka, C. E. Tin Decoration of Single-Wall Carbon Nanotubes and Graphene by Density Functional Theory Computations. *The Journal of Physical Chemistry C* **2011,** *115*, 15172-15181.
(512) Srivastava, M. K.; Wang, Y.; Kemper, A. F.; Cheng, H.-P. Density Functional Study of Gold and Iron Clusters on Perfect and Defected Graphene. *Physical Review B* **2012,** *85*, 165444.
(513) Parambhath, V. B.; Nagar, R.; Sethupathi, K.; Ramaprabhu, S. Investigation of Spillover Mechanism in Palladium Decorated Hydrogen Exfoliated Functionalized Graphene. *The Journal of Physical Chemistry C* **2011,** *115*, 15679-15685.
(514) Kunaseth, M.; Mudchimo, T.; Namuangruk, S.; Kungwan, N.; Promarak, V.; Jungsuttiwong, S. A Dft Study of Arsine Adsorption on Palladium Doped Graphene: Effects of Palladium Cluster Size. *Applied Surface Science* **2016,** *367*, 552-558.
(515) Martins, P. M.; Ferreira, C. G.; Silva, A. R.; Magalhães, B.; Alves, M. M.; Pereira, L.; Marques, P. A. A. P.; Melle-Franco, M.; Lanceros-Méndez, S. Tio2/Graphene and Tio2/Graphene Oxide Nanocomposites for Photocatalytic Applications: A Computer Modeling and Experimental Study. *Composites Part B: Engineering* **2018,** *145*, 39-46.
(516) Saha, A.; Moya, A.; Kahnt, A.; Iglesias, D.; Marchesan, S.; Wannemacher, R.; Prato, M.; Vilatela, J. J.; Guldi, D. M. Interfacial Charge Transfer in Functionalized Multi-Walled Carbon Nanotube@Tio2 Nanofibres. *Nanoscale* **2017,** *9*, 7911-7921.

(517) Long, R. Electronic Structure of Semiconducting and Metallic Tubes in Tio2/Carbon Nanotube Heterojunctions: Density Functional Theory Calculations. *The Journal of Physical Chemistry Letters* **2013,** *4*, 1340-1346.
(518) Kiarii, E. M.; Govender, K. K.; Ndungu, P. G.; Govender, P. P. Recent Advances in Titanium Dioxide/Graphene Photocatalyst Materials as Potentials of Energy Generation. *Bull. Mater. Sci.* **2018,** *41*, 75.
(519) Kashiwaya, S.; Morasch, J.; Streibel, V.; Toupance, T.; Jaegermann, W.; Klein, A. The Work Function of Tio2. *Surfaces* **2018,** *1*, 7.
(520) Gupta, S.; Carrizosa, S. B.; Jasinski, J.; Dimakis, N. Charge Transfer Dynamical Processes at Graphene-Transition Metal Oxides/Electrolyte Interface for Energy Storage: Insights from in-Situ Raman Spectroelectrochemistry. *AIP Advances* **2018,** *8*, 065225.
(521) Kim, G.; Jhi, S.-H.; Park, N.; Louie, S. G.; Cohen, M. L. Optimization of Metal Dispersion in Doped Graphitic Materials for Hydrogen Storage. *Physical Review B* **2008,** *78*, 085408.
(522) Tang, Y.; Yang, Z.; Dai, X. Trapping of Metal Atoms in the Defects on Graphene. *The Journal of Chemical Physics* **2011,** *135*, 224704.
(523) Ali, S.; Fu Liu, T.; Lian, Z.; Li, B.; Sheng Su, D. The Effect of Defects on the Catalytic Activity of Single Au Atom Supported Carbon Nanotubes and Reaction Mechanism for Co Oxidation. *PCCP* **2017,** *19*, 22344-22354.
(524) Ambrusi, R. E.; Luna, C. R.; Juan, A.; Pronsato, M. E. Dft Study of Rh-Decorated Pristine, B-Doped and Vacancy Defected Graphene for Hydrogen Adsorption. *RSC Advances* **2016,** *6*, 83926-83941.
(525) Dai, G.; Chen, L.; Zhao, X. Tungsten-Embedded Graphene: Theoretical Study on a Potential High-Activity Catalyst toward Co Oxidation. *Materials* **2018,** *11*, 1848.
(526) Jia, T.-T.; Lu, C.-H.; Ding, K.-N.; Zhang, Y.-F.; Chen, W.-K. Oxidation of Pdn (N=1–5) Clusters on Single Vacancy Graphene: A First-Principles Study. *Computational and Theoretical Chemistry* **2013,** *1020*, 91-99.
(527) Liu, X.; Li, L.; Meng, C.; Han, Y. Palladium Nanoparticles/Defective Graphene Composites as Oxygen Reduction Electrocatalysts: A First-Principles Study. *The Journal of Physical Chemistry C* **2012,** *116*, 2710-2719.
(528) Fampiou, I.; Ramasubramaniam, A. Binding of Pt Nanoclusters to Point Defects in Graphene: Adsorption, Morphology, and Electronic Structure. *The Journal of Physical Chemistry C* **2012,** *116*, 6543-6555.
(529) Gasper, R. J.; Ramasubramaniam, A. Density Functional Theory Studies of the Methanol Decomposition Reaction on Graphene-Supported Pt13 Nanoclusters. *The Journal of Physical Chemistry C* **2016,** *120*, 17408-17417.
(530) Yang, G. M.; Fan, X. F.; Shi, S.; Huang, H. H.; Zheng, W. T. Stability of Ptn Cluster on Free/Defective Graphene: A First-Principles Study. *Appl. Surf. Sci.* **2017,** *392*, 936-941.
(531) Shi, H.; Auerbach, S. M.; Ramasubramaniam, A. First-Principles Predictions of Structure–Function Relationships of Graphene-Supported Platinum Nanoclusters. *The Journal of Physical Chemistry C* **2016,** *120*, 11899-11909.
(532) García-Rodríguez, D. E.; Mendoza-Huizar, L. H.; Díaz, C. A Dft Study of Cu Nanoparticles Adsorbed on Defective Graphene. *Applied Surface Science* **2017,** *412*, 146-151.
(533) Lim, D.-H.; Negreira, A. S.; Wilcox, J. Dft Studies on the Interaction of Defective Graphene-Supported Fe and Al Nanoparticles. *The Journal of Physical Chemistry C* **2011,** *115*, 8961-8970.
(534) Sen, D.; Thapa, R.; Chattopadhyay, K. K. Small Pd Cluster Adsorbed Double Vacancy Defect Graphene Sheet for Hydrogen Storage: A First-Principles Study. *Int. J. Hydrogen Energy* **2013,** *38*, 3041-3049.
(535) Cheng, H.; Kvande, I.; Zhu, Y.-A.; Hammer, N.; Rønning, M.; Walmsley, J. C.; Li, P.; Qi, Z.; Zhou, X.-G.; Chen, D. Decoding Atomic-Level Structures of the Interface between Pt Sub-Nanocrystals and Nanostructured Carbon. *The Journal of Physical Chemistry C* **2018,** *122*, 7166-7178.
(536) Pavlov, S. V.; Kislenko, S. A. Graphene Electrochemistry: Edge Vs. Basal Plane Sites. *Journal of Physics: Conference Series* **2018,** *1092*, 012112.

(537) Yuan, W.; Zhou, Y.; Li, Y.; Li, C.; Peng, H.; Zhang, J.; Liu, Z.; Dai, L.; Shi, G. The Edge- and Basal-Plane-Specific Electrochemistry of a Single-Layer Graphene Sheet. *Scientific Reports* **2013,** *3*, 2248.
(538) Wei, N.; Chang, C.; Zhu, H.; Xu, Z. Mechanotunable Monatomic Metal Structures at Graphene Edges. *PCCP* **2014,** *16*, 10295-10300.
(539) Yang, N.; Yang, D.; Chen, L.; Liu, D.; Cai, M.; Fan, X. Design and Adjustment of the Graphene Work Function Via Size, Modification, Defects, and Doping: A First-Principle Theory Study. *Nanoscale Research Letters* **2017,** *12*, 642.
(540) Gholizadeh, R.; Yu, Y.-X. Work Functions of Pristine and Heteroatom-Doped Graphenes under Different External Electric Fields: An Ab Initio Dft Study. *The Journal of Physical Chemistry C* **2014,** *118*, 28274-28282.
(541) Kumar, P. V.; Bernardi, M.; Grossman, J. C. The Impact of Functionalization on the Stability, Work Function, and Photoluminescence of Reduced Graphene Oxide. *ACS Nano* **2013,** *7*, 1638-1645.
(542) Akada, K.; Terasawa, T.-o.; Imamura, G.; Obata, S.; Saiki, K. Control of Work Function of Graphene by Plasma Assisted Nitrogen Doping. *Appl. Phys. Lett.* **2014,** *104*, 131602.
(543) Park, M.; Kim, B.-H.; Kim, S.; Han, D.-S.; Kim, G.; Lee, K.-R. Improved Binding between Copper and Carbon Nanotubes in a Composite Using Oxygen-Containing Functional Groups. *Carbon* **2011,** *49*, 811-818.
(544) Mahmoodinia, M.; Åstrand, P.-O.; Chen, D. Tuning the Electronic Properties of Single-Atom Pt Catalysts by Functionalization of the Carbon Support Material. *The Journal of Physical Chemistry C* **2017,** *121*, 20802-20812.
(545) Li, J.; Wang, Y.; Song, J.; Gao, Q.; Zhang, J.; Zhang, J.; Zhai, D.; Zhou, J.; Liu, Q.; Xu, Z. P.et al. Theoretical and Experimental Evidence for the Carbon–Oxygen Group Enhancement of No Reduction. *Environmental Science & Technology* **2017,** *51*, 14209-14216.
(546) Charlier, J. C.; Arnaud, L.; Avilov, I. V.; Delgado, M.; Demoisson, F.; Espinosa, E. H.; Ewels, C. P.; Felten, A.; Guillot, J.; Ionescu, R.et al. Carbon Nanotubes Randomly Decorated with Gold Clusters: From Nano2hybrid Atomic Structures to Gas Sensing Prototypes. *Nanotechnology* **2009,** *20*, 375501.
(547) Makaremi, M.; Mortazavi, B.; Singh, C. V. Adsorption of Metallic, Metalloidic, and Nonmetallic Adatoms on Two-Dimensional C3n. *The Journal of Physical Chemistry C* **2017,** *121*, 18575-18583.
(548) Huang, X.; Yan, H.; Huang, L.; Zhang, X.; Lin, Y.; Li, J.; Xia, Y.; Ma, Y.; Sun, Z.; Wei, S.et al. Toward Understanding of the Support Effect on Pd1 Single-Atom-Catalyzed Hydrogenation Reactions. *The Journal of Physical Chemistry C* **2018**, DOI:10.1021/acs.jpcc.8b07181 10.1021/acs.jpcc.8b07181.
(549) Chen, P.; Chew, L. M.; Kostka, A.; Muhler, M.; Xia, W. The Structural and Electronic Promoting Effect of Nitrogen-Doped Carbon Nanotubes on Supported Pd Nanoparticles for Selective Olefin Hydrogenation. *Catalysis Science & Technology* **2013,** *3*, 1964-1971.
(550) Acharya, C. K.; Sullivan, D. I.; Turner, C. H. Characterizing the Interaction of Pt and Ptru Clusters with Boron-Doped, Nitrogen-Doped, and Activated Carbon: Density Functional Theory Calculations and Parameterization. *The Journal of Physical Chemistry C* **2008,** *112*, 13607-13622.
(551) Rangel, E.; Sansores, E. Theoretical Study of Hydrogen Adsorption on Nitrogen Doped Graphene Decorated with Palladium Clusters. *Int. J. Hydrogen Energy* **2014,** *39*, 6558-6566.
(552) He, Z.; Dong, B.; Wang, W.; Yang, G.; Cao, Y.; Wang, H.; Yang, Y.; Wang, Q.; Peng, F.; Yu, H. Elucidating Interaction between Palladium and N-Doped Carbon Nanotubes: Effect of Electronic Property on Activity for Nitrobenzene Hydrogenation. *ACS Catalysis* **2019**, DOI:10.1021/acscatal.8b03965 10.1021/acscatal.8b03965.
(553) Ning, X.; Li, Y.; Dong, B.; Wang, H.; Yu, H.; Peng, F.; Yang, Y. Electron Transfer Dependent Catalysis of Pt on N-Doped Carbon Nanotubes: Effects of Synthesis Method on Metal-Support Interaction. *J. Catal.* **2017,** *348*, 100-109.

(554) Ning, X.; Yu, H.; Peng, F.; Wang, H. Pt Nanoparticles Interacting with Graphitic Nitrogen of N-Doped Carbon Nanotubes: Effect of Electronic Properties on Activity for Aerobic Oxidation of Glycerol and Electro-Oxidation of Co. *J. Catal.* **2015,** *325*, 136-144.
(555) Yun, Y. S.; Park, H.; Yun, D.; Song, C. K.; Kim, T. Y.; Lee, K. R.; Kim, Y.; Han, J. W.; Yi, J. Tuning the Electronic State of Metal/Graphene Catalysts for the Control of Catalytic Activity Via N- and B-Doping into Graphene. *Chem. Commun.* **2018,** *54*, 7147-7150.
(556) Ambrusi, R. E.; Pronsato, M. E. Dft Study of Rh and Ti Dimers Decorating N-Doped Pyridinic and Pyrrolic Graphene for Molecular and Dissociative Hydrogen Adsorption. *Appl. Surf. Sci.* **2019,** *464*, 243-254.
(557) Porter, L. A.; Choi, H. C.; Schmeltzer, J. M.; Ribbe, A. E.; Elliott, L. C. C.; Buriak, J. M. Electroless Nanoparticle Film Deposition Compatible with Photolithography, Microcontact Printing, and Dip-Pen Nanolithography Patterning Technologies. *Nano Lett.* **2002,** *2*, 1369-1372.
(558) Shaikhutdinov, S. K.; Kochubey, D. I. Scanning Tunneling Microscopy Study of Porous Carbon Impregnated with Palladium Chloride. *Catal. Lett.* **1994,** *28*, 343-350.
(559) Simonov, P. A.; Troitskii, S. Y.; Likholobov, V. A. Preparation of the Pd/C Catalysts: A Molecular-Level Study of Active Site Formation. *Kinet. Catal.* **2000,** *41*, 255-269.
(560) Choi, H. C.; Shim, M.; Bangsaruntip, S.; Dai, H. Spontaneous Reduction of Metal Ions on the Sidewalls of Carbon Nanotubes. *J. Am. Chem. Soc.* **2002,** *124*, 9058-9059.
(561) Wei, Z. D.; Yan, C.; Tan, Y.; Li, L.; Sun, C. X.; Shao, Z. G.; Shen, P. K.; Dong, H. W. Spontaneous Reduction of Pt(Iv) onto the Sidewalls of Functionalized Multiwalled Carbon Nanotubes as Catalysts for Oxygen Reduction Reaction in Pemfcs. *The Journal of Physical Chemistry C* **2008,** *112*, 2671-2677.
(562) Chen, J.; Wang, M.; Liu, B.; Fan, Z.; Cui, K.; Kuang, Y. Platinum Catalysts Prepared with Functional Carbon Nanotube Defects and Its Improved Catalytic Performance for Methanol Oxidation. *The Journal of Physical Chemistry B* **2006,** *110*, 11775-11779.
(563) Kong, B.-S.; Geng, J.; Jung, H.-T. Layer-by-Layer Assembly of Graphene and Gold Nanoparticles by Vacuum Filtration and Spontaneous Reduction of Gold Ions. *Chem. Commun.* **2009**, DOI:10.1039/B821920F 10.1039/B821920F, 2174-2176.
(564) Benayad, A.; Shin, H.-J.; Park, H. K.; Yoon, S.-M.; Kim, K. K.; Jin, M. H.; Jeong, H.-K.; Lee, J. C.; Choi, J.-Y.; Lee, Y. H. Controlling Work Function of Reduced Graphite Oxide with Au-Ion Concentration. *Chem. Phys. Lett.* **2009,** *475*, 91-95.
(565) Qi, H.; Yu, P.; Wang, Y.; Han, G.; Liu, H.; Yi, Y.; Li, Y.; Mao, L. Graphdiyne Oxides as Excellent Substrate for Electroless Deposition of Pd Clusters with High Catalytic Activity. *J. Am. Chem. Soc.* **2015,** *137*, 5260-5263.
(566) Zhang, Z.; Sun, T.; Chen, C.; Xiao, F.; Gong, Z.; Wang, S. Bifunctional Nanocatalyst Based on Three-Dimensional Carbon Nanotube–Graphene Hydrogel Supported Pd Nanoparticles: One-Pot Synthesis and Its Catalytic Properties. *ACS Applied Materials & Interfaces* **2014,** *6*, 21035-21040.
(567) Sun, L.-z.; Yi, Q.-f. Spontaneous Reduction of Palladium Chloride on Surface of Carbon Materials to Produce Electrochemical Catalysts for Ethanol Oxidation. *New Carbon Materials* **2015,** *30*, 150-155.
(568) Sun, T.; Levin, B. D. A.; Guzman, J. J. L.; Enders, A.; Muller, D. A.; Angenent, L. T.; Lehmann, J. Rapid Electron Transfer by the Carbon Matrix in Natural Pyrogenic Carbon. *Nature Communications* **2017,** *8*, 14873.
(569) Corma, A.; Garcia, H.; Leyva, A. Catalytic Activity of Palladium Supported on Single Wall Carbon Nanotubes Compared to Palladium Supported on Activated Carbon: Study of the Heck and Suzuki Couplings, Aerobic Alcohol Oxidation and Selective Hydrogenation. *J. Mol. Catal. A: Chem.* **2005,** *230*, 97-105.
(570) Wang, X.; Huang, P.; Feng, L.; He, M.; Guo, S.; Shen, G.; Cui, D. Green Controllable Synthesis of Silver Nanomaterials on Graphene Oxide Sheets Via Spontaneous Reduction. *RSC Advances* **2012,** *2*, 3816-3822.

(571) Shin, D.-W.; Meng, X.; Lee, J. H.; Yu, S. M.; Yoo, J. H.; Lim, K. S.; Patole, S. P.; Yoo, J.-B. Doping and Dedoping in Swcnt Film by the Spontaneous Redox Process. *The Journal of Physical Chemistry C* **2011,** *115*, 18327-18332.
(572) Ma, S.-B.; Ahn, K.-Y.; Lee, E.-S.; Oh, K.-H.; Kim, K.-B. Synthesis and Characterization of Manganese Dioxide Spontaneously Coated on Carbon Nanotubes. *Carbon* **2007,** *45*, 375-382.
(573) Song, S.; Rao, R.; Yang, H.; Zhang, A. Cu2o/Mwcnts Prepared by Spontaneous Redox: Growth Mechanism and Superior Catalytic Activity. *The Journal of Physical Chemistry C* **2010,** *114*, 13998-14003.
(574) Liu, X.; Huber, T. A.; Kopac, M. C.; Pickup, P. G. Ru Oxide/Carbon Nanotube Composites for Supercapacitors Prepared by Spontaneous Reduction of Ru(Vi) and Ru(Vii). *Electrochim. Acta* **2009,** *54*, 7141-7147.
(575) Wu, J.; Ong, S. W.; Kang, H. C.; Tok, E. S. Hydrogen Adsorption on Mixed Platinum and Nickel Nanoclusters: The Influence of Cluster Composition and Graphene Support. *The Journal of Physical Chemistry C* **2010,** *114*, 21252-21261.
(576) Kim, B.-H.; Lee, K.-R.; Chung, Y.-C.; Park, M. Functionalization Effect on a Pt/Carbon Nanotube Composite Catalyst: A First-Principles Study. *PCCP* **2016,** *18*, 22687-22692.
(577) Fampiou, I.; Ramasubramaniam, A. Co Adsorption on Defective Graphene-Supported Pt13 Nanoclusters. *The Journal of Physical Chemistry C* **2013,** *117*, 19927-19933.
(578) Lim, D.-H.; Wilcox, J. Dft-Based Study on Oxygen Adsorption on Defective Graphene-Supported Pt Nanoparticles. *The Journal of Physical Chemistry C* **2011,** *115*, 22742-22747.
(579) Yumura, T.; Kimura, K.; Kobayashi, H.; Tanaka, R.; Okumura, N.; Yamabe, T. The Use of Nanometer-Sized Hydrographene Species for Support Material for Fuel Cell Electrode Catalysts: A Theoretical Proposal. *PCCP* **2009,** *11*, 8275-8284.
(580) Yumura, T.; Awano, T.; Kobayashi, H.; Yamabe, T. Platinum Clusters on Vacancy-Type Defects of Nanometer-Sized Graphene Patches. *Molecules (Basel, Switzerland)* **2012,** *17*, 7941-7960.
(581) Tang, Y.; Yang, Z.; Dai, X. A Theoretical Simulation on the Catalytic Oxidation of Co on Pt/Graphene. *PCCP* **2012,** *14*, 16566-16572.
(582) Tang, Y.; Dai, X.; Yang, Z.; Pan, L.; Chen, W.; Ma, D.; Lu, Z. Formation and Catalytic Activity of Pt Supported on Oxidized Graphene for the Co Oxidation Reaction. *PCCP* **2014,** *16*, 7887-7895.
(583) Zhang, X.; Lu, Z.; Xu, G.; Wang, T.; Ma, D.; Yang, Z.; Yang, L. Single Pt Atom Stabilized on Nitrogen Doped Graphene: Co Oxidation Readily Occurs Via the Tri-Molecular Eley–Rideal Mechanism. *PCCP* **2015,** *17*, 20006-20013.
(584) Lu, Y.-H.; Zhou, M.; Zhang, C.; Feng, Y.-P. Metal-Embedded Graphene: A Possible Catalyst with High Activity. *The Journal of Physical Chemistry C* **2009,** *113*, 20156-20160.
(585) Li, Y.; Zhou, Z.; Yu, G.; Chen, W.; Chen, Z. Co Catalytic Oxidation on Iron-Embedded Graphene: Computational Quest for Low-Cost Nanocatalysts. *The Journal of Physical Chemistry C* **2010,** *114*, 6250-6254.
(586) Wu, P.; Du, P.; Zhang, H.; Cai, C. Graphyne-Supported Single Fe Atom Catalysts for Co Oxidation. *PCCP* **2015,** *17*, 1441-1449.
(587) Tang, Y.; Zhou, J.; Shen, Z.; Chen, W.; Li, C.; Dai, X. High Catalytic Activity for Co Oxidation on Single Fe Atom Stabilized in Graphene Vacancies. *RSC Advances* **2016,** *6*, 93985-93996.
(588) Zhao, M. Y.; Zhao, R. M.; Niu, M. M.; Li, W.; Ma, Y. Q.; Li, Y.; Tang, Y. N.; Dai, X. Q. Promotion of Co Oxidation on the Fe/Nxclusters Embedded Graphene. *Appl. Phys. A* **2017,** *123*, 199.
(589) Deng, Q.; Zhao, L.; Gao, X.; Zhang, M.; Luo, Y.; Zhao, Y. Single Layer of Polymeric Cobalt Phthalocyanine: Promising Low-Cost and High-Activity Nanocatalysts for Co Oxidation. *Small* **2013,** *9*, 3506-3513.
(590) Tang, Y.; Ma, D.; Chen, W.; Dai, X. Improving the Adsorption Behavior and Reaction Activity of Co-Anchored Graphene Surface toward Co and O2 Molecules. *Sensors and Actuators B: Chemical* **2015,** *211*, 227-234.
(591) Xu, X.-Y.; Li, J.; Xu, H.; Xu, X.; Zhao, C. Dft Investigation of Ni-Doped Graphene: Catalytic Ability to Co Oxidation. *New J. Chem.* **2016,** *40*, 9361-9369.

(592) Song, E. H.; Wen, Z.; Jiang, Q. Co Catalytic Oxidation on Copper-Embedded Graphene. *The Journal of Physical Chemistry C* **2011,** *115*, 3678-3683.
(593) Esrafili, M. D.; Mousavian, P. A Dft Study on the Possibility of Using a Single Cu Atom Incorporated Nitrogen-Doped Graphene as a Promising and Highly Active Catalyst for Oxidation of Co. *Int. J. Quantum Chem 0*, e25857.
(594) Gu, Y.; Chen, X.; Cao, Y.; Zhuang, G.; Zhong, X.; Wang, J. Atomically Dispersed Pd Catalysts in Graphyne Nanopore: Formation and Reactivity. *Nanotechnology* **2017,** *28*, 295403.
(595) Esrafili, M. D.; Asadollahi, S. Exploring Different Reaction Mechanisms for Oxidation of Co over a Single Pd Atom Incorporated Nitrogen-Doped Graphene: A Dft Study. *Appl. Surf. Sci.* **2019,** *463*, 526-534.
(596) Jiang, Q.; Zhang, J.; Ao, Z.; Huang, H.; He, H.; Wu, Y. First Principles Study on the Co Oxidation on Mn-Embedded Divacancy Graphene. *Frontiers in chemistry* **2018,** *6*, 187-187.
(597) Tang, J.-Y.; Shen, J.-S.; Chen, L.; Jiang, J.-W.; Lu, J.; Zhao, X.; Dai, G.-L. Investigation of Carbon Monoxide Catalytic Oxidation on Vanadium-Embedded Graphene. *Monatshefte für Chemie - Chemical Monthly* **2018,** *149*, 1349-1356.
(598) Dai, G.; Chen, L.; Zhao, X. Catalytic Oxidation Mechanisms of Carbon Monoxide over Single and Double Vacancy Cr-Embedded Graphene. *Journal of Materials Science* **2019,** *54*, 1395-1408.
(599) Esrafili, M. D.; Heydari, S. Co Oxidation Catalyzed by a Single Ti Atom Supported on Divacancy Defective Graphene: A Dispersion-Corrected Dft Study. *ChemistrySelect* **2018,** *3*, 4471-4479.
(600) Jiang, Q. G.; Ao, Z. M.; Li, S.; Wen, Z. Density Functional Theory Calculations on the Co Catalytic Oxidation on Al-Embedded Graphene. *RSC Advances* **2014,** *4*, 20290-20296.
(601) Esrafili, M. D.; Nematollahi, P.; Abdollahpour, H. A Comparative Dft Study on the Co Oxidation Reaction over Al- and Ge-Embedded Graphene as Efficient Metal-Free Catalysts. *Appl. Surf. Sci.* **2016,** *378*, 418-425.
(602) Jiang, Q.; Deng, J. Ab Initio Study on the Co Oxidation on Zn-Doped Graphene. *AIP Conference Proceedings* **2018,** *1944*, 020067.
(603) Zhou, M.; Zhang, A.; Dai, Z.; Zhang, C.; Feng, Y. P. Greatly Enhanced Adsorption and Catalytic Activity of Au and Pt Clusters on Defective Graphene. *The Journal of Chemical Physics* **2010,** *132*, 194704.
(604) Fampiou, I.; Ramasubramaniam, A. Influence of Support Effects on Co Oxidation Kinetics on Co-Saturated Graphene-Supported Pt13 Nanoclusters. *The Journal of Physical Chemistry C* **2015,** *119*, 8703-8710.
(605) Yuan, D. W.; Liu, C.; Liu, Z. R. Structures and Catalytic Properties of Pdmaun (M+N=7) Bimetallic Clusters Supported on Graphene by First-Principles Studies. *Phys. Lett. A* **2014,** *378*, 408-415.
(606) Amaya-Roncancio, S.; García Blanco, A. A.; Linares, D. H.; Sapag, K. Dft Study of Hydrogen Adsorption on Ni/Graphene. *Appl. Surf. Sci.* **2018,** *447*, 254-260.
(607) Kim, G.; Jhi, S.-H.; Park, N. Effective Metal Dispersion in Pyridinelike Nitrogen Doped Graphenes for Hydrogen Storage. *Appl. Phys. Lett.* **2008,** *92*, 013106.
(608) Rangel, E.; Sansores, E.; Vallejo, E.; Hernández-Hernández, A.; López-Pérez, P. A. Study of the Interplay between N-Graphene Defects and Small Pd Clusters for Enhanced Hydrogen Storage Via a Spill-over Mechanism. *PCCP* **2016,** *18*, 33158-33170.
(609) Cabria, I.; López, M. J.; Fraile, S.; Alonso, J. A. Adsorption and Dissociation of Molecular Hydrogen on Palladium Clusters Supported on Graphene. *The Journal of Physical Chemistry C* **2012,** *116*, 21179-21189.
(610) D'Anna, V.; Duca, D.; Ferrante, F.; La Manna, G. Dft Studies on Catalytic Properties of Isolated and Carbon Nanotube Supported Pd9 Cluster–I: Adsorption, Fragmentation and Diffusion of Hydrogen. *PCCP* **2009,** *11*, 4077-4083.
(611) Kumar, D.; Govindaraja, T.; Krishnamurty, S.; Kaliaperumal, S.; Pal, S. Dissociative Chemisorption of Hydrogen Molecules on Defective Graphene-Supported Aluminium Clusters: A Computational Study. *PCCP* **2018,** *20*, 26506-26512.

(612) Verdinelli, V.; Juan, A.; German, E. Ruthenium Decorated Single Walled Carbon Nanotube for Molecular Hydrogen Storage: A First-Principle Study. *Int. J. Hydrogen Energy* **2019,** *44*, 8376-8383.
(613) Sharma, S.; Groves, M. N.; Fennell, J.; Soin, N.; Horswell, S. L.; Malardier-Jugroot, C. Carboxyl Group Enhanced Co Tolerant Go Supported Pt Catalysts: Dft and Electrochemical Analysis. *Chem. Mater.* **2014,** *26*, 6142-6151.
(614) Campos-Roldán, C. A.; Ramos-Sánchez, G.; Gonzalez-Huerta, R. G.; Vargas García, J. R.; Balbuena, P. B.; Alonso-Vante, N. Influence of Sp3–Sp2 Carbon Nanodomains on Metal/Support Interaction, Catalyst Durability, and Catalytic Activity for the Oxygen Reduction Reaction. *ACS Applied Materials & Interfaces* **2016,** *8*, 23260-23269.
(615) Chen, X.; Sun, S.; Li, F.; Wang, X.; Xia, D. The Interactions of Oxygen with Small Gold Clusters on Nitrogen-Doped Graphene. *Molecules* **2013,** *18*, 3279.
(616) Liu, S.; Huang, S. Theoretical Insights into the Activation of O2 by Pt Single Atom and Pt4 Nanocluster on Functionalized Graphene Support: Critical Role of Pt Positive Polarized Charges. *Carbon* **2017,** *115*, 11-17.
(617) Chesnokov, V. V.; Prosvirin, I. P.; Zaitseva, N. A.; Zaikovskii, V. I.; Molchanov, V. V. Effect of the Structure of Carbon Nanofibers on the State of an Active Component and on the Catalytic Properties of Pd/C Catalysts in the Selective Hydrogenation of 1,3-Butadiene. *Kinet. Catal.* **2002,** *43*, 838-846.
(618) Feng, Y.; Zhou, L.; Wan, Q.; Lin, S.; Guo, H. Selective Hydrogenation of 1,3-Butadiene Catalyzed by a Single Pd Atom Anchored on Graphene: The Importance of Dynamics. *Chemical science* **2018,** *9*, 5890-5896.
(619) Huang, X.; Xia, Y.; Cao, Y.; Zheng, X.; Pan, H.; Zhu, J.; Ma, C.; Wang, H.; Li, J.; You, R.et al. Enhancing Both Selectivity and Coking-Resistance of a Single-Atom Pd1/C3n4 Catalyst for Acetylene Hydrogenation. *Nano Research* **2017,** *10*, 1302-1312.
(620) Xu, Z.; Duong-Viet, C.; Liu, Y.; Baaziz, W.; Li, B.; Nguyen-Dinh, L.; Ersen, O.; Pham-Huu, C. Macroscopic Graphite Felt Containing Palladium Catalyst for Liquid-Phase Hydrogenation of Cinnamaldehyde. *Applied Catalysis B: Environmental* **2019,** *244*, 128-139.
(621) Qu, Y.; Yang, H.; Wang, S.; Chen, T.; Wang, G. Hydrogenation of Nitrobenzene to Aniline Catalyzed by C60-Stabilized Ni. *Catal. Commun.* **2017,** *97*, 83-87.
(622) Wenjing, S.; Lozano-Martin, M. C.; Esteban, G.-S.; Carolina, R.-B.; Weizheng, W.; Xiaodong, Y.; Belen, B.-B.; Antonio, G.-R.; Inmaculada, R.-R. New Insights in the Development of Carbon Supported Ruthenium Catalysts for Hydrogenation of Levulinic Acid. *Current Catalysis* **2018,** *7*, 129-137.
(623) Xiao, C.; Goh, T.-W.; Qi, Z.; Goes, S.; Brashler, K.; Perez, C.; Huang, W. Conversion of Levulinic Acid to Γ-Valerolactone over Few-Layer Graphene-Supported Ruthenium Catalysts. *ACS Catalysis* **2016,** *6*, 593-599.
(624) Tan, J.; Cui, J.; Cui, X.; Deng, T.; Li, X.; Zhu, Y.; Li, Y. Graphene-Modified Ru Nanocatalyst for Low-Temperature Hydrogenation of Carbonyl Groups. *ACS Catalysis* **2015,** *5*, 7379-7384.
(625) D'Anna, V.; Duca, D.; Ferrante, F.; La Manna, G. Dft Studies on Catalytic Properties of Isolated and Carbon Nanotube Supported Pd9 Cluster Part Ii. Hydro-Isomerization of Butene Isomers. *PCCP* **2010,** *12*, 1323-1330.
(626) Zhao, J.; Xu, J.; Xu, J.; Zhang, T.; Di, X.; Ni, J.; Li, X. Enhancement of Au/Ac Acetylene Hydrochlorination Catalyst Activity and Stability Via Nitrogen-Modified Activated Carbon Support. *Chem. Eng. J.* **2015,** *262*, 1152-1160.
(627) Deming, C. P.; Mercado, R.; Lu, J. E.; Gadiraju, V.; Khan, M.; Chen, S. Oxygen Electroreduction Catalyzed by Palladium Nanoparticles Supported on Nitrogen-Doped Graphene Quantum Dots: Impacts of Nitrogen Dopants. *ACS Sustainable Chemistry & Engineering* **2016,** *4*, 6580-6589.
(628) Jalili, S.; Goliaei, E. M.; Schofield, J. Silver Cluster Supported on Nitrogen-Doped Graphene as an Electrocatalyst with High Activity and Stability for Oxygen Reduction Reaction. *Int. J. Hydrogen Energy* **2017,** *42*, 14522-14533.

(629) Song, Y.; Chen, S. Graphene Quantum-Dot-Supported Platinum Nanoparticles: Defect-Mediated Electrocatalytic Activity in Oxygen Reduction. *ACS Applied Materials & Interfaces* **2014,** *6*, 14050-14060.
(630) Liu, J.; Jiao, M.; Mei, B.; Tong, Y.; Li, Y.; Ruan, M.; Song, P.; Sun, G.; Jiang, L.; Wang, Y.et al. Carbon-Supported Divacancy-Anchored Platinum Single-Atom Electrocatalysts with Superhigh Pt Utilization for the Oxygen Reduction Reaction. *Angew. Chem. Int. Ed.* **2019,** *58*, 1163-1167.
(631) Higgins, D.; Hoque, M. A.; Seo, M. H.; Wang, R.; Hassan, F.; Choi, J.-Y.; Pritzker, M.; Yu, A.; Zhang, J.; Chen, Z. Development and Simulation of Sulfur-Doped Graphene Supported Platinum with Exemplary Stability and Activity Towards Oxygen Reduction. *Adv. Funct. Mater.* **2014,** *24*, 4325-4336.
(632) Li, L.; Liu, H.; Wang, L.; Yue, S.; Tong, X.; Zaliznyak, T.; Taylor, G. T.; Wong, S. S. Chemical Strategies for Enhancing Activity and Charge Transfer in Ultrathin Pt Nanowires Immobilized onto Nanotube Supports for the Oxygen Reduction Reaction. *ACS Applied Materials & Interfaces* **2016,** *8*, 34280-34294.
(633) Dantas Ramos, A. L.; Alves, P. d. S.; Aranda, D. A. G.; Schmal, M. Characterization of Carbon Supported Palladium Catalysts: Inference of Electronic and Particle Size Effects Using Reaction Probes. *Applied Catalysis A: General* **2004,** *277*, 71-81.
(634) Giroir-Fendler, A.; Richard, D.; Gallezot, P. In *Stud. Surf. Sci. Catal.*; Guisnet, M.;Barrault, J.;Bouchoule, C.;Duprez, D.;Montassier, C.;Pérot, G., Eds.; Elsevier, 1988; Vol. 41.
(635) Richard, D.; Gallezot, P.; Neibecker, D.; Tkatchenko, I. Characterization and Selectivity in Cinnamaldehyde Hydrogenation of Graphite-Supported Platinum Catalysts Prepared from a Zero-Valent Platinum Complex. *Catal. Today* **1989,** *6*, 171-179.
(636) Liu, Z.-T.; Wang, C.-X.; Liu, Z.-W.; Lu, J. Selective Hydrogenation of Cinnamaldehyde over Pt-Supported Multi-Walled Carbon Nanotubes: Insights into the Tube-Size Effects. *Applied Catalysis A: General* **2008,** *344*, 114-123.
(637) Vu, H.; Gonçalves, F.; Philippe, R.; Lamouroux, E.; Corrias, M.; Kihn, Y.; Plee, D.; Kalck, P.; Serp, P. Bimetallic Catalysis on Carbon Nanotubes for the Selective Hydrogenation of Cinnamaldehyde. *J. Catal.* **2006,** *240*, 18-22.
(638) Cárdenas-Lizana, F.; Hao, Y.; Crespo-Quesada, M.; Yuranov, I.; Wang, X.; Keane, M. A.; Kiwi-Minsker, L. Selective Gas Phase Hydrogenation of P-Chloronitrobenzene over Pd Catalysts: Role of the Support. *ACS Catalysis* **2013,** *3*, 1386-1396.
(639) Yang, F.; Wang, M.; Liu, W.; Yang, B.; Wang, Y.; Luo, J.; Tang, Y.; Hou, L.; Li, Y.; Li, Z.et al. Atomically Dispersed Ni as the Active Site Towards Selective Hydrogenation of Nitroarenes. *Green Chemistry* **2019,** *21*, 704-711.
(640) Lou, Y.; Xu, J.; Wu, H.; Liu, J. Hollow Carbon Anchored Highly Dispersed Pd Species for Selective Hydrogenation of 3-Nitrostyrene: Metal-Carbon Interaction. *Chem. Commun.* **2018,** *54*, 13248-13251.
(641) Cao, S.; Monnier, J. R.; Williams, C. T.; Diao, W.; Regalbuto, J. R. Rational Nanoparticle Synthesis to Determine the Effects of Size, Support, and K Dopant on Ru Activity for Levulinic Acid Hydrogenation to Γ-Valerolactone. *J. Catal.* **2015,** *326*, 69-81.
(642) Nie, R.; Peng, X.; Zhang, H.; Yu, X.; Lu, X.; Zhou, D.; Xia, Q. Transfer Hydrogenation of Bio-Fuel with Formic Acid over Biomass-Derived N-Doped Carbon Supported Acid-Resistant Pd Catalyst. *Catalysis Science & Technology* **2017,** *7*, 627-634.
(643) Cheng, S.; Meng, X.; Shang, N.; Gao, S.; Feng, C.; Wang, C.; Wang, Z. Pd Supported on G-C3n4 Nanosheets: Mott–Schottky Heterojunction Catalyst for Transfer Hydrogenation of Nitroarenes Using Formic Acid as Hydrogen Source. *New J. Chem.* **2018,** *42*, 1771-1778.
(644) Luo, Q.; Zhang, W.; Fu, C.-F.; Yang, J. Single Pd Atom and Pd Dimer Embedded Graphene Catalyzed Formic Acid Dehydrogenation: A first-Principles Study. *Int. J. Hydrogen Energy* **2018,** *43*, 6997-7006.
(645) Shin, D. Y.; Kim, M.-S.; Kwon, J. A.; Shin, Y.-J.; Yoon, C. W.; Lim, D.-H. Fundamental Mechanisms of Reversible Dehydrogenation of Formate on N-Doped Graphene-Supported Pd Nanoparticles. *The Journal of Physical Chemistry C* **2019,** *123*, 1539-1549.

(646) Chen, W.; Ji, J.; Duan, X.; Qian, G.; Li, P.; Zhou, X.; Chen, D.; Yuan, W. Unique Reactivity in Pt/Cnt Catalyzed Hydrolytic Dehydrogenation of Ammonia Borane. *Chem. Commun.* **2014,** *50*, 2142-2144.
(647) Donoeva, B.; Masoud, N.; de Jongh, P. E. Carbon Support Surface Effects in the Gold-Catalyzed Oxidation of 5-Hydroxymethylfurfural. *ACS Catalysis* **2017,** *7*, 4581-4591.
(648) Wang, X.; Orikasa, Y.; Uchimoto, Y. Platinum-Based Electrocatalysts for the Oxygen-Reduction Reaction: Determining the Role of Pure Electronic Charge Transfer in Electrocatalysis. *ACS Catalysis* **2016,** *6*, 4195-4198.
(649) Yang, L.; Cheng, D.; Xu, H.; Zeng, X.; Wan, X.; Shui, J.; Xiang, Z.; Cao, D. Unveiling the High-Activity Origin of Single-Atom Iron Catalysts for Oxygen Reduction Reaction. *Proceedings of the National Academy of Sciences* **2018,** *115*, 6626-6631.
(650) Zandkarimi, B.; Alexandrova, A. N. Dynamics of Subnanometer Pt Clusters Can Break the Scaling Relationships in Catalysis. *The Journal of Physical Chemistry Letters* **2019,** *10*, 460-467.
(651) Lei, Z.; An, L.; Dang, L.; Zhao, M.; Shi, J.; Bai, S.; Cao, Y. Highly Dispersed Platinum Supported on Nitrogen-Containing Ordered Mesoporous Carbon for Methanol Electrochemical Oxidation. *Microporous Mesoporous Mater.* **2009,** *119*, 30-38.
(652) Sun, Y.; Du, C.; An, M.; Du, L.; Tan, Q.; Liu, C.; Gao, Y.; Yin, G. Boron-Doped Graphene as Promising Support for Platinum Catalyst with Superior Activity Towards the Methanol Electrooxidation Reaction. *J. Power Sources* **2015,** *300*, 245-253.
(653) Sun, Y.; Du, C.; Han, G.; Qu, Y.; Du, L.; Wang, Y.; Chen, G.; Gao, Y.; Yin, G. Boron, Nitrogen Co-Doped Graphene: A Superior Electrocatalyst Support and Enhancing Mechanism for Methanol Electrooxidation. *Electrochim. Acta* **2016,** *212*, 313-321.
(654) Jackson, C.; Smith, G. T.; Markiewicz, M.; Inwood, D. W.; Leach, A. S.; Whalley, P. S.; Kucernak, A. R.; Russell, A. E.; Kramer, D.; Levecque, P. B. J. Support Induced Charge Transfer Effects on Electrochemical Characteristics of Pt Nanoparticle Electrocatalysts. *J. Electroanal. Chem.* **2018,** *819*, 163-170.
(655) Zhou, G. Metal/Graphene Heterobilayers as Hydrogen Evolution Reaction Cathodes: A First-Principles Study. *PCCP* **2019**, DOI:10.1039/C8CP07725H 10.1039/C8CP07725H.
(656) He, T.; Zhang, C.; Du, A. Single-Atom Supported on Graphene Grain Boundary as an Efficient Electrocatalyst for Hydrogen Evolution Reaction. *Chem. Eng. Sci.* **2019,** *194*, 58-63.
(657) Cheng, N.; Stambula, S.; Wang, D.; Banis, M. N.; Liu, J.; Riese, A.; Xiao, B.; Li, R.; Sham, T.-K.; Liu, L.-M.et al. Platinum Single-Atom and Cluster Catalysis of the Hydrogen Evolution Reaction. *Nature Communications* **2016,** *7*, 13638.
(658) Lim, J.; Back, S.; Choi, C.; Jung, Y. Ultralow Overpotential of Hydrogen Evolution Reaction Using Fe-Doped Defective Graphene: A Density Functional Study. *ChemCatChem* **2018,** *10*, 4450-4455.
(659) Li, H.; Yu, K.; Li, C.; Tang, Z.; Guo, B.; Lei, X.; Fu, H.; Zhu, Z. Charge-Transfer Induced High Efficient Hydrogen Evolution of Mos2/Graphene Cocatalyst. *Scientific Reports* **2015,** *5*, 18730.
(660) Xing, W.; Zhang, Y.; Xue, Q.; Yan, Z. Highly Active Catalyst of Two-Dimensional Cos2/Graphene Nanocomposites for Hydrogen Evolution Reaction. *Nanoscale Research Letters* **2015,** *10*, 488.
(661) Singh, R.; Dutta, S. A Review on H2 Production through Photocatalytic Reactions Using Tio2/Tio2-Assisted Catalysts. *Fuel* **2018,** *220*, 607-620.
(662) Nguyen-Phan, T.-D.; Luo, S.; Liu, Z.; Gamalski, A. D.; Tao, J.; Xu, W.; Stach, E. A.; Polyansky, D. E.; Senanayake, S. D.; Fujita, E.et al. Striving toward Noble-Metal-Free Photocatalytic Water Splitting: The Hydrogenated-Graphene–Tio2 Prototype. *Chem. Mater.* **2015,** *27*, 6282-6296.
(663) Han, W.; Li, Z.; Li, Y.; Fan, X.; Zhang, F.; Zhang, G.; Peng, W. The Promoting Role of Different Carbon Allotropes Cocatalysts for Semiconductors in Photocatalytic Energy Generation and Pollutants Degradation. *Frontiers in chemistry* **2017,** *5*, 84-84.
(664) Leary, R.; Westwood, A. Carbonaceous Nanomaterials for the Enhancement of Tio2 Photocatalysis. *Carbon* **2011,** *49*, 741-772.
(665) Khalid, N. R.; Majid, A.; Tahir, M. B.; Niaz, N. A.; Khalid, S. Carbonaceous-Tio2 Nanomaterials for Photocatalytic Degradation of Pollutants: A Review. *Ceram. Int.* **2017,** *43*, 14552-14571.

(666) Morales-Torres, S.; Pastrana-Martínez, L. M.; Figueiredo, J. L.; Faria, J. L.; Silva, A. M. T. Design of Graphene-Based Tio2 Photocatalysts—a Review. *Environmental Science and Pollution Research* **2012,** *19*, 3676-3687.
(667) Tang, B.; Chen, H.; Peng, H.; Wang, Z.; Huang, W. Graphene Modified Tio_2 Composite Photocatalysts: Mechanism, Progress and Perspective. *Nanomaterials (Basel, Switzerland)* **2018,** *8*, 105.
(668) Upadhyay, R. K.; Soin, N.; Roy, S. S. Role of Graphene/Metal Oxide Composites as Photocatalysts, Adsorbents and Disinfectants in Water Treatment: A Review. *RSC Advances* **2014,** *4*, 3823-3851.
(669) Minella, M.; Sordello, F.; Minero, C. Photocatalytic Process in Tio2/Graphene Hybrid Materials. Evidence of Charge Separation by Electron Transfer from Reduced Graphene Oxide to Tio2. *Catal. Today* **2017,** *281*, 29-37.
(670) Gillespie, P. N. O.; Martsinovich, N. Electronic Structure and Charge Transfer in the Tio2 Rutile (110)/Graphene Composite Using Hybrid Dft Calculations. *The Journal of Physical Chemistry C* **2017,** *121*, 4158-4171.
(671) Hu, G.; Tang, B. Photocatalytic Mechanism of Graphene/Titanate Nanotubes Photocatalyst under Visible-Light Irradiation. *Mater. Chem. Phys.* **2013,** *138*, 608-614.
(672) Lu, K.-Q.; Zhang, N.; Han, C.; Li, F.; Chen, Z.; Xu, Y.-J. Insight into the Origin of Boosted Photosensitive Efficiency of Graphene from the Cooperative Experiment and Theory Study. *The Journal of Physical Chemistry C* **2016,** *120*, 27091-27103.
(673) Aleksandrzak, M.; Adamski, P.; Kukułka, W.; Zielinska, B.; Mijowska, E. Effect of Graphene Thickness on Photocatalytic Activity of Tio2-Graphene Nanocomposites. *Appl. Surf. Sci.* **2015,** *331*, 193-199.
(674) Gu, Y.; Xing, M.; Zhang, J. Synthesis and Photocatalytic Activity of Graphene Based Doped Tio2 Nanocomposites. *Appl. Surf. Sci.* **2014,** *319*, 8-15.
(675) Rajender, G.; Kumar, J.; Giri, P. K. Interfacial Charge Transfer in Oxygen Deficient Tio2-Graphene Quantum Dot Hybrid and Its Influence on the Enhanced Visible Light Photocatalysis. *Applied Catalysis B: Environmental* **2018,** *224*, 960-972.
(676) Qu, A.; Xie, H.; Xu, X.; Zhang, Y.; Wen, S.; Cui, Y. High Quantum Yield Graphene Quantum Dots Decorated Tio2 Nanotubes for Enhancing Photocatalytic Activity. *Appl. Surf. Sci.* **2016,** *375*, 230-241.
(677) Gao, H.; Li, X.; Lv, J.; Liu, G. Interfacial Charge Transfer and Enhanced Photocatalytic Mechanisms for the Hybrid Graphene/Anatase Tio2(001) Nanocomposites. *The Journal of Physical Chemistry C* **2013,** *117*, 16022-16027.
(678) Zhang, H.; Lv, X.; Li, Y.; Wang, Y.; Li, J. P25-Graphene Composite as a High Performance Photocatalyst. *ACS Nano* **2010,** *4*, 380-386.
(679) Liang, Y. T.; Vijayan, B. K.; Lyandres, O.; Gray, K. A.; Hersam, M. C. Effect of Dimensionality on the Photocatalytic Behavior of Carbon–Titania Nanosheet Composites: Charge Transfer at Nanomaterial Interfaces. *The Journal of Physical Chemistry Letters* **2012,** *3*, 1760-1765.
(680) Olowoyo, J. O.; Kumar, M.; Jain, S. L.; Babalola, J. O.; Vorontsov, A. V.; Kumar, U. Insights into Reinforced Photocatalytic Activity of the Cnt–Tio2 Nanocomposite for Co2 Reduction and Water Splitting. *The Journal of Physical Chemistry C* **2019,** *123*, 367-378.
(681) Yang, M.-Q.; Zhang, N.; Xu, Y.-J. Synthesis of Fullerene–, Carbon Nanotube–, and Graphene–Tio2 Nanocomposite Photocatalysts for Selective Oxidation: A Comparative Study. *ACS Applied Materials & Interfaces* **2013,** *5*, 1156-1164.
(682) Kamat, P. V.; Bedja, I.; Hotchandani, S. Photoinduced Charge Transfer between Carbon and Semiconductor Clusters. One-Electron Reduction of C60 in Colloidal Tio2 Semiconductor Suspensions. *The Journal of Physical Chemistry* **1994,** *98*, 9137-9142.
(683) Qi, K.; Selvaraj, R.; Al Fahdi, T.; Al-Kindy, S.; Kim, Y.; Wang, G.-C.; Tai, C.-W.; Sillanpää, M. Enhanced Photocatalytic Activity of Anatase-Tio2 Nanoparticles by Fullerene Modification: A Theoretical and Experimental Study. *Appl. Surf. Sci.* **2016,** *387*, 750-758.

(684) Zhang, L.; Wang, Y.; Xu, T.; Zhu, S.; Zhu, Y. Surface Hybridization Effect of C60 Molecules on Tio2 and Enhancement of the Photocatalytic Activity. *J. Mol. Catal. A: Chem.* **2010,** *331*, 7-14.
(685) Long, R.; Dai, Y.; Huang, B. Fullerene Interfaced with a Tio2(110) Surface May Not Form an Efficient Photovoltaic Heterojunction: First-Principles Investigation of Electronic Structures. *The Journal of Physical Chemistry Letters* **2013,** *4*, 2223-2229.
(686) Wang, S.; Liu, C.; Dai, K.; Cai, P.; Chen, H.; Yang, C.; Huang, Q. Fullerene C70–Tio2 Hybrids with Enhanced Photocatalytic Activity under Visible Light Irradiation. *Journal of Materials Chemistry A* **2015,** *3*, 21090-21098.
(687) Thomas, J. M.; Raja, R. Exploiting Nanospace for Asymmetric Catalysis: Confinement of Immobilized, Single-Site Chiral Catalysts Enhances Enantioselectivity. *Acc. Chem. Res.* **2008,** *41*, 708-720.
(688) Kosinov, N.; Liu, C.; Hensen, E. J. M.; Pidko, E. A. Engineering of Transition Metal Catalysts Confined in Zeolites. *Chem. Mater.* **2018,** *30*, 3177-3198.
(689) Santiso, E. E.; George, A. M.; Turner, C. H.; Kostov, M. K.; Gubbins, K. E.; Buongiorno-Nardelli, M.; Sliwinska-Bartkowiak, M. Adsorption and Catalysis: The Effect of Confinement on Chemical Reactions. *Appl. Surf. Sci.* **2005,** *252*, 766-777.
(690) Yang, F.; Deng, D.; Pan, X.; Fu, Q.; Bao, X. Understanding Nano Effects in Catalysis. *National Science Review* **2015,** *2*, 183-201.
(691) Weckhuysen, B. M.; Kitagawa, S.; Tsapatsis, M. Reactions in Confined Spaces. *ChemPhysChem* **2018,** *19*, 339-340.
(692) Jenny, J.; Krishnakanth, C.; Aditya, G.; Jeremiah, J. G. The Chemistry of Confined Spaces. *Curr. Org. Chem.* **2014,** *18*, 2002-2009.
(693) Sastre, G.; Corma, A. The Confinement Effect in Zeolites. *J. Mol. Catal. A: Chem.* **2009,** *305*, 3-7.
(694) Boscoboinik, J. A. Chemistry in Confined Space through the Eyes of Surface Science—2d Porous Materials. *J. Phys.: Condens. Matter* **2019,** *31*, 063001.
(695) Pan, X.; Bao, X. Reactions over Catalysts Confined in Carbon Nanotubes. *Chem. Commun.* **2008**, DOI:10.1039/B810994J 10.1039/B810994J, 6271-6281.
(696) Pan, X.; Bao, X. The Effects of Confinement inside Carbon Nanotubes on Catalysis. *Acc. Chem. Res.* **2011,** *44*, 553-562.
(697) Khlobystov, A. N. Carbon Nanotubes: From Nano Test Tube to Nano-Reactor. *ACS Nano* **2011,** *5*, 9306-9312.
(698) Miners, S. A.; Rance, G. A.; Khlobystov, A. N. Chemical Reactions Confined within Carbon Nanotubes. *Chem. Soc. Rev.* **2016,** *45*, 4727-4746.
(699) Axet, M. R.; Serp, P. In *Organic Nanoreactors*; Sadjadi, S., Ed.; Academic Press: Boston, 2016, DOI:https://doi.org/10.1016/B978-0-12-801713-5.00005-7 https://doi.org/10.1016/B978-0-12-801713-5.00005-7.
(700) Fu, Q.; Bao, X. Surface Chemistry and Catalysis Confined under Two-Dimensional Materials. *Chem. Soc. Rev.* **2017,** *46*, 1842-1874.
(701) Li, H.; Xiao, J.; Fu, Q.; Bao, X. Confined Catalysis under Two-Dimensional Materials. *Proceedings of the National Academy of Sciences* **2017,** *114*, 5930-5934.
(702) Jiang, J.; Sandler, S. I. Shape Versus Inverse-Shape Selective Adsorption of Alkane Isomers in Carbon Nanotubes. *The Journal of Chemical Physics* **2006,** *124*, 024717.
(703) Kärger, J.; Goepel , M.; Gläser, R. In *Nanotechnology in Catalysis*; Van de Voorde, M.;Sels, B., Eds.; Wiley-VCH, 2017, DOI:doi:10.1002/9783527699827.ch13 doi:10.1002/9783527699827.ch13.
(704) Xu, Y. Nanofluidics: Nanofluidics: A New Arena for Materials Science (Adv. Mater. 3/2018). *Adv. Mater.* **2018,** *30*, 1870019.
(705) Guo, S.; Meshot, E. R.; Kuykendall, T.; Cabrini, S.; Fornasiero, F. Nanofluidic Transport through Isolated Carbon Nanotube Channels: Advances, Controversies, and Challenges. *Adv. Mater.* **2015,** *27*, 5726-5737.

(706) Gao, J.; Feng, Y.; Guo, W.; Jiang, L. Nanofluidics in Two-Dimensional Layered Materials: Inspirations from Nature. *Chem. Soc. Rev.* **2017,** *46*, 5400-5424.
(707) Lev, D. G.; Gubbins, K. E.; Radhakrishnan, R.; Sliwinska-Bartkowiak, M. Phase Separation in Confined Systems. *Rep. Prog. Phys.* **1999,** *62*, 1573.
(708) Alba-Simionesco, C.; Coasne, B.; Dosseh, G.; Dudziak, G.; Gubbins, K. E.; Radhakrishnan, R.; Sliwinska-Bartkowiak, M. Effects of Confinement on Freezing and Melting. *J. Phys.: Condens. Matter* **2006,** *18*, R15.
(709) Long, Y.; Palmer, J. C.; Coasne, B.; Śliwinska-Bartkowiak, M.; Gubbins, K. E. Pressure Enhancement in Carbon Nanopores: A Major Confinement Effect. *PCCP* **2011,** *13*, 17163-17170.
(710) Gubbins, K. E.; Liu, Y.-C.; Moore, J. D.; Palmer, J. C. The Role of Molecular Modeling in Confined Systems: Impact and Prospects. *PCCP* **2011,** *13*, 58-85.
(711) Nørskov, J. K.; Abild-Pedersen, F.; Studt, F.; Bligaard, T. Density Functional Theory in Surface Chemistry and Catalysis. *Proceedings of the National Academy of Sciences* **2011,** *108*, 937-943.
(712) Niyogi, S.; Hamon, M. A.; Hu, H.; Zhao, B.; Bhowmik, P.; Sen, R.; Itkis, M. E.; Haddon, R. C. Chemistry of Single-Walled Carbon Nanotubes. *Acc. Chem. Res.* **2002,** *35*, 1105-1113.
(713) Zhong, J.; Chiou, J.; Dong, C.; Song, L.; Liu, C.; Xie, S.; Cheng, H.; Pong, W.-F.; Chang, C.; Chen, Y.et al. Probing Quantum Confinement of Single-Walled Carbon Nanotubes by Resonant Soft-X-Ray Emission Spectroscopy. *Appl. Phys. Lett.* **2008,** *93*, 023107.
(714) Martínez, J. I.; López, M. J.; Alonso, J. A. Theoretical Study of the Reactivity of Cesium with Benzene and Graphitic Cxhy Clusters. *The Journal of Chemical Physics* **2005,** *123*, 074303.
(715) Wei, G.-F.; Shang, C.; Liu, Z.-P. Confined Platinum Nanoparticle in Carbon Nanotube: Structure and Oxidation. *PCCP* **2015,** *17*, 2078-2087.
(716) Garg, I.; Sharma, H.; Dharamvir, K.; Jindal, V. K.; Kanhere, D. G. Dft Study of Aln (1−13) Clusters Encapsulated inside Single Walled Carbon Nanotubes. *The Journal of Physical Chemistry C* **2010,** *114*, 18762-18772.
(717) Zhang, F.; Pan, X.; Hu, Y.; Yu, L.; Chen, X.; Jiang, P.; Zhang, H.; Deng, S.; Zhang, J.; Bolin, T. B.et al. Tuning the Redox Activity of Encapsulated Metal Clusters Via the Metallic and Semiconducting Character of Carbon Nanotubes. *Proceedings of the National Academy of Sciences* **2013,** *110*, 14861-14866.
(718) Guo, S.; Pan, X.; Gao, H.; Yang, Z.; Zhao, J.; Bao, X. Probing the Electronic Effect of Carbon Nanotubes in Catalysis: Nh3 Synthesis with Ru Nanoparticles. *Chemistry – A European Journal* **2010,** *16*, 5379-5384.
(719) Trépanier, M.; Dalai, A. K.; Abatzoglou, N. Synthesis of Cnt-Supported Cobalt Nanoparticle Catalysts Using a Microemulsion Technique: Role of Nanoparticle Size on Reducibility, Activity and Selectivity in Fischer–Tropsch Reactions. *Applied Catalysis A: General* **2010,** *374*, 79-86.
(720) Zhang, G.; Xie, W.; Chen, Y.; Liu, F.; Chen, C. The Effect of Doping and Confinement on the Adsorption of Pt on Cnts Upon Be, B, N and O Doping: A Theoretical Study. *Journal of Inorganic and Organometallic Polymers and Materials* **2015,** *25*, 1502-1510.
(721) Prachi, C. Thermodynamics of Confined Gallium Clusters. *J. Phys.: Condens. Matter* **2015,** *27*, 445502.
(722) Fang, R. R.; He, Y. Z.; Zhang, K.; Li, H. Melting Behavior of Aluminum Nanowires in Carbon Nanotubes. *The Journal of Physical Chemistry C* **2014,** *118*, 7622-7629.
(723) Shao, J.; Yang, C.; Zhu, X.; Lu, X. Melting and Freezing of Au Nanoparticles Confined in Armchair Single-Walled Carbon Nanotubes. *The Journal of Physical Chemistry C* **2010,** *114*, 2896-2902.
(724) Arcidiacono, S.; Walther, J. H.; Poulikakos, D.; Passerone, D.; Koumoutsakos, P. Solidification of Gold Nanoparticles in Carbon Nanotubes. *Phys. Rev. Lett.* **2005,** *94*, 105502.
(725) Zhu, B. E.; Pan, Z. Y.; Hou, M.; Cheng, D.; Wang, Y. X. Melting Behaviour of Gold Nanowires in Carbon Nanotubes. *Mol. Phys.* **2011,** *109*, 527-533.
(726) Shi, R.; Shao, J.; Zhu, X.; Lu, X. On the Melting and Freezing of Au−Pt Nanoparticles Confined in Single-Walled Carbon Nanotubes. *The Journal of Physical Chemistry C* **2011,** *115*, 2961-2968.

(727) Akbarzadeh, H.; Abbaspour, M.; Salemi, S.; Abroodi, M. Investigation of Thermal Evolution of Copper Nanoclusters Encapsulated in Carbon Nanotubes: A Molecular Dynamics Study. *PCCP* **2015,** *17*, 12747-12759.
(728) Yufeng, G.; Wanlin, G. Structural Transformation of Partially Confined Copper Nanowires inside Defected Carbon Nanotubes. *Nanotechnology* **2006,** *17*, 4726.
(729) Cheng, D.; Lan, J. Thermal Behaviour of Pd Clusters inside Carbon Nanotubes: Insights into the Cluster-Size, Tube-Size and Metal–Tube Interaction Effects. *Molecular Simulation* **2010,** *36*, 805-814.
(730) Akbarzadeh, H.; Shamkhali, A. N. Melting Behavior of (Pdxpt1−X)N Nanoclusters Confined in Single-Walled Carbon Nanotubes: A Molecular Dynamics Investigation on the Effects of Chirality and Diameter of Nanotubes, and Size and Composition of Nanoclusters. *RSC Advances* **2015,** *5*, 23160-23173.
(731) Wei, H.; Wei, S.; Zhu, X.; Lu, X. Investigation of Structural, Thermal, and Dynamical Properties of Pd–Au–Pt Ternary Metal Nanoparticles Confined in Carbon Nanotubes Based on Md Simulation. *The Journal of Physical Chemistry C* **2017,** *121*, 12911-12920.
(732) Akbarzadeh, H.; Abbaspour, M.; Mehrjouei, E.; Ramezanzadeh, S. Pt–Co Nanocluster in Hollow Carbon Nanospheres. *J. Comput. Chem.* **2018,** *39*, 1267-1274.
(733) Akbarzadeh, H.; Shamkhali, A. N.; Abbaspour, M.; Salemi, S.; Attaran, Z. A Comprehensive Molecular Dynamics Investigation on Confinement of Ptncum Nanocluster inside Carbon Nanotubes. *Colloids and Surfaces A: Physicochemical and Engineering Aspects* **2017,** *522*, 433-444.
(734) Cheng, D.; Wang, W.; Huang, S. Thermal Evolution of a Platinum Cluster Encapsulated in Carbon Nanotubes. *The Journal of Physical Chemistry C* **2007,** *111*, 1631-1637.
(735) Ivanovskaya, V. V.; Köhler, C.; Seifert, G. $3d$ Metal Nanowires and Clusters inside Carbon Nanotubes: Structural, Electronic, and Magnetic Properties. *Physical Review B* **2007,** *75*, 075410.
(736) Tereshchuk, P.; Da Silva, J. L. F. Encapsulation of Small Magnetic Clusters in Fullerene Cages: A Density Functional Theory Investigation within Van Der Waals Corrections. *Physical Review B* **2012,** *85*, 195461.
(737) Kang, Y.-J.; Choi, J.; Moon, C.-Y.; Chang, K. J. Electronic and Magnetic Properties of Single-Wall Carbon Nanotubes Filled with Iron Atoms. *Physical Review B* **2005,** *71*, 115441.
(738) Weissmann, M.; García, G.; Kiwi, M.; Ramírez, R.; Fu, C.-C. Theoretical Study of Iron-Filled Carbon Nanotubes. *Physical Review B* **2006,** *73*, 125435.
(739) Horga, F. I.; Mañanes, A.; López, M. J.; Alonso, J. A. Electronic and Magnetic Properties of Fe Clusters inside Finite Zigzag Single-Wall Carbon Nanotubes. *Physical Review B* **2013,** *87*, 085402.
(740) Yuan, S.; Wang, X.; Li, P.; Li, F.; Yuan, S. Fe3c Cluster Confined in Single-Walled Carbon Nanotubes: A First-Principles Study. *J. Appl. Phys.* **2008,** *104*, 054310.
(741) Javan, M. B.; Tajabor, N.; Rezaee-Roknabadi, M.; Behdani, M. First Principles Study of Small Cobalt Clusters Encapsulated in C60 and C82 Spherical Nanocages. *Appl. Surf. Sci.* **2011,** *257*, 7586-7591.
(742) Kuznetsov, A. Magnetism of Co≪Sub≫13≪/Sub≫-Filled Carbon Nanotubes of Diverse Chiral Symmetry. *Journal of Modern Physics* **2013,** *Vol.04No.03*, 4.
(743) Ma, D.; Jia, S.; Zhao, D.; Lu, Z.; Yang, Z. O2 Activation on the Outer Surface of Carbon Nanotubes Modified by Encapsulated Iron Clusters. *Appl. Surf. Sci.* **2014,** *300*, 91-97.
(744) Yang, X.; Yu, H.; Peng, F.; Wang, H. Confined Iron Nanowires Enhance the Catalytic Activity of Carbon Nanotubes in the Aerobic Oxidation of Cyclohexane. *ChemSusChem* **2012,** *5*, 1213-1217.
(745) Xiao, J.; Pan, X.; Guo, S.; Ren, P.; Bao, X. Toward Fundamentals of Confined Catalysis in Carbon Nanotubes. *J. Am. Chem. Soc.* **2015,** *137*, 477-482.
(746) Xiao, J.; Pan, X.; Zhang, F.; Li, H.; Bao, X. Size-Dependence of Carbon Nanotube Confinement in Catalysis. *Chemical Science* **2017,** *8*, 278-283.

(747) Chen, W.; Pan, X.; Willinger, M.-G.; Su, D. S.; Bao, X. Facile Autoreduction of Iron Oxide/Carbon Nanotube Encapsulates. *J. Am. Chem. Soc.* **2006,** *128*, 3136-3137.
(748) Cao, F.; Zhong, K.; Gao, A.; Chen, C.; Li, Q.; Chen, Q. Reducing Reaction of Fe3o4 in Nanoscopic Reactors of a-Cnts. *The Journal of Physical Chemistry B* **2007,** *111*, 1724-1728.
(749) Chen, W.; Pan, X.; Bao, X. Tuning of Redox Properties of Iron and Iron Oxides Via Encapsulation within Carbon Nanotubes. *J. Am. Chem. Soc.* **2007,** *129*, 7421-7426.
(750) Li, Z.; Chen, Z.-X.; Kang, G.-J.; He, X. Does Confinement Effect Always Enhance Catalytic Activity? A Theoretical Study of H2 Dissociation on Cnt Supported Gold Clusters. *Catal. Today* **2011,** *165*, 25-31.
(751) Kowalczyk, P.; Terzyk, A. P.; Gauden, P. A.; Furmaniak, S.; Kaneko, K. Toward in Silico Modeling of Palladium–Hydrogen–Carbon Nanohorn Nanocomposites. *PCCP* **2014,** *16*, 11763-11769.
(752) Wang, Q.-Y.; Tong, Y.-C.; Yan, P.-J.; Xu, X.-J.; Li, Z. Attachment of Co to a (6, 6) Cnt with a Sc Adsorbate Atom. *Struct. Chem.* **2018**, DOI:10.1007/s11224-018-1202-5 10.1007/s11224-018-1202-5.
(753) Mu, R.; Fu, Q.; Jin, L.; Yu, L.; Fang, G.; Tan, D.; Bao, X. Visualizing Chemical Reactions Confined under Graphene. *Angew. Chem. Int. Ed.* **2012,** *51*, 4856-4859.
(754) Jin, L.; Fu, Q.; Dong, A.; Ning, Y.; Wang, Z.; Bluhm, H.; Bao, X. Surface Chemistry of Co on Ru(0001) under the Confinement of Graphene Cover. *The Journal of Physical Chemistry C* **2014,** *118*, 12391-12398.
(755) Wei, M.; Fu, Q.; Yang, Y.; Wei, W.; Crumlin, E.; Bluhm, H.; Bao, X. Modulation of Surface Chemistry of Co on Ni(111) by Surface Graphene and Carbidic Carbon. *The Journal of Physical Chemistry C* **2015,** *119*, 13590-13597.
(756) Yao, Y.; Fu, Q.; Zhang, Y. Y.; Weng, X.; Li, H.; Chen, M.; Jin, L.; Dong, A.; Mu, R.; Jiang, P.et al. Graphene Cover-Promoted Metal-Catalyzed Reactions. *Proceedings of the National Academy of Sciences* **2014,** *111*, 17023-17028.
(757) Sutter, P.; Sadowski, J. T.; Sutter, E. A. Chemistry under Cover: Tuning Metal−Graphene Interaction by Reactive Intercalation. *J. Am. Chem. Soc.* **2010,** *132*, 8175-8179.
(758) Chen, X.; Lin, Z.-Z. Single-Layer Graphdiyne-Covered Pt(111) Surface: Improved Catalysis Confined under Two-Dimensional Overlayer. *J. Nanopart. Res.* **2018,** *20*, 136.
(759) Wang, S.; Feng, Y.; Yu, M. a.; Wan, Q.; Lin, S. Confined Catalysis in the G-C3n4/Pt(111) Interface: Feasible Molecule Intercalation, Tunable Molecule–Metal Interaction, and Enhanced Reaction Activity of Co Oxidation. *ACS Applied Materials & Interfaces* **2017,** *9*, 33267-33273.
(760) Park, H. G.; Jung, Y. Carbon Nanofluidics of Rapid Water Transport for Energy Applications. *Chem. Soc. Rev.* **2014,** *43*, 565-576.
(761) Das, R.; Ali, M. E.; Hamid, S. B. A.; Ramakrishna, S.; Chowdhury, Z. Z. Carbon Nanotube Membranes for Water Purification: A Bright Future in Water Desalination. *Desalination* **2014,** *336*, 97-109.
(762) Guo, J.; He, J.; Zeng, B. Carbon Nanotube Based Nanopore and Nanofluidic Devices Towards Sensing Applications. *Current Nanoscience* **2016,** *12*, 421-428.
(763) Kärger, J., Goepel, M. and Gläser, R. In *Nanotechnology in Catalysis*; Sels, M. V. d. V. a. B., Ed.; Wiley, 2017, DOI:doi:10.1002/9783527699827.ch13 doi:10.1002/9783527699827.ch13.
(764) Jong Won, C.; Maria, A.; Hyung Gyu, P. In *Carbon Nanotubes Applications on Electron Devices*; Marulanda, J. M., Ed., 2011, DOI:10.5772/17370 10.5772/17370.
(765) Majumder, M.; Chopra, N.; Andrews, R.; Hinds, B. J. Enhanced Flow in Carbon Nanotubes. *Nature* **2005,** *438*, 44.
(766) Noy, A.; Park, H. G.; Fornasiero, F.; Holt, J. K.; Grigoropoulos, C. P.; Bakajin, O. Nanofluidics in Carbon Nanotubes. *Nano Today* **2007,** *2*, 22-29.
(767) Park, H. G.; Bakajin, O. In *Encyclopedia of Microfluidics and Nanofluidics*; Li, D., Ed.; Springer US: Boston, MA, 2008, DOI:10.1007/978-0-387-48998-8_1088 10.1007/978-0-387-48998-8_1088.

(768) Holt, J. K.; Park, H. G.; Wang, Y.; Stadermann, M.; Artyukhin, A. B.; Grigoropoulos, C. P.; Noy, A.; Bakajin, O. Fast Mass Transport through Sub-2-Nanometer Carbon Nanotubes. *Science* **2006,** *312*, 1034-1037.
(769) Mattia, D.; Gogotsi, Y. Review: Static and Dynamic Behavior of Liquids inside Carbon Nanotubes. *Microfluidics and Nanofluidics* **2008,** *5*, 289-305.
(770) Thompson, W. H. Perspective: Dynamics of Confined Liquids. *The Journal of Chemical Physics* **2018,** *149*, 170901.
(771) Skoulidas, A. I.; Ackerman, D. M.; Johnson, J. K.; Sholl, D. S. Rapid Transport of Gases in Carbon Nanotubes. *Phys. Rev. Lett.* **2002,** *89*, 185901.
(772) Ackerman, D. M.; Skoulidas, A. I.; Sholl, D. S.; Karl Johnson, J. Diffusivities of Ar and Ne in Carbon Nanotubes. *Molecular Simulation* **2003,** *29*, 677-684.
(773) Suga, K.; Mori, Y.; Moritani, R.; Kaneda, M. Combined Effects of Molecular Geometry and Nanoconfinement on Liquid Flows through Carbon Nanotubes. *Physical Review E* **2018,** *97*, 053109.
(774) Skoulidas, A. I.; Sholl, D. S.; Johnson, J. K. Adsorption and Diffusion of Carbon Dioxide and Nitrogen through Single-Walled Carbon Nanotube Membranes. *The Journal of Chemical Physics* **2006,** *124*, 054708.
(775) Chen, H.; Johnson, J. K.; Sholl, D. S. Transport Diffusion of Gases Is Rapid in Flexible Carbon Nanotubes. *The Journal of Physical Chemistry B* **2006,** *110*, 1971-1975.
(776) Bucior, B. J.; Kolmakov, G. V.; Male, J. M.; Liu, J.; Chen, D.-L.; Kumar, P.; Johnson, J. K. Adsorption and Diffusion of Fluids in Defective Carbon Nanotubes: Insights from Molecular Simulations. *Langmuir* **2017,** *33*, 11834-11844.
(777) Mao, Z.; Sinnott, S. B. A Computational Study of Molecular Diffusion and Dynamic Flow through Carbon Nanotubes. *The Journal of Physical Chemistry B* **2000,** *104*, 4618-4624.
(778) Liu, L.; Nicholson, D.; Bhatia, S. K. Interfacial Resistance and Length-Dependent Transport Diffusivities in Carbon Nanotubes. *The Journal of Physical Chemistry C* **2016,** *120*, 26363-26373.
(779) Chen, H.; Sholl, D. S. Rapid Diffusion of Ch4/H2 Mixtures in Single-Walled Carbon Nanotubes. *J. Am. Chem. Soc.* **2004,** *126*, 7778-7779.
(780) Krishna, R.; van Baten, J. M. Describing Binary Mixture Diffusion in Carbon Nanotubes with the Maxwell−Stefan Equations. An Investigation Using Molecular Dynamics Simulations. *Industrial & Engineering Chemistry Research* **2006,** *45*, 2084-2093.
(781) Liu, L.; Hu, C.; Nicholson, D.; Bhatia, S. K. Inhibitory Effect of Adsorbed Water on the Transport of Methane in Carbon Nanotubes. *Langmuir* **2017,** *33*, 6280-6291.
(782) Kalra, A.; Hummer, G.; Garde, S. Methane Partitioning and Transport in Hydrated Carbon Nanotubes. *The Journal of Physical Chemistry B* **2004,** *108*, 544-549.
(783) Kim, H. W.; Yoon, H. W.; Yoon, S.-M.; Yoo, B. M.; Ahn, B. K.; Cho, Y. H.; Shin, H. J.; Yang, H.; Paik, U.; Kwon, S.et al. Selective Gas Transport through Few-Layered Graphene and Graphene Oxide Membranes. *Science* **2013,** *342*, 91-95.
(784) Jiao, S.; Xu, Z. Selective Gas Diffusion in Graphene Oxides Membranes: A Molecular Dynamics Simulations Study. *ACS Applied Materials & Interfaces* **2015,** *7*, 9052-9059.
(785) Cai, Q.; Buts, A.; Seaton, N. A.; Biggs, M. J. A Pore Network Model for Diffusion in Nanoporous Carbons: Validation by Molecular Dynamics Simulation. *Chem. Eng. Sci.* **2008,** *63*, 3319-3327.
(786) Palmer, J. C.; Moore, J. D.; Brennan, J. K.; Gubbins, K. E. Adsorption and Diffusion of Argon in Disordered Nanoporous Carbons. *Adsorption* **2011,** *17*, 189-199.
(787) Yamada, Y.; Taguchi, K.; Ikuta, T.; Horibe, A.; Takahashi, K. Meniscus Motion and Void Generation inside Carbon Nanotubes. *The Journal of Physical Chemistry C* **2018,** *122*, 21910-21918.
(788) Goh, K.; Chen, Y. Controlling Water Transport in Carbon Nanotubes. *Nano Today* **2017,** *14*, 13-15.
(789) Alexiadis, A.; Kassinos, S. Molecular Simulation of Water in Carbon Nanotubes. *Chem. Rev.* **2008,** *108*, 5014-5034.

(790) Falk, K.; Sedlmeier, F.; Joly, L.; Netz, R. R.; Bocquet, L. Molecular Origin of Fast Water Transport in Carbon Nanotube Membranes: Superlubricity Versus Curvature Dependent Friction. *Nano Lett.* **2010,** *10*, 4067-4073.
(791) Barati Farimani, A.; Aluru, N. R. Spatial Diffusion of Water in Carbon Nanotubes: From Fickian to Ballistic Motion. *The Journal of Physical Chemistry B* **2011,** *115*, 12145-12149.
(792) Joseph, S.; Aluru, N. R. Why Are Carbon Nanotubes Fast Transporters of Water? *Nano Lett.* **2008,** *8*, 452-458.
(793) Li, J.-Y.; Wu, Z.-Q.; Xu, J.-J.; Chen, H.-Y.; Xia, X.-H. Water Transport within Carbon Nanotubes on a Wave. *PCCP* **2016,** *18*, 33204-33210.
(794) Nicholls, W. D.; Borg, M. K.; Lockerby, D. A.; Reese, J. M. Water Transport through Carbon Nanotubes with Defects. *Molecular Simulation* **2012,** *38*, 781-785.
(795) Gărăjeu, M.; Gouin, H.; Saccomandi, G. Scaling Navier-Stokes Equation in Nanotubes. *Physics of Fluids* **2013,** *25*, 082003.
(796) Thomas, J. A.; McGaughey, A. J. H. Reassessing Fast Water Transport through Carbon Nanotubes. *Nano Lett.* **2008,** *8*, 2788-2793.
(797) Chakraborty, S.; Kumar, H.; Dasgupta, C.; Maiti, P. K. Confined Water: Structure, Dynamics, and Thermodynamics. *Acc. Chem. Res.* **2017,** *50*, 2139-2146.
(798) Liu, H.; Yang, X.; Li, C.; Chen, J. Molecular Dynamics Simulation Study on the Microscopic Structure and the Diffusion Behavior of Methanol in Confined Carbon Nanotubes. **2011**, 430-436.
(799) Shao, Q.; Huang, L.; Zhou, J.; Lu, L.; Zhang, L.; Lu, X.; Jiang, S.; Gubbins, K. E.; Zhu, Y.; Shen, W. Molecular Dynamics Study on Diameter Effect in Structure of Ethanol Molecules Confined in Single-Walled Carbon Nanotubes. *The Journal of Physical Chemistry C* **2007,** *111*, 15677-15685.
(800) Zheng, J.; Lennon, E. M.; Tsao, H.-K.; Sheng, Y.-J.; Jiang, S. Transport of a Liquid Water and Methanol Mixture through Carbon Nanotubes under a Chemical Potential Gradient. *The Journal of Chemical Physics* **2005,** *122*, 214702.
(801) Ghoufi, A.; Szymczyk, A.; Malfreyt, P. Ultrafast Diffusion of Ionic Liquids Confined in Carbon Nanotubes. *Scientific Reports* **2016,** *6*, 28518.
(802) Chaban, V. V.; Prezhdo, O. V. Nanoscale Carbon Greatly Enhances Mobility of a Highly Viscous Ionic Liquid. *ACS Nano* **2014,** *8*, 8190-8197.
(803) Yang, H.; Liu, Y.; Zhang, H.; Li, Z.-S. Diffusion of Single Alkane Molecule in Carbon Nanotube Studied by Molecular Dynamics Simulation. *Polymer* **2006,** *47*, 7607-7610.
(804) Nair, R. R.; Wu, H. A.; Jayaram, P. N.; Grigorieva, I. V.; Geim, A. K. Unimpeded Permeation of Water through Helium-Leak–Tight Graphene-Based Membranes. *Science* **2012,** *335*, 442-444.
(805) Ban, S.; Xie, J.; Wang, Y.; Jing, B.; Liu, B.; Zhou, H. Insight into the Nanoscale Mechanism of Rapid H2o Transport within a Graphene Oxide Membrane: Impact of Oxygen Functional Group Clustering. *ACS Applied Materials & Interfaces* **2016,** *8*, 321-332.
(806) Kalugin, O. N.; Chaban, V. V.; Loskutov, V. V.; Prezhdo, O. V. Uniform Diffusion of Acetonitrile inside Carbon Nanotubes Favors Supercapacitor Performance. *Nano Lett.* **2008,** *8*, 2126-2130.
(807) Kondratyuk, P.; Yates, J. T. Molecular Views of Physical Adsorption inside and Outside of Single-Wall Carbon Nanotubes. *Acc. Chem. Res.* **2007,** *40*, 995-1004.
(808) Liu, X.; Pan, X.; Shen, W.; Ren, P.; Han, X.; Bao, X. Nmr Study of Preferential Endohedral Adsorption of Methanol in Multiwalled Carbon Nanotubes. *The Journal of Physical Chemistry C* **2012,** *116*, 7803-7809.
(809) Shen, W.; Li, X.; Zhang, H. The Initial Adsorption Process of Benzene in Double-Walled Carbon Nanotubes Studied by in Situ Solid-State Nmr. *RSC Advances* **2015,** *5*, 69848-69853.
(810) Ren, P.; Zheng, A.; Pan, X.; Han, X.; Bao, X. Dft Study on the Nmr Chemical Shifts of Molecules Confined in Carbon Nanotubes. *The Journal of Physical Chemistry C* **2013,** *117*, 23418-23424.
(811) Shim, Y.; Jung, Y.; Kim, H. J. Carbon Nanotubes in Benzene: Internal and External Solvation. *PCCP* **2011,** *13*, 3969-3978.
(812) Fomin, Y. D.; Tsiok, E. N.; Ryzhov, V. N. The Behavior of Benzene Confined in a Single Wall Carbon Nanotube. *J. Comput. Chem.* **2015,** *36*, 901-906.

(813) Huang, L.; Zhang, L.; Shao, Q.; Lu, L.; Lu, X.; Jiang, S.; Shen, W. Simulations of Binary Mixture Adsorption of Carbon Dioxide and Methane in Carbon Nanotubes: Temperature, Pressure, and Pore Size Effects. *The Journal of Physical Chemistry C* **2007,** *111*, 11912-11920.
(814) Cao, W.; Tow, G. M.; Lu, L.; Huang, L.; Lu, X. Diffusion of Co2/Ch4 Confined in Narrow Carbon Nanotube Bundles. *Mol. Phys.* **2016,** *114*, 2530-2540.
(815) Liu, L.; Nicholson, D.; Bhatia, S. K. Adsorption of Ch4 and Ch4/Co2 Mixtures in Carbon Nanotubes and Disordered Carbons: A Molecular Simulation Study. *Chem. Eng. Sci.* **2015,** *121*, 268-278.
(816) Kowalczyk, P.; Brualla, L.; Żywociński, A.; Bhatia, S. K. Single-Walled Carbon Nanotubes: Efficient Nanomaterials for Separation and on-Board Vehicle Storage of Hydrogen and Methane Mixture at Room Temperature? *The Journal of Physical Chemistry C* **2007,** *111*, 5250-5257.
(817) Xingling, T.; Zhigang, W.; Zaixing, Y.; Peng, X.; Bo, Z. Adsorptive Separation of Ethylene/Ethane Mixtures Using Carbon Nanotubes: A Molecular Dynamics Study. *J. Phys. D: Appl. Phys.* **2013,** *46*, 395302.
(818) Guan, J.; Pan, X.; Liu, X.; Bao, X. Syngas Segregation Induced by Confinement in Carbon Nanotubes: A Combined First-Principles and Monte Carlo Study. *The Journal of Physical Chemistry C* **2009,** *113*, 21687-21692.
(819) Gao, Y.; Xie, K.; Mi, S.; Liu, N.; Wang, W.; Huang, W. Preferential Oxidation of Co in a H2-Rich Stream over Multi-Walled Carbon Nanotubes Confined Ru Catalysts. *Int. J. Hydrogen Energy* **2013,** *38*, 16665-16676.
(820) Rodriguez, J.; Elola, M. D.; Laria, D. Confined Polar Mixtures within Cylindrical Nanocavities. *The Journal of Physical Chemistry B* **2010,** *114*, 7900-7908.
(821) Wells, R. H.; Thompson, W. H. What Determines the Location of a Small Solute in a Nanoconfined Liquid? *The Journal of Physical Chemistry B* **2015,** *119*, 12446-12454.
(822) Zhang, H.; Pan, X.; Han, X.; Liu, X.; Wang, X.; Shen, W.; Bao, X. Enhancing Chemical Reactions in a Confined Hydrophobic Environment: An Nmr Study of Benzene Hydroxylation in Carbon Nanotubes. *Chemical Science* **2013,** *4*, 1075-1078.
(823) Mataz, A.; Gregory, B. M. Effects of Confinement on Material Behaviour at the Nanometre Size Scale. *J. Phys.: Condens. Matter* **2005,** *17*, R461.
(824) Chaban, V. V.; Prezhdo, V. V.; Prezhdo, O. V. Confinement by Carbon Nanotubes Drastically Alters the Boiling and Critical Behavior of Water Droplets. *ACS Nano* **2012,** *6*, 2766-2773.
(825) Agrawal, K. V.; Shimizu, S.; Drahushuk, L. W.; Kilcoyne, D.; Strano, M. S. Observation of Extreme Phase Transition Temperatures of Water Confined inside Isolated Carbon Nanotubes. *Nature Nanotechnology* **2016,** *12*, 267.
(826) Chen, S.; Wu, G.; Sha, M.; Huang, S. Transition of Ionic Liquid [Bmim][Pf6] from Liquid to High-Melting-Point Crystal When Confined in Multiwalled Carbon Nanotubes. *J. Am. Chem. Soc.* **2007,** *129*, 2416-2417.
(827) Zhang, S.; Zhang, J.; Zhang, Y.; Deng, Y. Nanoconfined Ionic Liquids. *Chem. Rev.* **2017,** *117*, 6755-6833.
(828) Tessonnier, J.-P.; Ersen, O.; Weinberg, G.; Pham-Huu, C.; Su, D. S.; Schlögl, R. Selective Deposition of Metal Nanoparticles inside or Outside Multiwalled Carbon Nanotubes. *ACS Nano* **2009,** *3*, 2081-2089.
(829) Trang Nguyen, T.; Serp, P. Confinement of Metal Nanoparticles in Carbon Nanotubes. *ChemCatChem* **2013,** *5*, 3595-3603.
(830) Castillejos, E.; Debouttière, P.-J.; Roiban, L.; Solhy, A.; Martinez, V.; Kihn, Y.; Ersen, O.; Philippot, K.; Chaudret, B.; Serp, P. An Efficient Strategy to Drive Nanoparticles into Carbon Nanotubes and the Remarkable Effect of Confinement on Their Catalytic Performance. *Angew. Chem. Int. Ed.* **2009,** *48*, 2529-2533.
(831) Pan, X.; Fan, Z.; Chen, W.; Ding, Y.; Luo, H.; Bao, X. Enhanced Ethanol Production inside Carbon-Nanotube Reactors Containing Catalytic Particles. *Nature Materials* **2007,** *6*, 507.

(832) Li, X.; Hungria, T.; Garcia Marcelot, C.; Axet, M. R.; Fazzini, P. F.; Tan, R. P.; Serp, P.; Soulantica, K. Confinement Effects on the Shape and Composition of Bimetallic Nano-Objects in Carbon Nanotubes. *Chem. Commun.* **2016,** *52*, 2362-2365.

(833) Chen, Y. K.; Green, M. L. H.; Tsang, S. C. Synthesis of Carbon Nanotubes Filled with Long Continuous Crystals of Molybdenum Oxides. *Chem. Commun.* **1996**, DOI:10.1039/CC9960002489 10.1039/CC9960002489, 2489-2490.

(834) Kiang, C.-H.; Choi, J.-S.; Tran, T. T.; Bacher, A. D. Molecular Nanowires of 1 Nm Diameter from Capillary Filling of Single-Walled Carbon Nanotubes. *The Journal of Physical Chemistry B* **1999,** *103*, 7449-7451.

(835) Elías, A. L.; Rodríguez-Manzo, J. A.; McCartney, M. R.; Golberg, D.; Zamudio, A.; Baltazar, S. E.; López-Urías, F.; Muñoz-Sandoval, E.; Gu, L.; Tang, C. C.et al. Production and Characterization of Single-Crystal Feco Nanowires inside Carbon Nanotubes. *Nano Lett.* **2005,** *5*, 467-472.

(836) Grobert, N.; Mayne, M.; Terrones, M.; Sloan, J.; Dunin-Borkowski, R. E.; Kamalakaran, R.; Seeger, T.; Terrones, H.; Rühle, M.; Walton, D. R. M.et al. Alloy Nanowires: Invar inside Carbon Nanotubes. *Chem. Commun.* **2001**, DOI:10.1039/B100190F 10.1039/B100190F, 471-472.

(837) Eliseev, A. A.; Falaleev, N. S.; Verbitskiy, N. I.; Volykhov, A. A.; Yashina, L. V.; Kumskov, A. S.; Zhigalina, V. G.; Vasiliev, A. L.; Lukashin, A. V.; Sloan, J.et al. Size-Dependent Structure Relations between Nanotubes and Encapsulated Nanocrystals. *Nano Lett.* **2017,** *17*, 805-810.

(838) Kitaura, R.; Imazu, N.; Kobayashi, K.; Shinohara, H. Fabrication of Metal Nanowires in Carbon Nanotubes Via Versatile Nano-Template Reaction. *Nano Lett.* **2008,** *8*, 693-699.

(839) Govindaraj, A.; Satishkumar, B. C.; Nath, M.; Rao, C. N. R. Metal Nanowires and Intercalated Metal Layers in Single-Walled Carbon Nanotube Bundles. *Chem. Mater.* **2000,** *12*, 202-205.

(840) Kobayashi, K.; Kitaura, R.; Sasaki, K.; Kuroda, K.; Saito, T.; Shinohara, H. <I>in Situ</I> Observation of Gold Chloride Decomposition in a Confined Nanospace by Transmission Electron Microscopy. *MATERIALS TRANSACTIONS* **2014,** *55*, 461-465.

(841) Sloan, J.; M. Wright, D.; Bailey, S.; Brown, G.; P. E. York, A.; S. Coleman, K.; L. H. Green, M.; Sloan, J.; M. Wright, D.; L. Hutchison, J.et al. Capillarity and Silver Nanowire Formation Observed in Single Walled Carbon Nanotubes. *Chem. Commun.* **1999**, DOI:10.1039/A901572H 10.1039/A901572H, 699-700.

(842) Chan, L. H.; Hong, K. H.; Lai, S. H.; Liu, X. W.; Shih, H. C. The Formation and Characterization of Palladium Nanowires in Growing Carbon Nanotubes Using Microwave Plasma-Enhanced Chemical Vapor Deposition. *Thin Solid Films* **2003,** *423*, 27-32.

(843) Muramatsu, H.; Hayashi, T.; Kim, Y. A.; Shimamoto, D.; Endo, M.; Terrones, M.; Dresselhaus, M. S. Synthesis and Isolation of Molybdenum Atomic Wires. *Nano Lett.* **2008,** *8*, 237-240.

(844) Kitaura, R.; Nakanishi, R.; Saito, T.; Yoshikawa, H.; Awaga, K.; Shinohara, H. High-Yield Synthesis of Ultrathin Metal Nanowires in Carbon Nanotubes. *Angew. Chem. Int. Ed.* **2009,** *48*, 8298-8302.

(845) Medeiros, P. V. C.; Marks, S.; Wynn, J. M.; Vasylenko, A.; Ramasse, Q. M.; Quigley, D.; Sloan, J.; Morris, A. J. Single-Atom Scale Structural Selectivity in Te Nanowires Encapsulated inside Ultranarrow, Single-Walled Carbon Nanotubes. *ACS Nano* **2017,** *11*, 6178-6185.

(846) Vasylenko, A.; Marks, S.; Wynn, J. M.; Medeiros, P. V. C.; Ramasse, Q. M.; Morris, A. J.; Sloan, J.; Quigley, D. Electronic Structure Control of Sub-Nanometer 1d Snte Via Nanostructuring within Single-Walled Carbon Nanotubes. *ACS Nano* **2018,** *12*, 6023-6031.

(847) Manzetti, S. Molecular and Crystal Assembly inside the Carbon Nanotube: Encapsulation and Manufacturing Approaches. *Advances in Manufacturing* **2013,** *1*, 198-210.

(848) Guerret-Piécourt, C.; Bouar, Y. L.; Lolseau, A.; Pascard, H. Relation between Metal Electronic Structure and Morphology of Metal Compounds inside Carbon Nanotubes. *Nature* **1994,** *372*, 761.

(849) Prasad, B. R.; Lele, S. Stabilization of the Amorphous Phase inside Carbon Nanotubes: Solidification in a Constrained Geometry. *Philos. Mag. Lett.* **1994,** *70*, 357-361.

(850) Kim, H.; Kaufman, M. J.; Sigmund, W. M. Phase Transition of Iron inside Carbon Nanotubes under Electron Irradiation. *J. Mater. Res.* **2011,** *19*, 1835-1839.

(851) Yang, Z.; Guo, S.; Pan, X.; Wang, J.; Bao, X. Fen Nanoparticles Confined in Carbon Nanotubes for Co Hydrogenation. *Energy & Environmental Science* **2011,** *4*, 4500-4503.
(852) Hart, M.; Chen, J.; Michaelides, A.; Sella, A.; Shaffer, M. S. P.; Salzmann, C. G. One-Dimensional Arsenic Allotropes: Polymerization of Yellow Arsenic inside Single-Wall Carbon Nanotubes. *Angew. Chem. Int. Ed.* **2018,** *57*, 11649-11653.
(853) Sun, C.; Ma, M.; Yang, J.; Zhang, Y.; Chen, P.; Huang, W.; Dong, X. Phase-Controlled Synthesis of A-Nis Nanoparticles Confined in Carbon Nanorods for High Performance Supercapacitors. *Scientific Reports* **2014,** *4*, 7054.
(854) Giusca, C. E.; Stolojan, V.; Sloan, J.; Börrnert, F.; Shiozawa, H.; Sader, K.; Rümmeli, M. H.; Büchner, B.; Silva, S. R. P. Confined Crystals of the Smallest Phase-Change Material. *Nano Lett.* **2013,** *13*, 4020-4027.
(855) Pham-Huu, C.; Keller, N.; Estournès, C.; Ehret, G.; Grenèche, J. M.; Ledoux, M. J. Microstructural Investigation and Magnetic Properties of Cofe2o4 Nanowires Synthesized inside Carbon Nanotubes. *PCCP* **2003,** *5*, 3716-3723.
(856) Keller, N.; Pham-Huu, C.; Shiga, T.; Estournès, C.; Grenèche, J. M.; Ledoux, M. J. Mild Synthesis of Cofe2o4 Nanowires Using Carbon Nanotube Template: A High-Coercivity Material at Room Temperature. *J. Magn. Magn. Mater.* **2004,** *272-276*, 1642-1644.
(857) Pham-Huu, C.; Keller, N.; Estournès, C.; Ehret, G.; Ledoux, M. J. Synthesis of Cofe2o4 Nanowire in Carbon Nanotubes. A New Use of the Confinement Effect. *Chem. Commun.* **2002**, DOI:10.1039/B203787B 10.1039/B203787B, 1882-1883.
(858) Toste, F. D. Beyond the Molecule. *Acc. Chem. Res.* **2018,** *51*, 2980-2981.
(859) Yu, C.; He, J. Synergic Catalytic Effects in Confined Spaces. *Chem. Commun.* **2012,** *48*, 4933-4940.
(860) Tavasoli, A.; Anahid, S.; Nakhaeipour, A. Effects of Confinement in Carbon Nanotubes on the Performance and Lifetime of Fischer-Tropsch Iron Nano Catalysts. *Iranian Journal of Chemistry and Chemical Engineering (IJCCE)* **2010,** *29*, 1-12.
(861) Akbarzadeh, O.; Mohd Zabidi, N.; Abdul Wahab, Y.; Hamizi, N.; Chowdhury, Z.; Merican Aljunid Merican, Z.; Ab Rahman, M.; Akhter, S.; Rasouli, E.; Johan, M. Effect of Cobalt Catalyst Confinement in Carbon Nanotubes Support on Fischer-Tropsch Synthesis Performance. *Symmetry* **2018,** *10*, 572.
(862) Hatami, B.; Asghari, A.; Tavassoli, A.; Zamani, Y.; Zamaniyan, A. Effects of Functionalization of Carbon Nanotubes on Activity and Selectivity of Co/Cnt Catalysts in Fischer-Tropsch Synthesis. *Physical Chemistry Research* **2018,** *6*, 795-804.
(863) Abbaslou, R. M. M.; Soltan, J.; Dalai, A. K. Effects of Nanotubes Pore Size on the Catalytic Performances of Iron Catalysts Supported on Carbon Nanotubes for Fischer–Tropsch Synthesis. *Applied Catalysis A: General* **2010,** *379*, 129-134.
(864) Wang, C.; Pan, X.; Bao, X. Direct Production of Light Olefins from Syngas over a Carbon Nanotube Confined Iron Catalyst. *Chin. Sci. Bull.* **2010,** *55*, 1117-1119.
(865) Malek Abbaslou, R. M.; Tavasoli, A.; Dalai, A. K. Effect of Pre-Treatment on Physico-Chemical Properties and Stability of Carbon Nanotubes Supported Iron Fischer–Tropsch Catalysts. *Applied Catalysis A: General* **2009,** *355*, 33-41.
(866) Gu, B.; Zhou, C.; He, S.; Moldovan, S.; Chernavskii, P. A.; Ordomsky, V. V.; Khodakov, A. Y. Size and Promoter Effects on Iron Nanoparticles Confined in Carbon Nanotubes and Their Catalytic Performance in Light Olefin Synthesis from Syngas. *Catal. Today* **2019**, DOI:https://doi.org/10.1016/j.cattod.2019.05.054 https://doi.org/10.1016/j.cattod.2019.05.054.
(867) Chen, W.; Fan, Z.; Pan, X.; Bao, X. Effect of Confinement in Carbon Nanotubes on the Activity of Fischer−Tropsch Iron Catalyst. *J. Am. Chem. Soc.* **2008,** *130*, 9414-9419.
(868) Abbaslou, R. M. M.; Tavassoli, A.; Soltan, J.; Dalai, A. K. Iron Catalysts Supported on Carbon Nanotubes for Fischer–Tropsch Synthesis: Effect of Catalytic Site Position. *Applied Catalysis A: General* **2009,** *367*, 47-52.

(869) Chen, X.; Deng, D.; Pan, X.; Bao, X. Iron Catalyst Encapsulated in Carbon Nanotubes for Co Hydrogenation to Light Olefins. *Chinese Journal of Catalysis* **2015,** *36*, 1631-1637.
(870) Sun, Z.; Sun, B.; Qiao, M.; Wei, J.; Yue, Q.; Wang, C.; Deng, Y.; Kaliaguine, S.; Zhao, D. A General Chelate-Assisted Co-Assembly to Metallic Nanoparticles-Incorporated Ordered Mesoporous Carbon Catalysts for Fischer–Tropsch Synthesis. *J. Am. Chem. Soc.* **2012,** *134*, 17653-17660.
(871) Lu, Y.; Yan, Q.; Han, J.; Cao, B.; Street, J.; Yu, F. Fischer–Tropsch Synthesis of Olefin-Rich Liquid Hydrocarbons from Biomass-Derived Syngas over Carbon-Encapsulated Iron Carbide/Iron Nanoparticles Catalyst. *Fuel* **2017,** *193*, 369-384.
(872) Yu, G.; Sun, B.; Pei, Y.; Xie, S.; Yan, S.; Qiao, M.; Fan, K.; Zhang, X.; Zong, B. Fexoy@C Spheres as an Excellent Catalyst for Fischer−Tropsch Synthesis. *J. Am. Chem. Soc.* **2010,** *132*, 935-937.
(873) Ma, G.; Wang, X.; Xu, Y.; Wang, Q.; Wang, J.; Lin, J.; Wang, H.; Dong, C.; Zhang, C.; Ding, M. Enhanced Conversion of Syngas to Gasoline-Range Hydrocarbons over Carbon Encapsulated Bimetallic Femn Nanoparticles. *ACS Applied Energy Materials* **2018,** *1*, 4304-4312.
(874) Trépanier, M.; Tavasoli, A.; Dalai, A. K.; Abatzoglou, N. Fischer–Tropsch Synthesis over Carbon Nanotubes Supported Cobalt Catalysts in a Fixed Bed Reactor: Influence of Acid Treatment. *Fuel Process. Technol.* **2009,** *90*, 367-374.
(875) Xing, C.; Yang, G.; Wang, D.; Zeng, C.; Jin, Y.; Yang, R.; Suehiro, Y.; Tsubaki, N. Controllable Encapsulation of Cobalt Clusters inside Carbon Nanotubes as Effective Catalysts for Fischer–Tropsch Synthesis. *Catal. Today* **2013,** *215*, 24-28.
(876) Nakhaei Pour, A.; Housaindokht, M. R.; Kamali Shahri, S. M. Fischer–Tropsch Synthesis over Cobalt/Cnts Catalysts: Functionalized Support and Catalyst Preparation Effect on Activity and Kinetic Parameters. *Industrial & Engineering Chemistry Research* **2018,** *57*, 13639-13649.
(877) Fu, T.; Jiang, Y.; Lv, J.; Li, Z. Effect of Carbon Support on Fischer–Tropsch Synthesis Activity and Product Distribution over Co-Based Catalysts. *Fuel Process. Technol.* **2013,** *110*, 141-149.
(878) Surisetty Venkateswara, R.; Epelde, E.; Trépanier, M.; Kozinski, J.; Dalai Ajay, K. In *International Journal of Chemical Reactor Engineering*, 2012; Vol. 10.
(879) Zhu, Y.; Ye, Y.; Zhang, S.; Leong, M. E.; Tao, F. Synthesis and Catalysis of Location-Specific Cobalt Nanoparticles Supported by Multiwall Carbon Nanotubes for Fischer–Tropsch Synthesis. *Langmuir* **2012,** *28*, 8275-8280.
(880) Xie, W.; Zhang, Y.; Liew, K.; Li, J. Effect of Catalyst Confinement and Pore Size on Fischer-Tropsch Synthesis over Cobalt Supported on Carbon Nanotubes. *Science China Chemistry* **2012,** *55*, 1811-1818.
(881) Tavasoli, A.; Trépanier, M.; Dalai, A. K.; Abatzoglou, N. Effects of Confinement in Carbon Nanotubes on the Activity, Selectivity, and Lifetime of Fischer−Tropsch Co/Carbon Nanotube Catalysts. *Journal of Chemical & Engineering Data* **2010,** *55*, 2757-2763.
(882) Vosoughi, V.; Badoga, S.; Dalai, A. K.; Abatzoglou, N. Effect of Pretreatment on Physicochemical Properties and Performance of Multiwalled Carbon Nanotube Supported Cobalt Catalyst for Fischer–Tropsch Synthesis. *Industrial & Engineering Chemistry Research* **2016,** *55*, 6049-6059.
(883) Ha, K.-S.; Kwak, G.; Jun, K.-W.; Hwang, J.; Lee, J. Ordered Mesoporous Carbon Nanochannel Reactors for High-Performance Fischer–Tropsch Synthesis. *Chem. Commun.* **2013,** *49*, 5141-5143.
(884) Pendyala, V. R. R.; Jacobs, G.; Graham, U. M.; Shafer, W. D.; Martinelli, M.; Kong, L.; Davis, B. H. Fischer–Tropsch Synthesis: Influence of Acid Treatment and Preparation Method on Carbon Nanotube Supported Ruthenium Catalysts. *Industrial & Engineering Chemistry Research* **2017,** *56*, 6408-6418.
(885) Phaahlamohlaka, T. N.; Kumi, D. O.; Dlamini, M. W.; Jewell, L. L.; Coville, N. J. Ruthenium Nanoparticles Encapsulated inside Porous Hollow Carbon Spheres: A Novel Catalyst for Fischer–Tropsch Synthesis. *Catal. Today* **2016,** *275*, 76-83.
(886) Zhang, A. M.; Dong, J. L.; Xu, Q. H.; Rhee, H. K.; Li, X. L. Palladium Cluster Filled in Inner of Carbon Nanotubes and Their Catalytic Properties in Liquid Phase Benzene Hydrogenation. *Catal. Today* **2004,** *93-95*, 347-352.

(887) Ma, H.; Yu, T.; Pan, X.; Bao, X. Confinement Effect of Carbon Nanotubes on the Product Distribution of Selective Hydrogenation of Cinnamaldehyde. *Chinese Journal of Catalysis* **2017,** *38*, 1315-1321.
(888) Castillejos, E.; Jahjah, M.; Favier, I.; Orejón, A.; Pradel, C.; Teuma, E.; Masdeu-Bultó, A. M.; Serp, P.; Gómez, M. Synthesis of Platinum–Ruthenium Nanoparticles under Supercritical Co2 and Their Confinement in Carbon Nanotubes: Hydrogenation Applications. *ChemCatChem* **2012,** *4*, 118-122.
(889) Chen, Z.; Guan, Z.; Li, M.; Yang, Q.; Li, C. Enhancement of the Performance of a Platinum Nanocatalyst Confined within Carbon Nanotubes for Asymmetric Hydrogenation. *Angew. Chem. Int. Ed.* **2011,** *50*, 4913-4917.
(890) Guan, Z.; Lu, S.; Li, C. Highly Oxidized Pt Species Stabilized inside Carbon Nanotubes for Asymmetric Hydrogenation. *Chinese Journal of Catalysis* **2015,** *36*, 1535-1542.
(891) Guan, Z.; Lu, S.; Li, C. Enantioselective Hydrogenation of A,B-Unsaturated Carboxylic Acid over Cinchonidine-Modified Pd Nanoparticles Confined in Carbon Nanotubes. *J. Catal.* **2014,** *311*, 1-5.
(892) Yang, H.; Song, S.; Rao, R.; Wang, X.; Yu, Q.; Zhang, A. Enhanced Catalytic Activity of Benzene Hydrogenation over Nickel Confined in Carbon Nanotubes. *J. Mol. Catal. A: Chem.* **2010,** *323*, 33-39.
(893) Wang, J.; Lu, S.-m.; Li, J.; Li, C. A Remarkable Difference in Co2 Hydrogenation to Methanol on Pd Nanoparticles Supported inside and Outside of Carbon Nanotubes. *Chem. Commun.* **2015,** *51*, 17615-17618.
(894) Ran, M.; Liu, Y.; Chu, W.; Borgna, A. Enhanced Conversion of Cellobiose to Sugar Alcohols by Controlled Dispersion of Ruthenium Nanoparticles inside Carbon Nanotube Channels. *Catal. Lett.* **2013,** *143*, 1139-1144.
(895) Priecel, P.; Endot, N. A.; Carà, P. D.; Lopez-Sanchez, J. A. Fast Catalytic Hydrogenation of 2,5-Hydroxymethylfurfural to 2,5-Dimethylfuran with Ruthenium on Carbon Nanotubes. *Industrial & Engineering Chemistry Research* **2018,** *57*, 1991-2002.
(896) Wang, D.; Yang, G.; Ma, Q.; Wu, M.; Tan, Y.; Yoneyama, Y.; Tsubaki, N. Confinement Effect of Carbon Nanotubes: Copper Nanoparticles Filled Carbon Nanotubes for Hydrogenation of Methyl Acetate. *ACS Catalysis* **2012,** *2*, 1958-1966.
(897) Zheng, J.; Duan, X.; Lin, H.; Gu, Z.; Fang, H.; Li, J.; Yuan, Y. Silver Nanoparticles Confined in Carbon Nanotubes: On the Understanding of the Confinement Effect and Promotional Catalysis for the Selective Hydrogenation of Dimethyl Oxalate. *Nanoscale* **2016,** *8*, 5959-5967.
(898) Zhang, X.; Guo, Y. C.; Cheng Zhang, Z.; Gao, J. S.; Xu, C. M. High Performance of Carbon Nanotubes Confining Gold Nanoparticles for Selective Hydrogenation of 1,3-Butadiene and Cinnamaldehyde. *J. Catal.* **2012,** *292*, 213-226.
(899) Su, F.; Lee, F. Y.; Lv, L.; Liu, J.; Tian, X. N.; Zhao, X. S. Sandwiched Ruthenium/Carbon Nanostructures for Highly Active Heterogeneous Hydrogenation. *Adv. Funct. Mater.* **2007,** *17*, 1926-1931.
(900) Li, F.; Liang, J.; Wang, K.; Cao, B.; Zhu, W.; Song, H. Hydrogenation of M-Chloronitrobenzene over Amorphous Ni-B/Cnts Catalysts: Promoting Effect of Cnts Confinement on the Catalytic Performance. *The Canadian Journal of Chemical Engineering* **2017,** *95*, 2012-2017.
(901) Chen, T.; Lei, Y.; Yang, Q.; Wu, Y. Stable and Accessible Metal Catalysts Confined by Mesoporous Carbon Structures Derived from Multicomponent Colloidal Spheres. *Journal of Materials Chemistry A* **2017,** *5*, 3136-3139.
(902) Chen, G.; Gao, W.; Wang, X.; Huo, H.; Li, W.; Zhang, L.; Li, R.; Li, Z. Magnetic Nio Nanoparticles Confined within Open Ends Mwcnts: A Novel and Highly Active Catalyst for Hydrogenation and Synthesis of Imines. *RSC Advances* **2016,** *6*, 58805-58812.
(903) Chesnokov, V. V.; Svintsitskii, D. A.; Chichkan', A. S.; Parmon, V. N. Effect of the Structure of Carbon Support on the Selectivity of Pt/C Catalysts for the Hydrogenation of Acetylene to Ethylene. *Nanotechnologies in Russia* **2018,** *13*, 246-255.

(904) Wang, Y.; Rong, Z.; Wang, Y.; Zhang, P.; Wang, Y.; Qu, J. Ruthenium Nanoparticles Loaded on Multiwalled Carbon Nanotubes for Liquid-Phase Hydrogenation of Fine Chemicals: An Exploration of Confinement Effect. *J. Catal.* **2015,** *329*, 95-106.
(905) Aygün, M.; Chamberlain, T. W.; Gimenez-Lopez, M. d. C.; Khlobystov, A. N. Magnetically Recyclable Catalytic Carbon Nanoreactors. *Adv. Funct. Mater.* **2018,** *28*, 1802869.
(906) Shi, J.; Wang, Y.; Du, W.; Hou, Z. Synthesis of Graphene Encapsulated Fe3c in Carbon Nanotubes from Biomass and Its Catalysis Application. *Carbon* **2016,** *99*, 330-337.
(907) Xi, J.; Sun, H.; Wang, D.; Zhang, Z.; Duan, X.; Xiao, J.; Xiao, F.; Liu, L.; Wang, S. Confined-Interface-Directed Synthesis of Palladium Single-Atom Catalysts on Graphene/Amorphous Carbon. *Applied Catalysis B: Environmental* **2018,** *225*, 291-297.
(908) Peer, M.; Qajar, A.; Rajagopalan, R.; Foley, H. C. On the Effects of Confinement within a Catalyst Consisting of Platinum Embedded within Nanoporous Carbon for the Hydrogenation of Alkenes. *Carbon* **2014,** *66*, 459-466.
(909) Aygün, M.; Stoppiello, C. T.; Lebedeva, M. A.; Smith, E. F.; Gimenez-Lopez, M. d. C.; Khlobystov, A. N.; Chamberlain, T. W. Comparison of Alkene Hydrogenation in Carbon Nanoreactors of Different Diameters: Probing the Effects of Nanoscale Confinement on Ruthenium Nanoparticle Catalysis. *Journal of Materials Chemistry A* **2017,** *5*, 21467-21477.
(910) Lu, H.; Xu, B.; Wang, X.; Hu, Z.; Fan, Y. The Influence of Pd Particles Distribution Position on Pd/Cnts Catalyst for Acetylene Selective Hydrogenation. *Catal. Lett.* **2014,** *144*, 2198-2203.
(911) Xu, S.; Zhang, P.; Li, H.; Wei, H.; Li, L.; Li, B.; Wang, X. Ru Nanoparticles Confined in Carbon Nanotubes: Supercritical Co2 Assisted Preparation and Improved Catalytic Performances in Hydrogenation of D-Glucose. *RSC Advances* **2014,** *4*, 7079-7083.
(912) Ran, M.; Chu, W.; Liu, Y.; Borgna, A. Nano Ru Catalysts Supported on Carbon Nanotubes for Cellobiose Conversion to Sugar Alcohols: Effects of Cnt Channel Size. *RSC Advances* **2015,** *5*, 103669-103673.
(913) Wang, W.; Villa, A.; Kübel, C.; Hahn, H.; Wang, D. Tailoring the 3d Structure of Pd Nanocatalysts Supported on Mesoporous Carbon for Furfural Hydrogenation. *ChemNanoMat* **2018,** *4*, 1125-1132.
(914) Chamberlain, T. W.; Earley, J. H.; Anderson, D. P.; Khlobystov, A. N.; Bourne, R. A. Catalytic Nanoreactors in Continuous Flow: Hydrogenation inside Single-Walled Carbon Nanotubes Using Supercritical Co2. *Chem. Commun.* **2014,** *50*, 5200-5202.
(915) Tessonnier, J.-P.; Pesant, L.; Ehret, G.; Ledoux, M. J.; Pham-Huu, C. Pd Nanoparticles Introduced inside Multi-Walled Carbon Nanotubes for Selective Hydrogenation of Cinnamaldehyde into Hydrocinnamaldehyde. *Applied Catalysis A: General* **2005,** *288*, 203-210.
(916) Ma, H.; Wang, L.; Chen, L.; Dong, C.; Yu, W.; Huang, T.; Qian, Y. Pt Nanoparticles Deposited over Carbon Nanotubes for Selective Hydrogenation of Cinnamaldehyde. *Catal. Commun.* **2007,** *8*, 452-456.
(917) Guan, Z.; Lu, S.; Chen, Z.; Li, C. An Unexpected Effect of Water on the Asymmetric Hydrogenation of A-Ketoesters on Platinum Nanoparticles Confined in Carbon Nanotubes. *J. Catal.* **2013,** *305*, 19-26.
(918) Turner, C. H.; Johnson, J. K.; Gubbins, K. E. Effect of Confinement on Chemical Reaction Equilibria: The Reactions 2no⇔(No)2 and N2+3h2⇔2nh3 in Carbon Micropores. *The Journal of Chemical Physics* **2001,** *114*, 1851-1859.
(919) Qin, W.; Li, X. A Theoretical Study on the Catalytic Effect of Nanoparticle Confined in Carbon Nanotube. *Chem. Phys. Lett.* **2011,** *502*, 96-100.
(920) Rao, R.; Zhang, Q.; Liu, H.; Yang, H.; Ling, Q.; Yang, M.; Zhang, A.; Chen, W. Enhanced Catalytic Performance of Ceo2 Confined inside Carbon Nanotubes for Dehydrogenation of Ethylbenzene in the Presence of Co2. *J. Mol. Catal. A: Chem.* **2012,** *363-364*, 283-290.
(921) Li, C.; Sun, Y.; Zhang, A. Binary Ce–Mn Oxides Confined in Carbon Nanotubes as Efficient Catalysts for Ethylbenzene Dehydrogenation in the Presence of Carbon Dioxide. *RSC Advances* **2015,** *5*, 36394-36403.

(922) Zhang, J.; Müller, J.-O.; Zheng, W.; Wang, D.; Su, D.; Schlögl, R. Individual Fe−Co Alloy Nanoparticles on Carbon Nanotubes: Structural and Catalytic Properties. *Nano Lett.* **2008,** *8*, 2738-2743.
(923) Zheng, W.; Zhang, J.; Zhu, B.; Blume, R.; Zhang, Y.; Schlichte, K.; Schlögl, R.; Schüth, F.; Su, D. S. Structure–Function Correlations for Ru/Cnt in the Catalytic Decomposition of Ammonia. *ChemSusChem* **2010,** *3*, 226-230.
(924) Fu, T.; Wang, X.; Zheng, H.; Li, Z. Effect of Cu Location and Dispersion on Carbon Sphere Supported Cu Catalysts for Oxidative Carbonylation of Methanol to Dimethyl Carbonate. *Carbon* **2017,** *115*, 363-374.
(925) Panić, S.; Kukovecz, Á.; Boskovic, G. Design of Catalytic Carbon Nanotube-Based Reactor for Water Denitration – the Impact of Active Metal Confinement. *Applied Catalysis B: Environmental* **2018,** *225*, 207-217.
(926) Ding, T.-Y.; Zhao, Z.-G.; Ran, M.-F.; Yang, Y.-Y. Superior Activity of Pd Nanoparticles Confined in Carbon Nanotubes for Hydrogen Production from Formic Acid Decomposition at Ambient Temperature. *J. Colloid Interface Sci.* **2019,** *538*, 474-480.
(927) Dongil, A. B.; Pastor-Pérez, L.; Sepúlveda-Escribano, A.; García, R.; Escalona, N. Hydrodeoxygenation of Guaiacol: Tuning the Selectivity to Cyclohexene by Introducing Ni Nanoparticles inside Carbon Nanotubes. *Fuel* **2016,** *172*, 65-69.
(928) Zhang, F.; Jiao, F.; Pan, X.; Gao, K.; Xiao, J.; Zhang, S.; Bao, X. Tailoring the Oxidation Activity of Pt Nanoclusters Via Encapsulation. *ACS Catalysis* **2015,** *5*, 1381-1385.
(929) Sun, Y.; Li, X.; Wang, J.; Ning, W.; Fu, J.; Lu, X.; Hou, Z. Carbon Film Encapsulated Pt Nps for Selective Oxidation of Alcohols in Acidic Aqueous Solution. *Applied Catalysis B: Environmental* **2017,** *218*, 538-544.
(930) Yang, M.; Ling, Q.; Yang, H.; Li, C.; Zhang, A. Enhanced Catalytic Activity of K-Birnessite Mno2 Confined in Carbon Nanotubes for Selective Oxidation of Benzyl Alcohol. *Catal. Commun.* **2014,** *46*, 238-241.
(931) Castillejos, E.; Chico, R.; Bacsa, R.; Coco, S.; Espinet, P.; Pérez-Cadenas, M.; Guerrero-Ruiz, A.; Rodríguez-Ramos, I.; Serp, P. Selective Deposition of Gold Nanoparticles on or inside Carbon Nanotubes and Their Catalytic Activity for Preferential Oxidation of Co. *Eur. J. Inorg. Chem.* **2010,** *2010*, 5096-5102.
(932) Li, B.; Wang, C.; Yi, G.; Lin, H.; Yuan, Y. Enhanced Performance of Ru Nanoparticles Confined in Carbon Nanotubes for Co Preferential Oxidation in a H2-Rich Stream. *Catal. Today* **2011,** *164*, 74-79.
(933) Shi, L.; Zhang, G.; Wang, Y. Tailoring Catalytic Performance of Carbon Nanotubes Confined Cuoceo2 Catalysts for Co preferential Oxidation. *Int. J. Hydrogen Energy* **2018,** *43*, 18211-18219.
(934) Zhang, H.; Pan, X.; Liu , J.; Qian, W.; Wei, F.; Huang, Y.; Bao, X. Enhanced Catalytic Activity of Sub-Nanometer Titania Clusters Confined inside Double-Wall Carbon Nanotubes. *ChemSusChem* **2011,** *4*, 975-980.
(935) Shi, Z.-Q.; Dong, Z.-P.; Sun, J.; Zhang, F.-W.; Yang, H.-L.; Zhou, J.-H.; Zhu, X.-H.; Li, R. Filled Cobalt Nanoparticles into Carbon Nanotubes as a Rapid and High-Efficiency Catalyst for Selective Epoxidation of Styrene with Molecular Oxygen. *Chem. Eng. J.* **2014,** *237*, 81-87.
(936) Zhang, H.; Pan, X.; Bao, X. Facile Filling of Metal Particles in Small Carbon Nanotubes for Catalysis. *Journal of Energy Chemistry* **2013,** *22*, 251-256.
(937) Solomonsz, W. A.; Rance, G. A.; Suyetin, M.; La Torre, A.; Bichoutskaia, E.; Khlobystov, A. N. Controlling the Regioselectivity of the Hydrosilylation Reaction in Carbon Nanoreactors. *Chemistry – A European Journal* **2012,** *18*, 13180-13187.
(938) Solomonsz, W. A.; Rance, G. A.; Harris, B. J.; Khlobystov, A. N. Competitive Hydrosilylation in Carbon Nanoreactors: Probing the Effect of Nanoscale Confinement on Selectivity. *Nanoscale* **2013,** *5*, 12200-12205.
(939) Rance, G. A.; Solomonsz, W. A.; Khlobystov, A. N. Click Chemistry in Carbon Nanoreactors. *Chem. Commun.* **2013,** *49*, 1067-1069.

(940) Cornelio, B.; Saunders, A. R.; Solomonsz, W. A.; Laronze-Cochard, M.; Fontana, A.; Sapi, J.; Khlobystov, A. N.; Rance, G. A. Palladium Nanoparticles in Catalytic Carbon Nanoreactors: The Effect of Confinement on Suzuki–Miyaura Reactions. *Journal of Materials Chemistry A* **2015,** *3*, 3918-3927.

(941) Lodge, R. W.; Rance, G. A.; Fay, M. W.; Khlobystov, A. N. Movement of Palladium Nanoparticles in Hollow Graphitised Nanofibres: The Role of Migration and Coalescence in Nanocatalyst Sintering During the Suzuki–Miyaura Reaction. *Nanoscale* **2018,** *10*, 19046-19051.

(942) Shaikh, M.; Atyam, K. K.; Sahu, M.; Ranganath, K. V. S. Enhanced Reactivity and Selectivity of Asymmetric Oxa-Michael Addition of 2′-Hydroxychalcones in Carbon Confined Spaces. *Chem. Commun.* **2017,** *53*, 6029-6032.

(943) Wang, H.; Wang, Y.; Guo, Y.; Ren, X.-K.; Wu, L.; Liu, L.; Shi, Z.; Wang, Y. Pd Nanoparticles Confined within Triazine-Based Carbon Nitride Nts: An Efficient Catalyst for Knoevenagel Condensation-Reduction Cascade Reactions. *Catal. Today* **2018**, DOI:https://doi.org/10.1016/j.cattod.2018.04.020 https://doi.org/10.1016/j.cattod.2018.04.020.

(944) Russell, J.; Zapol, P.; Král, P.; Curtiss, L. A. Methane Bond Activation by Pt and Pd Subnanometer Clusters Supported on Graphene and Carbon Nanotubes. *Chem. Phys. Lett.* **2012,** *536*, 9-13.

(945) Tabassum, H.; Mahmood, A.; Zhu, B.; Liang, Z.; Zhong, R.; Guo, S.; Zou, R. Recent Advances in Confining Metal-Based Nanoparticles into Carbon Nanotubes for Electrochemical Energy Conversion and Storage Devices. *Energy & Environmental Science* **2019**, DOI:10.1039/C9EE00315K 10.1039/C9EE00315K.

(946) Deng, D.; Yu, L.; Chen, X.; Wang, G.; Jin, L.; Pan, X.; Deng, J.; Sun, G.; Bao, X. Iron Encapsulated within Pod-Like Carbon Nanotubes for Oxygen Reduction Reaction. *Angew. Chem.* **2013,** *125*, 389-393.

(947) Deng, J.; Ren, P.; Deng, D.; Yu, L.; Yang, F.; Bao, X. Highly Active and Durable Non-Precious-Metal Catalysts Encapsulated in Carbon Nanotubes for Hydrogen Evolution Reaction. *Energy & Environmental Science* **2014,** *7*, 1919-1923.

(948) Li, Y.; Lu, X.; Li, Y.; Zhang, X. Oxygen Evolution Reaction in Nanoconfined Carbon Nanotubes. *Physica E: Low-dimensional Systems and Nanostructures* **2018,** *99*, 1-5.

(949) Zhang, J.; Guo, S.; Wei, J.; Xu, Q.; Yan, W.; Fu, J.; Wang, S.; Cao, M.; Chen, Z. High-Efficiency Encapsulation of Pt Nanoparticles into the Channel of Carbon Nanotubes as an Enhanced Electrocatalyst for Methanol Oxidation. *Chemistry – A European Journal* **2013,** *19*, 16087-16092.

(950) Mezzavilla, S.; Baldizzone, C.; Swertz, A.-C.; Hodnik, N.; Pizzutilo, E.; Polymeros, G.; Keeley, G. P.; Knossalla, J.; Heggen, M.; Mayrhofer, K. J. J.et al. Structure–Activity–Stability Relationships for Space-Confined Ptxniy Nanoparticles in the Oxygen Reduction Reaction. *ACS Catalysis* **2016,** *6*, 8058-8068.

(951) Datta, A.; Kapri, S.; Bhattacharyya, S. Enhanced Catalytic Activity of Palladium Nanoparticles Confined inside Porous Carbon in Methanol Electro-Oxidation. *Green Chemistry* **2015,** *17*, 1572-1580.

(952) Song, A.; Yang, W.; Yang, W.; Sun, G.; Yin, X.; Gao, L.; Wang, Y.; Qin, X.; Shao, G. Facile Synthesis of Cobalt Nanoparticles Entirely Encapsulated in Slim Nitrogen-Doped Carbon Nanotubes as Oxygen Reduction Catalyst. *ACS Sustainable Chemistry & Engineering* **2017,** *5*, 3973-3981.

(953) Zhou, Y.; Chen, W.; Cui, P.; Zeng, J.; Lin, Z.; Kaxiras, E.; Zhang, Z. Enhancing the Hydrogen Activation Reactivity of Nonprecious Metal Substrates Via Confined Catalysis Underneath Graphene. *Nano Lett.* **2016,** *16*, 6058-6063.

(954) Park, Y.-C.; Tokiwa, H.; Kakinuma, K.; Watanabe, M.; Uchida, M. Effects of Carbon Supports on Pt Distribution, Ionomer Coverage and Cathode Performance for Polymer Electrolyte Fuel Cells. *J. Power Sources* **2016,** *315*, 179-191.

(955) Shchukin, D. G.; Sviridov, D. V. Photocatalytic Processes in Spatially Confined Micro- and Nanoreactors. *Journal of Photochemistry and Photobiology C: Photochemistry Reviews* **2006,** *7*, 23-39.

(956) Kurtoglu, A.; Walsh, D.; Khlobystov, A. N.; Gimenez-Lopez, M. d. C. Confinement of Platinum Catalysts in Carbon Nanocontainers to Control the Durability in the Oxygen Reduction Reaction. *Meeting Abstracts* **2015,** *MA2015-01*, 1875.

(957) Yang, J.; Li, L.; Yu, H.; Geng, H.; Li, C.; Dong, X. Co/N–C Nanotubes with Increased Coupling Sites by Space-Confined Pyrolysis for High Electrocatalytic Activity. *Green Energy & Environment* **2017,** *2*, 23-29.

(958) Wang, J.; Dong, Z.; Huang, J.; Li, J.; Jin, X.; Niu, J.; Sun, J.; Jin, J.; Ma, J. Filling Carbon Nanotubes with Ni–Fe Alloys Via Methylbenzene-Oriented Constant Current Electrodeposition for Hydrazine Electrocatalysis. *Appl. Surf. Sci.* **2013,** *270*, 128-132.

(959) Cui, T.; Dong, J.; Pan, X.; Yu, T.; Fu, Q.; Bao, X. Enhanced Hydrogen Evolution Reaction over Molybdenum Carbide Nanoparticles Confined inside Single-Walled Carbon Nanotubes. *Journal of Energy Chemistry* **2019,** *28*, 123-127.

(960) Chen, Z.; Wu, R.; Liu, Y.; Ha, Y.; Guo, Y.; Sun, D.; Liu, M.; Fang, F. Ultrafine Co Nanoparticles Encapsulated in Carbon-Nanotubes-Grafted Graphene Sheets as Advanced Electrocatalysts for the Hydrogen Evolution Reaction. *Adv. Mater.* **2018,** *30*, 1802011.

(961) Meng, J.; Liu, X.; Li, J.; Li, Q.; Zhao, C.; Xu, L.; Wang, X.; Liu, F.; Yang, W.; Xu, X.et al. General Oriented Synthesis of Precise Carbon-Confined Nanostructures by Low-Pressure Vapor Superassembly and Controlled Pyrolysis. *Nano Lett.* **2017,** *17*, 7773-7781.

(962) Zhang, L.; Hu, J.-S.; Huang, X.-H.; Song, J.; Lu, S.-Y. Particle-in-Box Nanostructured Materials Created Via Spatially Confined Pyrolysis as High Performance Bifunctional Catalysts for Electrochemical Overall Water Splitting. *Nano Energy* **2018,** *48*, 489-499.

(963) Guo, Y.; Yuan, P.; Zhang, J.; Xia, H.; Cheng, F.; Zhou, M.; Li, J.; Qiao, Y.; Mu, S.; Xu, Q. Co2p–Con Double Active Centers Confined in N-Doped Carbon Nanotube: Heterostructural Engineering for Trifunctional Catalysis toward Her, Orr, Oer, and Zn–Air Batteries Driven Water Splitting. *Adv. Funct. Mater.* **2018,** *28*, 1805641.

(964) Wang, J.; Gao, D.; Wang, G.; Miao, S.; Wu, H.; Li, J.; Bao, X. Cobalt Nanoparticles Encapsulated in Nitrogen-Doped Carbon as a Bifunctional Catalyst for Water Electrolysis. *Journal of Materials Chemistry A* **2014,** *2*, 20067-20074.

(965) Chen, X.; Zheng, J.; Zhong, X.; Jin, Y.; Zhuang, G.; Li, X.; Deng, S.; Wang, J.-g. Tuning the Confinement Space of N-Carbon Shell-Coated Ruthenium Nanoparticles: Highly Efficient Electrocatalysts for Hydrogen Evolution Reaction. *Catalysis Science & Technology* **2017,** *7*, 4964-4970.

(966) Suryanto, B. H. R.; Fang, T.; Cheong, S.; Tilley, R. D.; Zhao, C. From the inside-Out: Leached Metal Impurities in Multiwall Carbon Nanotubes for Purification or Electrocatalysis. *Journal of Materials Chemistry A* **2018,** *6*, 4686-4694.

(967) Mao, Z.; Hu, H.; Su, R.; Liu, P.; Li, Y.; Zhang, W.; Zhao, X.; Guo, J.; Guan, P.; Qin, G.et al. Confining Gold Nanoclusters in Highly Defective Graphitic Layers to Enhance the Methanol Electrooxidation Reaction. *ChemCatChem* **2018,** *10*, 141-147.

(968) Chen, Z.; Liu, C.; Zhao, X.; Yan, H.; Li, J.; Lyu, P.; Du, Y.; Xi, S.; Chi, K.; Chi, X.et al. Promoted Glycerol Oxidation Reaction in an Interface-Confined Hierarchically Structured Catalyst. *Adv. Mater. 0*, 1804763.

(969) Chen, W.; Fan, Z.; Zhang, B.; Ma, G.; Takanabe, K.; Zhang, X.; Lai, Z. Enhanced Visible-Light Activity of Titania Via Confinement inside Carbon Nanotubes. *J. Am. Chem. Soc.* **2011,** *133*, 14896-14899.

(970) Yang, D.; Feng, J.; Jiang, L.; Wu, X.; Sheng, L.; Jiang, Y.; Wei, T.; Fan, Z. Photocatalyst Interface Engineering: Spatially Confined Growth of Znfe2o4 within Graphene Networks as Excellent Visible-Light-Driven Photocatalysts. *Adv. Funct. Mater.* **2015,** *25*, 7080-7087.

(971) Cui, X.; Wang, Y.; Jiang, G.; Zhao, Z.; Xu, C.; Duan, A.; Liu, J.; Wei, Y.; Bai, W. The Encapsulation of Cds in Carbon Nanotubes for Stable and Efficient Photocatalysis. *Journal of Materials Chemistry A* **2014,** *2*, 20939-20946.

(972) Liu, J.; Liu, R.; Li, H.; Kong, W.; Huang, H.; Liu, Y.; Kang, Z. Au Nanoparticles in Carbon Nanotubes with High Photocatalytic Activity for Hydrocarbon Selective Oxidation. *Dalton Transactions* **2014,** *43*, 12982-12988.
(973) Cui, T.; Pan, X.; Dong, J.; Miao, S.; Miao, D.; Bao, X. A Versatile Method for the Encapsulation of Various Non-Precious Metal Nanoparticles inside Single-Walled Carbon Nanotubes. *Nano Research* **2018,** *11*, 3132-3144.
(974) Zhu, J.; Li, M.; Lu, M.; Zhu, J. Effect of Structural Properties on Catalytic Performance in Citral Selective Hydrogenation over Carbon–Titania Composite Supported Pd Catalyst. *Catalysis Science & Technology* **2013,** *3*, 737-744.
(975) Yuan, G.; Keane, M. A. Liquid Phase Catalytic Hydrodechlorination of 2,4-Dichlorophenol over Carbon Supported Palladium: An Evaluation of Transport Limitations. *Chem. Eng. Sci.* **2003,** *58*, 257-267.
(976) Zhu, J.; Wu, F.; Li, M.; Zhu, J.; van Ommen, J. G.; Lefferts, L. Influence of Internal Diffusion on Selective Hydrogenation of 4-Carboxybenzaldehyde over Palladium Catalysts Supported on Carbon Nanofiber Coated Monolith. *Applied Catalysis A: General* **2015,** *498*, 222-229.
(977) Merenov, A. S.; Nelson, A.; Abraham, M. A. Support Effects of Nickel on Activated Carbon as a Catalyst for Vapor Phase Methanol Carbonylation. *Catal. Today* **2000,** *55*, 91-101.
(978) Bergault, I.; Fouilloux, P.; Joly-Vuillemin, C.; Delmas, H. Kinetics and Intraparticle Diffusion Modelling of a Complex Multistep Reaction: Hydrogenation of Acetophenone over a Rhodium Catalyst. *J. Catal.* **1998,** *175*, 328-337.
(979) Prins, R. Hydrogen Spillover. Facts and Fiction. *Chem. Rev.* **2012,** *112*, 2714-2738.
(980) Boudart, M.; Vannice, M. A.; Benson, J. E. In *Z. Phys. Chem.*, 1969; Vol. 64.
(981) Conner, W. C.; Falconer, J. L. Spillover in Heterogeneous Catalysis. *Chem. Rev.* **1995,** *95*, 759-788.
(982) Medenbach, L.; Escher, I.; Köwitsch, N.; Armbrüster, M.; Zedler, L.; Dietzek, B.; Adelhelm, P. Sulfur Spillover on Carbon Materials and Possible Impacts on Metal–Sulfur Batteries. *Angew. Chem. Int. Ed.* **2018,** *57*, 13666-13670.
(983) Juarez-Mosqueda, R.; Mavrandonakis, A.; Kuc, A. B.; Pettersson, L. G. M.; Heine, T. Theoretical Analysis of Hydrogen Spillover Mechanism on Carbon Nanotubes. *Frontiers in Chemistry* **2015,** *3*.
(984) Psofogiannakis, G. M.; Froudakis, G. E. Dft Study of the Hydrogen Spillover Mechanism on Pt-Doped Graphite. *The Journal of Physical Chemistry C* **2009,** *113*, 14908-14915.
(985) Teichner, S. J. Recent Studies in Hydrogen and Oxygen Spillover and Their Impact on Catalysis. *Applied Catalysis* **1990,** *62*, 1-10.
(986) Pyle, D. S.; Gray, E. M.; Webb, C. J. Hydrogen Storage in Carbon Nanostructures Via Spillover. *Int. J. Hydrogen Energy* **2016,** *41*, 19098-19113.
(987) Wang, L.; Yang, R. T. Hydrogen Storage on Carbon-Based Adsorbents and Storage at Ambient Temperature by Hydrogen Spillover. *Catalysis Reviews* **2010,** *52*, 411-461.
(988) Wang, L.; Yang, R. T. New Sorbents for Hydrogen Storage by Hydrogen Spillover – a Review. *Energy & Environmental Science* **2008,** *1*, 268-279.
(989) Psofogiannakis, G. M.; Froudakis, G. E. Fundamental Studies and Perceptions on the Spillover Mechanism for Hydrogen Storage. *Chem. Commun.* **2011,** *47*, 7933-7943.
(990) Tozzini, V.; Pellegrini, V. Prospects for Hydrogen Storage in Graphene. *PCCP* **2013,** *15*, 80-89.
(991) Konda, S. K.; Chen, A. Palladium Based Nanomaterials for Enhanced Hydrogen Spillover and Storage. *Mater. Today* **2016,** *19*, 100-108.
(992) Choi, M.; Yook, S.; Kim, H. Hydrogen Spillover in Encapsulated Metal Catalysts: New Opportunities for Designing Advanced Hydroprocessing Catalysts. *ChemCatChem* **2015,** *7*, 1048-1057.
(993) Yadav, S.; Zhu, Z.; Singh, C. V. Defect Engineering of Graphene for Effective Hydrogen Storage. *Int. J. Hydrogen Energy* **2014,** *39*, 4981-4995.
(994) Mattera, L.; Rosatelli, F.; Salvo, C.; Tommasini, F.; Valbusa, U.; Vidali, G. Selective Adsorption of 1h2 and 2h2 on the (0001) Graphite Surface. *Surf. Sci.* **1980,** *93*, 515-525.

(995) Costanzo, F.; Silvestrelli, P. L.; Ancilotto, F. Physisorption, Diffusion, and Chemisorption Pathways of H2 Molecule on Graphene and on (2,2) Carbon Nanotube by First Principles Calculations. *Journal of Chemical Theory and Computation* **2012,** *8*, 1288-1294.
(996) Carlos, P. H.; Rafael, R. Diffusion of Hydrogen in Graphite: A Molecular Dynamics Simulation. *J. Phys. D: Appl. Phys.* **2010,** *43*, 255402.
(997) Petucci, J.; LeBlond, C.; Karimi, M.; Vidali, G. Diffusion, Adsorption, and Desorption of Molecular Hydrogen on Graphene and in Graphite. *The Journal of Chemical Physics* **2013,** *139*, 044706.
(998) Miura, Y.; Kasai, H.; Diño, W.; Nakanishi, H.; Sugimoto, T. First Principles Studies for the Dissociative Adsorption of H2 on Graphene. *J. Appl. Phys.* **2003,** *93*, 3395-3400.
(999) Jiang, Q. G.; Ao, Z. M.; Zheng, W. T.; Li, S.; Jiang, Q. Enhanced Hydrogen Sensing Properties of Graphene by Introducing a Mono-Atom-Vacancy. *PCCP* **2013,** *15*, 21016-21022.
(1000) McKay, H.; Wales, D. J.; Jenkins, S. J.; Verges, J. A.; de Andres, P. L. Hydrogen on Graphene under Stress: Molecular Dissociation and Gap Opening. *Physical Review B* **2010,** *81*, 075425.
(1001) Ferro, Y.; Marinelli, F.; Allouche, A. Density Functional Theory Investigation of the Diffusion and Recombination of H on a Graphite Surface. *Chem. Phys. Lett.* **2003,** *368*, 609-615.
(1002) Ferro, Y.; Marinelli, F.; Jelea, A.; Allouche, A. Adsorption, Diffusion, and Recombination of Hydrogen on Pure and Boron-Doped Graphite Surfaces. *The Journal of Chemical Physics* **2004,** *120*, 11882-11888.
(1003) Agerico Diño, W.; Miura, Y.; Nakanishi, H.; Kasai, H.; Sugimoto, T. Stable Hydrogen Configurations between Graphite Layers. *J. Phys. Soc. Jpn.* **2003,** *72*, 1867-1870.
(1004) Hornekær, L.; Rauls, E.; Xu, W.; Šljivančanin, Ž.; Otero, R.; Stensgaard, I.; Lægsgaard, E.; Hammer, B.; Besenbacher, F. Clustering of Chemisorbed H(D) Atoms on the Graphite (0001) Surface Due to Preferential Sticking. *Phys. Rev. Lett.* **2006,** *97*, 186102.
(1005) Andree, A.; Lay, M. L.; Zecho, T.; Küpper, J. Pair Formation and Clustering of D on the Basal Plane of Graphite. *Chem. Phys. Lett.* **2006,** *425*, 99-104.
(1006) Khazaei, M.; Bahramy, M. S.; Ranjbar, A.; Mizuseki, H.; Kawazoe, Y. Geometrical Indications of Adsorbed Hydrogen Atoms on Graphite Producing Star and Ellipsoidal Like Features in Scanning Tunneling Microscopy Images: Ab Initio Study. *Carbon* **2009,** *47*, 3306-3312.
(1007) Ferro, Y.; Morisset, S.; Allouche, A. Evidence of Hydrogenated Hexamers on Graphite. *Chem. Phys. Lett.* **2009,** *478*, 42-44.
(1008) Lin, Y.; Ding, F.; Yakobson, B. I. Hydrogen Storage by Spillover on Graphene as a Phase Nucleation Process. *Physical Review B* **2008,** *78*, 041402.
(1009) Tsao, C.-S.; Liu, Y.; Chuang, H.-Y.; Tseng, H.-H.; Chen, T.-Y.; Chen, C.-H.; Yu, M.-S.; Li, Q.; Lueking, A.; Chen, S.-H. Hydrogen Spillover Effect of Pt-Doped Activated Carbon Studied by Inelastic Neutron Scattering. *The Journal of Physical Chemistry Letters* **2011,** *2*, 2322-2325.
(1010) Lachawiec, A. J.; Yang, R. T. Reverse Spillover of Hydrogen on Carbon-Based Nanomaterials: Evidence of Recombination Using Isotopic Exchange. *The Journal of Physical Chemistry C* **2009,** *113*, 13933-13939.
(1011) Menéndez, J. A.; Radovic, L. R.; Xia, B.; Phillips, J. Low-Temperature Generation of Basic Carbon Surfaces by Hydrogen Spillover. *The Journal of Physical Chemistry* **1996,** *100*, 17243-17248.
(1012) Hornekær, L.; Šljivančanin, Ž.; Xu, W.; Otero, R.; Rauls, E.; Stensgaard, I.; Lægsgaard, E.; Hammer, B.; Besenbacher, F. Metastable Structures and Recombination Pathways for Atomic Hydrogen on the Graphite (0001) Surface. *Phys. Rev. Lett.* **2006,** *96*, 156104.
(1013) Zecho, T.; Güttler, A.; Sha, X.; Lemoine, D.; Jackson, B.; Küppers, J. Abstraction of D Chemisorbed on Graphite (0001) with Gaseous H Atoms. *Chem. Phys. Lett.* **2002,** *366*, 188-195.
(1014) Sha, X.; Jackson, B.; Lemoine, D. Quantum Studies of Eley–Rideal Reactions between H Atoms on a Graphite Surface. *The Journal of Chemical Physics* **2002,** *116*, 7158-7169.
(1015) Casolo, S.; Tantardini, G. F.; Martinazzo, R. Insights into H2 Formation in Space from Ab Initio Molecular Dynamics. *Proceedings of the National Academy of Sciences of the United States of America* **2013,** *110*, 6674-6677.

(1016) Dumont, F.; Picaud, F.; Ramseyer, C.; Girardet, C.; Ferro, Y.; Allouche, A. Model for Thermal Desorption of Hydrogen Atoms from a Graphite Surface Based on Kinetic Monte Carlo Simulations. *Physical Review B* **2008,** *77*, 233401.
(1017) Chen, L.; Cooper, A. C.; Pez, G. P.; Cheng, H. Mechanistic Study on Hydrogen Spillover onto Graphitic Carbon Materials. *The Journal of Physical Chemistry C* **2007,** *111*, 18995-19000.
(1018) Ao, Z. M.; Peeters, F. M. Electric Field Activated Hydrogen Dissociative Adsorption to Nitrogen-Doped Graphene. *The Journal of Physical Chemistry C* **2010,** *114*, 14503-14509.
(1019) Wang, N.; Wang, L.; Tan, Q.; Pan, Y.-X. Effects of Hydroxyl Group on H2 Dissociation on Graphene: A Density Functional Theory Study. *Journal of Energy Chemistry* **2013,** *22*, 493-497.
(1020) Han, S. S.; Kim, H.; Park, N. Effect of Shuttling Catalyst on the Migration of Hydrogen Adatoms: A Strategy for the Facile Hydrogenation of Graphene. *The Journal of Physical Chemistry C* **2011,** *115*, 24696-24701.
(1021) Nguyen, M.-T.; Phong, P. N. Accelerating Dynamics of H on Graphene by Coadsorbates. *The Journal of Physical Chemistry A* **2017,** *121*, 5520-5523.
(1022) Hensen, E. J. M.; Lardinois, G. M. H. J.; de Beer, V. H. J.; van Veen, J. A. R.; van Santen, R. A. Hydrogen–Deuterium Equilibration over Transition Metal Sulfide Catalysts: On the Synergetic Effect in Como Catalysts. *J. Catal.* **1999,** *187*, 95-108.
(1023) Levy, R. B.; Boudart, M. The Kinetics and Mechanism of Spillover. *J. Catal.* **1974,** *32*, 304-314.
(1024) Psofogiannakis, G. M.; Froudakis, G. E. Dft Study of Hydrogen Storage by Spillover on Graphite with Oxygen Surface Groups. *J. Am. Chem. Soc.* **2009,** *131*, 15133-15135.
(1025) Lueking, A. D.; Psofogiannakis, G.; Froudakis, G. E. Atomic Hydrogen Diffusion on Doped and Chemically Modified Graphene. *The Journal of Physical Chemistry C* **2013,** *117*, 6312-6319.
(1026) Blankenship Ii, T. S.; Balahmar, N.; Mokaya, R. Oxygen-Rich Microporous Carbons with Exceptional Hydrogen Storage Capacity. *Nature Communications* **2017,** *8*, 1545.
(1027) Li, Q.; Lueking, A. D. Effect of Surface Oxygen Groups and Water on Hydrogen Spillover in Pt-Doped Activated Carbon. *The Journal of Physical Chemistry C* **2011,** *115*, 4273-4282.
(1028) Dong Jin, S.; Tae-Jin, P.; Son-Ki, I. Effect of Surface Oxygen Groups of Carbon Supports on the Characteristics of Pd/C Catalysts. *Carbon* **1993,** *31*, 427-435.
(1029) Psofogiannakis, G. M.; Steriotis, T. A.; Bourlinos, A. B.; Kouvelos, E. P.; Charalambopoulou, G. C.; Stubos, A. K.; Froudakis, G. E. Enhanced Hydrogen Storage by Spillover on Metal-Doped Carbon Foam: An Experimental and Computational Study. *Nanoscale* **2011,** *3*, 933-936.
(1030) Wang, Z.; Yang, F. H.; Yang, R. T. Enhanced Hydrogen Spillover on Carbon Surfaces Modified by Oxygen Plasma. *The Journal of Physical Chemistry C* **2010,** *114*, 1601-1609.
(1031) Li, Q.; Wang, H.; Xia, H.; Wei, S.; Yang, J. Density Functional Study of Hydrogen Adsorption and Diffusion on Ni-Loaded Graphene and Graphene Oxide. *Int. J. Quantum Chem* **2014,** *114*, 879-884.
(1032) Pham, V. H.; Dang, T. T.; Singh, K.; Hur, S. H.; Shin, E. W.; Kim, J. S.; Lee, M. A.; Baeck, S. H.; Chung, J. S. A Catalytic and Efficient Route for Reduction of Graphene Oxide by Hydrogen Spillover. *Journal of Materials Chemistry A* **2013,** *1*, 1070-1077.
(1033) Sun, K. G.; Chung, J. S.; Hur, S. H. Durability Improvement of Pt/Rgo Catalysts for Pemfc by Low-Temperature Self-Catalyzed Reduction. *Nanoscale Research Letters* **2015,** *10*, 257.
(1034) Sha, X.; Jackson, B. The Location of Adsorbed Hydrogen in Graphite Nanostructures. *J. Am. Chem. Soc.* **2004,** *126*, 13095-13099.
(1035) Di; ntilde; o, W. A.; Nakanishi, H.; Kasai, H.; Sugimoto, T.; Kondo, T. H₂ Dissociative Adsorption at the Zigzag Edges of Graphite. *e-Journal of Surface Science and Nanotechnology* **2004,** *2*, 77-80.
(1036) Diño, W. A.; Miura, Y.; Nakanishi, H.; Kasai, H.; Sugimoto, T.; Kondo, T. H2 Dissociative Adsorption at the Armchair Edges of Graphite. *Solid State Commun.* **2004,** *132*, 713-718.
(1037) Allouche, A.; Ferro, Y. Dissociative Adsorption of Small Molecules at Vacancies on the Graphite (0001) Surface. *Carbon* **2006,** *44*, 3320-3327.

(1038) Sunnardianto, G. K.; Maruyama, I.; Kusakabe, K. Dissociation-Chemisorption Pathways of H2 Molecule on Graphene Activated by a Hydrogenated Mono-Vacancy V11. *Advanced Science, Engineering and Medicine* **2016,** *8*, 421-426.
(1039) Sunnardianto, G. K.; Larasati, I. A.; Triawan, F.; Aamer, A. M. Effect of Charge on Graphene Vacancy for Hydrogen Storage Application. *MATEC Web Conf.* **2018,** *197*, 04001.
(1040) Sunnardianto, G. K.; Maruyama, I.; Kusakabe, K. Storing-Hydrogen Processes on Graphene Activated by Atomic-Vacancies. *Int. J. Hydrogen Energy* **2017,** *42*, 23691-23697.
(1041) Yang, F. H.; Yang, R. T. Ab Initio Molecular Orbital Study of Adsorption of Atomic Hydrogen on Graphite:: Insight into Hydrogen Storage in Carbon Nanotubes. *Carbon* **2002,** *40*, 437-444.
(1042) Takahashi, K.; Isobe, S.; Omori, K.; Mashoff, T.; Convertino, D.; Miseikis, V.; Coletti, C.; Tozzini, V.; Heun, S. Revealing the Multibonding State between Hydrogen and Graphene-Supported Ti Clusters. *The Journal of Physical Chemistry C* **2016,** *120*, 12974-12979.
(1043) Kumar, E. M.; P, S.; Thapa, R. Hydrogen Spillover on Dv (555-777) Graphene – Vanadium Cluster System: First Principles Study. *AIP Conference Proceedings* **2015,** *1665*, 080036.
(1044) Faye, O.; Eduok, U.; Szpunar, J.; Szpunar, B.; Samoura, A.; Beye, A. Hydrogen Storage on Bare Cu Atom and Cu-Functionalized Boron-Doped Graphene: A First Principles Study. *Int. J. Hydrogen Energy* **2017,** *42*, 4233-4243.
(1045) Rungnim, C.; Faungnawakij, K.; Sano, N.; Kungwan, N.; Namuangruk, S. Hydrogen Storage Performance of Platinum Supported Carbon Nanohorns: A Dft Study of Reaction Mechanisms, Thermodynamics, and Kinetics. *Int. J. Hydrogen Energy* **2018,** *43*, 23336-23345.
(1046) Méndez-Camacho, R.; Guirado-López, R. A. Adsorption and Diffusion of Hydrogen on C60-Supported Ptn Clusters. *The Journal of Physical Chemistry C* **2013,** *117*, 10059-10069.
(1047) Ferreira-Aparicio, P. New Insights into Proton Surface Mobility Processes in Pemfc Catalysts Using Isotopic Exchange Methods. *ACS Applied Materials & Interfaces* **2009,** *1*, 1946-1957.
(1048) Huidobro, A.; Sepúlveda-Escribano, A.; Rodríguez-Reinoso, F. In *Stud. Surf. Sci. Catal.*; Guerrero-Ruiz, A.;Rodríguez-Ramos, I., Eds.; Elsevier, 2001; Vol. 138.
(1049) López, M. J.; Blanco-Rey, M.; Juaristi, J. I.; Alducin, M.; Alonso, J. A. Manipulating the Magnetic Moment of Palladium Clusters by Adsorption and Dissociation of Molecular Hydrogen. *The Journal of Physical Chemistry C* **2017,** *121*, 20756-20762.
(1050) Alonso, J. A.; López, M. J. In *Handbook of Materials Modeling: Applications: Current and Emerging Materials*; Andreoni, W.;Yip, S., Eds.; Springer International Publishing: Cham, 2018, DOI:10.1007/978-3-319-50257-1_32-1 10.1007/978-3-319-50257-1_32-1.
(1051) Contescu, C. I.; van Benthem, K.; Li, S.; Bonifacio, C. S.; Pennycook, S. J.; Jena, P.; Gallego, N. C. Single Pd Atoms in Activated Carbon Fibers and Their Contribution to Hydrogen Storage. *Carbon* **2011,** *49*, 4050-4058.
(1052) Dag, S.; Ozturk, Y.; Ciraci, S.; Yildirim, T. Adsorption and Dissociation of Hydrogen Molecules on Bare and Functionalized Carbon Nanotubes. *Physical Review B* **2005,** *72*, 155404.
(1053) López-Corral, I.; Germán, E.; Juan, A.; Volpe, M. A.; Brizuela, G. P. Dft Study of Hydrogen Adsorption on Palladium Decorated Graphene. *The Journal of Physical Chemistry C* **2011,** *115*, 4315-4323.
(1054) López-Corral, I.; Germán, E.; Juan, A.; Volpe, M. A.; Brizuela, G. P. Hydrogen Adsorption on Palladium Dimer Decorated Graphene: A Bonding Study. *Int. J. Hydrogen Energy* **2012,** *37*, 6653-6665.
(1055) Pantha, N.; Khaniya, A.; Adhikari, N. P. Hydrogen Storage on Palladium Adsorbed Graphene: A Density Functional Theory Study. *Int. J. Mod Phys B* **2015,** *29*, 1550143.
(1056) Choudhary, A.; Malakkal, L.; Siripurapu, R. K.; Szpunar, B.; Szpunar, J. First Principles Calculations of Hydrogen Storage on Cu and Pd-Decorated Graphene. *Int. J. Hydrogen Energy* **2016,** *41*, 17652-17656.
(1057) Granja, A.; Alonso, J. A.; Cabria, I.; López, M. J. Competition between Molecular and Dissociative Adsorption of Hydrogen on Palladium Clusters Deposited on Defective Graphene. *RSC Advances* **2015,** *5*, 47945-47953.

(1058) Granja-DelRío, A.; Alonso, J. A.; López, M. J. Steric and Chemical Effects on the Hydrogen Adsorption and Dissociation on Free and Graphene–Supported Palladium Clusters. *Computational and Theoretical Chemistry* **2017,** *1107*, 23-29.
(1059) López-Corral, I.; de Celis, J.; Juan, A.; Irigoyen, B. Dft Study of H2 Adsorption on Pd-Decorated Single Walled Carbon Nanotubes with C-Vacancies. *Int. J. Hydrogen Energy* **2012,** *37*, 10156-10164.
(1060) Ma, L.; Zhang, J.-M.; Xu, K.-W. Hydrogen Storage on Nitrogen Induced Defects in Palladium-Decorated Graphene: A First-Principles Study. *Appl. Surf. Sci.* **2014,** *292*, 921-927.
(1061) Ma, L.; Zhang, J.-M.; Xu, K.-W.; Ji, V. Hydrogen Adsorption and Storage on Palladium-Decorated Graphene with Boron Dopants and Vacancy Defects: A First-Principles Study. *Physica E: Low-dimensional Systems and Nanostructures* **2015,** *66*, 40-47.
(1062) Faye, O.; Szpunar, J. A.; Szpunar, B.; Beye, A. C. Hydrogen Adsorption and Storage on Palladium – Functionalized Graphene with Nh-Dopant: A First Principles Calculation. *Appl. Surf. Sci.* **2017,** *392*, 362-374.
(1063) Ramos-Castillo, C. M.; Reveles, J. U.; Zope, R. R.; de Coss, R. Palladium Clusters Supported on Graphene Monovacancies for Hydrogen Storage. *The Journal of Physical Chemistry C* **2015,** *119*, 8402-8409.
(1064) Zhou, Q.; Wang, C.; Fu, Z.; Yuan, L.; Yang, X.; Tang, Y.; Zhang, H. Hydrogen Adsorption on Palladium Anchored Defected Graphene with B-Doping: A Theoretical Study. *Int. J. Hydrogen Energy* **2015,** *40*, 2473-2483.
(1065) Singh, A. K.; Ribas, M. A.; Yakobson, B. I. H-Spillover through the Catalyst Saturation: An Ab Initio Thermodynamics Study. *ACS Nano* **2009,** *3*, 1657-1662.
(1066) Schaefer, S.; Fierro, V.; Szczurek, A.; Izquierdo, M. T.; Celzard, A. Physisorption, Chemisorption and Spill-over Contributions to Hydrogen Storage. *Int. J. Hydrogen Energy* **2016,** *41*, 17442-17452.
(1067) Albers, P. W.; Lennon, D.; Parker, S. F. In *Experimental Methods in the Physical Sciences*; Fernandez-Alonso, F.;Price, D. L., Eds.; Academic Press, 2017; Vol. 49.
(1068) Mitchell, P. C. H.; Ramirez-Cuesta, A. J.; Parker, S. F.; Tomkinson, J.; Thompsett, D. Hydrogen Spillover on Carbon-Supported Metal Catalysts Studied by Inelastic Neutron Scattering. Surface Vibrational States and Hydrogen Riding Modes. *The Journal of Physical Chemistry B* **2003,** *107*, 6838-6845.
(1069) Pontiroli, D.; Aramini, M.; Gaboardi, M.; Mazzani, M.; Sanna, S.; Caracciolo, F.; Carretta, P.; Cavallari, C.; Rols, S.; Tatti, R.et al. Tracking the Hydrogen Motion in Defective Graphene. *The Journal of Physical Chemistry C* **2014,** *118*, 7110-7116.
(1070) Mitchell, P. C. H.; Ramirez-Cuesta, A. J.; Parker, S. F.; Tomkinson, J. Inelastic Neutron Scattering in Spectroscopic Studies of Hydrogen on Carbon-Supported Catalysts-Experimental Spectra and Computed Spectra of Model Systems. *J. Mol. Struct.* **2003,** *651-653*, 781-785.
(1071) Albers, P.; Burmeister, R.; Seibold, K.; Prescher, G.; Parker, S. F.; Ross, D. K. Investigations of Palladium Catalysts on Different Carbon Supports. *J. Catal.* **1999,** *181*, 145-154.
(1072) Albers, P. W.; Krauter, J. G. E.; Ross, D. K.; Heidenreich, R. G.; Köhler, K.; Parker, S. F. Identification of Surface States on Finely Divided Supported Palladium Catalysts by Means of Inelastic Incoherent Neutron Scattering. *Langmuir* **2004,** *20*, 8254-8260.
(1073) Sheng, W.; Kattel, S.; Yao, S.; Yan, B.; Liang, Z.; Hawxhurst, C. J.; Wu, Q.; Chen, J. G. Electrochemical Reduction of Co2 to Synthesis Gas with Controlled Co/H2 Ratios. *Energy & Environmental Science* **2017,** *10*, 1180-1185.
(1074) Bugaev, A. L.; Guda, A. A.; Lazzarini, A.; Lomachenko, K. A.; Groppo, E.; Pellegrini, R.; Piovano, A.; Emerich, H.; Soldatov, A. V.; Bugaev, L. A.et al. In Situ Formation of Hydrides and Carbides in Palladium Catalyst: When Xanes Is Better Than Exafs and Xrd. *Catal. Today* **2017,** *283*, 119-126.
(1075) Contescu, C. I.; Brown, C. M.; Liu, Y.; Bhat, V. V.; Gallego, N. C. Detection of Hydrogen Spillover in Palladium-Modified Activated Carbon Fibers During Hydrogen Adsorption. *The Journal of Physical Chemistry C* **2009,** *113*, 5886-5890.

(1076) Tsao, C.-S.; Li, M.; Zhang, Y.; Leao, J. B.; Chiang, W.-S.; Chung, T.-Y.; Tzeng, Y.-R.; Yu, M.-S.; Chen, S.-H. Probing the Room Temperature Spatial Distribution of Hydrogen in Nanoporous Carbon by Use of Small-Angle Neutron Scattering. *The Journal of Physical Chemistry C* **2010,** *114*, 19895-19900.
(1077) Bhowmick, R.; Rajasekaran, S.; Friebel, D.; Beasley, C.; Jiao, L.; Ogasawara, H.; Dai, H.; Clemens, B.; Nilsson, A. Hydrogen Spillover in Pt-Single-Walled Carbon Nanotube Composites: Formation of Stable C−H Bonds. *J. Am. Chem. Soc.* **2011,** *133*, 5580-5586.
(1078) Dinadayalane, T. C.; Leszczynski, J. In *Practical Aspects of Computational Chemistry: Methods, Concepts and Applications*; Leszczynski, J.;Shukla, M. K., Eds.; Springer Netherlands: Dordrecht, 2010, DOI:10.1007/978-90-481-2687-3_14 10.1007/978-90-481-2687-3_14.
(1079) Lin, C.; Yang, Z.; Xu, T.; Zhao, Y. An in Situ Electrical Study on Primary Hydrogen Spillover from Nanocatalysts to Amorphous Carbon Support. *Appl. Phys. Lett.* **2008,** *93*, 233110.
(1080) Liu, X. M.; Tang, Y.; Xu, E. S.; Fitzgibbons, T. C.; Larsen, G. S.; Gutierrez, H. R.; Tseng, H.-H.; Yu, M.-S.; Tsao, C.-S.; Badding, J. V.et al. Evidence for Ambient-Temperature Reversible Catalytic Hydrogenation in Pt-Doped Carbons. *Nano Lett.* **2013,** *13*, 137-141.
(1081) Blackburn, J. L.; Engtrakul, C.; Bult, J. B.; Hurst, K.; Zhao, Y.; Xu, Q.; Parilla, P. A.; Simpson, L. J.; Rocha, J.-D. R.; Hudson, M. R.et al. Spectroscopic Identification of Hydrogen Spillover Species in Ruthenium-Modified High Surface Area Carbons by Diffuse Reflectance Infrared Fourier Transform Spectroscopy. *The Journal of Physical Chemistry C* **2012,** *116*, 26744-26755.
(1082) Yang, F.; Hu, B.; Xia, W.; Peng, B.; Shen, J.; Muhler, M. On the Nature of Spillover Hydrogen Species on Platinum/Nitrogen-Doped Mesoporous Carbon Composites: A Temperature-Programmed Nitrobenzene Desorption Study. *J. Catal.* **2018,** *365*, 55-62.
(1083) Keren, E.; Soffer, A. Simultaneous Electronic and Ionic Surface Conduction of Catalyst Supports: A General Mechanism for Spillover: The Role of Water in the Pd-Catalyzed Hydrogenation of a Carbon Surface. *J. Catal.* **1977,** *50*, 43-55.
(1084) Roland, U.; Braunschweig, T.; Roessner, F. On the Nature of Spilt-over Hydrogen. *J. Mol. Catal. A: Chem.* **1997,** *127*, 61-84.
(1085) Zhao, W.; Luo, L.; Chen, T.; Li, Z.; Zhang, Z.; Wang, H.; Rao, J.; Feo, L.; Fan, M. Synthesis and Characterization of Pt-N-Doped Activated Biocarbon Composites for Hydrogen Storage. *Composites Part B: Engineering* **2019,** *161*, 464-472.
(1086) Lu, C.; Zhu, Q.; Zhang, X.; Ji, H.; Zhou, Y.; Wang, H.; Liu, Q.; Nie, J.; Han, W.; Li, X. Decoration of Pd Nanoparticles with N and S Doped Carbon Quantum Dots as a Robust Catalyst for the Chemoselective Hydrogenation Reaction. *ACS Sustainable Chemistry & Engineering* **2019,** *7*, 8542-8553.
(1087) Chung, T.-Y.; Tsao, C.-S.; Tseng, H.-P.; Chen, C.-H.; Yu, M.-S. Effects of Oxygen Functional Groups on the Enhancement of the Hydrogen Spillover of Pd-Doped Activated Carbon. *J. Colloid Interface Sci.* **2015,** *441*, 98-105.
(1088) Anbia, M.; Mandegarzad, S. Enhanced Hydrogen Sorption on Modified Mil-101 with Pt/Cmk-3 by Hydrogen Spillover Effect. *J. Alloys Compd.* **2012,** *532*, 61-67.
(1089) Wang, Y.; Wang, K.; Guan, C.; He, Z.; Lu, Z.; Chen, T.; Liu, J.; Tan, X.; Yang Tan, T. T.; Li, C. M. Surface Functionalization-Enhanced Spillover Effect on Hydrogen Storage of Ni–B Nanoalloy-Doped Activated Carbon. *Int. J. Hydrogen Energy* **2011,** *36*, 13663-13668.
(1090) Badenes, P.; Daza, L.; Rodriguez-Ramos, I.; Guerrero-Ruiz, A. In *Stud. Surf. Sci. Catal.*; Li, C.;Xin, Q., Eds.; Elsevier, 1997; Vol. 112.
(1091) Das, T. K.; Banerjee, S.; Pandey, M.; Vishwanadh, B.; Kshirsagar, R. J.; Sudarsan, V. Effect of Surface Functional Groups on Hydrogen Adsorption Properties of Pd Dispersed Reduced Graphene Oxide. *Int. J. Hydrogen Energy* **2017,** *42*, 8032-8041.
(1092) Wang, L.; Yang, F. H.; Yang, R. T.; Miller, M. A. Effect of Surface Oxygen Groups in Carbons on Hydrogen Storage by Spillover. *Industrial & Engineering Chemistry Research* **2009,** *48*, 2920-2926.

(1093) García-García, F. R.; Bion, N.; Duprez, D.; Rodríguez-Ramos, I.; Guerrero-Ruiz, A. H2/D2 Isotopic Exchange: A Tool to Characterize Complex Hydrogen Interaction with Carbon-Supported Ruthenium Catalysts. *Catal. Today* **2016,** *259*, 9-18.
(1094) Bhat, V. V.; Contescu, C. I.; Gallego, N. C. The Role of Destabilization of Palladium Hydride in the Hydrogen Uptake of Pd-Containing Activated Carbons. *Nanotechnology* **2009,** *20*, 204011.
(1095) Lueking, A. D.; Yang, R. T. Hydrogen Spillover to Enhance Hydrogen Storage—Study of the Effect of Carbon Physicochemical Properties. *Applied Catalysis A: General* **2004,** *265*, 259-268.
(1096) Wang, L.; Yang, R. T. Molecular Hydrogen and Spiltover Hydrogen Storage on High Surface Area Carbon Sorbents. *Carbon* **2012,** *50*, 3134-3140.
(1097) Tsao, C.-S.; Tzeng, Y.-R.; Yu, M.-S.; Wang, C.-Y.; Tseng, H.-H.; Chung, T.-Y.; Wu, H.-C.; Yamamoto, T.; Kaneko, K.; Chen, S.-H. Effect of Catalyst Size on Hydrogen Storage Capacity of Pt-Impregnated Active Carbon Via Spillover. *The Journal of Physical Chemistry Letters* **2010,** *1*, 1060-1063.
(1098) Zieliński, M.; Wojcieszak, R.; Monteverdi, S.; Mercy, M.; Bettahar, M. M. Hydrogen Storage in Nickel Catalysts Supported on Activated Carbon. *Int. J. Hydrogen Energy* **2007,** *32*, 1024-1032.
(1099) Geng, Z.; Wang, D.; Zhang, C.; Zhou, X.; Xin, H.; Liu, X.; Cai, M. Spillover Enhanced Hydrogen Uptake of Pt/Pd Doped Corncob-Derived Activated Carbon with Ultra-High Surface Area at High Pressure. *Int. J. Hydrogen Energy* **2014,** *39*, 13643-13649.
(1100) Itoi, H.; Nishihara, H.; Kobayashi, S.; Ittisanronnachai, S.; Ishii, T.; Berenguer, R.; Ito, M.; Matsumura, D.; Kyotani, T. Fine Dispersion of Pt4–5 Subnanoclusters and Pt Single Atoms over Porous Carbon Supports and Their Structural Analyses with X-Ray Absorption Spectroscopy. *The Journal of Physical Chemistry C* **2017,** *121*, 7892-7902.
(1101) Nishihara, H.; Ohtake, F.; Castro-Muñiz, A.; Itoi, H.; Ito, M.; Hayasaka, Y.; Maruyama, J.; Kondo, J. N.; Osuga, R.; Kyotani, T. Enhanced Hydrogen Chemisorption and Spillover on Non-Metallic Nickel Subnanoclusters. *Journal of Materials Chemistry A* **2018,** *6*, 12523-12531.
(1102) Pevzner, S.; Pri-Bar, I.; Lutzky, I.; Ben-Yehuda, E.; Ruse, E.; Regev, O. Carbon Allotropes Accelerate Hydrogenation Via Spillover Mechanism. *The Journal of Physical Chemistry C* **2014,** *118*, 27164-27169.
(1103) Nishihara, H.; Ittisanronnachai, S.; Itoi, H.; Li, L.-X.; Suzuki, K.; Nagashima, U.; Ogawa, H.; Kyotani, T.; Ito, M. Experimental and Theoretical Studies of Hydrogen/Deuterium Spillover on Pt-Loaded Zeolite-Templated Carbon. *The Journal of Physical Chemistry C* **2014,** *118*, 9551-9559.
(1104) Razzhivina, I. A.; Badun, G. A.; Chernysheva, M. G.; Garshev, A. V.; Shevchenko, V. P.; Shevchenko, K. V.; Nagaev, I. Y.; Shchepina, N. E. Hydrogen Spillover through a Gas Phase. *Mendeleev Commun.* **2016,** *26*, 59-60.
(1105) Baumgarten, E.; Maschke, L. Hydrogen Spillover through the Gas Phase: Reaction with Graphite and Activated Carbon. *Applied Catalysis A: General* **2000,** *202*, 171-177.
(1106) Yang, F. H.; Lachawiec, A. J.; Yang, R. T. Adsorption of Spillover Hydrogen Atoms on Single-Wall Carbon Nanotubes. *The Journal of Physical Chemistry B* **2006,** *110*, 6236-6244.
(1107) Lachawiec, A. J.; Qi, G.; Yang, R. T. Hydrogen Storage in Nanostructured Carbons by Spillover: Bridge-Building Enhancement. *Langmuir* **2005,** *21*, 11418-11424.
(1108) Boudart, M.; Aldag, A. W.; Vannice, M. A. On the Slow Uptake of Hydrogen by Platinized Carbon. *J. Catal.* **1970,** *18*, 46-51.
(1109) Nishihara, H.; Simura, T.; Kyotani, T. Enhanced Hydrogen Spillover to Fullerene at Ambient Temperature. *Chem. Commun.* **2018,** *54*, 3327-3330.
(1110) Furimsky, E. In *Carbons and Carbon Supported Catalysts in Hydroprocessing*; The Royal Society of Chemistry, 2008, DOI:10.1039/9781847558411-00022 10.1039/9781847558411-00022.
(1111) Srinivas, S. T.; Rao, P. K. Direct Observation of Hydrogen Spillover on Carbon-Supported Platinum and Its Influence on the Hydrogenation of Benzene. *J. Catal.* **1994,** *148*, 470-477.
(1112) Wojcieszak, R.; Zieliński, M.; Monteverdi, S.; Bettahar, M. M. Study of Nickel Nanoparticles Supported on Activated Carbon Prepared by Aqueous Hydrazine Reduction. *J. Colloid Interface Sci.* **2006,** *299*, 238-248.

(1113) Chen, H.; Yang, H.; Briker, Y.; Fairbridge, C.; Omotoso, O.; Ding, L.; Zheng, Y.; Ring, Z. Effect of Hydrogen Spillover on the Hydrogenation of 1-Hexene over Diluted Carbon Molecular Sieve Supported Pt Catalyst. *Catal. Today* **2007,** *125*, 256-262.
(1114) Cheng, Z. X.; Yuan, S. B.; Fan, J. W.; Zhu, Q. M.; Zhen, M. S. In *Stud. Surf. Sci. Catal.*; Li, C.;Xin, Q., Eds.; Elsevier, 1997; Vol. 112.
(1115) Liang, X.-L.; Dong, X.; Lin, G.-D.; Zhang, H.-B. Carbon Nanotube-Supported Pd–Zno Catalyst for Hydrogenation of Co2 to Methanol. *Applied Catalysis B: Environmental* **2009,** *88*, 315-322.
(1116) Pinilla, J. L.; García, A. B.; Philippot, K.; Lara, P.; García-Suárez, E. J.; Millan, M. Carbon-Supported Pd Nanoparticles as Catalysts for Anthracene Hydrogenation. *Fuel* **2014,** *116*, 729-735.
(1117) Hao, Y.; Wang, X.; Perret, N.; Cárdenas-Lizana, F.; Keane, M. A. Support Effects in the Gas Phase Hydrogenation of Butyronitrile over Palladium. *Catalysis, Structure & Reactivity* **2015,** *1*, 4-10.
(1118) Zhang, Z. G.; Okada, K.; Yamamoto, M.; Yoshida, T. Hydrogenation of Anthracene over Active Carbon-Supported Nickel Catalyst. *Catal. Today* **1998,** *45*, 361-366.
(1119) Zhang, Z.-G.; Yoshida, T. Behavior of Hydrogen Transfer in the Hydrogenation of Anthracene over Activated Carbon. *Energy & Fuels* **2001,** *15*, 708-713.
(1120) Coloma, F.; Sepúlveda-Escribano, A.; Fierro, J. L. G.; Rodríguez-Reinoso, F. Gas Phase Hydrogenation of Crotonaldehyde over Pt/Activated Carbon Catalysts. Influence of the Oxygen Surface Groups on the Support. *Applied Catalysis A: General* **1997,** *150*, 165-183.
(1121) Fujimoto, K.; Asaoka, S.; Kunugi, T. Reverse Spillover of Hydrogen as a Key Process of the Dehydrogenation of Paraffin over Metal Supported Carbon Catalysts. *Revista Portuguesa de Quimica* **1977,** *19*, 298.
(1122) Fujimoto, K.; Toyoshi, S. In *Stud. Surf. Sci. Catal.*; Seivama, T.;Tanabe, K., Eds.; Elsevier, 1981; Vol. 7.
(1123) Jiang, N.; Rao, K. S. R.; Jin, M.-J.; Park, S.-E. Effect of Hydrogen Spillover in Decalin Dehydrogenation over Supported Pt Catalysts. *Applied Catalysis A: General* **2012,** *425-426*, 62-67.
(1124) Lin, S. S. Y.; Yang, J.; Kung, H. H. Transition Metal-Decorated Activated Carbon Catalysts for Dehydrogenation of Naalh4. *Int. J. Hydrogen Energy* **2012,** *37*, 2737-2741.
(1125) Tan, C.-Y.; Tsai, W.-T. Catalytic and Inhibitive Effects of Pd and Pt Decorated Mwcnts on the Dehydrogenation Behavior of Lialh4. *Int. J. Hydrogen Energy* **2015,** *40*, 10185-10193.
(1126) Fujimoto, K. Spillover of Hydrogen on Carbon and Its Role in Catalytic Hydrocarbon Reforming. *Journal of The Japan Petroleum Institute* **1984,** *27*, 463-471.
(1127) Kariya, N.; Fukuoka, A.; Ichikawa, M. Efficient Evolution of Hydrogen from Liquid Cycloalkanes over Pt-Containing Catalysts Supported on Active Carbons under "Wet–Dry Multiphase Conditions". *Applied Catalysis A: General* **2002,** *233*, 91-102.
(1128) Biniwale, R. B.; Kariya, N.; Ichikawa, M. Dehydrogenation of Cyclohexane over Ni Based Catalystssupported on Activated Carbon Using Spray-Pulsed Reactor and Enhancement in Activity by Addition of a Small Amount of Pt. *Catal. Lett.* **2005,** *105*, 83-87.
(1129) Yoshio, U.; Takeshi, S.; Takaji, K. Dehydrogenation of Cyclohexanol to Cyclohexanone on Supported Nickel Catalysts. *Chem. Lett.* **1989,** *18*, 777-780.
(1130) Pande, J. V.; Shukla, A.; Biniwale, R. B. Catalytic Dehydrogenation of Cyclohexane over Ag-M/Acc Catalysts for Hydrogen Supply. *Int. J. Hydrogen Energy* **2012,** *37*, 6756-6763.
(1131) Weigle, J. C.; Phillips, J. Novel Dual-Bed Reactors: Utilization of Hydrogen Spillover in Reactor Design. *Langmuir* **2004,** *20*, 1189-1193.
(1132) Baker, R. T. K.; Rodriguez, N.; Mastalir, Á.; Wild, U.; Schlögl, R.; Wootsch, A.; Paál, Z. Platinum/Graphite Nanofiber Catalysts of Various Structure: Characterization and Catalytic Properties. *The Journal of Physical Chemistry B* **2004,** *108*, 14348-14355.
(1133) Weigle, J. C.; Phillips, J. Modeling Hydrogen Spillover in Dual-Bed Catalytic Reactors. *AlChE J.* **2004,** *50*, 821-828.

(1134) Paál, Z.; Wootsch, A.; Schlögl, R.; Wild, U. Carbon Accumulation, Deactivation and Reactivation of Pt Catalysts Upon Exposure to Hydrocarbons. *Applied Catalysis A: General* **2005,** *282*, 135-145.
(1135) Baker, R. T. K.; Laubernds, K.; Wootsch, A.; Paál, Z. Pt/Graphite Nanofiber Catalyst in N-Hexane Test Reaction. *J. Catal.* **2000,** *193*, 165-167.
(1136) Paál, Z.; Teschner, D.; Rodriguez, N. M.; Baker, R. T. K.; Tóth, L.; Wild, U.; Schlögl, R. Rh/Gnf Catalysts: Characterization and Catalytic Performance in Methylcyclopentane Reactions. *Catal. Today* **2005,** *102-103*, 254-258.
(1137) Ma, X.-M.; Lin, G.-D.; Zhang, H.-B. Co-Decorated Carbon Nanotube-Supported Co–Mo–K Sulfide Catalyst for Higher Alcohol Synthesis. *Catal. Lett.* **2006,** *111*, 141-151.
(1138) Phaahlamohlaka, T. N.; Kumi, D. O.; Dlamini, M. W.; Forbes, R.; Jewell, L. L.; Billing, D. G.; Coville, N. J. Effects of Co and Ru Intimacy in Fischer–Tropsch Catalysts Using Hollow Carbon Sphere Supports: Assessment of the Hydrogen Spillover Processes. *ACS Catalysis* **2017,** *7*, 1568-1578.
(1139) Ji, L.-l.; Li, H.; Zhang, W.; Sun, S.; Gao, C.; Bao, J.; Ma, Y.-s. Synthesis of Higher Alcohols from Syngas over Alkali Promoted K-Co-Mo Catalysts Supported on Multi-Walled Carbon Nanotubes. *Chin. J. Chem. Phys.* **2017,** *30*, 333-338.
(1140) Karimi, A.; Nasernejad, B.; Rashidi, A. M. Particle Size Control Effect on Activity and Selectivity of Functionalized Cnt-Supported Cobalt Catalyst in Fischer-Tropsch Synthesis. *Korean J. Chem. Eng.* **2012,** *29*, 1516-1524.
(1141) Karimi, A.; Nasernejad, B.; Rashidi, A. M.; Tavasoli, A.; Pourkhalil, M. Functional Group Effect on Carbon Nanotube (Cnt)-Supported Cobalt Catalysts in Fischer–Tropsch Synthesis Activity, Selectivity and Stability. *Fuel* **2014,** *117*, 1045-1051.
(1142) Karimi, A.; Tavasoli, A.; Davari, M.; Mohajeri, A. Surface Chemistry Improvement of Carbon Nanotube (Cnt) Supported Fischer–Tropsch Nanocatalysts. *Journal of Nanoanalysis* **2014,** *1*, 82-92.
(1143) Ban, C.; Yang, S.; Kim, H.; Kim, D. H. Effect of Cu Addition to Carbon-Supported Ru Catalysts on Hydrogenation of Alginic Acid into Sugar Alcohols. *Applied Catalysis A: General* **2019,** *578*, 98-104.
(1144) Chang, H.; Phillips, J.; Heck, R. Catalytic Synergism in Physical Mixtures. *Langmuir* **1996,** *12*, 2756-2761.
(1145) Chang, H.; Phillips, J. Catalytic Synergism in Physical Mixtures of Supported Iron−Cerium and Supported Noble Metal for Hydroisomerization of 1,3-Butadiene. *Langmuir* **1997,** *13*, 477-482.
(1146) Lu, W. C.; Chang, H.; Phillips, J. Novel Multimetallic Hydroisomerization Catalysts. *J. Catal.* **1994,** *146*, 608-612.
(1147) Amorim, C.; Yuan, G.; Patterson, P. M.; Keane, M. A. Catalytic Hydrodechlorination over Pd Supported on Amorphous and Structured Carbon. *J. Catal.* **2005,** *234*, 268-281.
(1148) Amorim, C.; Keane, M. A. Palladium Supported on Structured and Nonstructured Carbon: A Consideration of Pd Particle Size and the Nature of Reactive Hydrogen. *J. Colloid Interface Sci.* **2008,** *322*, 196-208.
(1149) Amorim, C.; Wang, X.; Keane, M. A. Application of Hydrodechlorination in Environmental Pollution Control: Comparison of the Performance of Supported and Unsupported Pd and Ni Catalysts. *Chinese Journal of Catalysis* **2011,** *32*, 746-755.
(1150) Wu, Z.; Mao, Y.; Wang, X.; Zhang, M. Preparation of a Cu–Ru/Carbon Nanotube Catalyst for Hydrogenolysis of Glycerol to 1,2-Propanediolviahydrogen Spillover. *Green Chemistry* **2011,** *13*, 1311-1316.
(1151) Wu, Z.; Duan, Y.; Ge, S.; Yip, A. C. K.; Yang, F.; Li, Y.; Dou, T. Promoting Hydrolysis of Ammonia Borane over Multiwalled Carbon Nanotube-Supported Ru Catalysts Via Hydrogen Spillover. *Catal. Commun.* **2017,** *91*, 10-15.
(1152) Ranade, V. S.; Prins, R. Hydrogenolysis of Benzylic Alcohols on Rhodium Catalysts. *Chemistry – A European Journal* **2000,** *6*, 313-320.

(1153) Yook, S.; Shin, H.; Kim, H.; Choi, M. Selective Dissociation of Dihydrogen over Dioxygen on a Hindered Platinum Surface for the Direct Synthesis of Hydrogen Peroxide. *ChemCatChem* **2014,** *6*, 2836-2842.
(1154) Ramirez-Cuesta, A. J.; Mitchell, P. C. H.; Parker, S. F.; Tomkinson, J.; Thompsett, D. In *Stud. Surf. Sci. Catal.*; Guerrero-Ruiz, A.;Rodríguez-Ramos, I., Eds.; Elsevier, 2001; Vol. 138.
(1155) Liu, W.-J.; Wu, B.-L.; Cha, C.-S. Surface Diffusion and the Spillover of H-Adatoms and Oxygen-Containing Surface Species on the Surface of Carbon Black and Pt/C Porous Electrodes. *J. Electroanal. Chem.* **1999,** *476*, 101-108.
(1156) Ferreira-Aparicio, P. In *New and Future Developments in Catalysis*; Suib, S. L., Ed.; Elsevier: Amsterdam, 2013, DOI:https://doi.org/10.1016/B978-0-444-53880-2.00017-X https://doi.org/10.1016/B978-0-444-53880-2.00017-X.
(1157) Lee, T. K.; Jung, J. H.; Kim, J. B.; Hur, S. H. Improved Durability of Pt/Cnt Catalysts by the Low Temperature Self-Catalyzed Reduction for the Pem Fuel Cells. *Int. J. Hydrogen Energy* **2012,** *37*, 17992-18000.
(1158) Broom, D. P.; Hirscher, M. Irreproducibility in Hydrogen Storage Material Research. *Energy & Environmental Science* **2016,** *9*, 3368-3380.
(1159) Radovic, L. R.; Silva-Tapia, A. B.; Vallejos-Burgos, F. Oxygen Migration on the Graphene Surface. 1. Origin of Epoxide Groups. *Carbon* **2011,** *49*, 4218-4225.
(1160) Mul, G.; Kapteijn, F.; Doornkamp, C.; Moulijn, J. A. Transition Metal Oxide Catalyzed Carbon Black Oxidation: A Study With18o2. *J. Catal.* **1998,** *179*, 258-266.
(1161) Baumgarten, E.; Schuck, A. Investigations About Coke Burning and Oxygen Spillover. *React. Kinet. Catal. Lett.* **1997,** *61*, 3-12.
(1162) Baumgarten, E.; Schuck, A. Investigations About Gas Phase Oxygen Spillover. *React. Kinet. Catal. Lett.* **1997,** *62*, 209-216.
(1163) Kamp, C. J.; Perez Garza, H. H.; Fredriksson, H.; Kasemo, B.; Andersson, B.; Skoglundh, M. Nanofabricated Catalyst Particles for the Investigation of Catalytic Carbon Oxidation by Oxygen Spillover. *Langmuir* **2017,** *33*, 4903-4912.
(1164) Lee, S. M.; Lee, Y. H.; Hwang, Y. G.; Hahn, J. R.; Kang, H. Defect-Induced Oxidation of Graphite. *Phys. Rev. Lett.* **1999,** *82*, 217-220.
(1165) Xu, Y.-J.; Li, J.-Q. The Interaction of Molecular Oxygen with Active Sites of Graphite: A Theoretical Study. *Chem. Phys. Lett.* **2004,** *400*, 406-412.
(1166) Zhu, X. Y.; Lee, S. M.; Lee, Y. H.; Frauenheim, T. Adsorption and Desorption of an ${O}_{2}$ Molecule on Carbon Nanotubes. *Physical Review Letters* **2000,** *85*, 2757-2760.
(1167) Dag, S.; Gülseren, O.; Yildirim, T.; Ciraci, S. Oxygenation of Carbon Nanotubes: Atomic Structure, Energetics, and Electronic Structure. *Physical Review B* **2003,** *67*, 165424.
(1168) Jiang, J.; Yi, B. Thickness Effects of a Carbon-Supported Platinum Catalyst Layer on the Electrochemical Reduction of Oxygen in Sulfuric Acid Solution. *J. Electroanal. Chem.* **2005,** *577*, 107-115.
(1169) Tian, L.-L.; Yang, J.; Weng, M.-Y.; Tan, R.; Zheng, J.-X.; Chen, H.-B.; Zhuang, Q.-C.; Dai, L.-M.; Pan, F. Fast Diffusion of O2 on Nitrogen-Doped Graphene to Enhance Oxygen Reduction and Its Application for High-Rate Zn–Air Batteries. *ACS Applied Materials & Interfaces* **2017,** *9*, 7125-7130.
(1170) Qi, X.; Song, W.; Shi, J. Density Functional Theory Study the Effects of Oxygen-Containing Functional Groups on Oxygen Molecules and Oxygen Atoms Adsorbed on Carbonaceous Materials. *PLOS ONE* **2017,** *12*, e0173864.
(1171) Srivastava, D.; Susi, T.; Borghei, M.; Kari, L. Dissociation of Oxygen on Pristine and Nitrogen-Doped Carbon Nanotubes: A Spin-Polarized Density Functional Study. *RSC Advances* **2014,** *4*, 15225-15235.
(1172) Scardamaglia, M.; Susi, T.; Struzzi, C.; Snyders, R.; Di Santo, G.; Petaccia, L.; Bittencourt, C. Spectroscopic Observation of Oxygen Dissociation on Nitrogen-Doped Graphene. *Scientific Reports* **2017,** *7*, 7960.

(1173) Zhou, Q.; Yang, X.; Fu, Z.; Wang, C.; Yuan, L.; Zhang, H.; Tang, Y. Dft Study of Oxygen Adsorption on Vacancy and Stone–Wales Defected Single-Walled Carbon Nanotubes with Cr-Doped. *Physica E: Low-dimensional Systems and Nanostructures* **2015,** *65*, 77-83.
(1174) Radovic, L. R.; Suarez, A.; Vallejos-Burgos, F.; Sofo, J. O. Oxygen Migration on the Graphene Surface. 2. Thermochemistry of Basal-Plane Diffusion (Hopping). *Carbon* **2011,** *49*, 4226-4238.
(1175) Yafei, D.; Shuang, N.; Zhenyu, L.; Jinlong, Y. Diffusion and Desorption of Oxygen Atoms on Graphene. *J. Phys.: Condens. Matter* **2013,** *25*, 405301.
(1176) Manh-Thuong, N. An Ab initio Study of Oxygen on Strained Graphene. *J. Phys.: Condens. Matter* **2013,** *25*, 395301.
(1177) Mehmood, F.; Pachter, R.; Lu, W.; Boeckl, J. J. Adsorption and Diffusion of Oxygen on Single-Layer Graphene with Topological Defects. *The Journal of Physical Chemistry C* **2013,** *117*, 10366-10374.
(1178) Suarez, A. M.; Radovic, L. R.; Bar-Ziv, E.; Sofo, J. O. Gate-Voltage Control of Oxygen Diffusion on Graphene. *Phys. Rev. Lett.* **2011,** *106*, 146802.
(1179) Šljivančanin, Ž.; Milošević, A. S.; Popović, Z. S.; Vukajlović, F. R. Binding of Atomic Oxygen on Graphene from Small Epoxy Clusters to a Fully Oxidized Surface. *Carbon* **2013,** *54*, 482-488.
(1180) Lawson, D. B.; Beregszaszy, E. J. Incremental Oxidation of the Surface of Monolayer and Bilayer Graphene: A Computational Study. *Physica E: Low-dimensional Systems and Nanostructures* **2015,** *68*, 164-170.
(1181) Kumar, P. V.; Bardhan, N. M.; Chen, G.-Y.; Li, Z.; Belcher, A. M.; Grossman, J. C. New Insights into the Thermal Reduction of Graphene Oxide: Impact of Oxygen Clustering. *Carbon* **2016,** *100*, 90-98.
(1182) Liu, Z.; Jiang, L.; Sheng, L.; Zhou, Q.; Wei, T.; Zhang, B.; Fan, Z. Oxygen Clusters Distributed in Graphene with "Paddy Land" Structure: Ultrahigh Capacitance and Rate Performance for Supercapacitors. *Adv. Funct. Mater.* **2018,** *28*, 1705258.
(1183) Yan, J.-A.; Xian, L.; Chou, M. Y. Structural and Electronic Properties of Oxidized Graphene. *Phys. Rev. Lett.* **2009,** *103*, 086802.
(1184) Yang, M.; Wang, L.; Li, M.; Hou, T.; Li, Y. Structural Stability and O2 Dissociation on Nitrogen-Doped Graphene with Transition Metal Atoms Embedded: A First-Principles Study. *AIP Advances* **2015,** *5*, 067136.
(1185) Zhou, Q.; Yong, Y.; Su, X.; Ju, W.; Fu, Z.; Li, X. Adsorption Behavior of O2 on Vacancy-Defected Graphene with Transition-Metal Dopants: A Theoretical Study. *Int. J. Mod Phys B 0*, 1850304.
(1186) Nasehnia, F.; Seifi, M. Adsorption of Molecular Oxygen on Viiib Transition Metal-Doped Graphene: A Dft Study. *Mod. Phys. Lett. B* **2014,** *28*, 1450237.
(1187) Li, X.; Liu, L.; Wang, M.; Wang, Z. Adsorption and Dissociation of O2 on Ni-Doped (5, 5) Swcnt: A Dft Study. *Appl. Surf. Sci.* **2016,** *370*, 6-10.
(1188) Zheng, Y.; Xiao, W.; Cho, M.; Cho, K. Density Functional Theory Calculations for the Oxygen Dissociation on Nitrogen and Transition Metal Doped Graphenes. *Chem. Phys. Lett.* **2013,** *586*, 104-107.
(1189) Zhang, P.; Hou, X.; Mi, J.; Liu, L.; Dong, M. Oxygen Reduction Reaction on M-S4 Embedded Graphene: A Density Functional Theory Study. *Chem. Phys. Lett.* **2015,** *641*, 112-116.
(1190) Orellana, W. Catalytic Properties of Transition Metal–N4 Moieties in Graphene for the Oxygen Reduction Reaction: Evidence of Spin-Dependent Mechanisms. *The Journal of Physical Chemistry C* **2013,** *117*, 9812-9818.
(1191) Omidvar, A. Dissociation of O2 Molecule on Fe/Nx Clusters Embedded in C60 Fullerene, Carbon Nanotube and Graphene. *Synth. Met.* **2017,** *234*, 38-46.
(1192) Novotny, Z.; Netzer, F. P.; Dohnálek, Z. Cerium Oxide Nanoclusters on Graphene/Ru(0001): Intercalation of Oxygen Via Spillover. *ACS Nano* **2015,** *9*, 8617-8626.
(1193) Hayes, K. E.; Lee, H.-S. First Principles Studies of the Electronic Properties and Catalytic Activity of Single-Walled Carbon Nanotube Doped with Pt Clusters and Chains. *Chem. Phys.* **2012,** *393*, 96-106.

(1194) Ciambelli, P.; D'Amore, M.; Palma, V.; Vaccaro, S. Catalytic Oxidation of an Amorphous Carbon Black. *Combust. Flame* **1994,** *99*, 413-421.
(1195) Simonsen, S. B.; Dahl, S.; Johnson, E.; Helveg, S. Ceria-Catalyzed Soot Oxidation Studied by Environmental Transmission Electron Microscopy. *J. Catal.* **2008,** *255*, 1-5.
(1196) Mul, G.; Neeft, J. P. A.; Kapteijn, F.; Moulijn, J. A. The Formation of Carbon Surface Oxygen Complexes by Oxygen and Ozone. The Effect of Transition Metal Oxides. *Carbon* **1998,** *36*, 1269-1276.
(1197) Zeng, L.; Turek, T.; Weber, A. P. Spillover-Bedingte Reichweite Von Aktivierten Sauerstoffatomen in Der Katalytischen Rußoxidation an Nanopartikel-Schichtsystemen. *Chem. Ing. Tech.* **2011,** *83*, 1276-1281.
(1198) Baumgarten, E.; Dedek, B. Ftir Spectroscopic Investigation of Oxygen Spillover Especially through the Gas-Phase. A Reaction Interesting in Coke Burning. *React. Kinet. Catal. Lett.* **1999,** *67*, 21-28.
(1199) Zeng, L.; Weber, A. P. Transportmechanismen Für Aktivierten Sauerstoff in Der Katalytischen Rußoxidation An nanopartikel-Schichtsystemen. *Chem. Ing. Tech.* **2012,** *84*, 295-300.
(1200) Kalinkin, A. V.; Sorokin, A. M.; Smirnov, M. Y.; Bukhtiyarov, V. I. Size Effect in the Oxidation of Platinum Nanoparticles on Graphite with Nitrogen Dioxide: An Xps and Stm Study. *Kinet. Catal.* **2014,** *55*, 354-360.
(1201) Wu, G.; Wang, X.; Guan, N.; Li, L. Palladium on Graphene as Efficient Catalyst for Solvent-Free Aerobic Oxidation of Aromatic Alcohols: Role of Graphene Support. *Applied Catalysis B: Environmental* **2013,** *136-137*, 177-185.
(1202) Toebes, M. L.; Zhang, Y.; Hájek, J.; Alexander Nijhuis, T.; Bitter, J. H.; Jos van Dillen, A.; Murzin, D. Y.; Koningsberger, D. C.; de Jong, K. P. Support Effects in the Hydrogenation of Cinnamaldehyde over Carbon Nanofiber-Supported Platinum Catalysts: Characterization and Catalysis. *J. Catal.* **2004,** *226*, 215-225.
(1203) Toebes, M. L.; Alexander Nijhuis, T.; Hájek, J.; Bitter, J. H.; Jos van Dillen, A.; Murzin, D. Y.; de Jong, K. P. Support Effects in Hydrogenation of Cinnamaldehyde over Carbon Nanofiber-Supported Platinum Catalysts: Kinetic Modeling. *Chem. Eng. Sci.* **2005,** *60*, 5682-5695.
(1204) Plomp, A. J.; Vuori, H.; Krause, A. O. I.; de Jong, K. P.; Bitter, J. H. Particle Size Effects for Carbon Nanofiber Supported Platinum and Ruthenium Catalysts for the Selective Hydrogenation of Cinnamaldehyde. *Applied Catalysis A: General* **2008,** *351*, 9-15.
(1205) Toebes, M. L.; Prinsloo, F. F.; Bitter, J. H.; van Dillen, A. J.; de Jong, K. P. Influence of Oxygen-Containing Surface Groups on the Activity and Selectivity of Carbon Nanofiber-Supported Ruthenium Catalysts in the Hydrogenation of Cinnamaldehyde. *J. Catal.* **2003,** *214*, 78-87.
(1206) Solhy, A.; Machado, B. F.; Beausoleil, J.; Kihn, Y.; Gonçalves, F.; Pereira, M. F. R.; Órfão, J. J. M.; Figueiredo, J. L.; Faria, J. L.; Serp, P. Mwcnt Activation and Its Influence on the Catalytic Performance of Pt/Mwcnt Catalysts for Selective Hydrogenation. *Carbon* **2008,** *46*, 1194-1207.
(1207) Machado, B. F.; Gomes, H. T.; Serp, P.; Kalck, P.; Faria, J. L. Liquid-Phase Hydrogenation of Unsaturated Aldehydes: Enhancing Selectivity of Multiwalled Carbon Nanotube-Supported Catalysts by Thermal Activation. *ChemCatChem* **2010,** *2*, 190-197.
(1208) Lazzarini, A.; Piovano, A.; Pellegrini, R.; Leofanti, G.; Agostini, G.; Rudić, S.; Chierotti, M. R.; Gobetto, R.; Battiato, A.; Spoto, G.et al. A Comprehensive Approach to Investigate the Structural and Surface Properties of Activated Carbons and Related Pd-Based Catalysts. *Catalysis Science & Technology* **2016,** *6*, 4910-4922.
(1209) Wang, Y.; Yao, J.; Li, H.; Su, D.; Antonietti, M. Highly Selective Hydrogenation of Phenol and Derivatives over a Pd@Carbon Nitride Catalyst in Aqueous Media. *J. Am. Chem. Soc.* **2011,** *133*, 2362-2365.
(1210) Makowski, P.; Demir Cakan, R.; Antonietti, M.; Goettmann, F.; Titirici, M.-M. Selective Partial Hydrogenation of Hydroxy Aromatic Derivatives with Palladium Nanoparticles Supported on Hydrophilic Carbon. *Chem. Commun.* **2008**, DOI:10.1039/B717928F 10.1039/B717928F, 999-1001.

(1211) Jiang, H.; Yu, X.; Nie, R.; Lu, X.; Zhou, D.; Xia, Q. Selective Hydrogenation of Aromatic Carboxylic Acids over Basic N-Doped Mesoporous Carbon Supported Palladium Catalysts. *Applied Catalysis A: General* **2016,** *520*, 73-81.
(1212) Aksoylu, A. E.; Madalena, M.; Freitas, A.; Pereira, M. F. R.; Figueiredo, J. L. The Effects of Different Activated Carbon Supports and Support Modifications on the Properties of Pt/Ac Catalysts. *Carbon* **2001,** *39*, 175-185.
(1213) Zanutelo, C.; Landers, R.; Carvalho, W. A.; Cobo, A. J. G. Carbon Support Treatment Effect on Ru/C Catalyst Performance for Benzene Partial Hydrogenation. *Applied Catalysis A: General* **2011,** *409-410*, 174-180.
(1214) Lin, S. D.; Vannice, M. A. Hydrogenation of Aromatic Hydrocarbons over Supported Pt Catalysts .I. Benzene Hydrogenation. *J. Catal.* **1993,** *143*, 539-553.
(1215) Fraga, M. A.; Mendes, M. J.; Jordão, E. Examination of the Surface Chemistry of Activated Carbon on Enantioselective Hydrogenation of Methyl Pyruvate over Pt/C Catalysts. *J. Mol. Catal. A: Chem.* **2002,** *179*, 243-251.
(1216) Tang, T.; Yin, C.; Xiao, N.; Guo, M.; Xiao, F.-S. High Activity in Catalytic Oxidation of Benzyl Alcohol with Molecular Oxygen over Carboxylic-Functionalized Carbon Nanofiber-Supported Ruthenium Catalysts. *Catal. Lett.* **2009,** *127*, 400-405.
(1217) Cordoba, M.; Miranda, C.; Lederhos, C.; Coloma-Pascual, F.; Ardila, A.; Fuentes, G. A.; Pouilloux, Y.; Ramírez, A. Catalytic Performance of Co3o4 on Different Activated Carbon Supports in the Benzyl Alcohol Oxidation. *Catalysts* **2017,** *7*, 384.
(1218) Wang, X.; Li, N.; Webb, J. A.; Pfefferle, L. D.; Haller, G. L. Effect of Surface Oxygen Containing Groups on the Catalytic Activity of Multi-Walled Carbon Nanotube Supported Pt Catalyst. *Applied Catalysis B: Environmental* **2010,** *101*, 21-30.
(1219) Wang, X.; Li, N.; Pfefferle, L. D.; Haller, G. L. Pt−Co Bimetallic Catalyst Supported on Single-Walled Carbon Nanotubes: Effect of Alloy Formation and Oxygen Containing Groups. *The Journal of Physical Chemistry C* **2010,** *114*, 16996-17002.
(1220) Amorim, C.; Keane, M. A. Effect of Surface Acid Groups Associated with Amorphous and Structured Carbon on the Catalytic Hydrodechlorination of Chlorobenzenes. *Journal of Chemical Technology & Biotechnology* **2008,** *83*, 662-672.
(1221) Carmo, M.; Brandalise, M.; Neto, A. O.; Spinacé, E. V.; Taylor, A. D.; Linardi, M.; Rocha Poço, J. G. Enhanced Activity Observed for Sulfuric Acid and Chlorosulfuric Acid Functionalized Carbon Black as Ptru and Ptsn Electrocatalyst Support for Dmfc and Defc Applications. *Int. J. Hydrogen Energy* **2011,** *36*, 14659-14667.
(1222) Gharibi, H.; Yasi, F.; Kazemeini, M.; Heydari, A.; Golmohammadi, F. Fabrication of Mea Based on Sulfonic Acid Functionalized Carbon Supported Platinum Nanoparticles for Oxygen Reduction Reaction in Pemfcs. *RSC Advances* **2015,** *5*, 85775-85784.
(1223) Pak, C.; Joo, S. H.; You, D. J.; Kim, J. M.; Chang, H.; Seung, D. In *Stud. Surf. Sci. Catal.*; Zhao, D.;Qiu, S.;Tang, Y.;Yu, C., Eds.; Elsevier, 2007; Vol. 165.
(1224) Sun, Z.-P.; Zhang, X.-G.; Liu, R.-L.; Liang, Y.-Y.; Li, H.-L. A Simple Approach Towards Sulfonated Multi-Walled Carbon Nanotubes Supported by Pd Catalysts for Methanol Electro-Oxidation. *J. Power Sources* **2008,** *185*, 801-806.
(1225) Yang, S.; Zhang, X.; Mi, H.; Ye, X. Pd Nanoparticles Supported on Functionalized Multi-Walled Carbon Nanotubes (Mwcnts) and Electrooxidation for Formic Acid. *J. Power Sources* **2008,** *175*, 26-32.
(1226) Sun, Z.-P.; Zhang, X.-G.; Tong, H.; Liang, Y.-Y.; Li, H.-L. Sulfonation of Ordered Mesoporous Carbon Supported Pd Catalysts for Formic Acid Electrooxidation. *J. Colloid Interface Sci.* **2009,** *337*, 614-618.
(1227) Sun, Z.-P.; Zhang, X.-G.; Liang, Y.-Y.; Li, H.-L. A Facile Approach Towards Sulfonate Functionalization of Multi-Walled Carbon Nanotubes as Pd Catalyst Support for Ethylene Glycol Electro-Oxidation. *J. Power Sources* **2009,** *191*, 366-370.

(1228) Selvarani, G.; Sahu, A. K.; Choudhury, N. A.; Sridhar, P.; Pitchumani, S.; Shukla, A. K. A Phenyl-Sulfonic Acid Anchored Carbon-Supported Platinum Catalyst for Polymer Electrolyte Fuel Cell Electrodes. *Electrochim. Acta* **2007,** *52*, 4871-4877.
(1229) He, D.; Mu, S.; Pan, M. Perfluorosulfonic Acid-Functionalized Pt/Carbon Nanotube Catalysts with Enhanced Stability and Performance for Use in Proton Exchange Membrane Fuel Cells. *Carbon* **2011,** *49*, 82-88.
(1230) Carmo, M.; Roepke, T.; Roth, C.; dos Santos, A. M.; Poco, J. G. R.; Linardi, M. A Novel Electrocatalyst Support with Proton Conductive Properties for Polymer Electrolyte Membrane Fuel Cell Applications. *J. Power Sources* **2009,** *191*, 330-337.
(1231) Xu, Z.; Qi, Z.; Kaufman, A. Superior Catalysts for Proton Exchange Membrane Fuel Cells: Sulfonation of Carbon-Supported Catalysts Using Sulfate Salts. *Electrochem. Solid-State Lett.* **2005,** *8*, A313-A315.
(1232) Hung, T.-F.; Wang, B.; Tsai, C.-W.; Tu, M.-H.; Wang, G.-X.; Liu, R.-S.; Tsai, D. P.; Lo, M.-Y.; Shy, D.-S.; Xing, X.-K. Sulfonation of Graphene Nanosheet-Supported Platinum Via a Simple Thermal-Treatment toward Its Oxygen Reduction Activity in Acid Medium. *Int. J. Hydrogen Energy* **2012,** *37*, 14205-14210.
(1233) He, D.; Kou, Z.; Xiong, Y.; Cheng, K.; Chen, X.; Pan, M.; Mu, S. Simultaneous Sulfonation and Reduction of Graphene Oxide as Highly Efficient Supports for Metal Nanocatalysts. *Carbon* **2014,** *66*, 312-319.
(1234) Yang, H.-P.; Lin, Q.; Zhang, H.-W.; Li, G.-D.; Fan, L.-D.; Chai, X.-Y.; Zhang, Q.-L.; Liu, J.-H.; He, C.-X. Platinum/Nitrogen-Doped Carbon/Carbon Cloth: A Bifunctional Catalyst for the Electrochemical Reduction and Carboxylation of Co2 with Excellent Efficiency. *Chem. Commun.* **2018,** *54*, 4108-4111.
(1235) Purceno, A. D.; Machado, B. F.; Teixeira, A. P. C.; Medeiros, T. V.; Benyounes, A.; Beausoleil, J.; Menezes, H. C.; Cardeal, Z. L.; Lago, R. M.; Serp, P. Magnetic Amphiphilic Hybrid Carbon Nanotubes Containing N-Doped and Undoped Sections: Powerful Tensioactive Nanostructures. *Nanoscale* **2015,** *7*, 294-300.
(1236) Liu, X.; Dai, L. Carbon-Based Metal-Free Catalysts. *Nature Reviews Materials* **2016,** *1*, 16064.
(1237) *Carbon-Based Metal-Free Catalysts: Design and Applications*; Wiley-VCH Verlag GmbH & Co. KGaA: Weinheim, Germany, 2018.
(1238) Tang, P.; Hu, G.; Li, M.; Ma, D. Graphene-Based Metal-Free Catalysts for Catalytic Reactions in the Liquid Phase. *ACS Catalysis* **2016,** *6*, 6948-6958.
(1239) Hu, C.; Liu, D.; Xiao, Y.; Dai, L. Functionalization of Graphene Materials by Heteroatom-Doping for Energy Conversion and Storage. *Progress in Natural Science: Materials International* **2018,** *28*, 121-132.
(1240) Navalon, S.; Dhakshinamoorthy, A.; Alvaro, M.; Antonietti, M.; García, H. Active Sites on Graphene-Based Materials as Metal-Free Catalysts. *Chem. Soc. Rev.* **2017,** *46*, 4501-4529.
(1241) Hara, M.; Yoshida, T.; Takagaki, A.; Takata, T.; Kondo, J. N.; Hayashi, S.; Domen, K. A Carbon Material as a Strong Protonic Acid. *Angew. Chem. Int. Ed.* **2004,** *43*, 2955-2958.
(1242) Garg, B.; Bisht, T.; Ling, Y.-C. Graphene-Based Nanomaterials as Heterogeneous Acid Catalysts: A Comprehensive Perspective. *Molecules* **2014,** *19*, 14582.
(1243) Li, B.; Su, D. The Nucleophilicity of the Oxygen Functional Groups on Carbon Materials: A Dft Analysis. *Chemistry – A European Journal* **2014,** *20*, 7890-7894.
(1244) Guo, D.; Shibuya, R.; Akiba, C.; Saji, S.; Kondo, T.; Nakamura, J. Active Sites of Nitrogen-Doped Carbon Materials for Oxygen Reduction Reaction Clarified Using Model Catalysts. *Science* **2016,** *351*, 361-365.
(1245) Deldari, H. Suitable Catalysts for Hydroisomerization of Long-Chain Normal Paraffins. *Applied Catalysis A: General* **2005,** *293*, 1-10.
(1246) Fernandes, S.; Andrade, M.; Ania, C. O.; Martins, A.; Pires, J.; Carvalho, A. P. Pt/Carbon Materials as Bi-Functional Catalysts for N-Decane Hydroisomerization. *Microporous Mesoporous Mater.* **2012,** *163*, 21-28.

(1247) Contreras, R. C.; Guicheret, B.; Machado, B. F.; Rivera-Cárcamo, C.; Curiel Alvarez, M. A.; Valdez Salas, B.; Ruttert, M.; Placke, T.; Favre Réguillon, A.; Vanoye, L.et al. Effect of Mesoporous Carbon Support Nature and Pretreatments on Palladium Loading, Dispersion and Apparent Catalytic Activity in Hydrogenation of Myrcene. *J. Catal.* **2019,** *372*, 226-244.
(1248) Meier, J. A.; Hill, L. W. Carbon Black Catalyzed Olefin Isomerization: I. A Heterogeneous Site Model Based on Rate Dependence on Catalyst Concentration. *J. Catal.* **1974,** *32*, 80-87.
(1249) Trawczyński, J.; Suppan, S.; Sayag, C.; Djéga-Mariadassou, G. Surface Acidity of the Activated Cbc. *Fuel Process. Technol.* **2002,** *77-78*, 317-324.
(1250) Said, S. Synthesis and Functionalization of Ordered Mesoporous Carbons Supported Pt Nanoparticles for Hydroconversion of N-Heptane. *New J. Chem.* **2018,** *42*, 14517-14529.
(1251) Hita, I.; Palos, R.; Arandes, J. M.; Hill, J. M.; Castaño, P. Petcoke-Derived Functionalized Activated Carbon as Support in a Bifunctional Catalyst for Tire Oil Hydroprocessing. *Fuel Process. Technol.* **2016,** *144*, 239-247.
(1252) Hita, I.; Cordero-Lanzac, T.; Gallardo, A.; Arandes, J. M.; Rodríguez-Mirasol, J.; Bilbao, J.; Cordero, T.; Castaño, P. Phosphorus-Containing Activated Carbon as Acid Support in a Bifunctional Pt–Pd Catalyst for Tire Oil Hydrocracking. *Catal. Commun.* **2016,** *78*, 48-51.
(1253) Lazaridis, P. A.; Karakoulia, S. A.; Teodorescu, C.; Apostol, N.; Macovei, D.; Panteli, A.; Delimitis, A.; Coman, S. M.; Parvulescu, V. I.; Triantafyllidis, K. S. High Hexitols Selectivity in Cellulose Hydrolytic Hydrogenation over Platinum (Pt) Vs. Ruthenium (Ru) Catalysts Supported on Micro/Mesoporous Carbon. *Applied Catalysis B: Environmental* **2017,** *214*, 1-14.
(1254) Adsuar-García, M. D.; Flores-Lasluisa, J. X.; Azar, F. Z.; Román-Martínez, M. C. Carbon-Black-Supported Ru Catalysts for the Valorization of Cellulose through Hydrolytic Hydrogenation. *Catalysts* **2018,** *8*, 572.
(1255) Han, J. W.; Lee, H. Direct Conversion of Cellulose into Sorbitol Using Dual-Functionalized Catalysts in Neutral Aqueous Solution. *Catal. Commun.* **2012,** *19*, 115-118.
(1256) Deng, W.; Tan, X.; Fang, W.; Zhang, Q.; Wang, Y. Conversion of Cellulose into Sorbitol over Carbon Nanotube-Supported Ruthenium Catalyst. *Catal. Lett.* **2009,** *133*, 167.
(1257) Wang, Y.; Rong, Z.; Wang, Y.; Wang, T.; Du, Q.; Wang, Y.; Qu, J. Graphene-Based Metal/Acid Bifunctional Catalyst for the Conversion of Levulinic Acid to Γ-Valerolactone. *ACS Sustainable Chemistry & Engineering* **2017,** *5*, 1538-1548.
(1258) de Clippel, F.; Dusselier, M.; Van Rompaey, R.; Vanelderen, P.; Dijkmans, J.; Makshina, E.; Giebeler, L.; Oswald, S.; Baron, G. V.; Denayer, J. F. M.et al. Fast and Selective Sugar Conversion to Alkyl Lactate and Lactic Acid with Bifunctional Carbon–Silica Catalysts. *J. Am. Chem. Soc.* **2012,** *134*, 10089-10101.
(1259) Hu, L.; Lin, L.; Wu, Z.; Zhou, S.; Liu, S. Chemocatalytic Hydrolysis of Cellulose into Glucose over Solid Acid Catalysts. *Applied Catalysis B: Environmental* **2015,** *174-175*, 225-243.
(1260) Barbaro, P.; Liguori, F.; Linares, N.; Marrodan, C. M. Heterogeneous Bifunctional Metal/Acid Catalysts for Selective Chemical Processes. *Eur. J. Inorg. Chem.* **2012,** *2012*, 3807-3823.
(1261) Kobayashi, H.; Ito, Y.; Komanoya, T.; Hosaka, Y.; Dhepe, P. L.; Kasai, K.; Hara, K.; Fukuoka, A. Synthesis of Sugar Alcohols by Hydrolytic Hydrogenation of Cellulose over Supported Metal Catalysts. *Green Chemistry* **2011,** *13*, 326-333.
(1262) Luo, C.; Wang, S.; Liu, H. Cellulose Conversion into Polyols Catalyzed by Reversibly Formed Acids and Supported Ruthenium Clusters in Hot Water. *Angew. Chem. Int. Ed.* **2007,** *46*, 7636-7639.
(1263) Suganuma, S.; Nakajima, K.; Kitano, M.; Yamaguchi, D.; Kato, H.; Hayashi, S.; Hara, M. Hydrolysis of Cellulose by Amorphous Carbon Bearing So3h, Cooh, and Oh Groups. *J. Am. Chem. Soc.* **2008,** *130*, 12787-12793.
(1264) Yabushita, M.; Kobayashi, H.; Hara, K.; Fukuoka, A. Quantitative Evaluation of Ball-Milling Effects on the Hydrolysis of Cellulose Catalysed by Activated Carbon. *Catalysis Science & Technology* **2014,** *4*, 2312-2317.

(1265) Kobayashi, H.; Yabushita, M.; Komanoya, T.; Hara, K.; Fujita, I.; Fukuoka, A. High-Yielding One-Pot Synthesis of Glucose from Cellulose Using Simple Activated Carbons and Trace Hydrochloric Acid. *ACS Catalysis* **2013,** *3*, 581-587.
(1266) Chung, P.-W.; Charmot, A.; Olatunji-Ojo, O. A.; Durkin, K. A.; Katz, A. Hydrolysis Catalysis of Miscanthus Xylan to Xylose Using Weak-Acid Surface Sites. *ACS Catalysis* **2014,** *4*, 302-310.
(1267) Yang, Z.; Huang, R.; Qi, W.; Tong, L.; Su, R.; He, Z. Hydrolysis of Cellulose by Sulfonated Magnetic Reduced Graphene Oxide. *Chem. Eng. J.* **2015,** *280*, 90-98.
(1268) Zhang, M.; Wu, M.; Liu, Q.; Wang, X.; Lv, T.; Jia, L. Graphene Oxide Mediated Cellulose-Derived Carbon as a Highly Selective Catalyst for the Hydrolysis of Cellulose to Glucose. *Applied Catalysis A: General* **2017,** *543*, 218-224.
(1269) Komanoya, T.; Kobayashi, H.; Hara, K.; Chun, W.-J.; Fukuoka, A. Catalysis and Characterization of Carbon-Supported Ruthenium for Cellulose Hydrolysis. *Applied Catalysis A: General* **2011,** *407*, 188-194.
(1270) Kobayashi, H.; Komanoya , T.; Hara, K.; Fukuoka, A. Water-Tolerant Mesoporous-Carbon-Supported Ruthenium Catalysts for the Hydrolysis of Cellulose to Glucose. *ChemSusChem* **2010,** *3*, 440-443.
(1271) Kitano, M.; Yamaguchi, D.; Suganuma, S.; Nakajima, K.; Kato, H.; Hayashi, S.; Hara, M. Adsorption-Enhanced Hydrolysis of B-1,4-Glucan on Graphene-Based Amorphous Carbon Bearing So3h, Cooh, and Oh Groups. *Langmuir* **2009,** *25*, 5068-5075.
(1272) Suganuma, S.; Nakajima, K.; Kitano, M.; Yamaguchi, D.; Kato, H.; Hayashi, S.; Hara, M. Synthesis and Acid Catalysis of Cellulose-Derived Carbon-Based Solid Acid. *Solid State Sciences* **2010,** *12*, 1029-1034.
(1273) Wang, D.; Niu, W.; Tan, M.; Wu, M.; Zheng, X.; Li, Y.; Tsubaki, N. Pt Nanocatalysts Supported on Reduced Graphene Oxide for Selective Conversion of Cellulose or Cellobiose to Sorbitol. *ChemSusChem* **2014,** *7*, 1398-1406.
(1274) Kobayashi, H.; Matsuhashi, H.; Komanoya, T.; Hara, K.; Fukuoka, A. Transfer Hydrogenation of Cellulose to Sugar Alcohols over Supported Ruthenium Catalysts. *Chem. Commun.* **2011,** *47*, 2366-2368.
(1275) Shrotri, A.; Kobayashi, H.; Tanksale, A.; Fukuoka, A.; Beltramini, J. Transfer Hydrogenation of Cellulose-Based Oligomers over Carbon-Supported Ruthenium Catalyst in a Fixed-Bed Reactor. *ChemCatChem* **2014,** *6*, 1349-1356.
(1276) Pang, J.; Wang, A.; Zheng, M.; Zhang, Y.; Huang, Y.; Chen, X.; Zhang, T. Catalytic Conversion of Cellulose to Hexitols with Mesoporous Carbon Supported Ni-Based Bimetallic Catalysts. *Green Chemistry* **2012,** *14*, 614-617.
(1277) Van de Vyver, S.; Geboers, J.; Schutyser, W.; Dusselier, M.; Eloy, P.; Dornez, E.; Seo, J. W.; Courtin, C. M.; Gaigneaux, E. M.; Jacobs, P. A.et al. Tuning the Acid/Metal Balance of Carbon Nanofiber-Supported Nickel Catalysts for Hydrolytic Hydrogenation of Cellulose. *ChemSusChem* **2012,** *5*, 1549-1558.
(1278) Piskun, A. S.; van de Bovenkamp, H. H.; Rasrendra, C. B.; Winkelman, J. G. M.; Heeres, H. J. Kinetic Modeling of Levulinic Acid Hydrogenation to Γ-Valerolactone in Water Using a Carbon Supported Ru Catalyst. *Applied Catalysis A: General* **2016,** *525*, 158-167.
(1279) Ding, D.; Wang, J.; Xi, J.; Liu, X.; Lu, G.; Wang, Y. High-Yield Production of Levulinic Acid from Cellulose and Its Upgrading to Γ-Valerolactone. *Green Chemistry* **2014,** *16*, 3846-3853.
(1280) Yan, Z.-p.; Lin, L.; Liu, S. Synthesis of Γ-Valerolactone by Hydrogenation of Biomass-Derived Levulinic Acid over Ru/C Catalyst. *Energy & Fuels* **2009,** *23*, 3853-3858.
(1281) Piskun, A. S.; de Haan, J. E.; Wilbers, E.; van de Bovenkamp, H. H.; Tang, Z.; Heeres, H. J. Hydrogenation of Levulinic Acid to Γ-Valerolactone in Water Using Millimeter Sized Supported Ru Catalysts in a Packed Bed Reactor. *ACS Sustainable Chemistry & Engineering* **2016,** *4*, 2939-2950.
(1282) Manzer, L. E. Catalytic Synthesis of A-Methylene-Γ-Valerolactone: A Biomass-Derived Acrylic Monomer. *Applied Catalysis A: General* **2004,** *272*, 249-256.

(1283) Du, X.; Liu, Y.; Wang, J.; Cao, Y.; Fan, K. Catalytic Conversion of Biomass-Derived Levulinic Acid into Γ-Valerolactone Using Iridium Nanoparticles Supported on Carbon Nanotubes. *Chinese Journal of Catalysis* **2013,** *34*, 993-1001.
(1284) Park, J. Y.; Kim, M. A.; Lee, S. J.; Jung, J.; Jang, H. M.; Upare, P. P.; Hwang, Y. K.; Chang, J.-S.; Park, J. K. Preparation and Characterization of Carbon-Encapsulated Iron Nanoparticles and Their Catalytic Activity in the Hydrogenation of Levulinic Acid. *Journal of Materials Science* **2015,** *50*, 334-343.
(1285) Shimizu, K.-i.; Kanno, S.; Kon, K. Hydrogenation of Levulinic Acid to Γ-Valerolactone by Ni and Moox Co-Loaded Carbon Catalysts. *Green Chemistry* **2014,** *16*, 3899-3903.
(1286) Yan, K.; Lafleur, T.; Liao, J. Facile Synthesis of Palladium Nanoparticles Supported on Multi-Walled Carbon Nanotube for Efficient Hydrogenation of Biomass-Derived Levulinic Acid. *J. Nanopart. Res.* **2013,** *15*, 1906.
(1287) Upare, P. P.; Lee, J.-M.; Hwang, D. W.; Halligudi, S. B.; Hwang, Y. K.; Chang, J.-S. Selective Hydrogenation of Levulinic Acid to Γ-Valerolactone over Carbon-Supported Noble Metal Catalysts. *Journal of Industrial and Engineering Chemistry* **2011,** *17*, 287-292.
(1288) Velisoju, V. K.; Peddakasu, G. B.; Gutta, N.; Boosa, V.; Kandula, M.; Chary, K. V. R.; Akula, V. Influence of Support for Ru and Water Role on Product Selectivity in the Vapor-Phase Hydrogenation of Levulinic Acid to Γ-Valerolactone: Investigation by Probe-Adsorbed Fourier Transform Infrared Spectroscopy. *The Journal of Physical Chemistry C* **2018,** *122*, 19670-19677.
(1289) Galletti, A. M. R.; Antonetti, C.; De Luise, V.; Martinelli, M. A Sustainable Process for the Production of Γ-Valerolactone by Hydrogenation of Biomass-Derived Levulinic Acid. *Green Chemistry* **2012,** *14*, 688-694.
(1290) Abdelrahman, O. A.; Heyden, A.; Bond, J. Q. Analysis of Kinetics and Reaction Pathways in the Aqueous-Phase Hydrogenation of Levulinic Acid to Form Γ-Valerolactone over Ru/C. *ACS Catalysis* **2014,** *4*, 1171-1181.
(1291) Yao, Y.; Wang, Z.; Zhao, S.; Wang, D.; Wu, Z.; Zhang, M. A Stable and Effective Ru/Polyethersulfone Catalyst for Levulinic Acid Hydrogenation to Γ-Valerolactone in Aqueous Solution. *Catal. Today* **2014,** *234*, 245-250.
(1292) Abdelrahman, O. A.; Luo, H. Y.; Heyden, A.; Román-Leshkov, Y.; Bond, J. Q. Toward Rational Design of Stable, Supported Metal Catalysts for Aqueous-Phase Processing: Insights from the Hydrogenation of Levulinic Acid. *J. Catal.* **2015,** *329*, 10-21.
(1293) Goyal, R.; Sarkar, B.; Lucus, N.; Bordoloi, A. Acid–Base Cooperative Catalysis over Mesoporous Nitrogen-Rich Carbon. *ChemCatChem* **2014,** *6*, 3091-3095.
(1294) Vilé, G.; Albani, D.; Nachtegaal, M.; Chen, Z.; Dontsova, D.; Antonietti, M.; López, N.; Pérez-Ramírez, J. A Stable Single-Site Palladium Catalyst for Hydrogenations. *Angew. Chem. Int. Ed.* **2015,** *54*, 11265-11269.
(1295) Liu, W.; Chen, Y.; Qi, H.; Zhang, L.; Yan, W.; Liu, X.; Yang, X.; Miao, S.; Wang, W.; Liu, C.et al. A Durable Nickel Single-Atom Catalyst for Hydrogenation Reactions and Cellulose Valorization under Harsh Conditions. *Angew. Chem.* **2018,** *130*, 7189-7193.
(1296) Yan, H.; Lv, H.; Yi, H.; Liu, W.; Xia, Y.; Huang, X.; Huang, W.; Wei, S.; Wu, X.; Lu, J. Understanding the Underlying Mechanism of Improved Selectivity in Pd1 Single-Atom Catalyzed Hydrogenation Reaction. *J. Catal.* **2018,** *366*, 70-79.
(1297) Li, J.; Liu, G.; Long, X.; Gao, G.; Wu, J.; Li, F. Different Active Sites in a Bifunctional Co@N-Doped Graphene Shells Based Catalyst for the Oxidative Dehydrogenation and Hydrogenation Reactions. *J. Catal.* **2017,** *355*, 53-62.
(1298) Long, J.; Shen, K.; Li, Y. Bifunctional N-Doped Co@C Catalysts for Base-Free Transfer Hydrogenations of Nitriles: Controllable Selectivity to Primary Amines Vs Imines. *ACS Catalysis* **2017,** *7*, 275-284.
(1299) Li, J.; Liu, J.-l.; Zhou, H.-j.; Fu, Y. Catalytic Transfer Hydrogenation of Furfural to Furfuryl Alcohol over Nitrogen-Doped Carbon-Supported Iron Catalysts. *ChemSusChem* **2016,** *9*, 1339-1347.
(1300) Jia, L.; Bulushev, D. A.; Podyacheva, O. Y.; Boronin, A. I.; Kibis, L. S.; Gerasimov, E. Y.; Beloshapkin, S.; Seryak, I. A.; Ismagilov, Z. R.; Ross, J. R. H. Pt Nanoclusters Stabilized by N-

Doped Carbon Nanofibers for Hydrogen Production from Formic Acid. *J. Catal.* **2013,** *307*, 94-102.
(1301) Han, X.; Li, C.; Guo, Y.; Liu, X.; Zhang, Y.; Wang, Y. N-Doped Carbon Supported Pt Catalyst for Base-Free Oxidation of 5-Hydroxymethylfurfural to 2,5-Furandicarboxylic Acid. *Applied Catalysis A: General* **2016,** *526*, 1-8.
(1302) Bai, C.; Li, A.; Yao, X.; Liu, H.; Li, Y. Efficient and Selective Aerobic Oxidation of Alcohols Catalysed by Mof-Derived Co Catalysts. *Green Chemistry* **2016,** *18*, 1061-1069.
(1303) Zhong, W.; Liu, H.; Bai, C.; Liao, S.; Li, Y. Base-Free Oxidation of Alcohols to Esters at Room Temperature and Atmospheric Conditions Using Nanoscale Co-Based Catalysts. *ACS Catalysis* **2015,** *5*, 1850-1856.
(1304) Su, H.; Zhang, K.-X.; Zhang, B.; Wang, H.-H.; Yu, Q.-Y.; Li, X.-H.; Antonietti, M.; Chen, J.-S. Activating Cobalt Nanoparticles Via the Mott–Schottky Effect in Nitrogen-Rich Carbon Shells for Base-Free Aerobic Oxidation of Alcohols to Esters. *J. Am. Chem. Soc.* **2017,** *139*, 811-818.
(1305) Zhang, P.; Gong, Y.; Li, H.; Chen, Z.; Wang, Y. Solvent-Free Aerobic Oxidation of Hydrocarbons and Alcohols with Pd@N-Doped Carbon from Glucose. *Nature Communications* **2013,** *4*, 1593.
(1306) Dai, J.; Zou, H.; Shi, Z.; Yang, H.; Wang, R.; Zhang, Z.; Qiu, S. Janus N-Doped Carbon@Silica Hollow Spheres as Multifunctional Amphiphilic Nanoreactors for Base-Free Aerobic Oxidation of Alcohols in Water. *ACS Applied Materials & Interfaces* **2018,** *10*, 33474-33483.
(1307) Markus, H.; Mäki-Arvela, P.; Kumar, N.; Kul'kova, N. V.; Eklund, P.; Sjöholm, R.; Holmbom, B.; Salmi, T.; Murzin, D. Y. Hydrogenolysis of Hydroxymatairesinol over Carbon-Supported Palladium Catalysts. *Catal. Lett.* **2005,** *103*, 125-131.
(1308) Markus, H.; Plomp, A. J.; Sandberg, T.; Nieminen, V.; Bitter, J. H.; Murzin, D. Y. Dehydrogenation of Hydroxymatairesinol to Oxomatairesinol over Carbon Nanofibre-Supported Palladium Catalysts. *J. Mol. Catal. A: Chem.* **2007,** *274*, 42-49.
(1309) Dong, X.; Wang, Y.; Yu, Y.; Zhang, M. Density Functional Theory Investigation on the Synthesis Mechanism of Vinyl Acetate from Acetylene and Acetic Acid Catalyzed by Ordered Mesoporous Carbon-Supported Zinc Acetate. *Industrial & Engineering Chemistry Research* **2018,** *57*, 7363-7373.
(1310) Fitzer, E. Book Review: Chemistry and Physics of Carbon, Vol. 1 and 2. Edited by P. L. Walker Jr. *Angewandte Chemie International Edition in English* **1967,** *6*, 1092-1093.
(1311) Brodie Benjamin, C. Xiii. On the Atomic Weight of Graphite. *Philosophical Transactions of the Royal Society of London* **1859,** *149*, 249-259.
(1312) Inagaki, M.; Kang, F. In *Materials Science and Engineering of Carbon: Fundamentals (Second Edition)*; Inagaki, M.;Kang, F., Eds.; Butterworth-Heinemann: Oxford, 2014, DOI:https://doi.org/10.1016/B978-0-12-800858-4.00001-2 https://doi.org/10.1016/B978-0-12-800858-4.00001-2.
(1313) Rupprechter, G. In *Surface and Interface Science*; Wandelt, K., Ed.; Wiley, 2015, DOI:doi:10.1002/9783527680573.ch39 doi:10.1002/9783527680573.ch39.
(1314) Gunter, P. L. J.; Niemantsverdriet, J. W.; Ribeiro, F. H.; Somorjai, G. A. Surface Science Approach to Modeling Supported Catalysts. *Catalysis Reviews* **1997,** *39*, 77-168.
(1315) Gao, F.; Goodman, D. W. Model Catalysts: Simulating the Complexities of Heterogeneous Catalysts. *Annu. Rev. Phys. Chem.* **2012,** *63*, 265-286.
(1316) Tian, W.; Li, W.; Yu, W.; Liu, X. A Review on Lattice Defects in Graphene: Types, Generation, Effects and Regulation. *Micromachines* **2017,** *8*, 163.
(1317) Lungerich, D.; Papaianina, O.; Feofanov, M.; Liu, J.; Devarajulu, M.; Troyanov, S. I.; Maier, S.; Amsharov, K. Dehydrative Π-Extension to Nanographenes with Zig-Zag Edges. *Nature Communications* **2018,** *9*, 4756.
(1318) Padilha, J. E.; Amorim, R. G.; Rocha, A. R.; da Silva, A. J. R.; Fazzio, A. Energetics and Stability of Vacancies in Carbon Nanotubes. *Solid State Commun.* **2011,** *151*, 482-486.
(1319) Gao, X.; Liu, H.; Wang, D.; Zhang, J. Graphdiyne: Synthesis, Properties, and Applications. *Chem. Soc. Rev.* **2019,** *48*, 908-936.

(1320) Liu, J.; Wang, H.; Antonietti, M. Graphitic Carbon Nitride “Reloaded”: Emerging Applications Beyond (Photo)Catalysis. *Chem. Soc. Rev.* **2016,** *45*, 2308-2326.